Cell biological consequences of inherited mitochondrial complex I deficiency: a radical study

Front cover: living human skin fibroblasts loaded with the superoxide specific dye hydroethidine

Cover design by Joost Verkaart

Printed by Ponsen & Looijen, Wageningen

Cell biological consequences of inherited mitochondrial complex I deficiency: a radical study

Een wetenschappelijke proeve op het gebied van de Medische Wetenschappen

PROEFSCHRIFT

ter verkrijging van de graad van doctor
aan de Radboud Universiteit Nijmegen,
op gezag van Rector Magnificus Prof. mr. S.C.J.J. Kortmann,
volgens besluit van het College van Decanen
in het openbaar te verdedigen op donderdag 5 juli 2007
om 10.30 uur precies

door

Sjoerd Adrianus Johannes Verkaart

geboren op 10 december 1977
te Bergen op Zoom

Promotor:

Prof. dr. J.A.M. Smeitink

Copromotores:

Dr. P.H.G.M. Willems

Dr. W.J.H. Koopman

Manuscriptcommissie:

Prof. dr. B. Wieringa (voorzitter)

Prof. dr. R. de Groot

Prof. dr. I. Braakman

TABLE OF CONTENTS

CHAPTER I

Introduction

To perform the complicated tasks associated with normal life our body requires a sufficient supply of energy and water, which is mainly provided by the intake of nutrition and fluids. Although the human body can be deprived of food for two to eight weeks, survival without water is usually limited to three to four days. The story becomes completely different with respect to our need of oxygen. Although some people can survive for almost nine minutes with one gasp of breath (lying motionless submerged in water) most of us can last for only one or two minutes. The reason that we are so heavily dependent on breathing air, engulfing a substantial amount of oxygen, lies at the heart of our cells, in organelles called mitochondria.

Mitochondria, the basics

Mitochondria are essential organelles, present in large numbers in virtually every cell. Together with the glycolytic pathway in the cytosol, mitochondria are responsible for the generation of ATP (adenosine triphosphate), the major form of cellular energy. Mitochondrial ATP production is an aerobe process, which consumes ~98% of the oxygen we breathe (68). Mitochondria are composed of a double membrane system, which separates two aqueous compartments (the mitochondrial matrix and inter membrane space; IMS) from the cellular environment (**Fig. 1**). Whereas the outer mitochondrial membrane (OMM) is almost freely permeable to small solutes the inner mitochondrial membrane (IMM) is not.

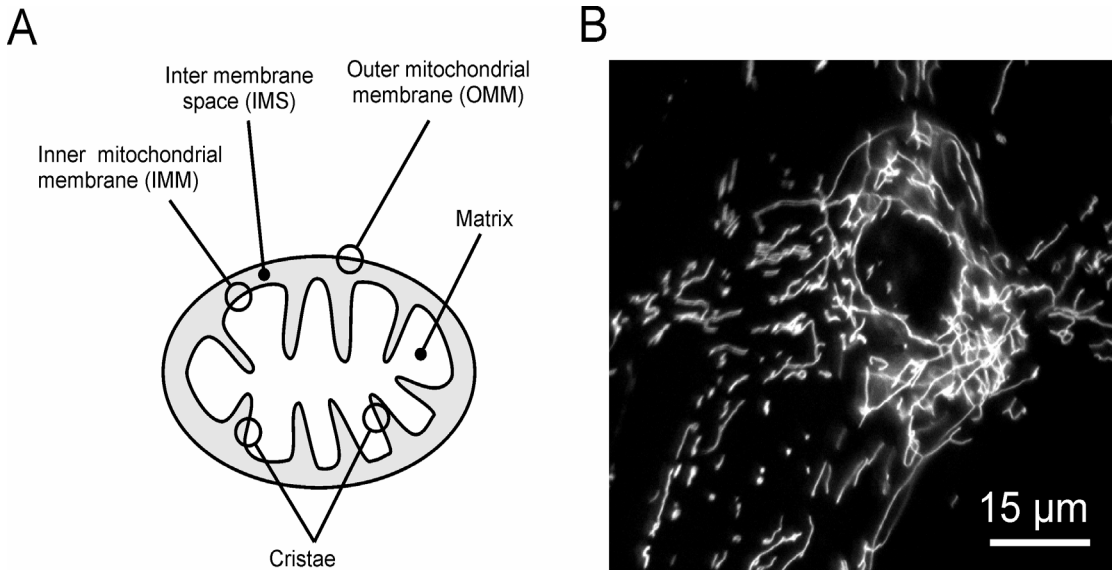

Figure 1: Overview of mitochondrial structure and mitochondrial reticulum in living cells - **A**) Schematic representation of the mitochondrial structure. **B**) Confocal image of the mitochondrial reticulum in a single living human skin fibroblast visualized with rhodamine 123 (R123). Image was acquired after R123 pulse staining, averaged (N=32) and contrast optimized according ref. 136.

Furthermore, the IMM is highly invaginated (cristae) and protrudes into the mitochondrial matrix (68). In addition mitochondria contain multiple copies of their own genetic material, present as circular double stranded DNA molecules (mtDNA) in the mitochondrial matrix. In living cells, mitochondria (Greek: mitos = thread + khondrion = granule) are very dynamic structures that are mobile and continuously change shape by fission and fusion. As a result, mitochondria occur as individual bean-shaped objects, elongated filaments or as part of an interconnected mitochondrial reticulum (**Fig. 1**, 46).

Mitochondrial and cellular function is tightly integrated

In addition of being the major generators of cellular ATP, mitochondria are also involved in many other biochemical and cellular processes. For example, they harbor essential components of biochemical pathways for the biosynthesis of iron-sulfur clusters, heme, pyrimidines, amino acids, phospholipids and nucleotides and for the breakdown of fatty acids (68,152,161). Furthermore, mitochondria are central to cellular (patho)physiology given their critical roles in heat generation (237), transduction of electrical signals (112), calcium homeostasis (25,213,293), generation of reactive oxygen- and nitrogen species (ROS/RNS; 14,65,209,265) and apoptosis (8,98).

The mitochondrial oxidative phosphorylation system

Virtually all mitochondrial functions require the presence of a sufficiently negative membrane potential ($\Delta\Psi$) across the IMM (68). Maintaining a proper $\Delta\Psi$ is essential for ATP generation, mitochondrial fusion and transport of calcium ions and other solutes across the IMM (24,63,115,168,283). During aerobic conditions, generation of $\Delta\Psi$ and ATP production are coupled via the mitochondrial oxidative phosphorylation (OXPHOS) system (**Fig. 2**). This system is embedded in the IMM and composed of five multi-protein assemblies (62).

The first four complexes, together with two electron carriers (ubiquinone and cytochrome *c*), constitute the electron transport chain (ETC). Oxidation of reduced nicotinamide adenine dinucleotide (NADH) at complex I (CI or NADH:ubiquinone oxidoreductase, EC 1.6.5.3.) and succinate at complex II (CII or succinate:ubiquinone oxidoreductase, EC 1.3.5.1.) liberates electrons that are subsequently transported to complex III (CIII or ubiquinol:cytochrome *c* oxidoreductase, EC 1.10.2.2) and IV (CIV or cytochrome *c* oxidase, EC 1.9.3.1). At the latter complex the electrons are finally donated to molecular oxygen resulting in the formation of water. During electron transport, the energy released is utilized to expel protons (H^+) from the mitochondrial matrix into the IMS (at CI, CIII and CIV), resulting in an inside-negative

membrane potential ($\Delta\Psi$) across the IMM. The electrochemical proton gradient is used by complex V (CV or F_1F_0-ATPase, EC 3.6.3.14) to drive the synthesis of ATP from ADP (adenosine diphosphate) and P_i (inorganic phosphate) in the mitochondrial matrix.

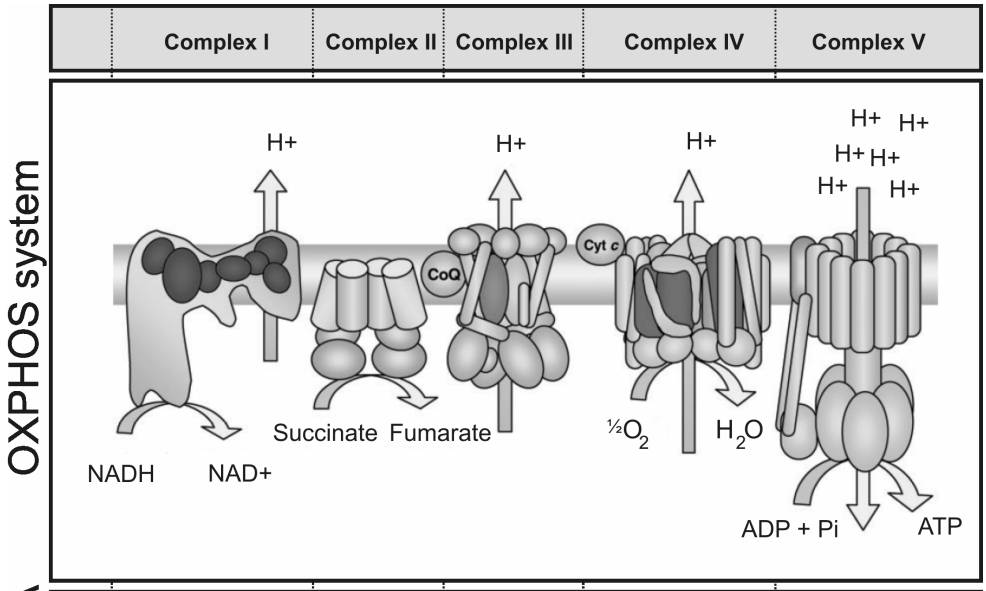

		Complex I	Complex II	Complex III	Complex IV	Complex V
mtDNA		ND1 ND2 ND3 ND4 ND4L ND5 ND6		Cyt b	COXI COXII COXIII	ATPase 6
nDNA		B17.2L NDUFA1 NDUFS1 NDUFS2 NDUFS3 NDUFS4 NDUFS6 NDUFS7 NDUFS8 NDUFV1 NDUFV2	SDHA SDHB SDHC SDHD	BSC1L UQCRB	COX10 COX15 LRPPRC SCO1 SCO2	ATP12
Total	MtDNA subunits	7	0	1	3	2
	NDNA subunits	38	4	10	10	~14

Figure 2: The mitochondrial oxidative phosphorylation system - Creative drawing of the oxidative phosphorylation system adapted from ref. 301. Top: respiratory chain complexes, representing complex I-V. OXPHOS system: nuclear-encoded subunits are shown in light grey. Subunits of mitochondrial origin, embedded in the midst of nuclear-encoded subunits, are shown in darker grey. mtDNA: subunit encoded by the mtDNA in which disease-causing mutations have been identified (120). nDNA: nuclear-encoded subunit in which disease-causing mutations have been found (references: see text and ref. 120). Recently disease-causing mutations have been identified in the nuclear-encoded proteins COQ2 (206) and PDSS2 (158) involved in the biosynthesis of coenzyme Q, not shown. Total: number of structural components of the oxidative phosphorylation system. Abbreviations: see text.

The OXPHOS system consists of at least 89 different proteins (62). Only a small subset of these proteins is derived from the mtDNA (seven for CI, one for CIII, three for CIV and two for CV) whereas the remainder is encoded by the nuclear genome (nDNA) (242). Therefore, the large majority of the OXPHOS subunits, together with many other nuclear-encoded mitochondrial proteins (>1000) need to be imported from the cytosol. This task is carried out by a dedicated mitochondrial protein import machinery consisting of a translocase in the OMM (TOM complex) and a translocase in the IMM (TIM complex; 295), the latter of which is $\Delta\Psi$-driven and requires ATP.

Importantly, given the large number of different OXPHOS proteins and their bi-genomic nature, biosynthesis of functional OXPHOS complexes requires coordination between nuclear and mitochondrial transcription/translation machineries (225). Within the mitochondrion, OXPHOS complexes are assembled and maintained by specific proteinaceous factors (53,62,185,284,285,287). Currently, detailed mechanistic insights into the regulation of OXPHOS expression and assembly are lacking (192).

Deficiency of the oxidative phosphorylation system

Mitochondrial dysfunction is associated with a variety of human diseases including cancer, diabetes, neurodegenerative disorders such as Parkinson, Alzheimer and Huntington disease and inborn errors of metabolism (1,14,88,101,161,230,242,248,291,302) Furthermore, functional deterioration of mitochondria has been observed during normal aging (96,269). Although the term ‘mitochondrial dysfunction’ is rather broad, it usually refers to disturbances of the OXPHOS system. For inborn errors of metabolism, deficiencies of the OXPHOS system have an estimated incidence of at least 1 in 5000 live births. OXPHOS disorders are genetically and clinically heterogeneous and the biochemical defect is either isolated or combined, meaning that one or more OXPHOS complexes are affected (120). Furthermore, OXPHOS defects can be systemic or occur in a tissue specific manner. The latter is likely caused by different types of cells/tissues being more or less sensitive to malfunction of individual OXPHOS complexes (218).

OXPHOS deficiency predominantly affects tissues with a high energy demand including skeletal muscle, heart and brain. Clinically, the deficiency can present itself at any age but is often seen as an early-onset, progressive metabolic syndrome associated with a diverse array of neurological, neuromuscular, cardiac and endocrine disorders (62,274,302). Most patients suffer from Leigh or Leigh-like syndrome (120,148,210) and die within a few years after the first clinical manifestations.

Due to the bi-genomic origin of complex I, III, IV and V, OXPHOS deficiency can be caused by mtDNA mutations, which are maternally inherited, and/or nDNA mutations (**Fig 2.** 33,107,264,274,292,30). Therefore, different modes of inheritance (maternal, autosomal recessive or dominant and X-linked) can contribute to the genetic heterogeneity of OXPHOS disorders (120). In most patients, the decrease in OXPHOS activity is associated with a deficiency of CI (OMIM 252010) making it the most frequently encountered enzymatic deficiency (157,224,288).

Complex I: composition, biogenesis and disease

Mammalian complex I (CI) is the largest enzyme of the OXPHOS system. Its structure is L-shaped and consists of a hydrophobic part, embedded in the IMM and a hydrophilic part, perpendicularly protruding into the mitochondrial matrix (**Fig. 3**, 81,90). CI couples the oxidation and reduction of NADH and ubiquinone, respectively, to the translocation of protons across the IMM (104). Oxidation of NADH liberates two electrons which are transferred to the primary electron acceptor of CI, a non-covalently bound flavin mononucleotide (FMN). Subsequently, the electrons are transported via a series of eight iron-sulfur clusters to their final electron acceptor ubiquinone (CoQ), resulting in the formation of ubiquinol ($CoQH_2$) and the translocation of four protons to the IMS (103). Although different mechanistic models have been proposed for the above process (103,187,280), its exact molecular mechanism remains to be determined.

Mammalian CI has a molecular mass of approximately 1 MDa and consists of 45 structural subunits (**Fig. 3**) 14 of which (including all mtDNA-encoded proteins) are evolutionary conserved (44,45,83). The latter proteins constitute the catalytic core of CI and carry the substrate binding site, all redox centers and, in principle, suffice to perform the bioenergetic functions of CI. In addition, mammalian CI has 31 nuclear-encoded 'accessory' subunits, which functions are largely unknown (104,118). CI assembly involves the coordinated combination of individual subunits in evolutionary conserved protein modules (82,272,287). Next, these modules are assembled to a fully functional complex. CI assembly requires assistance of specific assembly factors including NDUFAF1 (286), B17.2L (185) and Ecsit (285). In addition, biochemical, structural and functional approaches suggest that CI complexes are organized into higher order supercomplexes that also contain CIII and CIV (27,227,228,229). It is hypothesized that these supercomplexes allow efficient substrate channeling between complexes, stabilize the structure of the participating complexes and prevent leakage of reactive intermediates (229).

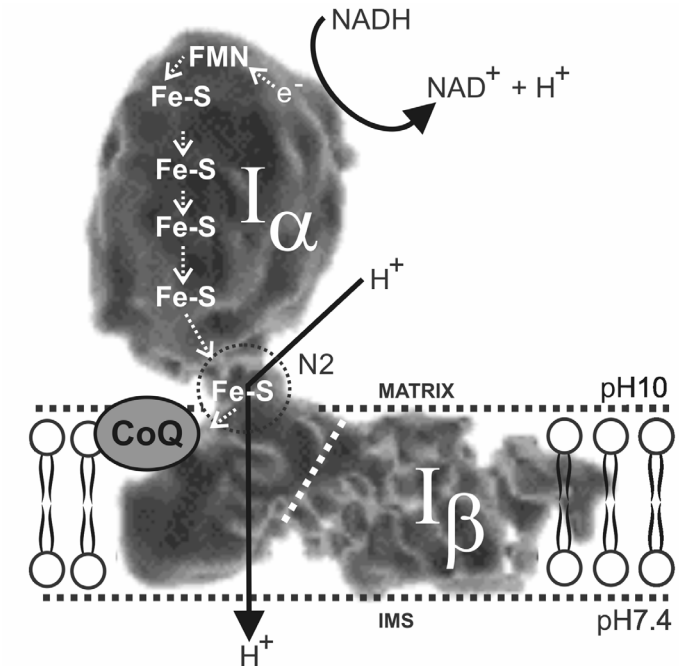

Iα#	
HUMAN	***Bos taurus***
DAP13	B17.2
GRIM19	B16.6
NDUFA1	**MWFE**
NDUFA2	B8
NDUFA3	B9
NDUFA5	B13
NDUFA6	B14
NDUFA7	B14.5a
NDUFA8	PGIV
NDUFA9	39-kDa
NDUFA10	B14.7
NDUFA11	42-kDa
NDUFAB1*	SDAP*
NDUFB4*	B15*
NDUFS1	**75-kDa**
NDUFS2	**49-kDa**
NDUFS3	**30-kDa**
NDUFS4	**18-kDa**
NDUFS5	15-kDa
NDUFS6	**13-kDa**
NDUFS7	**PSST**
NDUFS8	**TYKY**
NDUFV1	**51-kDa**
NDUFV2	**24-kDa**
NDUFV3	10-kDa
ND6	**ND6**

Iβ#	
HUMAN	***Bos taurus***
NDUFAB1*	SDAP*
NDUFB4*	B15*
NDUFB1	MNLL
NDUFB2	AGGG
NDUFB3	B12
NDUFB5	SGDH
NDUFB6	B17
NDUFB7	B18
NDUFB8	ASHI
NDUFB9	B22
NDUFB10	PDSW
NDUFB11	ESSS
NDUFC1	KFYI
NDUFC2	B14.5b
ND4	**ND4**
ND5	**ND5**

Not assigned%	
HUMAN	***Bos taurus***
NDUFA4	MLRQ
ND1	**ND1**
ND2	**ND2**
ND3	**ND3**
ND4L	**ND4L**

Figure 3: Structural composition of mammalian complex I - Complex I structure was adapted from ref. 90 and CI subunit composition and annotation were based on ref. 104. #With the aid of chaotropic agents, bovine CI can be divided into an alpha (Iα) and beta (Iβ) subcomplex. Subunits in which a disease-causing mutation is identified are shown in bold; mtDNA-encoded subunits are underlined. Asterisks indicate that protein is present in substochiometric amounts. %Not assigned: subunits which belong to complex I but could not be assigned to the Iα or Iβ subcomplex.

In most pediatric cases, CI deficiency is caused by mutations in nDNA-encoded structural CI subunits (246). Thus far, autosomal recessive mutations have been demonstrated in the NDUFA1, NDUFS1, NDUFS2, NDUFS3, NDUFS4, NDUFS6, NDUFS7, NDUFS8, NDUFV1 and NDUFV2 subunits of CI and in the CI assembly factor B17.2L (22,40,41,74,120,130,165,205). Regarding the possible consequences of these mutations, concentrations of lactic acid and Kreb's cycle intermediates as well as lactate:pyruvate ratios can be increased in body fluids and cells of patients with CI deficiency (71,157,204). The latter phenomenon results from a disturbed mitochondrial NADH/NAD^+ redox balance in which accumulation of NADH as a result of CI deficiency leads to inhibition of the Kreb's cycle and thereby accumulation of Kreb's cycle intermediates and pyruvate. The latter is converted into lactic acid by NADH-dependent lactate dehydrogenases, resulting in an elevated lactate:pyruvate ratio (248).

Studies on fibroblasts from patients with an isolated CI deficiency revealed aberrations in cellular and mitochondrial calcium handling and calcium-stimulated mitochondrial ATP production during hormone stimulation (281,282,283). Another cellular study revealed that mitochondrial morphology was aberrant in CI deficient patient fibroblasts (ranging from fragmented to highly elongated) and positively correlated with residual CI activity (139). This suggests that CI deficiency affects mitochondrial structure or *vice versa*.

Complex I deficiency: Involvement of free radicals

Over 90% of the cellular reactive oxygen species (ROS) is produced by mitochondria as a normal consequence of electron transport (14,68). This ROS results from the fact that a small portion of molecular oxygen (~0.2%), consumed by the ETC, is incompletely reduced thereby resulting in the formation of reactive intermediates (255). ROS comprise a group of chemically diverse molecules like superoxide (O_2^-), hydrogen peroxide (H_2O_2) and hydroxyl radical ($OH^\cdot$) (117) with different (patho)biological actions (**Fig. 4**).

The primary source of cellular ROS is O_2^-, which is mainly generated at CI in living cells (2,144,175,184,255). Superoxide is membrane impermeable and fairly reactive. Under normal conditions virtually all O_2^- is enzymatically converted into H_2O_2 by the combined action of manganese superoxide dismutase (MnSOD) in the mitochondrial matrix and copper-zinc superoxide dismutase (CuZnSOD) in the cytosol (117,208). In contrast to O_2^-, H_2O_2 is not very reactive and can cross membranes readily (6,254). Mitochondria-generated H_2O_2 can be degraded by the enzymatic action of glutathione-dependent peroxidases (113) or peroxiredoxins (122), causing thiol oxidation of glutathione and thioredoxin which may be used as a regulatory signal (106,117).

Mitochondrial O_2^- can also react with nitric oxide (NO) resulting in formation of the reactive nitrogen species (RNS) peroxynitrite ($ONOO^-$), (117). NO itself can easily diffuse into mitochondria and may also be produced there by the action of nitric oxide synthases (38,86). As formation of $ONOO^-$ is faster than the decomposition of O_2^- by MnSOD (207), $ONOO^-$ generation by this reaction is possibly biologically relevant. When not properly scavenged, O_2^- can damage iron-sulfur proteins thereby liberating ferrous iron (Fe^{2+}) (276). In an alternative reaction although not confirmed *in vivo*, O_2^- can be protonated to the membrane permeable hydroperoxyl radical ($HO_2^\cdot$) that, on its turn, can induce lipid peroxidation (7,117). The importance of a functional mitochondrial O_2^- scavenging system is stressed by results obtained in mice in which the gene for MnSOD was ablated. These mice die of a mitochondrial disorder shortly after birth (110,149).

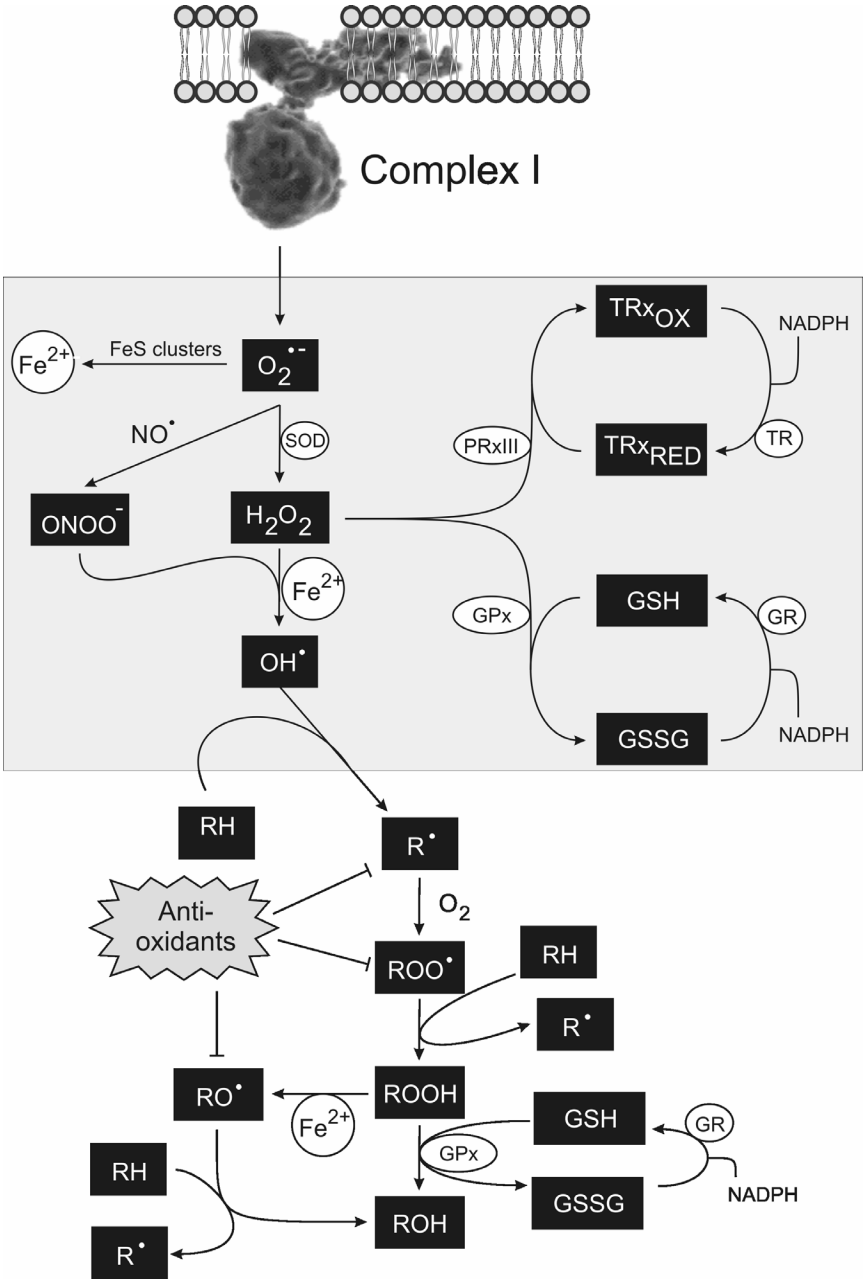

Figure 4: Overview of mitochondrial free radical metabolism - Schematic overview of mitochondrial ROS reactions adapted from ref. 117. Superoxide ($O_2^{\cdot-}$) produced by CI can be dismutated by superoxide dismutase (SOD) to hydrogen peroxide (H_2O_2) but can also react with iron–sulfur proteins producing ferrous iron (Fe^{2+}) and nitric oxide (NO) to form peroxynitrite ($ONOO^-$). H_2O_2 can be degraded by peroxiredoxin III (PRxIII) or by glutathione peroxidases (GPx) which use thioredoxin (Trx) or glutathione (GSH) as electron donors, respectively. In the presence of Fe^{2+}, H_2O_2 breaks down to form the hydroxyl radical ($OH^{\cdot}$) whereas the breakdown of $ONOO^-$ results in a species with similar reactivity as $OH^{\cdot}$. $OH^{\cdot}$ can remove $H^{\cdot}$ from lipids (RH) initiating formation of peroxolipids ($ROO^{\cdot}$) which can start a cycle of lipid peroxidation that includes the formation of peroxides (ROOH) and alkoxy radicals ($RO^{\cdot}$). These can be detoxified to alcohols (ROH) by the action of antioxidants and glutathione peroxidase 4. GR: glutathione reductase; GSSG: oxidized GSH; NADPH: nicotinamide adenine dinucleotide phosphate reduced form); TR, thioredoxin reductase; TRx, thioredoxin.

When H_2O_2 levels become too high, this molecule can participate in the Fenton reaction comprising the Fe^{2+}-catalyzed formation of the extremely reactive hydroxyl radical ($OH^{\cdot}$). Within a lipid environment, hydroxyl radicals initiate lipid peroxidation. In non-lipid environments, this radical can induce non-specific damage to all biological molecules at its site of production. Currently, no enzymatic scavenging system for hydroxyl radicals has been identified.

Next to enzymatic systems, several non-enzymatic ROS scavenging systems exist that protect the cell from the detrimental effects of ROS/RNS during normophysiological conditions. These include membrane-bound vitamin E (with α-tocopherol being the most effective form), vitamin C (ascorbic acid), and glutathione (GSH; L-γ-glutamyl-L-cysteinyl-glycine) (56). GSH is the predominant low-molecular-weight thiol in animal cells and is important in the protection against oxidative damage, both by direct reaction with ROS and as electron donor for peroxidases (111,297) Because of the high intracellular GSH concentration (0.5-10 mM) the 2GSH/GSSG couple is believed to be the major determinant for cellular redox homeostasis and antioxidative capacity (226,297).

A small part of the ROS produced is believed to function in cellular signal transduction (80,153). However, excessive production of ROS/RNS can overwhelm cellular antioxidant mechanisms and inflict damage to all major cellular biomolecules including DNA, lipids and proteins (117,208). Changes in ROS/RNS levels as a consequence of CI deficiency may alter mitochondrial and/or cellular redox homeostasis leading to activation of redox-sensitive signaling pathways (65,265). Evidence has been provided that these pathways modulate cellular calcium signaling (28), regulate cellular antioxidant capacity (204,296) and control mitochondrial biogenesis (147,171,172).

Aim and outline of this thesis

At present, our understanding of the consequences of CI mutations at the cellular level is very limited. This lack of insight severely hampers the rational design and testing of effective therapeutics. Since CI is a major contributor to cellular ROS production, disturbances in the function of this complex due to an inherited mutation in one of its subunits could result in increased free radical levels. Such an increase might result in cellular damage and/or alterations in cellular signaling pathways (80,153,208). Previous studies using isolated mitochondrial preparations demonstrated that **(I)** a decrease in CI activity is associated with increased ROS levels and induction of lipid damage (16,160,204) **(II)** conditions of oxidative or nitrosative stress can result in CI protein modifications and a reduced activity

(18,26,47,55,196,263). However, given the tight interconnection between mitochondrial and cellular function, the use of isolated mitochondria precludes proper evaluation of the cell biological consequences of CI deficiency, in relation to human disease.

Therefore, **the aim of the research described in this thesis** was to gain more insight into the consequences of human CI deficiency with respect to free radical biology in the context of the living cell. To investigate this, we used two model systems: one in which CI deficiency was induced by rotenone in healthy control cells and another where a cohort of patient-derived fibroblasts with an inherited CI deficiency was used. With the aid of chemical and genetically-encoded fluorescent reporter molecules, life-cell imaging, biochemical, immuno-histochemical and enzymatic techniques, the quantitative relationship between CI protein expression, ROS levels, lipid peroxidation and redox homeostasis in human CI deficiency at the (sub)cellular level was investigated.

In **chapter 2** a novel method for simultaneous quantification of oxidative stress and cell spreading in CI deficiency is described and validated. Using the method described in the previous chapter, **chapter 3** and **4** investigate the effect of the vitamin E-derived antioxidant Trolox on cellular oxygen radical levels and CI expression and activity. **Chapter 3** demonstrates that increased cellular ROS levels in patient cells are normalized by Trolox-treatment. In parallel, Trolox increased the expression of fully assembled CI and its activity. Comparison of the Trolox-induced change in CI expression and activity revealed a variable intrinsic catalytic problem in the patient cell lines. In **chapter 4** Trolox was used as a tool to investigate the pathological mechanism of CI deficiency in a subset of patient cell lines with a mutated NDUFS4 subunit. This revealed that, although these patient cells displayed only a catalytically inactive CI subcomplex of reduced size on native gels, substantial biochemical CI activity was present within the context of the intact cell. This suggests that the mutations in the NDUFS4 subunit lead to CI destabilization. In **chapter 5**, a cohort of 21 CI deficient patient cell lines was studied to determine the relationship between superoxide levels, expression of fully assembled CI protein and CI activity. It was demonstrated that human CI deficiency results from decreased expression of fully assembled CI, which is paralleled by a proportional increase in cellular O_2^- levels. **Chapter 6** investigated whether patient cells displayed alterations in mitochondrial/cellular redox state and extent of lipid peroxidation. No aberrations in redox status and lipid peroxidation were observed, suggesting that the cells successfully adapted to the increased ROS levels described in **chapter 3-5**. **Chapter 7** describes the findings obtained using the rotenone model and the effect of the mitochondria-targeted antioxidant Mitoquinone (MitoQ). It is demonstrated that chronic partial CI inhibition

induces mitochondrial branching, and increases O_2^- and lipid peroxidation in control cells. The presence of MitoQ effectively blocked the rotenone-induced mitochondrial branching and lipid peroxidation without, however, reducing the elevated O_2^--levels. These findings suggest that CI deficiency can alter mitochondrial morphology via O_2^- induced lipid peroxidation. Finally, **chapter 8** summarizes and discusses the results obtained.

CHAPTER II

Simultaneous quantification of oxidative stress and cell spreading using 5-(and-6)-chloromethyl-2',7'-dichlorofluorescein

Werner J.H. Koopman[a,c,d]
Sjoerd Verkaart[a,b,d,e]
Sjenet E. van Emst-de Vries[a,d]
Sander Grefte[a]
Jan A.M. Smeitink[b,d,e]
Peter H.G.M. Willems[a,c,d]

[a]Department of Membrane Biochemistry, [b]Department of Pediatrics, [c]Microscopical Imaging Centre, [d]Nijmegen Centre for Molecular Life Sciences (NCMLS), [e]Nijmegen Centre for Mitochondrial Disorders (NCMD), Department of Pediatrics, Radboud University Nijmegen Medical Centre

Cytometry A. **2006**, 69(12):1184-1192.

ABSTRACT

Background – Mitochondrial dysfunction may lead to increased oxidative stress and consequent changes in cell spreading. Here, we describe and validate a novel method for simultaneous quantification of these two parameters.

Methods – Human skin fibroblasts were loaded with 5-(and-6)-chloromethyl-2',7'-dichlorodihydrofluorescein (CM-H_2DCF) and its oxidative conversion into CM-DCF was monitored as a function of time by video-rate confocal microscopy and real-time image averaging. Cell size was determined after binarization of the acquired images.

Results – At the lowest practical laser output, CM-DCF formation occurred with zero order kinetics, indicating that [CM-H_2DCF] was not rate-limiting and that the rate of [CM-DCF] formation ($V_{CM\text{-}DCF}$) was a function of the cellular oxidant level. Analysis of fibroblasts of a healthy control subject and a patient with a deficiency of NADH:ubiquinone oxidoreductase, the first complex of the oxidative phosphorylation system, revealed a significant increase in cellular oxidant level in the latter cells that was, however, not accompanied by a change in cell spreading. Conversely, chronic treatment with 6-hydroxy-2,5,7,8-tetramethylchroman-2-carboxylic acid (Trolox), a derivative of vitamin E, markedly decreased the oxidant level and cell spreading in both control and patient fibroblasts.

Conclusions – We present a reliable method for simultaneous quantification of oxidant levels and cell spreading in living cells.

INTRODUCTION

In mammalian cells, the vast majority (>90%) of reactive oxygen species (ROS) is produced as a consequence of electron transport through the mitochondrial electron transport chain (ETC; (14,68). The primary ROS species formed by the ETC is superoxide ($O_2^{\cdot-}$), with major production sites at CI and CIII (144). Superoxide can react with nitric oxide (NO) to form extremely reactive peroxinitrite ($ONOO^-$). The latter reactive nitrogen species (RNS) exists in fast dynamic equilibrium with its conjugated acid ONOOH. In the absence of carbon dioxide, $ONOO^-$/ONOOH decays to harmless nitrate (NO_3^-), reactive nitrogen dioxide (NO_2), and the highly reactive hydroxyl radical ($OH^{\cdot}$); (56).

Under normophysiological conditions, several enzymatic and non-enzymatic systems exist that protect the cell from the detrimental effects of oxidants. Antioxidant enzymes include catalases, superoxide dismutases (SODs), peroxiredoxins and glutathione peroxidases. Thus, once formed, the majority of superoxide is dismutated to hydrogen peroxide (H_2O_2) by the combined activity of mitochondrial MnSOD and cytosolic CuZnSOD. Hydrogen peroxide is subsequently decomposed to water and oxygen by the action of catalase and various peroxidases. In the presence of iron(II), however, H_2O_2 can be converted into $OH^{\cdot}$ by the Fenton reaction. If this reaction is not properly counterbalanced by ferritin and/or heme oxygenase (HOx), $OH^{\cdot}$ can induce serious damage to lipids, proteins, carbohydrates and DNA (209). The major non-enzymatic defense systems consist of membrane-bound vitamin E, vitamin C (ascorbic acid), and glutathione (GSH; L-γ-glutamyl-L-cysteinyl-glycine; (56)). In general, these antioxidants act by terminating a chain reaction of oxidizing events (270).

Oxidative stress occurs when the generation of oxidants is not appropriately counterbalanced by the cell's antioxidant systems (14,65,265,296). This imbalance will change the cellular redox environment, thereby activating specific redox-sensitive signaling pathways (65,265). Evidence has been provided that these pathways, among others, regulate mitochondrial biogenesis (146,171,172), cellular antioxidant capacity (204,296), Ca^{2+} homeostasis (28) and cell adhesion and spreading (13,23,51,239,294). The oxidative conversion of 2',7'-dichlorodihydrofluorescein (H_2DCF) into 2',7'-dichlorofluorescein (DCF) has been widely applied to measure oxidant levels in both cell free systems and living cells (51,87,178,239,262). Here, we describe the establishment of a reliable protocol for simultaneous quantification of oxidant levels and cell spreading based on video-rate confocal microscopy of cells loaded with 5-(and-6)-chloromethyl-2',7'-dichlorodihydrofluorescein (CM-H_2DCF). This protocol was subsequently used to assess the effects of a deficiency of the

first and largest multi-subunit complex of the mitochondrial oxidative phosphorylation system, NADH:ubiquinone oxidoreductase, on the oxidant levels and spreading of cultured skin fibroblasts derived from a patient with a pathological mutation in one of the nuclear-encoded subunits of this enzyme. It was found that oxidant levels were increased but cell spreading was normal in patient fibroblasts.

MATERIALS AND METHODS

Cell culture – Fibroblasts were derived from a skin biopsy of a healthy control subject (culture number #5120) and a patient with isolated complex I (CI) deficiency (culture number #5170) following informed parental consent and according to the relevant Institutional Review Boards. The deficiency was confirmed in both muscle tissue and cultured skin fibroblasts and screening for the presence of DNA alterations in each of the known nuclear-encoded CI genes revealed a mutation in the NDUFS2 subunit (155). The patient was negative with respect to mtDNA alterations previously known to cause CI deficiency.
Fibroblasts were cultured in medium M199 containing 5 mg/l Tween 20, 10% (v/v) fetal calf serum, 100 IU/ml penicillin and 100 IU/ml streptomycin (Invitrogen, Breda, The Netherlands). For confocal imaging, cells were seeded on glass coverslips (Ø 22 mm) and cultured to ~70% confluence in a humidified atmosphere (95% air, 5% CO_2) at 37^{o} C.

Video-rate confocal imaging of CM-DCF fluorescence – Cytosolic oxidant levels were quantified with 5-(and-6)-chloromethyl-2',7'-dichlorodihydrofluorescein diacetate (CM-H_2DCFDA; Molecular Probes). Stock solutions (1 mM) were prepared in DMSO, saturated with N_2 gas to prevent oxidation, and stored at -20° C. Fibroblasts were incubated for 10 min at 37° C in a HEPES-Tris (HT) medium (132 mM NaCl, 4.2 mM KCl, 1 mM $CaCl_2$, 1 mM $MgCl_2$, 5.5 mM D-glucose and 10 mM HEPES, pH 7.4) containing 1 μM CM-H_2DCFDA. After thorough washing to remove non-hydrolysed dye, coverslips were mounted in an incubation chamber placed on the stage of an inverted microscope (Nikon Diaphot, Tokyo, Japan) attached to an Oz confocal microscope (Noran Instruments, Middleton, WI, USA). Cells were placed in HT-medium and measurements were performed at 20° C in the dark. In the axial direction, human skin fibroblasts fitted fully within 3 consecutive 1 μm thick optical sections. This demonstrates that the height of the fibroblasts is ≤ 3 μm. Therefore, to prevent exclusion of mitochondrial structures from the image in the axial direction, no confocal slit was used. This equals an axial section thickness of 10 μm. The light from an Argon ion laser (488 nm; Omnichrome, Chino, CA, USA) was delivered to the cells via a x40 oil immersion planapochromat objective (NA 1.4; Nikon). Fluorescence emission light was directed through a 500 nm LP barrier filter (Chroma Technology Corp., Brattleboro, VT, USA) and quantified using a photomultiplier tube at 8-bit resolution (Hamamatsu Photonics, Bridgewater, NJ, USA). Hardware and image acquisition were controlled by Intervision software running under IRIX 6.2 on an Indy workstation (Silicon Graphics Inc., Mountain View, CA, USA) equipped

with 512 Mb memory. Images (512x480 pixels) were collected at 30 Hz with a pixel dwell-time of 100 ns.

Data analysis – Image analysis was performed using Image Pro Plus 5.1 (Media Cybernetics, Silver Spring, MD, USA) as described in the Results section. Numerical results were visualized using Origin Pro 7.5 (Originlabs, Northampton, MA, USA) and values from multiple experiments were expressed as means ± SE (standard error). Statistical significance (Bonferroni corrected) was assessed using Student's t-test. During linear regression analysis, the degree of bivariate correlation between sets of data was analyzed by calculating Pearson's R. This parameter expresses the proportion of total variation that is explained by the regression. If R is ±1, the total variation in the fit can be explained in terms of the regression curve (58). For R>0 the correlation is positive, for R<0 the correlation is negative. Similarly, R^2 was used as a measure of the goodness of the fit during non-linear regression (Levenberg-Marquardt method).

Chemicals – Cell culture materials were obtained from Gibco (Gaithersburg, MD, USA). All other reagents were from Sigma (St. Louis, MO, USA).

RESULTS

Visualization of CM-DCF fluorescence by video-rate confocal microscopy – DCF (2',7'-dichlorofluorescein) has been shown to be prone to passive leakage across the plasma membrane (124,257). Therefore, we here used a DCF variant with chloromethyl groups (CM-DCF), which greatly reduce passive dye leakage (93). Skin fibroblasts were incubated for 10 min at 37° C in HT medium containing 1 µM CM-H_2DCFDA. During this period, the acetate groups are cleaved off by intracellular esterases, yielding non-fluorescent CM-H_2DCF, which is then oxidized by intracellular oxidants to form the highly fluorescent product CM-DCF (5-(and-6)-chloromethyl-2',7'-dichlorofluorescein). At the end of the loading period, cells were thoroughly washed to remove non-hydrolysed CM-H_2DCFDA. CM-DCF fluorescence was monitored by video-rate confocal microscopy and real-time image averaging. Excitation was at 488 nm and emission light was directed through a 500 nm long-pass barrier filter onto the photomultiplier tube (29). For maximal sensitivity, images were acquired using an objective with a high numerical aperture (1.4). Black level and brightness settings were adjusted to achieve an optimal dynamic range of grey values within the recorded image. Images were routinely captured at 10 s intervals. At each time point, 30 images (512x480 pixels) were acquired at 30 Hz and averaged in real time to increase the signal-to-noise ratio (138). The latter setting resulted in a pixel dwell-time of 100 ns. All measurements were performed in the dark and excitation light was fully shielded between images using a hardware shutter. This experimental approach permitted acquisition of high quality images at minimal laser intensities. CM-DCF fluorescence was observed throughout the cell but was clearly higher in the nucleoplasm (**Fig. 1A**; inset). This might be due to a higher viscosity of the nuclear compartment, which enhances the excitation efficiency of CM-DCF (134).

CM-DCF fluorescence increases as a function of laser intensity – Previous reports have shown that laser light stimulates CM-DCF formation (29,32,87,162,257). To assess the relative importance of this photo-oxidation process, CM-H_2DCF-loaded fibroblasts were excited at increasing laser intensities and CM-DCF fluorescence was recorded. For quantitative evaluation of the changes in CM-DCF fluorescence intensity, regions of interest (ROIs), encompassing either the whole cell (dotted lines) or an intracellular region of maximum size (solid lines), were defined (**Fig. 1A**). For each ROI, fluorescence emission intensity was expressed as average greylevel value per pixel. Before further analysis, each

trace was corrected for background by subtracting the fluorescence obtained from an extracellular ROI (marked 'B'). At laser intensities ≤ 6% (subcellular ROIs) and ≤ 7% (whole cell ROIs), CM-DCF fluorescence increased linearly with time ($R>0.99$, $p<0.0001$). The rate of fluorescence increase ($V_{CM\text{-}DCF}$) clearly depended on the laser intensity (**Fig. 1B**) and was proportional for both the whole cell and the intracellular region (**Fig. 1C**). Based on these findings, we used the lowest practical laser intensity of 4%, equaling a laser output at the laser head of 34 µW, in the remainder of the study.

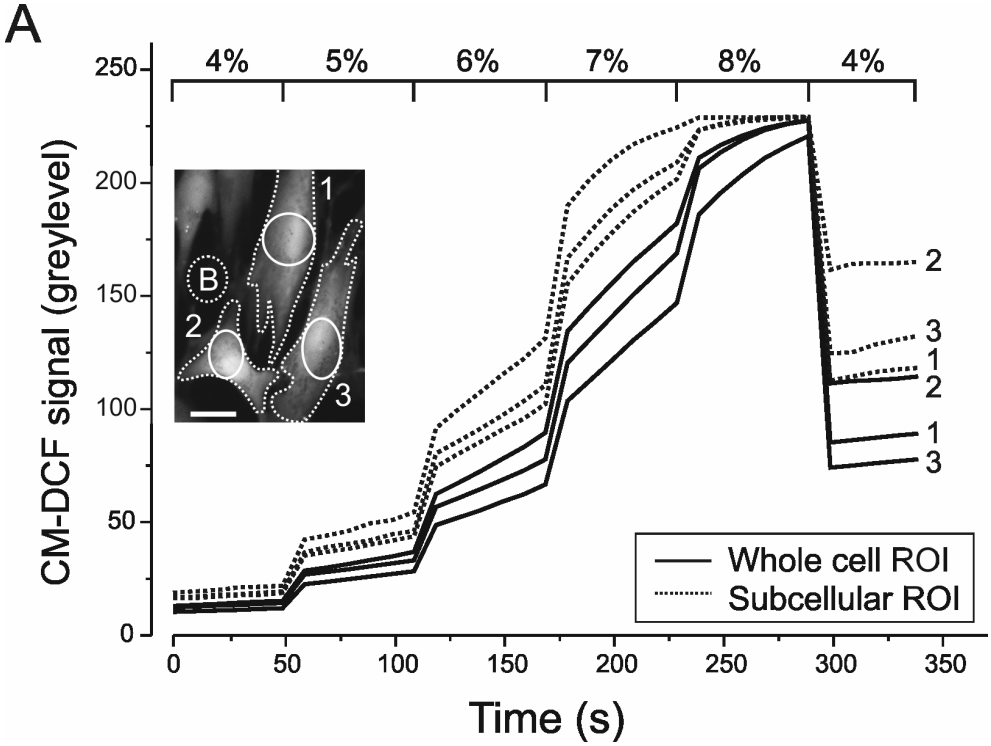

Figure 1: Effect of laser power on CM-DCF formation – (**A**) The inset shows a confocal image of human skin fibroblasts incubated with CM-H_2DCFDA for 10 min. The image was contrast-optimized to reveal cellular structures. Dotted lines indicate whole cell regions of interest (ROIs; marked 1, 2 and 3). Ovals correspond to intracellular ROIs and a background ROI (marked 'B'). The scale bar indicates 15 µm. The graph shows the time course of the background-corrected CM-DCF fluorescence as a function of laser power for the whole cell (continuous lines) and subcellular ROIs (dotted lines). (**B**) Average rate of CM-DCF fluorescence increase ($V_{CM\text{-}DCF}$) for whole cell (black bars) and subcellular ROIs. (**C**) Relationship between whole cell (x-axis) and subcellular (y-axis) $V_{CM\text{-}DCF}$ as a function of laser power. All data points obtained for 4% , 5% and 6% laser intensity were on a straight line that passed through the origin (intercept=-2.1E-4±0.0002; $R=0.999$, $p=0.003$). (**D**) CM-DCF fluorescence change as a function of time at 4% laser intensity. The upper traces represent subcellular ROIs, the lower trace corresponds to an extracellular ROI. A linear fit (straight line) was calculated to the first 11 data points for each cell (grey box). Linearity was observed during the first 200 s of recording. After this period, both intra- and extracellular signals increased supra-linearly. For all linear fits, $R>0.99$ and $p<0.0001$. The slope of the line fitted to the background signal did not differ from zero (slope=-6.9E-5±1.1E-4).

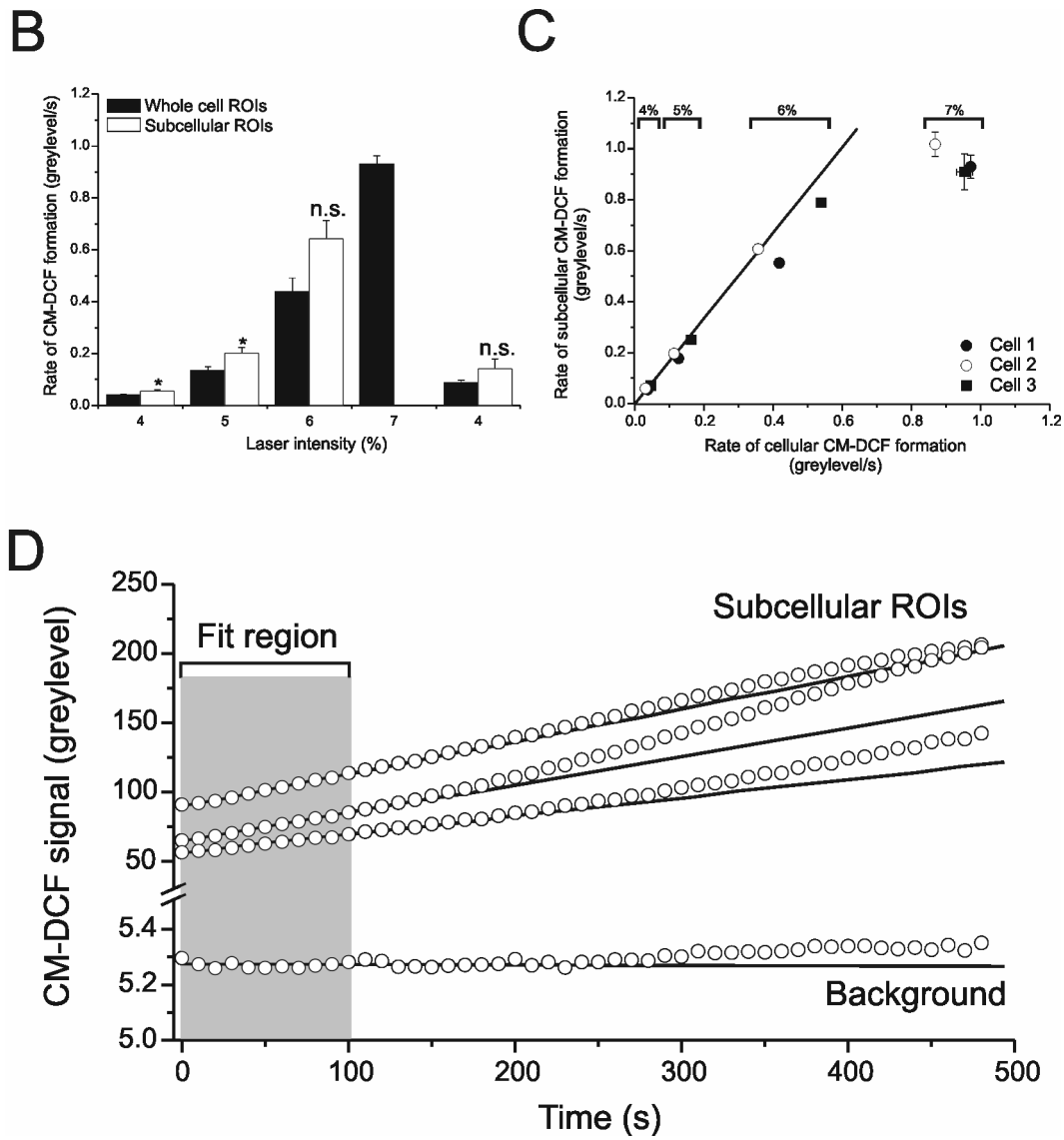

CM-DCF fluorescence increases linearly during low laser intensity illumination – We next investigated the linearity of the increase in CM-DCF fluorescence during prolonged illumination at the lowest practical laser intensity (4%). For each of the traces shown in **figure 1D**, a linear fit was made to the first 11 data points indicated with 'fit region' ($R>0.99$ and $p<0.0001$). The figure shows that linearity was observed for maximally 200 s, indicating that the slope of the fit to the first 20 data points can be taken as a reliable measure of $V_{CM\text{-}DCF}$. At longer times, both the intracellular and background fluorescence started to deviate from linearity. In view of these results, we decided to routinely use a recording time of less than 200 s for quantitative analysis of intracellular CM-DCF signals.

CM-DCF fluorescence increases faster in the presence of hydrogen peroxide – Previous work using epidermal keratinocytes and skin fibroblasts revealed that CM-DCF fluorescence

increased more rapidly in the presence of H_2O_2 (109,129). To assess whether linearity was maintained under these conditions, fibroblasts were acutely treated with 100 µM H_2O_2. **Figure 2B** shows that this treatment stepwise increased the fluorescence signal to a new and higher level. Thereafter, the signal continued to increase linearly (R>0.99, p<0.0001) but at a 3-fold faster rate than before application of the oxidant (**Fig. 2C**). Importantly, this result demonstrates that our method is quantitative at least up to oxidant levels that cause a 3-fold increase in $V_{CM\text{-}DCF}$. Of note, the cell size remained unaltered in the course of the experiment (**Fig. 2A**).

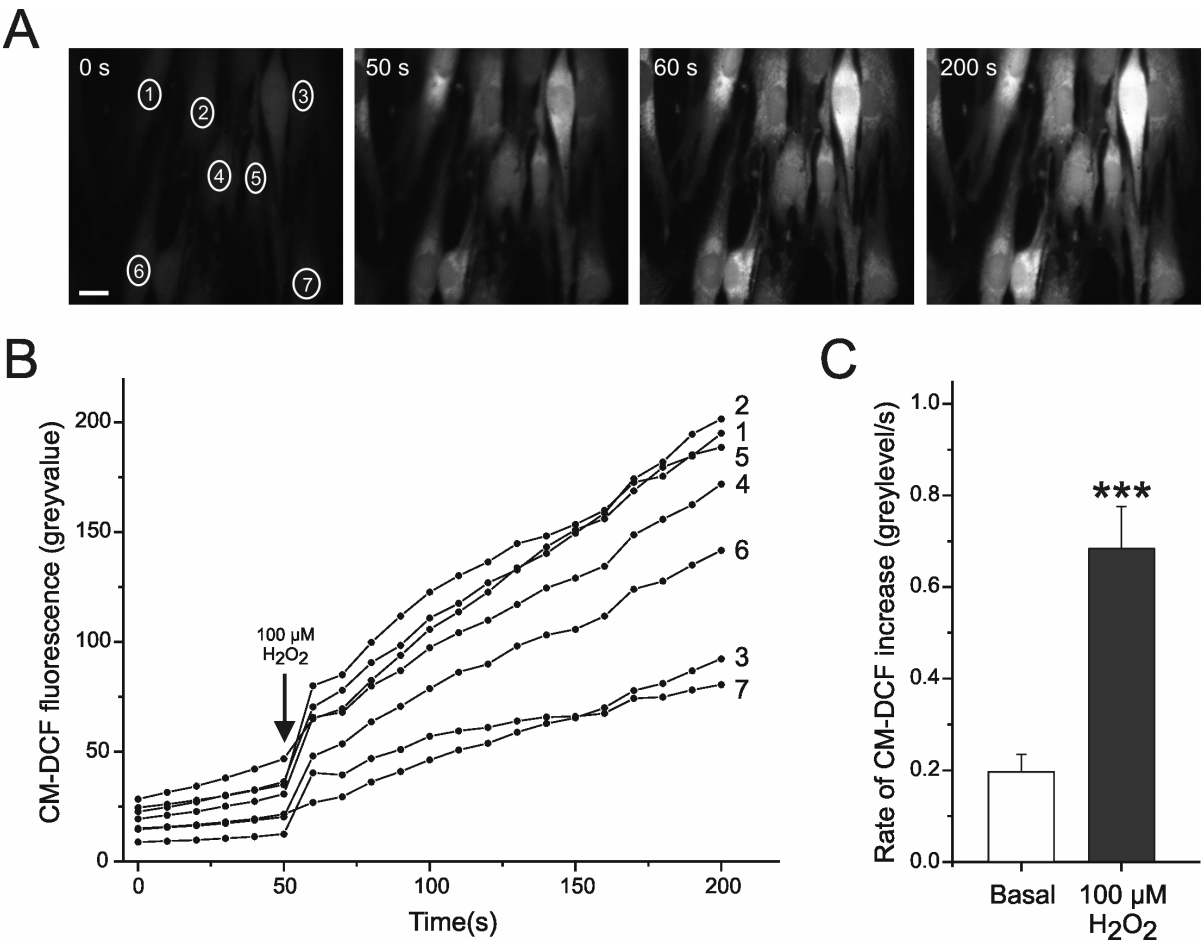

Figure 2: Linearity of CM-DCF formation and effect of hydrogen peroxide – (**A**) Confocal images of control human skin fibroblasts following incubation with CM-H_2DCFDA. Ovals indicate seven intracellular ROIs, used for analysis. The indicated times correspond to the trace in panel B. The scale bar indicates 15 µm. (**B**) Effect of acute hydrogen peroxide application (H_2O_2; 100 µM) on the background-corrected CM-DCF signal for the individual ROIs. Linearity was observed for both the pre- and post-H_2O_2 traces. For all linear fits, R>0.95 and p<0.0001. (**C**) Average rate of CM-DCF formation ($V_{CM\text{-}DCF}$) calculated for the cells in panel B. This rate was more than three-fold increased by H_2O_2 (p<0.001).

The rate of CM-DCF formation is increased in patient fibroblasts – Next, we determined whether $V_{CM\text{-}DCF}$ was altered in fibroblasts of a patient with isolated CI deficiency. Fibroblasts were loaded with 1 µM CM-H_2DCFDA for exactly 10 min at 37° C, thoroughly washed, and subjected to confocal analysis of CM-DCF fluorescence. CM-DCF fluorescence was quantified using an intracellular ROI of maximum size. Analysis of the first image shows that, relative to control, CM-DCF fluorescence was 2.5-fold increased in patient fibroblasts (**Fig. 3A**). Essentially the same result was obtained when $V_{CM\text{-}DCF}$ was measured over de next 200 s at a capture rate of one image every 10 seconds (**Fig. 3B**).

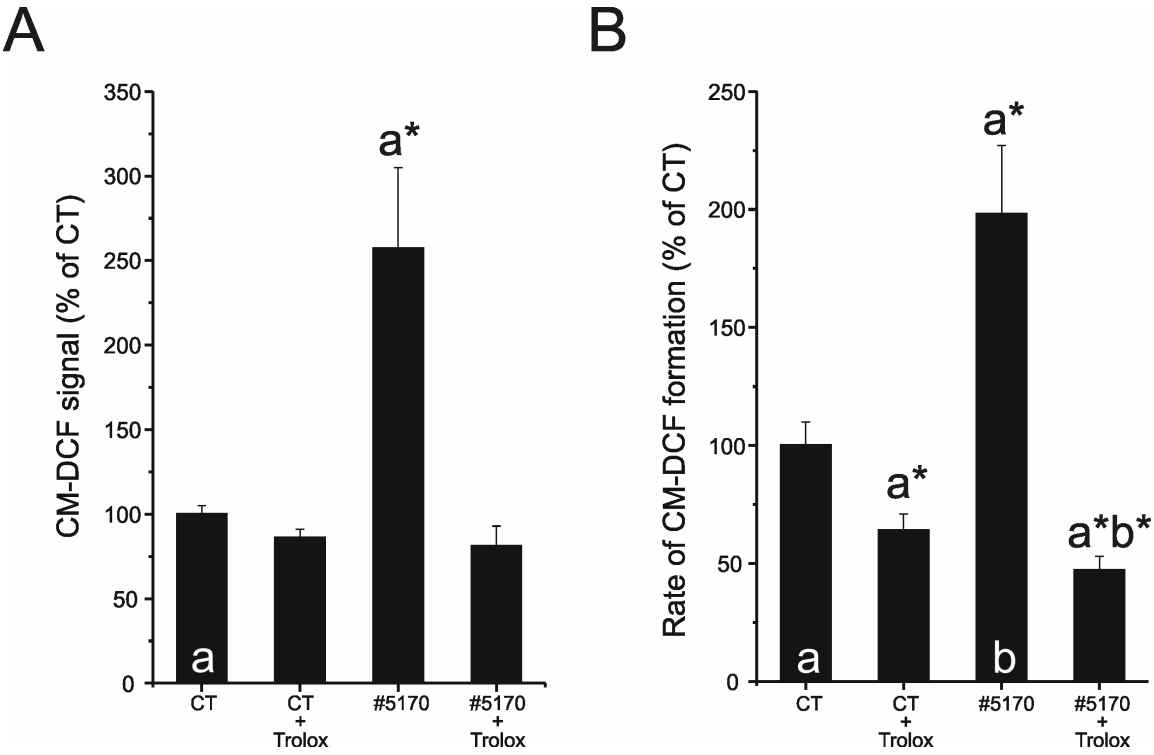

Figure 3: Trolox normalizes increased cellular oxidant levels in CI deficient patient fibroblasts – (**A**) Effect of chronic Trolox treatment (0.5 mM, 96 h) on the CM-DCF signal obtained from the first image taken (expressed as % of vehicle-treated control measured on the same day) in control fibroblasts (CT) and cells of a patient (#5170) with isolated CI deficiency. (**B**) Effect of Trolox on the rate of CM-DCF formation (expressed as % of control) in control (CT) and patient (#5170) fibroblasts, calculated from a sequence of images captured at 0.1 Hz over a period of 200 s. Average values were obtained from N=18 cells (CT), N=25 cells (CT+Trolox), N=17 cells (#5170) and N=19 cells (#5170+Trolox) measured during two independent experiments. In this figure a* and b* indicate significant differences ($p<0.05$) with column a and b, respectively.

The rate of CM-DCF formation is decreased upon chronic antioxidant treatment – The above result is compatible with an imbalance between oxidant production and detoxification in patient fibroblasts. To augment cellular antioxidant levels, cells were cultured in the

continuous presence of the antioxidant 6-hydroxy-2,5,7,8-tetramethylchroman-2-carboxylic acid or Trolox (0.5 mM, 96 h). Analysis of the first image demonstrates that Trolox completely normalized the increase in CM-DCF fluorescence in patient fibroblasts (**Fig. 3A**). Again, essentially the same result was obtained when assessing $V_{CM\text{-}DCF}$ over a measuring period of 200 s (**Fig. 3B**). In contrast to the first-image measurement, the time-sequence measurement revealed a significant decrease in $V_{CM\text{-}DCF}$ in control fibroblasts following antioxidant treatment. Importantly, all time courses were linear for 200 s ($R>0.95$ and $p<0.0001$).

Cell spreading is unaltered in isolated complex I deficiency – It has been shown that increased cellular oxidant levels induce enlargement and flattening of human diploid fibroblasts (294). Conversely, oxidant scavenging was demonstrated to inhibit spreading of NIH-3T3 fibroblasts (51). To assess whether in CI deficient patient fibroblast the increase in cellular oxidant levels was accompanied by an increased cell spreading, we developed a protocol for computer-assisted quantification of the latter parameter from CM-DCF-stained cells (**Fig. 4**). Starting from the last 'RAW' image of a time-sequence measurement (**Figs. 4A** and **4F**; image A), which has the most optimal signal-to-noise-ratio, we first produced an image with an even higher contrast by evenly redistributing the intensity histogram around the centre of the intensity scale using a bell contrast optimization (**Figs. 4B** and **4F**; image B). Next, the image was linearly contrast-stretched (**Fig. 4G**) to obtain the highest possible dynamic range (**Fig. 4C**). The latter image was then binarized by thresholding to discriminate cellular pixels from background pixels (**Fig. 4D**). Finally, remaining background noise pixels were removed by a single 3x3 median filter with a strength of 1 (**Fig. 4E**). As a consequence of the latter operation, the number of black (marked '0') and white pixels ('255') in the image increased and decreased, respectively (**Fig. 4H**). Given their very flat morphology (138), counting the total number of white pixels in the image is a good estimate of the degree of fibroblast spreading. In this study, we used a x40 objective and no additional software zoom. Therefore, the pixel size equaled 0.188 µm (138). By multiplying the pixel size by the number of pixels per cell, it was found that control and patient fibroblasts did not significantly differ in their degree of spreading (total white pixel areas of 2440±470 μm^2 and 2127±417μm^2 for control and patient fibroblasts, respectively) (**Fig. 4I**). These values are in good agreement with our previous results obtained with R123-stained fibroblasts (2266±125 μm^2; 138).

Cell size is reduced upon chronic antioxidant treatment – Chronic treatment with the vitamin E-derived antioxidant Trolox (0.5 mM, 96 h) significantly reduced the spreading of control and patient fibroblasts by 40% and 27%, respectively (**Fig. 4I**).

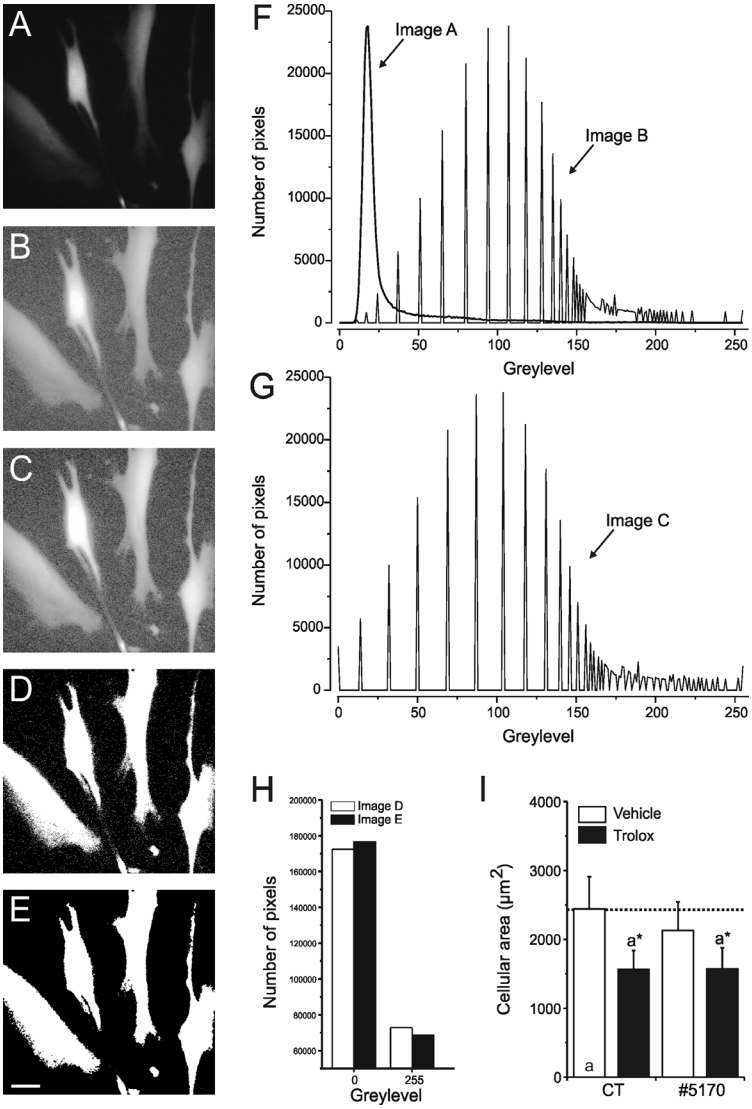

Figure 4: Cell size is not different between control and patient fibroblasts but significantly decreased by Trolox treatment – (**A**) Confocal image of control human skin fibroblasts following incubation with CM-H_2DCFDA. (**B**) Image depicted in panel A after a bell contrast stretch. (**C**) Image in panel B after a linear contrast stretch. (**D**) Image in panel C after thresholding. (**E**) Image in panel D after median filtering. (**F**) Intensity histogram for images A and B. (**G**) Intensity histogram of image C. (**H**) Intensity histogram for the black (greylevel=0) and white (greylevel=256) pixels in images D (open bars) and E (black bars). (**I**) Reduction in cell spreading induced by chronic Trolox treatment (0.5 mM, 96 h) in control (CT) and patient (#5170) fibroblasts. Averages were calculated for N=27 cells (CT), N=34 cells (CT+Trolox), N=26 cells (#5170) and N=26 cells #5170+Trolox) measured during four independent experiments. In this figure a* indicates a significant difference ($p<0.05$) with column a.

DISCUSSION

Increased cellular oxidant levels have been implicated in cell spreading (13,23,51,239,294). Here, we present a novel protocol for simultaneous quantification of oxidant levels and cell spreading using CM-DCF (5-(and-6)-chloromethyl-2',7'-dichlorofluorescein). Because dysfunction of mitochondria has been associated with increased oxidant levels (14,68,136,209,247) we compared both parameters between healthy control fibroblasts and cells from a patient with isolated CI deficiency. Following method validation, we observed that control and patient displayed similar spreading but that the latter displayed significantly increased oxidant levels. Both parameters were significantly reduced upon chronic treatment with the antioxidant Trolox.

The rate of CM-DCF formation is a function of laser intensity – We observed that $V_{CM\text{-}DCF}$ increased as a function of laser intensity. It has been suggested that photo-oxidation of CM-DCF might involve singlet oxygen ($^1O_2$), a highly oxidizing species that can be generated by irradiation with visible (λ>300 nm) laser light (138). However, previous work has shown that $^1O_2$ does not directly stimulate CM-DCF formation but induces the formation of a semiquinone radical (CM-DCF$^{\cdot-}$), which reacts with O_2 to form O_2^- (29,87). This radical is dismutated by SOD to H_2O_2 (138), which then stimulates the formation CM-DCF (see above). Our findings show that the relative contribution of the photo-oxidation process was minimal at the lowest practical laser intensity of 4%, equaling a laser output of 34 µW. To maximize the sensitivity of fluorescence detection at this low laser intensity, we used a long-pass instead of a band-pass emission filter. Furthermore, we applied optimal black level and brightness settings, whereas the signal-to-noise ratio was improved by real-time image averaging (138).

Intracellular formation of CM-DCF follows a zero order reaction mechanism – Using the lowest practical laser intensity, we observed that CM-DCF fluorescence increased linearly with time for maximally 200 s. This means that during this time the oxidative conversion of CM-H_2DCF to CM-DCF proceeded according to a zero order reaction (235), written as the equation: $[CM-DCF]_t = V_{CM-DCF} \cdot t + [CM-DCF]_0$. In this equation, $V_{CM\text{-}DCF}$ is independent of [CM-H_2DCF] and therefore solely determined by the steady-state oxidant level (178). The zero order model predicts that $V_{CM\text{-}DCF}$ increases as a function of $[CM\text{-}DCF]_0$, determined from the first image taken at 10 min after the onset of loading and following thorough

washing to remove non-hydrolysed dye. Indeed, comparison of **figures 3A** and **3B** shows that $V_{CM\text{-}DCF}$ changed proportionally with $[CM\text{-}DCF]_0$ in both control and patient fibroblasts. Similarly, both parameters increased to the same extent upon addition of H_2O_2 (**Fig. 2**). Beyond a measuring time of 200 s, however, the increase in CM-DCF fluorescence started to deviate from linearity. This may suggest that CM-DCF, once formed in sufficient quantities, stimulates the conversion of CM-H_2DCF into CM-DCF. Alternatively, cellular oxidant levels might increase upon prolonged laser illumination thereby accelerating the formation of CM-DCF. Taken together, our results demonstrate that normalization of the CM-DCF time trace (*i.e.* dividing by $[CM\text{-}DCF]_0$) is not appropriate since this would lead to underestimation of $V_{CM\text{-}DCF}$ at higher $[CM\text{-}DCF]_0$. In addition, they show that the rate of CM-DCF formation ($V_{CM\text{-}DCF}$) is constant and therefore solely determined by the level of cellular oxidants.

Oxidative formation of CM-DCF in living cells – Acute application of H_2O_2 readily increased $V_{CM\text{-}DCF}$ in human skin fibroblasts. This is in agreement with earlier findings in these cells and human epidermal keratinocytes (109,129). In a cell-free system, however, H_2O_2 but also superoxide (O_2^-), Fe(III), glutathione peroxidase and cytochrome *c* were found to be unable to convert H_2DCF into its fluorescent product (99). On the other hand, DCF formation was readily stimulated in the presence of horseradish peroxidase, Fe(II), catalase, Cu/Zn-SOD, xanthine oxidase, peroxynitrite ($ONOO^-$) and nitric oxide (NO) (99,124,190). Together, these results are compatible with the idea that intact cells contain catalysts, like transition metal ions, heme peroxidases and/or CuZnSOD that promote the H_2O_2-induced oxidation of the H_2DCF. Indeed, overexpression of CuZnSOD was demonstrated to enhance H_2O_2-induced DCF formation in human epidermal keratinocytes and murine macrophages (129). Therefore, we conclude that the formation of CM-DCF in cellular systems can best be considered as a marker of oxidant levels rather than as a direct reporter of a specific ROS/RNS species.

Oxidant levels are increased in patient cells and reduced by Trolox – $[CM\text{-}DCF]_0$, determined from the first image, appeared significantly higher in patient fibroblasts as compared to control fibroblasts, indicating a higher $V_{CM\text{-}DCF}$ (**Fig. 3A**). Indeed, $V_{CM\text{-}DCF}$, determined from the whole sequence of images, was higher in patient cells (**Fig. 3B**). These findings demonstrate that the higher value of $V_{CM\text{-}DCF}$ observed in patient cells is not due to photo-oxidation. Therefore, it can be concluded that oxidant levels are significantly increased in

complex I deficient patient fibroblasts, reflecting an imbalance between their production and detoxification (14,65,265,296). To augment their antioxidant capacity, cells were cultured in the presence of the vitamin E derivative Trolox. This treatment fully normalized $[CM\text{-}DCF]_0$ and $V_{CM\text{-}DCF}$ in patient fibroblasts and lowered these parameters in control fibroblasts. Trolox is a phenolic antioxidant with a chromane structure similar to vitamin E but without the polyisoprenoid hydrophobic tail (259). It has been described for vitamin E that its antioxidant action is exerted through the phenolic hydroxyl group, which readily donates its hydrogen to, for instance, polyunsaturated fatty acid peroxyl radicals ($PUFAOO^{\cdot}$), thereby forming a stable lipid species (212). In this reaction, vitamin E is converted into a relatively unreactive free radical, because the unpaired electron is delocalized into the aromatic ring. In vitro evidence suggests that the Trolox radical then can be regenerated by ascorbate, resulting in the formation of an ascorbyl radical (212). However, the lipophylicity (log *P*) of Trolox (3.23) is 3-fold less that that of vitamin E (9.60; (259)). Therefore, Trolox is probably less efficient in the detoxification of $PUFAOO^{\cdot}$.

Cell spreading is similar in control and patient cells and reduced by Trolox – Evidence in the literature shows that exogenous oxidants induce flattening and enlarge the size of human embryonic lung-derived diploid fibroblasts (294). Similarly, oxidants appear to be required for the integrin-mediated adhesion and spreading of NIH-3T3 fibroblasts (51). In the latter study, treatment with the antioxidant N-acetyl-cysteine (NAC) delayed cell attachment and reduced cell spreading. Although CI-deficient patient cells displayed 3-fold higher oxidant levels, we observed no difference in cell spreading between control and patient cells. In contrast, Trolox treatment lowered oxidant levels and decreased cell spreading for both control and patient fibroblasts. Evidence in the literature suggests that Trolox treatment diminishes cell proliferation (222), implying a link between Trolox, antioxidant levels, degree of cell spreading and cell cycle phase. In summary, our results suggest involvement of oxidants in the regulation of cell spreading in Trolox-treated, but not untreated, cells. This discrepancy might be caused by hitherto unknown non-oxidant (signaling) activity of Trolox, as described for vitamin E (232).

Acknowledgements: This work was supported by equipment grants of ZON (Netherlands Organization for Health Research and Development, No: 903-46-176), NWO (Netherlands Organization for Scientific Research, No: 911-02-008) and the European Union's sixth framework Programme for Research, Priority 1 'Life sciences, genomics and biotechnology for health', contract number LSHM-CT-2004-503116.

CHAPTER III

Cellular and molecular basis of nuclear-inherited isolated NADH:ubiquinone oxidoreductase deficiency: Improvement by chronic treatment with a vitamin E analogue

Sjoerd Verkaart[a,b,d,e]
Peter H.G.M. Willems[a,c,d]
Henk-Jan Visch[a,b,d,e]
Sander Grefte[a]
Richard J. Rodenburg[b,d,e]
Sjenet E. van Emst-de Vries[a,d]
Lambertus W.P.J. van den Heuvel[b,d,e]
Jan A.M. Smeitink[b,d,e]
Leo G.J. Nijtmans[b,d,e]
Werner J.H. Koopman[a,c,d]

[a]Department of Membrane Biochemistry, [b]Department of Pediatrics, [c]Microscopical Imaging Centre, [d]Nijmegen Centre for Molecular Life Sciences (NCMLS), [e]Nijmegen Centre for Mitochondrial Disorders (NCMD), Department of Pediatrics, Radboud University Nijmegen Medical Centre

Submitted

ABSTRACT

Isolated deficiency of mitochondrial complex I (NADH:ubiquinone oxidoreductase) is associated with a wide variety of clinical phenotypes such as Leigh syndrome, encephalomyopathy and cardiomyopathy for which currently no treatment strategy is available. To gain insight into the cellular and molecular basis of this deficiency we combined live cell imaging and blue native gel electrophoresis followed by Western blotting and in-gel activity measurement to assess the relationship between cellular reactive oxygen species (ROS) level and complex I amount and activity in skin fibroblast cell lines of three healthy control subjects and six children with disease causing mutations in nuclear complex I genes. Compared to control cell lines, patient fibroblasts displayed a markedly higher ROS level and a variable decrease in complex I amount and in-gel activity. When normalized to one of the controls, the ratio between amount and activity was 1 for the two other controls and to a variable extent below 1 for the patients, indicating a defect in both expression and intrinsic catalytic activity of the complex. In all cell lines, control as well as patient, the ROS level was dramatically reduced following chronic treatment with the water-soluble vitamin E analogue Trolox, revealing its activity as an antioxidant. In each case, this effect of Trolox was accompanied by a substantial increase in the amount of complex I. But, whereas the ratio between the increase in amount and the increase in activity did not differ from 1 for the controls, it varied from 0.1 to 0.8 for the patients. Our data provide experimental evidence that chronic antioxidant treatment may be beneficial to those complex I deficient patients that display a relatively mild decrease in intrinsic activity of the complex.

INTRODUCTION

The mitochondrial oxidative phosphorylation (OXPHOS) system consists of five multi-protein complexes (I-V) and is essential for the production of the vast majority of cellular ATP and various other mitochondrial activities including organelle fusion, Ca^{2+} uptake and metabolite exchange (24,168,246). Deficiency of the OXPHOS system is associated with a wide range of neuromuscular, cardiac, and endocrine disorders and, more recently, has also been implicated in age-related diseases and various forms of cancer (242,291,302). Although OXPHOS deficiency can occur at any given age, the onset is usually within the first 2 years of life. In 40% of the early-onset cases, the decrease in OXPHOS activity is associated with an isolated (25%) or combined (15%) deficiency of complex I (246). Human complex I (NADH:ubiquinone oxidoreductase; EC 1.6.5.3) consists of 7 mitochondrial DNA-encoded (mtDNA) and 38 nuclear DNA-encoded (nDNA) subunits (45). In the majority of early-onset patients, complex I deficiency (OMIM 252010) is caused by mutations in nuclear-encoded subunits (22,40,120,130). Additionally, disease causing mutations have been found in the nuclear-encoded complex I assembly factor B17.2L (185). Recent work has shown that disease causing mutations may reduce the assembly/stability of the complex I holocomplex, resulting in reduced rates of NADH oxidation (116,271). However, other evidence suggests that such mutations may also primarily decrease the intrinsic catalytic activity of the holocomplex (127).

At present, the pathophysiological mechanisms linking defects in complex I genes to cellular dysfunction and disease are poorly understood. Mutations in nDNA-encoded complex I subunits can alter mitochondrial shape and induce aberrations in mitochondrial and cellular Ca^{2+} and ATP handling (139,281,283). Furthermore, it is widely accepted that normal OXPHOS function is accompanied by the generation of superoxide and derived reactive oxygen species (ROS) and evidence has been provided that the production of these oxidants is increased in isolated complex I deficiency (116,137,160,204,266,277).

Other evidence suggests that these oxidants, if not adequately neutralized by the cell's antioxidant mechanisms, can act as important mediators of oxidative injury. Thus, specific proteins of adult bovine submitochondrial particle complexes were found to exhibit a basal level of oxidative damage (52).

It was proposed that steady leakage of electrons from the electron transport chain and ensuing formation of superoxide causes increasing damage to specific OXPHOS complexes ultimately leading to dysfunction of the OXPHOS system. More recently, in-vitro assays with

the flavoprotein fraction of bovine complex I revealed that NADH-induced superoxide production can cause specific oxidative modifications of the 51-kDa (NDUFV1) subunit, resulting in a decrease in electron transfer activity (47). In another study, using isolated perfused rat hearts following ischemia reperfusion, increases in complex I-mediated ROS production were found to be accompanied by thiol modifications of matrix-facing complex I subunits (266). Finally, recent work revealed that increases in mitochondrial ROS production can lead to accelerated degradation of newly synthesized mitochondrial proteins (17). It was suggested that consequent down-regulation of the most sensitive OXPHOS complexes may further increase mitochondrial superoxide production, which is compatible with the progressive nature of complex I deficiency.

In accordance with the above findings, antioxidants were found to improve OXPHOS function in superoxide dismutase 2 null mice (102). Furthermore, chronic antioxidant treatment was shown to increase CV activity and ATP synthesis in cybrids containing the mtDNA of patients with the T8993G mtDNA mutation associated with impaired oxidative phosphorylation in NARP (neuropathy, ataxia and retinitis pigmentosa) and MILS (maternally inherited Leigh's syndrome) (166). Likewise, chronic oral administration of high concentrations of vitamin E was found to prevent the loss of mitochondrial function and reduce protein and lipid oxidation in brain and liver of aging mice (180). These beneficial effects were paralleled by an increased lifespan, better neurological performance and higher exploratory activity. Regarding human complex I deficiency, patients have been found to respond differentially to antioxidant treatment (e.g. ref. 193).

Together, these findings indicate that superoxide and derived ROS may play an important role in the pathogenesis of disorders associated with defects of the OXPHOS system. Here, we combined live cell imaging microscopy and blue native gel electrophoresis followed by Western blotting and in-gel activity measurement to assess the relationship between cellular ROS levels and complex I expression and activity in nuclear-inherited isolated complex I deficiency. The data presented provide evidence that the amount and cellular activity of complex I are under regulatory control of the cell's oxidative balance. Furthermore, they show that cellular ROS levels are significantly increased in nuclear-inherited isolated complex I deficiency and that this increase is associated with a decrease in complex I amount. Most importantly, they demonstrate that apart from the amount also the intrinsic activity of complex I may be significantly decreased in these patients. Finally, our finding that chronic antioxidant treatment increases the amount of complex I provides an experimental basis for using antioxidants to treat complex I deficient patients. Here it should be noted,

however, that such treatment may only be beneficial to patients that have a predominant complex I expression rather than an intrinsic catalytic defect.

MATERIALS AND METHODS

Patient skin fibroblasts – Fibroblasts were obtained from skin biopsies of three healthy subjects and six complex I deficient children in the age range of 0-5 years following informed parental consent and according to the relevant Institutional Review Boards (245). The deficiency was confirmed in both muscle tissue and cultured skin fibroblasts. Patients were screened for the presence of DNA alterations in each of the known nuclear-encoded complex I genes and found to carry mutations in either the *NDUFS1* (#6173), *NDUFS2* (#5170), *NDUFS7* (#5175), *NDUFS8* (#6603) or *NDUFV1* (#5866, #5171) gene (**Table 1**). All patients were shown to be negative with respect to mitochondrial DNA alterations associated with complex I deficiency. Fibroblasts were cultured in medium 199 with Earle's salt supplemented with 10% (v/v) fetal calf serum, 100 IU/ml penicillin and 100 IU/ml streptomycin in a humidified atmosphere of 95% air and 5% CO2 at 37^{o} C. Cell cycle analysis revealed no differences between the various cell lines (139).

Table 1. Control and patient fibroblasts

CELL LINE[$]	MUTATED SUBUNIT	MUTATION[@]	CLINICAL PHENOTYPE[%]	REFERENCE
CT1 (#5120)	None	None	n.a.	**[283]**
CT2 (#5119)	None	None	n.a.	**[139]**
CT3 (#5118)	None	None	n.a.	**[139]**
P1 (#6603)	*NDUFS8*	R94C	L/LL	**[139]**
P2 (#6173)	*NDUFS1*	R557X/D618N	L/LD	**[283]**
P3 (#5170)	*NDUFS2*	R228Q	HCEM	**[155]**
P4 (#5866)	*NDUFV1*	R59X/T423M	MLM/LL	**[234]**
P5 (#5175)	*NDUFS7*	V122M	L/LL	**[268]**
P6 (#5171)	*NDUFV1*	R59X/T423M	MLM/LL	**[234]**

[$]CT and P indicate control and patient cell lines, respectively. Numbers indicate the designation of the cell lines within the Nijmegen Centre for Mitochondrial Disorders (NCMD). [@]Mutations are given at the protein level. [%]Clinical phenotype: L/LD, Leigh syndrome and leukodystrophy; L/LL, Leigh syndrome and Leigh-like syndrome; MLM, macrocephaly, leukodystrophy and myoclonic epilepsy; HCEM, hypertrophic cardiomyopathy and encephalomyopathy. **Abbreviations**: n.a., not appropriate.

Quantification of cellular reactive oxygen species level – Cellular reactive oxygen species levels were quantified as described previously (137). Briefly, fibroblasts were incubated in HEPES-Tris medium (132 mM NaCl, 4.2 mM KCl, 1 mM $CaCl_2$, 1 mM $MgCl_2$, 5.5 mM D-glucose and 10 mM HEPES, pH 7.4) containing 1 µM 5-(and-6)-chloromethyl-2',7'-dichlorodihydrofluorescein diacetate (CM-H_2DCFDA; Molecular Probes) for 10 min at 37^{o} C. During this period, the acetate groups are cleaved by intracellular esterases yielding

dichlorodihydrofluorescein (CM-H_2DCF), which is then oxidized by oxidants to form highly fluorescent dichlorofluorescein (CM-DCF). After loading, the cells were thoroughly washed and transferred to the stage of an Oz confocal microscope (Noran Instruments, Middleton, WI, USA). Routinely, CM-DCF fluorescence was monitored during 200 s at a 10 s-interval. After background correction, the rate of CM-DCF fluorescence increase during the first 150 s was determined as a measure of the cellular ROS level. On each measuring day, the average rate obtained with #5120 control fibroblasts was set at 100%, to which all values were related. All recordings were carried out at minimal laser intensity using identical hardware settings.

Blue native PAGE, Western blot analysis and in-gel activity measurement – Cultured skin fibroblasts were harvested by trypsinization, washed with ice-cold phosphate-buffered saline (PBS; Braun, Melsungen, Germany) and resuspended (approx. $2 \cdot 10^6$ cells) in 100 µl ice-cold PBS. For preparation of a mitochondria-enriched fraction, cells were incubated with 2 mg/ml digitonin (Biosciences Inc., La Jolla, CA, USA) in a final volume of 200 µl for 10 min on ice. Next, 1 ml ice-cold PBS was added followed by centrifugation (5 min; 10,000g; 4° C). Mitochondrial pellets were washed twice with 1 ml ice-cold PBS and stored overnight (-20° C). Pellets were solubilized in 100 µl ACBT buffer (Fluka, Steinheim, Germany) containing 1.5 M aminocaproic acid and 75 mM Bis-Tris/HCl (pH 7.0). To extract mitochondrial protein complexes, 20 µl 10% (w/v) β-lauryl maltoside was added and the solution was incubated for 10 min on ice. After centrifugation (30 min; 10,000g; 4° C), 10 µl of BN sample buffer (Biorad Laboratories, Hercules, CA, USA) was added to the supernatant. Blue native PAGE, Western blotting using a monoclonal antibody against the NDUFA9 (39-kDa) subunit of complex I (Molecular Probes) at a dilution of 1:1000, and in-gel activity measurement were performed as described previously (182). For quantitative analysis, gels were loaded with exactly 10 µg of mitochondrial protein.

Data analysis – After Western blotting, luminescent signals were quantitatively analyzed by exposing illumination films to the blots for different periods of time (5-180 s). Films that displayed sub-maximal, non-saturated, signals were scanned using a G690 Imaging Densitometer (Biorad). From these scans, the integrated optical density of each band was determined and background corrected.

The resulting numerical values were normalized to those obtained with control cells on the same blot. For quantitative analysis of in-gel activity, gels were scanned directly. Numerical results were visualized using Origin Pro 7.5 (OriginLab Corp., Northampton, MA, USA) and presented as the mean ± SEM. Statistical differences were determined using either a two-population or one-population Student's t-test (Bonferroni corrected).

Chemicals – Culture materials were obtained from Invitrogen (Breda, The Netherlands), all other reagents were from Sigma-Aldrich (St. Louis, MO, USA).

RESULTS

Cellular ROS levels are decreased by the water-soluble vitamin E derivative Trolox – To quantify cellular ROS levels, healthy control fibroblasts (#5120) were loaded with non-fluorescent CM-H_2DCFDA (5-(and-6)-chloromethyl-2',7'-dichlorodihydrofluorescein diacetate; 1 µM) for 10 min, thoroughly washed to remove excess CM-H_2DCFDA, and monitored for the conversion of intracellularly trapped CM-H_2DCF into fluorescent CM-DCF. Video-imaging microscopy revealed that CM-DCF fluorescence was uniformly distributed throughout the cell (**Fig. 1A**) and increased linearly with time (**Fig. 1B**; open symbols). Importantly, this linearity indicates that that the amount of CM-H_2DCF is not rate-limiting (137). Acute application of Trolox (6-Hydroxy-2,5,7,8-tetramethylchroman-2-carboxylic acid) instantaneously decreased the rate of CM-DCF formation by ~50% (**Fig. 1B**; filled symbols and inset).

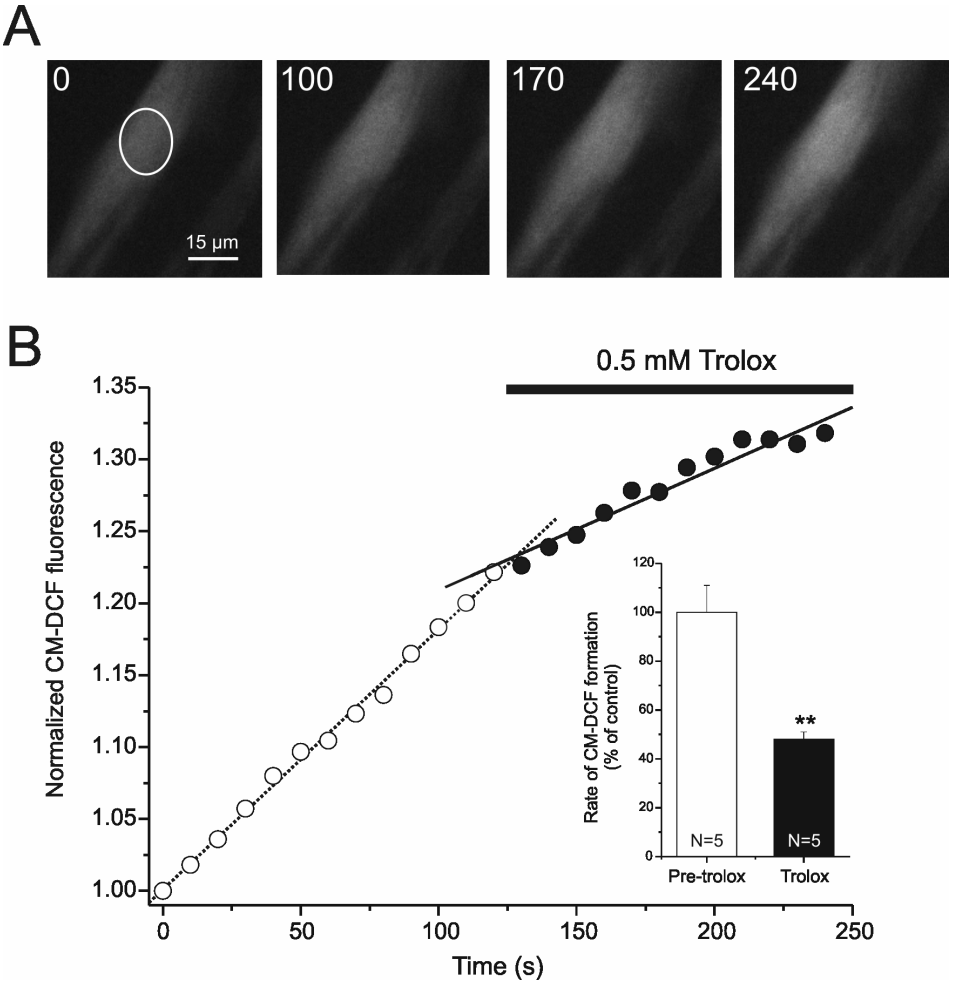

Fig. 1: Effect of acute and chronic Trolox treatment on cellular ROS levels. (**A**) Fluorescent images of control fibroblasts (#5120) at the indicated time points after removal of non-hydrolyzed CM-H_2DCFDA, showing the intracellular conversion of non-fluorescent CM-H_2DCF into fluorescent CM-DCF. Fluorescence at time zero originates from CM-DCF produced during the loading period. The white circle represents the region of interest used for quantitative analysis. (**B**) Effect of acute application of Trolox on the rate of CM-H_2DCF oxidation in control fibroblasts. Trolox (0.5 mM) was added at the indicated time point (black bar). Lines indicate a linear fit to the time course before (open symbols; slope=0.00181±3.4·10^{-5}, R=0.99, p<0.0001) and after (filled symbols; slope=8.5·10^{-4}±5.2·10^{-5}, R=0.98, p<0.0001) addition of Trolox. The inset shows that Trolox decreased the rate of CM-DCF formation by 50% (N=5 cells). (**C**) Rate of CM-DCF formation in control cells cultured in the absence (open bar; N=19 cells) and presence (black bar; N=16 cells) of 0.5 mM Trolox for 96 h. (**D**) Rate of CM-DCF formation following acute application of 1 mM hydrogen peroxide (H_2O_2) to the untreated (open bar; N=19 cells) and Trolox-treated (black bar; N=16 cells) cells.

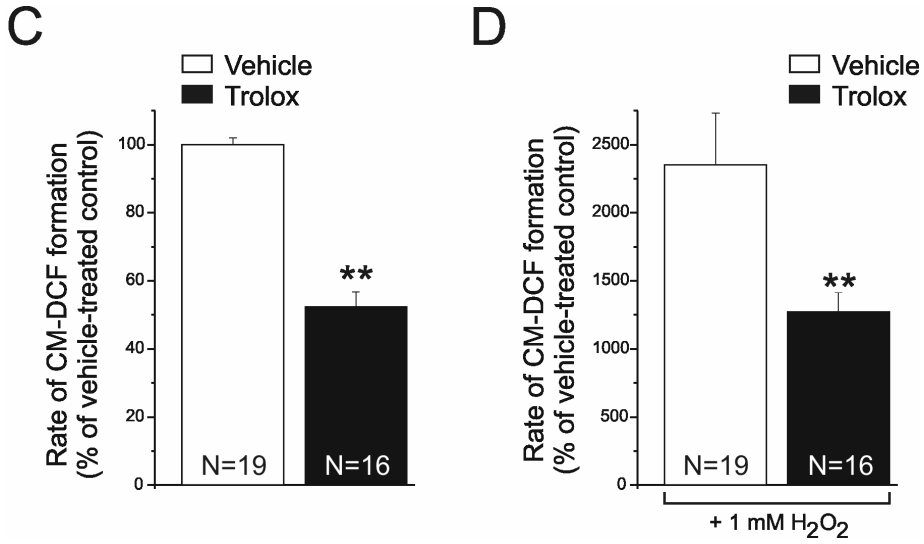

We showed before that acute application of exogenous hydrogen peroxide (H_2O_2) readily increased the rate of CM-DCF formation in human skin fibroblasts (137). To assess the effect of Trolox on the H_2O_2-induced increase in the rate of CM-DCF formation, healthy control cells were cultured in the presence of Trolox (0.5 mM) for 96 h, loaded with CM-H2DCF, and subsequently treated with 1 mM H_2O_2. In the absence of H_2O_2, the rate of CM-DCF formation was significantly lower in Trolox-treated cells (Fig. 1C). Subsequent addition of H_2O_2 increased the rate of CM-DCF formation 23- and 12-fold in vehicle- and Trolox-treated cells, respectively (**Fig. 1D**). These findings demonstrate the effectiveness of Trolox as an antioxidant in human skin fibroblasts.

Trolox normalizes increased cellular ROS levels in complex I deficient patient fibroblasts – The rate of CM-DCF fluorescence increase did not significantly differ between the three control cell lines (100±2%, 100±11% and 125±13% for #5120 (412 cells), #5119, (48 cells), and #5118, (61 cells), respectively). In all patient cell lines analyzed, the rate of CM-DCF

formation was significantly higher than in each of the controls (Fig. 2; open bars). Chronic treatment with Trolox (0.5 mM) for 96 h significantly decreased the rate of CM-DCF formation in both healthy control cells and complex I deficient cells (filled bars).

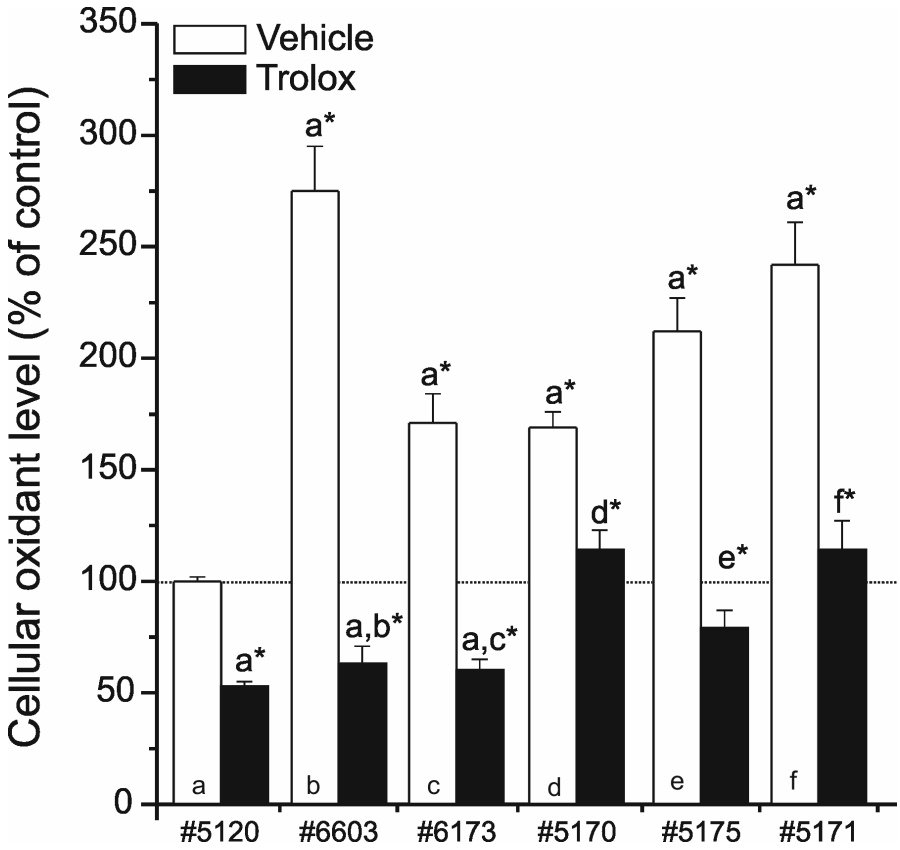

Fig. 2: Effect of Trolox on cellular ROS levels in human fibroblasts. Patient fibroblasts displayed cellular ROS levels that were significantly increased as compared to control (open bars) and efficiently reduced by chronic Trolox treatment (0.5 mM, 96 h; closed bars). Note that chronic Trolox also decreased the cellular ROS level in control cell line #5120. The data presented are from individual cells measured on 2-6 days. On each measuring day, the mean value obtained with vehicle-treated #5120 control cells was set at 100%, to which all values obtained that day including those obtained with the #5120 control cells themselves were related. Depicted are the mean ± SEM of 236 (#5120; bar a), 117 (#6603; bar b), 87 (#6173; bar c), 124 (#5170; bar d), 76 (#5175; bar e) and 78 (#5171; bar f) vehicle-treated cells and 159 (#5120), 31 (#6603), 56 (#6173), 62 (#5170), 47 (#5175) and 32 (#5171) Trolox-treated cells. *Significantly different from the indicated vehicle-treated condition ($p<0.05$).

Amount and activity of complex I are variably decreased in complex I deficient patient fibroblasts – To assess the cellular and molecular basis of the decrease in complex I activity in complex I deficient fibroblasts, we performed blue native PAGE followed by Western-blot

analysis (WB) and in-gel activity measurement (IGA) (271,272). First, the linearity of the IGA assay was determined in a dilution experiment using a mitochondrial fraction of control #5120 (**Fig. 3A**). For normalization, the integrated optical densities of the bands obtained with 10 µg of sample protein were set at 100%.

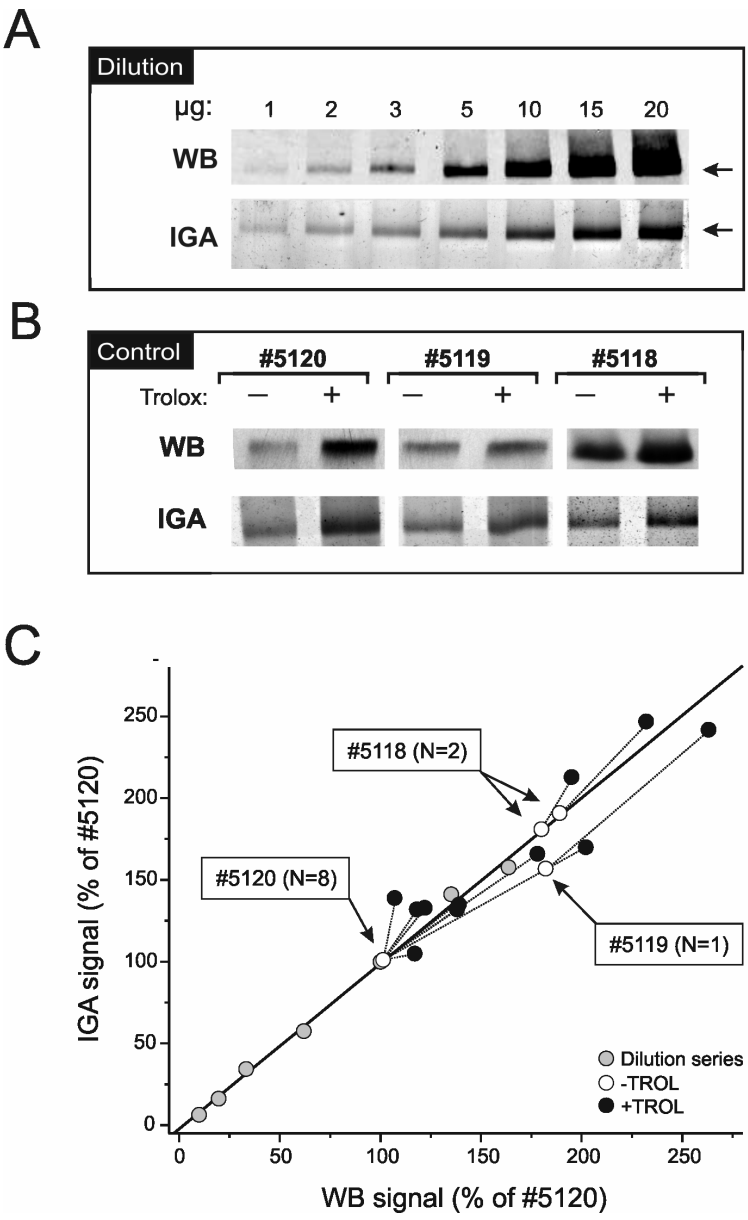

Fig. 3: Effect of Trolox on complex I amount and activity in control fibroblasts. Mitochondrial protein complexes were separated by blue native PAGE followed by Western blot detection (WB) of complex I assemblies and measurement of their in-gel activity (IGA). Complex I assemblies were visualized using a monoclonal antibody against the 39-kDa (NDUFA9) subunit. (**A**) To determine the relationship between the signal on the Western blot (WB) and the signal on the activity gel (IGA), a dilution series was prepared from a mitochondria-enriched fraction of control cell line #5120. The amount of protein is indicated above each lane. (**B**) Chronic Trolox treatment (0.5 mM, 96 h) increased the expression and activity of fully assembled complex I in control fibroblasts. For quantitative comparison, gels were loaded with exactly 10 µg of sample protein. The blots and gels shown in this panel are representative of 8 (#5120), 1 (#5119) and 2 (#5118) independent experiments. Of note, each blot and each gel depicted in this figure is contrast optimized for better visualization of the effect of Trolox, which precludes direct comparison by eye. (**C**) Relationship between the integrated optical densities of the WB signals and corresponding IGA signals for the dilution series in panel A (grey symbols) and vehicle- (open symbols) and Trolox-treated (black symbols) control cell lines in panel B. For each blot and each gel, the integrated optical density obtained with 10 µg of sample protein of control cell line #5120 was set at 100%, to which all other values were related. The continuous line indicates a linear fit to the dilution data (R=0.998, slope=1.01±0.03, intercept=-2.32±2.81%, $p<0.0001$). The fitted line was statistically identical to the line y=x. Corresponding data points are connected by a dotted line.

Plotting of the normalized IGA values as a function of the normalized WB values revealed a linear relationship with a slope of 1.01±0.03 (R=0.998, p<0.0001) (**Fig. 3C**, grey symbols). In the remainder of this study, blue native PAGE gels were routinely loaded with exactly 10 µg of sample protein and the integrated optical densities obtained with mitochondria-enriched fractions of control and patient cell lines were expressed relative to that of control #5120 present on the same gel. Importantly, exposure times of the blots were chosen such that saturation of the illumination films was prevented. **Figure 3B** (left lanes indicated with a minus sign) shows that all three control cell lines expressed only the fully assembled, catalytically active complex. Of note, the blots and gels depicted in this figure are contrast optimized for better visualization of the effect of Trolox and can therefore not be directly compared by eye. Densitometric analysis revealed a y=x relationship (slope of 0.92±0.06, R=0.98, p<0.0001) between IGA values and corresponding WB values, indicating that the activity per complex is the same for the control cell lines (**Fig. 3C**, open symbols).

Analysis of the patient cell lines showed the presence of a catalytically active complex, the size of which did not differ from control (**Fig. 4A**, left lanes indicated with a minus sign). In three patient cell lines (#6173, #5171, #5866), also a second complex of lower molecular weight was observed. In contrast to the active complex, this subcomplex appeared inactive in the IGA assay. **Figure 4B** (open symbols) shows that in all patient cell lines the amount of active complex was significantly lower than control (#5120). Furthermore, this figure shows that in all patient cell lines the activity of this complex was less than expected on the basis of its amount (i.e. all data points were below the line obtained with the control cell lines).

Trolox increases the amount and activity of complex I in control and patient fibroblasts – Chronic treatment with Trolox markedly increased complex I amount and activity in control fibroblasts (**Fig. 3B**, right lanes indicated with a plus sign). The regression line for the Trolox-treated control cells (**Fig. 3C**, black symbols) had a slope of 0.86±0.11 (R=0.93, p<0.0001), which was not significantly different from the line of identity, indicating that the intrinsic activity of the wild-type complexes was not altered. Similarly to control fibroblasts, all patient fibroblasts displayed an increase in active complex and, for three cell lines (#6173, #5171, and #5866), also in partially assembled subcomplex (**Fig. 4A**, right lanes indicated with a plus sign).

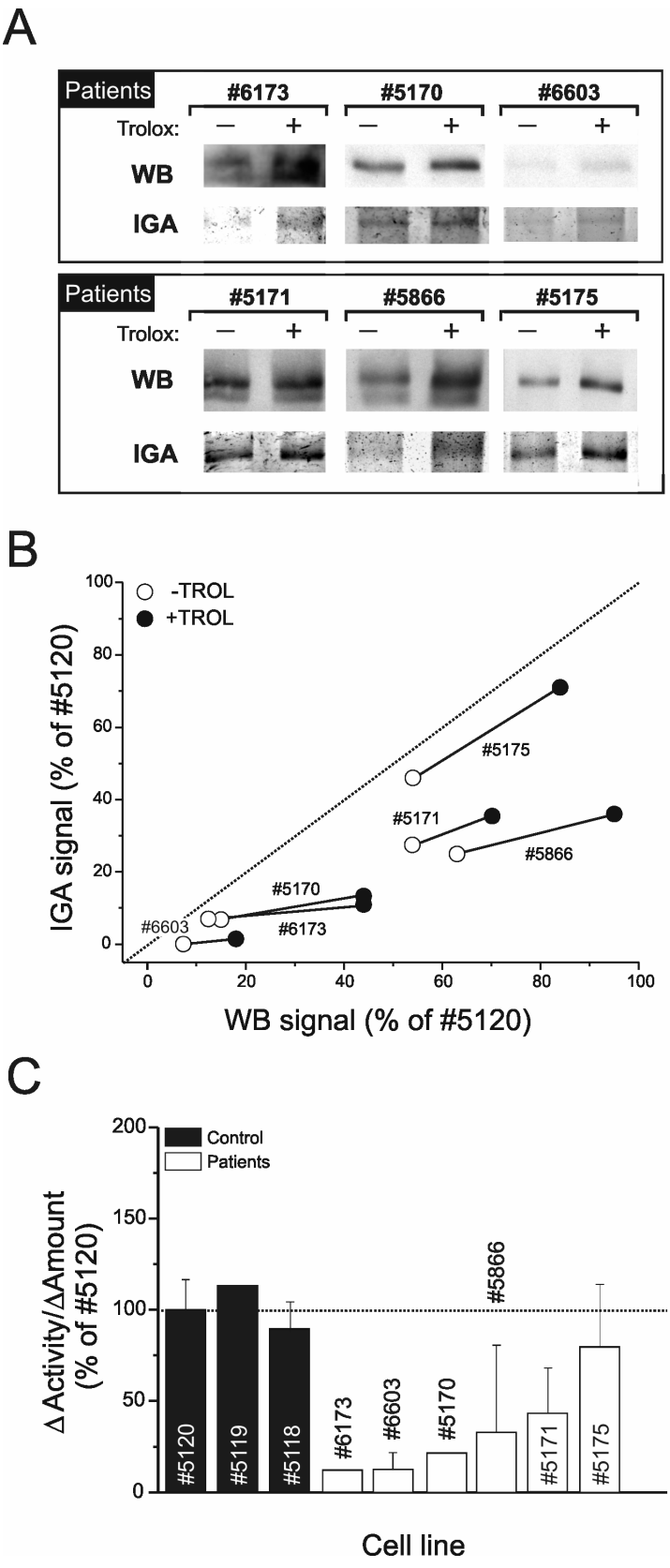

Fig. 4: Effect of Trolox on complex I amount and activity in patient fibroblasts. (**A**) Chronic Trolox treatment (0.5 mM, 96 h) increased the amount (WB) and activity (IGA) of complex I in patient fibroblasts. Experimental details are as described in the caption of **figure 3**. The blots and gels shown in this panel are representative of 1 (#6173), 1 (#5170), 2 (#6603), 2 (#5171), 3 (#5866) and 4 (#5175) independent experiments, are contrast optimized for presentation purposes and can therefore not be directly compared by eye. (**B**) Relationship between the between the integrated optical densities of the WB signals and corresponding IGA signals, expressed as percentage of control #5120, for vehicle- (open symbols) and Trolox-treated (closed symbols) patient cell lines. All patient values are below the line of identity (dotted line) observed for the control cell lines (see, **Fig. 3C**). (**C**) Ratio between the Trolox-induced increase in complex I activity and the corresponding increase in complex I amount (Δactivity/Δamount) as a measure of the intrinsic catalytic activity of the complex in control cell lines (closed bars) and patient cell lines (open bars). The average ratio over all experiments obtained with control cell line #5120 was set at 100% (dotted line), to which all values including those of control cell line #5120 itself were related. The data presented are from 8 (#5120), 1 (#5119), 2 (#5118), 1 (#6173), 2 (#6603), 1 (#5170), 3 (#5866), 2 (#5171), and 4 (#5175) independent experiments. Error bars represent standard deviation (n>2 experiments) or difference between duplicate values (n=2).

Control experiments with isolated heart mitochondria demonstrated that acute exposure to Trolox (0.5 mM, 15 min) did not alter the amount and/or in-gel activity of the active complex (not shown). The importance of this finding is that it makes it highly unlikely that Trolox exerts its effect by stabilizing the complex during β-lauryl maltoside extraction and subsequent native electrophoretic separation and/or increasing its in-gel activity. Calculation of the ratio between the Trolox-induced increase in complex I activity (Δactivity) and the corresponding increase in complex I amount (Δamount) as a measure of the intrinsic catalytic activity of the complex, revealed that compared to control #5120, for which the average ratio was set at 100%, all patients displayed a catalytic defect, which was smallest in patient cell line #5175 and largest in patient cell line #6173 (**Fig. 4C**). Comparison of **figures 4B** and **4C** furthermore shows that patient cell lines with the largest intrinsic catalytic defect (#6173, #6603, #5170) display the lowest amount of active complex, whereas patient cell lines with a higher intrinsic catalytic activity show also a higher expression of this complex.

DISCUSSION

Pathogenic mutations in nuclear-encoded subunits of the first and largest complex of the OXPHOS system lead to a reduction in total cellular activity of this enzyme and are associated with a broad spectrum of clinical manifestations that occur directly after birth or during early childhood (242,246,291,302). Here we analyzed cultured skin fibroblasts of six children with disease causing mutations in nuclear complex I genes and show that they expressed a catalytically active complex, the size of which did not differ from control, but the amount and intrinsic catalytic activity of which were decreased to a variable degree. Extrapolation of the results obtained in this study to the whole population of isolated complex I deficient patients means that some patients may have primarily a relatively mild expression problem (#5175 of this study), other patients may have a relatively mild expression problem combined with a relatively mild intrinsic catalytic problem (#5171 and #5866 of this study), and again other patients may have a severe expression problem and a severe intrinsic catalytic problem (#6173, #6603 and #5170 of this study). By far the most important consequence of our findings is that therapeutic strategies aimed at improving the expression of complex I in nuclear-inherited complex I deficiency are only meaningful if the fully assembled complex has a substantial residual activity. Thus, the data obtained with Trolox may provide an experimental basis for antioxidant treatment of complex I deficient patients in which primarily the expression of complex I is reduced rather than the activity per complex. In this context, our results may explain the observation that complex I deficient patients respond differentially to antioxidant treatment (193).

The present study demonstrates that blue native gel electrophoresis in combination with Western blotting and in-gel activity measurement is a powerful tool to establish the relative contribution of an expression defect and an intrinsic catalytic defect to the decrease in total cellular complex I activity in isolated human complex I deficiency. All three control cell lines harbored the fully assembled, catalytically active complex and a line of identity was observed between the amount and activity when expressed relative to the values obtained with control cell line #5120, indicating that the intrinsic catalytic activity was the same for the three control cell lines. Chronic Trolox treatment significantly increased both parameters and also in this case the obtained data points lie on the line of identity. The latter result indicates that Trolox does not alter the intrinsic catalytic activity of the complex and, thus, primarily acts by increasing its expression. All six patient cell lines expressed significantly less active complex than the control. Importantly, control experiments revealed that this reduction in amount of

active complex was not due to experimental procedures because Western blot analysis of mitochondrial enriched fractions confirmed that all six patient cell lines contained significantly less 39 kDa subunit than control (in press). In agreement with our results, the NDUFS1-Q522K mutation has only recently been published to be associated with a marked reduction in complex I amount and activity and a significant increase in mitochondrial superoxide and derived ROS levels (116). Most importantly, these patient cells showed an enhanced mitochondrial susceptibility to ROS damage. Here, we made use of the ability of Trolox to increase the amount of active complex I to identify patient cell lines with an intrinsic catalytic defect and to determine the severity of this defect. In all but one case (#5175), chronic Trolox treatment increased the in-gel activity (expressed relative to the value obtained with control cell line #5120) with a smaller factor than the amount of active complex (expressed relative to the value obtained with control cell line #5120), clearly demonstrating the presence of a catalytic defect. Three of the patient cell lines displayed an additional, catalytically inactive complex, the size of which was markedly smaller than that of the active complex. Chronic Trolox treatment also increased the amount of this subcomplex. At present, it is not clear whether this subcomplex constitutes an assembly intermediate or a breakdown product.

Thus far, only few studies have addressed the effect of pathogenic mutations on the intrinsic catalytic activity of complex I. Two of the mutations studied here, NDUFS2-R228Q (#5170) and NDUFS7-V122M (#5175), have been analyzed in great detail in the yeast Yarrowia lipolytica (3,127). In contrast to the present findings, these mutations did not reduce the complex I content in the yeast. Moreover, the NDUFS2-R228Q mutation did not alter the intrinsic catalytic activity of the complex, whereas in the case of the NDUFS7-V122M mutation the intrinsic catalytic activity was virtually halved. In another study, however, using the fungus Neurospora crassa, the latter mutation had no major effect on the catalytic activity of complex I (67). The same observation was reached with the NDUFV1-T423M mutation and the authors concluded that diminished formation and or stability of the complex are the major factors in cellular complex I deficiency. Both groups used essentially the same analysis methods, suggesting that the observed discrepancies are due to the use of different model systems. In the present study we used the original patient cell lines and yet again obtained other results with these mutations. Taken together, these findings stress the importance of the model system that is chosen for the analysis of pathogenic mutations.

All five mutated subunits investigated here constitute part of the minimal form or “core” of the complex, which furthermore contains the nuclear-encoded NDUFV2 and NDUFS3 subunits

and the seven mitochondrial-encoded subunits (35). NADH is oxidized at the NDUFV1 subunit and the high-energy electrons freed during this reaction are delivered via flavine mononucleotide, which is non-covalently bound to this subunit, onto a chain of iron-sulfur clusters, of which the last one, which is contained in the NDUFS7 subunit, donates the electrons to ubiquinone. Because all five subunits investigated in this study contain one or more iron-sulfur clusters, it remains to be established whether the variable decreases in intrinsic catalytic activity are due to a more or lesser efficient transport of electrons through the mutated forms of these subunits.

Another intriguing question deals with the origin of the ROS. Are they derived from superoxide generated by abnormal functioning complexes or are they produced by other enzyme systems as a consequence of increased NADH and/or ambient oxygen levels (2). A further question that needs to be resolved is whether the decrease in complex I amount results from the use of imperfectly fitting building blocks, which might slow down the assembly process or accelerate the breakdown process, or whether it is a consequence of, for instance, ROS damage. The data obtained with Trolox suggest that at least part of the decrease in complex I amount can be explained by an increase in cellular ROS.

Evidence that complex I expression may be controlled by the cell's oxidative balance – Trolox is a phenolic antioxidant with a chromane structure similar to vitamin E but without the hydrophobic polyisoprenoid tail of the latter (259). Vitamin E exerts its antioxidant action through the phenolic hydroxyl group, which readily donates its hydrogen to, for instance, polyunsaturated fatty acid peroxyl radicals, thereby forming a stable lipid species (212). In this reaction, vitamin E is converted into a relatively unreactive free radical. In vitro evidence suggests that this vitamin E radical can be regenerated by ascorbate, resulting in the formation of an ascorbyl radical (212). Chronic Trolox treatment significantly increased the amount of fully assembled, catalytically active complex I in healthy control fibroblasts, which may suggest that total cellular complex I activity is controlled by the cell's oxidative balance primarily through regulation of its amount. Using bovine heart submitochondrial particles, it was shown that the decrease in complex I activity induced by peroxidation of cardiolipin was reversed upon addition of exogenous cardiolipin, indicating an effect of peroxidized cardiolipin on the activity per complex rather than on its amount (195). It has been demonstrated that depletion of cardiolipin also causes an increase in ROS production (49), possibly leading to oxidative damage of complex I (17,47,52). Similarly, enhanced ROS generation was found to be associated with thiol modifications in several matrix-facing

subunits of complex I and a reduction in complex I-linked respiration (266). It remains to be established whether Trolox acts by directly reversing ROS damage in patient fibroblasts. Recent work has shown that overexpression of Mitofusin-2 (Mfn2) increased not only the complexity of the mitochondrial network but also the expression of complex I subunits, suggesting a link between mitochondrial morphology and complex I expression (203). An interesting option might therefore be that Trolox acts through a change in mitochondrial network morphology to alter complex I expression.

Acknowledgements: This work was supported by equipment grants of ZON (Netherlands Organization for Health Research and Development, No: 903-46-176), NWO (Netherlands Organization for Scientific Research, No: 911-02-008) and the European Union's 6th Framework Programme for Research, Priority 1 "Life sciences, genomics and biotechnology for health" (No: LSHM-CT-2004-503116).

CHAPTER IV

Patients with a mutation in the NDUFS4 subunit of NADH:ubiquinone oxidoreductase display an active but unstable form of the enzyme

Sjoerd Verkaart[a,b,d,e]
Werner J.H. Koopman[a,c,d]
Sjenet E. van Emst-de Vries[a,d]
Richard J. Rodenburg[b,d,e]
Lambertus W.P.J. van den Heuvel[b,d,e]
Leo G.J. Nijtmans[b,d,e]
Jan A.M. Smeitink[b,d,e]
Peter H.G.M. Willems[a,c,d]

[a]Department of Membrane Biochemistry, [b]Department of Pediatrics, [c]Microscopical Imaging Centre, [d]Nijmegen Centre for Molecular Life Sciences (NCMLS), [e]Nijmegen Centre for Mitochondrial Disorders (NCMD), Department of Pediatrics, Radboud University Nijmegen Medical Centre

In preparation

ABSTRACT

Genetic defects in mitochondrial oxidative phosphorylation (OXPHOS) are most frequently observed in a small subgroup of the 38 nuclear-encoded subunits that comprise the first and largest complex (CI; NADH:ubiquinone oxidoreductase) of the electron transport chain. Malfunction of this enzyme is associated with a wide array of clinical symptoms and is established by measurement of the rotenone-sensitive oxidation of NADH in the presence of coenzyme Q1 in both a crude homogenate from skeletal muscle and a mitochondria-enriched fraction from cultured skin fibroblasts. Using this diagnostic assay, we and others have found that mitochondria-enriched fractions from patient fibroblasts carrying a mutation in the *NDUFS4* gene, display a significant residual CI activity, whereas, in sharp contrast, blue native analysis of these fractions followed by in-gel activity measurement reveals only an inactive subcomplex of ~830 kDa. To exclude that this discrepancy is due to a lack of sensitivity of the in-gel activity assay, we here treated NDUFS4 mutant fibroblasts with the water-soluble analog of vitamin E, Trolox, shown before to markedly increase the amount and activity of CI, and determined the activity of this complex in both assays. The data presented demonstrate that Trolox significantly increased the activity of CI in the diagnostic assay, without causing the appearance of any active complex on the blue native gel. Based on these findings it is concluded that the NDUFS4 subunit, which belongs to the so-called supernumerary subunits, primarily stabilizes the active complex. Moreover, our data provide experimental proof that the administration of analogues of vitamin E might be beneficial for the treatment of CI deficient patients with a mutation in the *NDUFS4* gene.

INTRODUCTION

Complex I (NADH:ubiquinone oxidoreductase; EC 1.6.5.3.) of the oxidative phosphorylation (OXPHOS) system catalyses the transfer of electrons from NADH to ubiquinone and uses part of their energy to translocate protons across the inner mitochondrial membrane (103). Mammalian complex I (CI) consists of 45 subunits together having a molecular weight of close to 1 MDa. Seven of these subunits are products of the mitochondrial genome, whereas the remainder is encoded by the nuclear genome (44,45,83). The core of the complex, which can perform all bioenergetic functions, comprises the seven subunits encoded by the mitochondrial genome and seven of the subunits encoded by the nuclear genome namely the NDUFS1 (75-kDa), NDUFV1 (51-kDa), NDUFS2 (49-kDa), NDUFS3 (30-kDa), NDUFV2 (24-kDa), NDUFS7 (PSST) and NDUFS8 (TYKY) subunit (104). The remaining 31 subunits encoded by the nuclear genome are the so-called supernumerary subunits, involved in stabilization and/or assembly of the complex.

Malfunction of CI (OMIM 252010) is the most frequently encountered defect of the OXPHOS system and is associated with a wide variety of clinical signs and symptoms (246). The enzymatic diagnosis involves the measurement of the rotenone-sensitive oxidation of NADH in the presence of coenzyme Q1 under Vmax conditions in both a crude homogenate of skeletal muscle and a mitochondria enriched fraction from cultured skin fibroblasts (245). As far as the nuclear genome is concerned, disease-causing mutations have been identified in all seven core subunits (20,21,22,156,157,234,268), three of the supernumerary subunits (NDUFS4, NDUFS6 and NDUFA1 (40,74,130), and the CI-specific chaperone B17.2L (185).

Live cell imaging of cultured skin fibroblasts revealed that these mutations were associated with alterations in mitochondrial length and degree of branching (138), decreased Ca^{2+}-stimulated mitochondrial ATP production (281,283) and increased superoxide and derived reactive oxygen species (ROS) levels (116,277,277,278). Furthermore, blue native analysis of mitochondria-enriched fractions followed by Western blotting and in-gel activity measurement demonstrated that in all mutant fibroblasts the amount of active CI was significantly decreased (130,185,199,223,271,278,279). Using the same analysis technique, we recently showed that chronic treatment with the water-soluble analog of vitamin E, Trolox, caused a significant increase in the amount of fully assembled CI in both healthy control fibroblasts and fibroblasts of patients with a mutation in either the *NDUFS1*, *NDUFS2*, *NDUFS8*, *NDUFS7*, or *NDUFV1*gene (278). Importantly, in the patient cell lines, this increase in CI amount was paralleled by lower than proportional increase in CI activity,

indicating that the reduction in cellular CI activity is due to a decrease in both the amount and the intrinsic catalytic activity of the complex.

Unexpectedly, blue native analysis of mitochondria-enriched preparations from cultured skin fibroblasts of patients with a mutation in the *NDUFS4* gene revealed only an inactive subcomplex of ~830 kDa (223,271), whereas the same preparations displayed a marked rotenone-sensitive NADH:ubiquinone oxidoreductase activity in the spectrophotometric assay (40,223,271). To exclude that this discrepancy is due to a lack of sensitivity of the in-gel activity measurement, we here treated NDUFS4 mutant fibroblasts with Trolox and determined the activity of CI in both assays. It was found that Trolox markedly increased the rotenone-sensitive NADH:ubiquinone oxidoreductase capacity, without causing, however, the appearance of any active complex on the blue native gel. Based on these results we conclude that the NDUFS4 subunit primarily stabilizes the active complex.

MATERIALS AND METHODS

Patient skin fibroblasts – Fibroblasts were obtained from skin biopsies of a healthy subject and five CI deficient children in the age range of 0-5 years following informed parental consent and according to relevant institutional review boards (245). Pathogenic mutations were identified in the NDUFS4 subunit of patients #4608 (K158fs; (40)), #4827 (R106X; (40)), #5260 (R106X; (40) and #5737 (VPEEHI67/VEKSIstop; (**unpublished**)) and in the NDUFS8 subunit of patient #6603 (R94C; (**unpublished**)). Fibroblasts were cultured in medium 199 with Earle's salt supplemented with 10% (v/v) fetal calf serum, 100 IU/ml penicillin and 100 IU/ml streptomycin in a humidified atmosphere of 95% air and 5% CO_2 at 37° C.

Enzyme activity measurement – Rotenone-sensitive NADH:ubiquinone oxidoreductase activity was measured in a mitochondria-enriched fraction from cultured skin fibroblasts as described previously (245). Values are expressed as mU/mg protein.

Blue native PAGE, Western blot analysis and in-gel activity measurement – Quantitative measurement of CI expression and in-gel activity was performed as described previously (277). Briefly, cultured skin fibroblasts were harvested by trypsinization, washed with ice-cold phosphate-buffered saline (PBS) and resuspended (approx. $2 \cdot 10^6$ cells) in 100 µl ice-cold PBS. For preparation of a mitochondria-enriched fraction, cells were incubated with 2 mg/ml digitonin (Biosciences Inc., La Jolla, CA, USA) in a final volume of 200 µl for 10 min on ice. Next, 1 ml ice-cold PBS was added followed by centrifugation (5 min; 10,000g; 4° C). Mitochondrial pellets were washed twice with 1 ml ice-cold PBS and stored overnight (-20° C). Pellets were solubilized in 100 µl ACBT buffer (Fluka, Steinheim, Germany) containing 1.5 M aminocaproic acid and 75 mM Bis-Tris/HCl (pH 7.0). To extract mitochondrial protein complexes, 20 µl 10% (w/v) β-lauryl maltoside was added and the solution was incubated for 10 min on ice. After centrifugation (30 min; 10,000g; 4° C), 10 µl of Blue native sample buffer (Biorad Laboratories, Hercules, CA, USA) was added to the supernatant. Polyacrylamide gels were loaded with exactly 20 µg of mitochondrial protein and subjected to blue native electrophoresis. In-gel activity measurement was performed as described previously (182). For quantitative analysis of the amount of complex, gels were blotted onto PVDF membranes and immunodecorated with primary antibodies against the NDUFA9 (39-kDa) subunit of CI and the 70-kDa subunit of CII (Molecular Probes) at a dilution of 1:1000 and 1:10000, respectively. This step was followed by incubation with IRDye 800CW-conjugated

goat polyclonal anti-mouse IgG (Li-cor Biosciences, Lincoln, USA) at a dilution of 1:10000 as a secondary antibody. Finally, blots were dried and quantified using the Odyssey Infrared Imaging System (Li-cor Biosciences).

Quantification of reactive oxygen species (ROS) levels – Quantitative determination of cellular ROS levels was performed as described previously (137,278,279). Briefly, fibroblasts, grown to ~70% confluence on glass coverslips (Ø 24 mm), were incubated in a HEPES-Tris medium (132 mM NaCl, 4.2 mM KCl, 1 mM $CaCl_2$, 1 mM $MgCl_2$, 5.5 mM D-glucose and 10 mM HEPES, pH 7.4) containing 1 μM CM-H_2DCFDA for 10 min at 37 °C. After thorough washing to remove non-hydrolyzed CM-H_2DCFDA, the increase in CM-DCF fluorescence intensity was monitored as a function of time using a video-rate confocal microscope (Oz; Noran Instruments, Middleton, WI, USA) attached to an inverted microscope (Nikon, Diaphot, Tokyo, Japan) equipped with a 40x oil immersion planapochromat objective (NA 1.4; Nikon). Cells were excited with light from an argon ion laser (488 nm; Omnichrome, Chino, CA, USA) and fluorescence emission light was directed by a 500 nm LP barrier filter (Chroma Technology Corp., Rockingham, VT, USA) onto a photomultiplier tube (Hamamatsu Photonics, Bridgewater, NJ, USA). After background correction, the rate of CM-DCF formation was calculated from the slope of the line fitted to the fluorescence intensity versus time. In each experiment, the average value obtained with healthy fibroblasts was set at 100%, to which all other values were related.

Quantification of cellular NAD(P)H levels – For measurement of cellular NAD(P)H levels, fibroblasts were seeded on glass coverslips (Ø 24 mm) and cultured to ~70% confluence. Immediately prior to measurement, fibroblasts were transferred to HEPES-Tris medium and coverslips were mounted in an incubation chamber placed on the stage of an inverted microscope (Axiovert 200 M, Carl Zeiss, Jena, Germany) equipped with a Zeiss 40x/1.3 NA Plan NeoFluar objective. The cells were excited at 360 nm using a monochromator (Polychrome IV, TILL Photonics, Gräfelfing, Germany). Fluorescence emission light was directed by a 415DCLP dichroic mirror (Omega Optical Inc., Brattleboro, VT, USA) through a 510WB40 emission filter (Omega Optical Inc.) onto a CoolSNAP HQ monochrome CCD-camera (Roper Scientific, Vianen, The Netherlands). The imaging setup was controlled by Metafluor 6.0 software (Molecular Devices Corporation, Downingtown, PA, USA). Routinely, 10 fields of view were analyzed per coverslip using an image capturing time of 100 milliseconds. The mean fluorescence intensity was determined in an intracellular region of

interest and, for purpose of background correction, an extracellular region of identical size. Quantitative image analysis was performed with Metamorph 6.1 (Molecular Devices Corporation). In each experiment, the average value obtained with healthy fibroblasts was set at 100%, to which all other values were related.

Data analysis – Processing and analysis of fluorescence images and densitometer scans was performed with Image Pro Plus 5.1 (Media Cybernetics, San Diego, CA, USA) and Metamorph 6.1 (Molecular Devices Corporation). Numerical results were visualized using Origin Pro 7.5 (OriginLab Corp., Northampton, MA, USA) and are expressed as means ± SE. Statistical differences between average values were determined using an independent two-population Student's *t*-test (Bonferroni corrected). P-values <0.05 were considered significant.

Chemicals – Culture materials were obtained from Invitrogen (Breda, The Netherlands). All other reagents were from Sigma-Aldrich (St. Louis, MO, USA).

RESULTS

Previously, we and others have reported that mitochondria-enriched fractions from cultured skin fibroblasts of patients with a mutation in the *NDUFS4* gene contained an inactive subcomplex of CI when separated on a blue native polyacrylamide (BNP) gel (223,271). Remarkably, however, the same fractions were found to exhibit a significant rotenone-sensitive NADH:ubiquinone oxidoreductase capacity when analyzed in a spectrophotometric assay (40). A plausible explanation for these disparate results might be that the in-gel activity assay lacks sufficient sensitivity. To address this possibility, we here assessed the effect of chronic treatment of cultured skin fibroblasts with Trolox, a water-soluble analog of vitamin E, on the oxidative capacity of CI as determined in the above two assays. We showed before that this maneuver resulted in an increase in the amount and, as a consequence, in-gel activity of the fully assembled complex in cultured skin fibroblasts of both healthy control subjects and patients with a mutation in either the *NDUFS1*, *NDUFS2*, *NDUFS7*, *NDUFS8* or *NDUFV1* gene (278). Importantly, parallel measurements revealed a marked decrease in cellular ROS levels, suggesting a regulatory role for cellular oxidants in the expression of the fully assembled and catalytically active complex.

Mutations in the NDUFS4 gene cause variable expression of an inactive CI subcomplex – **Figure 1** confirms previous findings that fibroblasts of patients with a mutation in the *NDUFS4* gene do not express detectable amounts of the fully assembled (upper panel) and catalytically active (middle panel) complex (band a). Instead, they expressed variable amounts (upper panel) of a catalytically inactive (middle panel) CI subcomplex with a molecular weight of approximately 830 kDa (band b). For comparison, we analyzed fibroblasts of a patient with a mutation in the *NDUFS8* gene (lane 6). The latter cells clearly expressed the fully assembled and catalytically active complex, albeit at a very low level. Comparison of the band intensities obtained with this patient and the four NDUFS4 patients already indicates that the absence of any in-gel activity in the latter patients is not likely to be due to a lack of sensitivity of this assay.

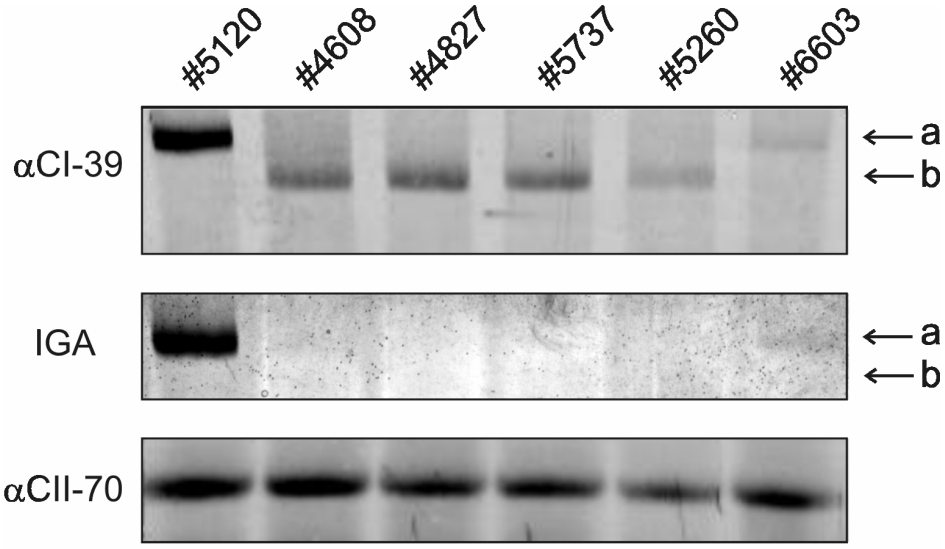

Figure 1: Blue native gel analysis of CI amount and activity in a mitochondria-enriched fraction of NDUFS4 mutant fibroblasts - Mitochondria-enriched fractions from cultured skin fibroblasts of a healthy subject (lane 1), four patients with a mutation in the *NDUFS4* gene (lanes 2-5) and one patient with a mutation in the *NDUFS8* gene (lane 6) were subjected to blue native PAGE followed by either Western blotting using specific antibodies against the NDUFA9 subunit of CI (αCI-39; upper lane) and the 70-kDa subunit of CII (αCII-70; lower panel) or in-gel activity measurement (IGA; middle panel). All four NDUFS4 preparations showed a single inactive subcomplex of ~830 kDa. Note that the relatively small amount of fully assembled CI obtained with the mitochondria-enriched fraction of the NDUFS8 mutant fibroblasts gave a clear band on the activity gel (lane 6; upper and middle panel, respectively). Cell line codes are as follows: #5120 (healthy control fibroblasts), #4608 (NDUFS4-K158fs), #4827 (NDUFS4-R106X), #5737 (NDUFS4-VPEEHI67/VEKSIstop), #5260 (NDUFS4-R106X) and #6603 (NDUFS8-R94C). a, fully assembled complex. b, inactive subcomplex.

Trolox normalizes cellular ROS levels in fibroblasts of patients with a mutation in the NDUFS4 gene – **Figure 2** (open bars) shows that cellular ROS levels were significantly increased in cultured fibroblasts of the NDUFS4 patients. In this respect, these patient fibroblasts do not differ from those with mutations in other nuclear CI genes (see also, 279). Moreover, in accordance with this result, we recently showed that fibroblasts of all five NDUFS4 patients at our disposal displayed a significantly increased cellular superoxide level (277). Here, we show that chronic treatment of these patient cell lines with 0.5 mM Trolox for 72 h caused a marked reduction in cellular ROS levels (**Fig. 2**, closed bars). This finding clearly demonstrates the effectiveness of this antioxidant in fibroblasts of NDUFS4 patients. As reported before, Trolox also reduced these levels in healthy control cells (278).

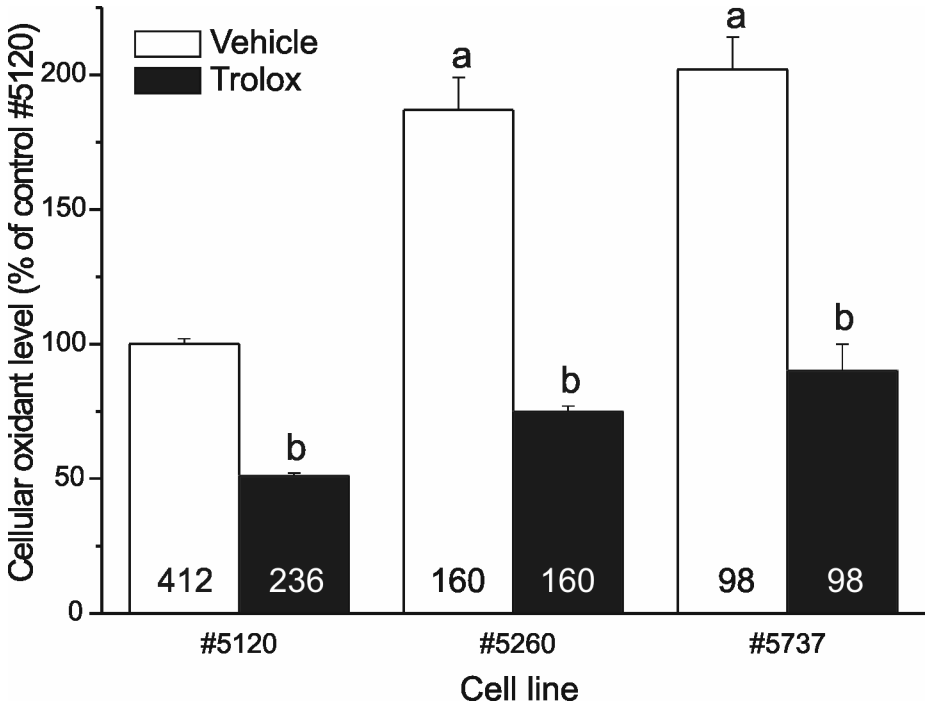

Figure 2: Effect of chronic Trolox treatment on ROS levels in NDUFS4 mutant fibroblasts - Cultured skin fibroblasts, chronically treated with either vehicle (open bars) or 0.5 mM Trolox (closed bars) for 72 h, were loaded with CM-H_2DCFDA, thoroughly washed to remove non-hydrolyzed dye, and monitored for the rate of fluorescence increase as a measure of intracellular ROS levels by video-rate confocal microscopy. In each experiment, the average rate of CM-DCF fluorescence increase obtained with vehicle-treated healthy control fibroblasts (#5120) was set at 100%, to which all other values were related. Note that chronic Trolox-treatment also decreased intracellular ROS levels in healthy control cells. The values depicted are from three independent measurements performed on three different days and represent the mean ± SE of 412 (#5120), 160 (#5260) and 98 (#5737) vehicle-treated cells and 236 (#5120), 160 (#5260) and 98 (#5737) Trolox-treated cells. a, significantly different from vehicle-treated healthy control fibroblasts. b, significantly different from corresponding vehicle-treated fibroblasts. Cell line codes are as follows: #5120 (healthy control fibroblasts), #5260 (NDUFS4-R106X) and #5737 (NDUFS4-VPEEHI67/VEKSIstop).

Trolox increases the rotenone-sensitive CI capacity in a mitochondria-enriched fraction without causing the appearance of an active complex on a BNP gel – **Table 1** shows that the rotenone-sensitive NADH:oxidoreductase capacity as determined in a mitochondria-enriched fraction is still 20% of control in cultured skin fibroblasts of patients with a mutation in the *NDUFS4* gene. Chronic treatment of these patient cells with Trolox significantly increased the rotenone-sensitive NADH:oxidoreductase capacity in this assay. In sharp contrast, however, this maneuver did not result in the appearance of an active form of CI on a blue native gel (**Fig. 3**). The experiment was performed in triplicate and in all three cases the amount of inactive subcomplex tended to be increased in the Trolox-treated cells.

Table 1. Effect of Trolox and rotenone on NADH:ubiquinone oxidoreductase activity and NAD(P)H fluorescence

Cell line[$]	NADH:ubiquinone oxidoreductase activity (mU/mg)[#]		NAD(P)H autofluorescence (% of vehicle-treated healthy control)[&]	
	VEHICLE	TROLOX	VEHICLE	ROTENONE
Healthy control (#5120)	22±3 (n=5)	29±5 (n=5)	100±2 (n=143)	132±8[b] (n=22)
NDUFS4-R106X (#5260)	4.1±1[a] (n=5)	10±1[b] (n=5)	132±4[a] (n=114)	179±24[a,b] (n=19)
NDUFS4-VPEEHI67/VEKSIstop (#5737)	3.7±1[a] (n=6)	7.1±1[b] (n=6)	127±6[a] (n=70)	176±10[a,b] (n=22)

[$]Numbers indicate the designation of the cell lines within the Nijmegen Centre for Mitochondrial Disorders (NCMD). [#]Values depicted are mean ± SEM expressed as mU/mg protein of vehicle- or Trolox-treated (0.5 mM, 72h) cells; numbers between brackets represent the number of assays. [&]Values depicted are mean ± SEM expressed as percentage of vehicle-treated control; values between brackets represent the numbers of cells measured on at least 3 days. Statistics: [a]significantly different from vehicle-treated healthy control, [b]significantly different from the corresponding vehicle-treated cells.

Patient fibroblasts with a mutation in the NDUFS4 gene display a significant rotenone-sensitive NADH-oxidizing activity – To support our conclusion that fibroblasts of NDUFS4 patients express a functionally active CI, we determined the effect of short-term rotenone treatment (1 µM, 2 min) on cellular NAD(P)H autofluorescence. **Table 1** shows that NAD(P)H autofluorescence was significantly increased in untreated patient fibroblasts. This result is in agreement with the reduction in rotenone-sensitive NADH:oxidoreductase capacity observed in the spectrophotometric assay. Most importantly, however, the table shows that short-term rotenone treatment resulted in a marked increase in NAD(P)H autofluorescence in the patient cell lines, indicating the presence of a substantial rotenone-sensitive NADH-oxidizing capacity. Also in this case, NAD(P)H autofluorescence was significantly higher in patient fibroblasts as compared to healthy fibroblasts. The latter result may be indicative for an altered energy metabolism in response to the CI deficient condition.

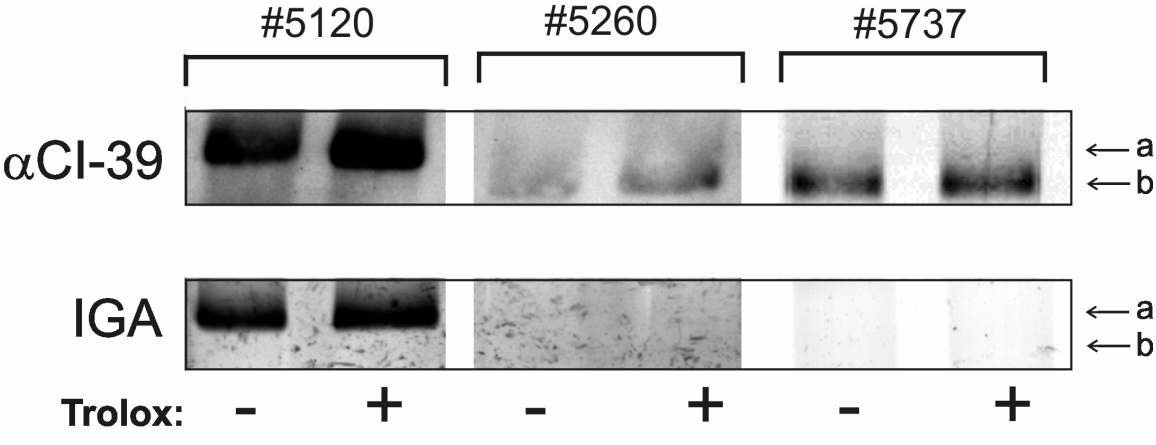

Figure 3: Effect of chronic Trolox treatment on CI amount and activity in a mitochondria-enriched fraction of NDUFS4 mutant fibroblasts - Mitochondria-enriched fractions from cultured skin fibroblasts, chronically treated with either vehicle (-) or 0.5 mM Trolox (+) for 72 h, were subjected to blue native PAGE followed by either Western blotting (upper lanes) or in-gel activity measurement (lower lanes) as described in the caption to figure 1. Note that Trolox readily increases the amount and activity of the fully assembled complex (band a) in healthy control fibroblasts, without causing the appearance of any active band in NDUFS4 mutant fibroblasts. The data presented are representative for three individual experiments. Cell line codes are as follows: #5120 (healthy control fibroblasts), #5260 (NDUFS4-R106X) and #5737 (NDUFS4-VPEEHI67/VEKSIstop). a, fully assembled active complex. b, inactive subcomplex.

DISCUSSION

The major conclusion of this study is that patient fibroblasts with a mutation in the *NDUFS4* gene contain an active form of CI that is, however, relatively labile as compared to that of healthy control cells. Evidence comes from the current finding that chronic treatment of NDUFS4 mutant fibroblasts with the vitamin E analogue Trolox markedly increased the rotenone-sensitive NADH:ubiquinone oxidoreductase capacity in a mitochondria-enriched fraction without causing the appearance of any active complex on a blue native gel. Furthermore, in agreement with the above conclusion, live cell imaging of these fibroblasts revealed a substantial rotenone-sensitive NADH consumption. Importantly, our data provide experimental proof that the administration of vitamin E analogues may be beneficial for the treatment of CI deficient patients with a mutation in the *NDUFS4* gene.

The present study sheds light on puzzling data obtained by us and others regarding the presence of an active form of CI in patients with a mutation in the *NDUFS4* gene. Previous studies by Papa and co-workers failed to detect any NDUFS4 protein on a whole cell Western blot from cultured skin fibroblasts of patients with a five base-pair duplication (K158fs; (273); #4608 of this study), leading to a 14-amino acid C-terminal extension, or a base-pair deletion (W97X; (39)) or non-sense mutation (W15X; (199)), both resulting in a premature stop codon (223). Intriguingly, in the case of the first two patients, mitochondria-enriched fractions were found to display a significant rotenone-sensitive NADH:ubiquinone oxidoreductase capacity (40,223). However, contradictory results were obtained with the third patient. Our group found a low but detectable activity (40), whereas Papa and co-workers found no activity at all (116,199,223). In addition to the fibroblast cell line with the five base-pair duplication (#4608), we here investigated fibroblast cell lines of three more patients with a mutation in the *NDUFS4* gene. Two unrelated patients had the same non-sense mutation (R106X; #4827 (39) and #5260 (40)), whereas the third patient carried a deletion/frameshift mutation (VPEEHI67/VEKSIstop; #5737 (**unpublished**)). All three mutations result in premature translation termination and, thus, to the probable absence of any NDUFS4 protein (see above). Whereas the original studies already showed that mitochondria-enriched fractions of patient cell lines #4827 (39) and #5260 (40) exhibited a significant rotenone-sensitive NADH:ubiquinone oxidoreductase capacity, we here show that this was also the case for the patient with the deletion/frameshift mutation (#5737). Moreover, we show that intact fibroblasts of these patients displayed a marked rotenone-sensitive NADH consumption. Taken together, these findings are in agreement with the idea that

patient fibroblasts with a mutation in the *NDUFS4* gene fail to express this subunit but nevertheless display a significant CI activity.

Blue native gel electrophoresis followed by Western blotting and in-gel activity measurement is a widely used tool in the analysis of CI deficiency. In agreement with previous results by us and others (223,271), we were unable to detect any active form of CI on a blue native gel of mitochondria-enriched preparations from NDUFS4 mutant fibroblasts. One can argue that the absence of any detectable in-gel activity is due to a lack of sensitivity of this analysis technique. However, we here show that doubling of the rotenone-sensitive NADH:ubiquinone oxidoreductase capacity by chronic treatment of patient cell lines #5260 and #5737 with the vitamin E analogue Trolox did not result in the appearance of any active form of CI on the gel. Moreover, inclusion of a patient with a mutation in the *NDUFS8* gene, revealed that even at very low levels of CI expression, in-gel activity was readily detectable (see also, 278). Taken together, these findings are compatible with the idea that patients with a mutation in the *NDUFS4* gene contain an active form of CI that is, however, relatively labile and falls apart during blue native gel electrophoresis. This then suggests that the NDUFS4 subunit may function primarily to stabilize CI. Additional evidence for a stabilizing role comes from earlier findings that mutations in this subunit not only decrease the activity of CI but also that of CIII (39). Thus far, evidence has been provided that CI is stabilized by the complex-specific chaperones B17.2L (185) and NDUFAF1 (286).

Using an antibody against the NDUFA9 subunit, all four preparations were found to contain an inactive subcomplex with a molecular weight of approximately 830 kDa. In agreement with this result, Scacco et al. reported the presence of an inactive subcomplex of similar size for two other NDUFS4 patients (223). At present, it is unclear whether the inactive form of CI, detected on a blue native gel from NDUFS4 mutant fibroblasts, represents an assembly intermediate or a breakdown product. Scacco et al. observed that this subcomplex was still associated with the inner mitochondrial membrane (223). Ugalde et al. showed that in addition to the NDUFA9 subunit this subcomplex contained the NDUFS3 and NDUFS5 subunit (271), whereas Scacco et al. demonstrated the additional presence of the NDUFS7, NDUFB6 and NDUFA6 subunit (223). Intriguingly, an inactive subcomplex of similar size was observed on a blue native gel of patients with mutations in either the *NDUFS1* gene (116,278), *NDUFV1* gene (185,278) or *NDUFS6* gene (130), but not the *NDUFS2*, *NDUFS7* or *NDUFS8* gene (278). In-gel activity measurements revealed that NDUFS1 and NDUFV1 mutant fibroblasts (278), but not NDUFS4 mutant fibroblasts (**this study**), contained in addition to the inactive subcomplex also the active complex. Importantly, Iuso et al.

demonstrated that the inactive subcomplex of patient fibroblasts with a mutation in the *NDUFS1* gene showed no immunostaining with polyclonal antibodies directed against either the N-terminus or the phosphorylated C-terminus of the NDUFS4 subunit (116). Similarly, Ogilvie et al. observed that the inactive subcomplex of NDUFV1 mutant fibroblasts contained no NDUFS4 subunit (185). These results are compatible with the idea that the presence of the NDUFS4 subunit is required for the stabilization of the fully assembled complex. Ogilvie et al. showed that the assembly factor B17.2L associated with the subcomplex and not with the fully assembled complex in fibroblasts of patients with a mutation in either the NDUFV1 gene or the NDUFS4 gene (185), indicating that the absence of the NDUFS4 subunit does not interfere with the binding of this assembly factor.

Using an anti-NDUFS1 antibody, Papa and co-workers co-immunoprecipitated the NDUFV2 subunit from NDUFS4 mutant fibroblasts, suggesting that both subunits are present in the same subcomplex (194). The fact that the NDUFS4 subunit is absent in the inactive subcomplex of NDUFV1 (185) and NDUFS1 (116) mutant fibroblasts (185), may suggest that it is associated with the NDUFS1/NDUFV2 containing subcomplex. Detailed analysis of the composition of this subcomplex will show whether it represents the NADH dehydrogenase module (284). According to our hypothesis, this module then associates with the remainder of the complex, containing at least the NDUFA9, NDUFS3, NDUFS5, NDUFS7, NDUFB6 and NDUFA6 subunit (223,271), in an NDUFS4-dependent manner.

Acknowledgements: This work was supported by equipment grants of ZON (Netherlands Organization for Health Research and Development, No: 903-46-176), NWO (Netherlands Organization for Scientific Research, No: 911-02-008) and the European Community's sixth Framework Programme for Research, Priority 1 "Life sciences, genomics and biotechnology for health", contract number LSHM-CT-2004-503116.

CHAPTER V

Superoxide production is inversely related to complex I activity in inherited complex I deficiency

Sjoerd Verkaart[a,b,d,e]
Werner J.H. Koopman[a,c,d]
Sjenet E. van Emst-de Vries[a,d]
Leo G.J. Nijtmans [b,d,e]
Lambertus W.P.J. van den Heuvel[b,d,e]
Jan A.M. Smeitink[b,d,e]
Peter H.G.M. Willems[a,c,d]

[a]Department of Membrane Biochemistry, [b]Department of Pediatrics, [c]Microscopical Imaging Centre, [d]Nijmegen Centre for Molecular Life Sciences (NCMLS), [e]Nijmegen Centre for Mitochondrial Disorders (NCMD), Department of Pediatrics, Radboud University Nijmegen Medical Centre

BBA Molecular Mechanisms of Disease, **2007** 1772(3):373-381.

ABSTRACT

Deficiency of NADH:ubiquinone oxidoreductase or complex I (CI) is the most common cause of disorders of the oxidative phosphorylation system in humans. Using life cell imaging and blue-native electrophoresis we quantitatively compared superoxide production and CI amount and activity in cultured skin fibroblasts of 7 healthy control subjects and 21 children with inherited isolated CI deficiency. Thirteen children had a disease causing mutation in one of the nuclear-encoded CI subunits, whereas in the remainder the genetic cause of the disease is not yet established. Superoxide production was significantly increased in all but two of the patient cell lines. An inverse relationship with the amount and residual activity of CI was observed. In agreement with this finding, rotenone, a potent inhibitor of CI activity, dose-dependently increased superoxide production in healthy control cells. Also in this case an inverse relationship with the residual activity of CI was observed. In sharp contrast, however, rotenone did not decrease the amount of CI. The data presented show that superoxide production is increased in inherited CI deficiency and that this increase is primarily a consequence of the reduction in cellular CI activity and not of a further leakage of electrons from mutationally malformed complexes.

INTRODUCTION

The mitochondrial oxidative phosphorylation (OXPHOS) system consists of five multiprotein complexes: NADH:ubiquinone oxidoreductase (complex I or CI), succinate-dehydrogenase-ubiquinone oxidoreductase (CII), ubiquinol:cytochrome *c* oxidoreductase (CIII), cytochrome *c* oxidase (CIV) and F_0F_1-ATP synthase (CV) (246). The first four complexes (CI-CIV), together with two electron carriers (coenzyme Q_{10} and cytochrome *c*), constitute the respiratory chain that utilizes the energy of NADH and succinate, oxidized at CI and CII, respectively, to translocate protons from the mitochondrial matrix into the intermembrane space. The latter results in a negative potential ($\Delta\psi$) across the inner mitochondrial membrane, which is crucial for the maintenance of mitochondrial integrity (68).

Dysfunction of the OXPHOS system is associated with a wide array of clinical manifestations, ranging from single lesions in Leber's hereditary optic neuropathy or maternally-inherited nonsyndromic deafness to more widespread lesions including myopathies, encephalomyopathies, cardiopathies, or complex multisystem syndromes (62,242,274,302). Inherited disorders of the OXPHOS system are observed once every 10,000 live births and the most frequently occurring enzymatic deficiency is found in CI (EC 1.6.5.3), which catalyzes the transfer of electrons from NADH to coenzyme Q_{10}. In human heart, this complex consists of at least 45 different subunits, together having a molecular weight close to 1 MDa (45). With the aid of differential extraction techniques, CI can be subdivided into a flavoprotein (FP), iron-sulfur protein (IP) and hydrophobic protein (HP) fraction. The catalytic core of the complex comprises 14 evolutionary conserved subunits, 2 of which reside in the FP fraction, 5 in the IP fraction and 7 in the HP fraction (81). In humans, these core subunits are encoded by the nuclear *NDUFV1* and *NDUFV2* genes, the nuclear *NDUFS1*, *NDUFS2*, *NDUFS3*, *NDUFS7* and *NDUFS8* genes and the mitochondrial *ND1-ND6* and *ND4L* genes. Thus far, disease causing mutations have been identified in all 14 core subunits (246) and, as far as the nuclear genome is concerned, in genes encoding supernumerary subunits NDUFS4 (246) and NDUFS6 (130) and assembly factor B17.2L (185).

The pathophysiological mechanisms linking defects in CI genes to cellular dysfunction and disease are only partially understood. To obtain insight into these mechanisms, we use skin fibroblasts of patients with inherited isolated CI deficiency and study the biogenesis of CI and cytopathological consequences of its dysfunction. Native gel electrophoresis and in-gel activity assays revealed that mutations in CI subunits (NDUFS2, NDUFS4, NDUFS7 and

NDUFS8) markedly reduced the expression of the fully assembled, catalytically active complex (271). At the cell physiological level, this reduction was found to be associated with disturbed mitochondrial Ca^{2+} handling and ensuing ATP production during hormone stimulation (281,283).

Partial inhibition of CI activity by chronic treatment with rotenone significantly increased superoxide production and lipid peroxidation in cultured skin fibroblasts of healthy control subjects (136). Similarly, the formation of superoxide-derived hydroxyl radicals and lipid peroxidation products was found to be increased in fibroblasts of three patients with a reduced rotenone-sensitive NADH-cytochrome *c* reductase (CI and CIII) activity (160). At pathological concentrations, superoxide and its derived reactive oxygen species are hazardous for the cell. At physiological concentrations, however, they play important roles in a variety of signaling processes (65). In fibroblasts of healthy control subjects we observed that the increase in superoxide production induced by chronic rotenone treatment was associated with a marked increase in mitochondrial length and degree of branching (136). Moreover, in patient fibroblasts we found that this parameter was linearly correlated with the residual activity of CI (139). Based on these observations, we hypothesized that the increase in mitochondrial length and degree of branching constitutes an adaptive response to protect against the consequences of CI deficiency. In agreement with this idea, recent evidence showed that a more complex mitochondrial network, induced by manipulating mitochondrial fusion, protected against radical-induced mitochondrial depolarization possibly by allowing a more effective sharing of intra-mitochondrial antioxidants (181).

To obtain a quantitative understanding of the relationship between CI deficiency and superoxide production, we here compare superoxide production and amount and activity of CI between cultured skin fibroblasts of 7 healthy control subjects and 21 children with inherited isolated CI deficiency. The data presented show that superoxide production is increased in virtually all patient cell lines but to a variable degree and that the extent of increase is inversely proportional to the amount and activity of CI.

MATERIALS AND METHODS

Patient skin fibroblasts – Fibroblasts were derived from skin biopsies of 21 CI deficient children in the age range of 0-5 years, 2 age-matched healthy children and 5 healthy adults following informed consent and according to relevant institutional review boards (Smeitink et al., 2001). **Table 1** shows that superoxide production did not differ between adult (CT1-CT5) and age-matched (CT6 and CT7) control cell lines. For 11 patients the biochemical analysis, mutations and clinical phenotypes were described before (P1, P2 (234); P4-P6 (155); P7, P8, P9, P11 (40); P12 (268)), for 3 patients (P3, P10, P13) these data are not yet reported, whereas for the remaining 8 patients the mutations are hitherto unknown (P14-P21 (271). Fibroblasts were cultured in medium 199 with Earle's salt supplemented with 10% (v/v) fetal calf serum, 100 IU/ml penicillin and 100 IU/ml streptomycin in a humidified atmosphere of 95% air and 5% CO_2 at 37^o C. Measurements were performed within 5 passages after the start of the culture. The passage number at the onset of the culture is given in **Table 1**.

Enzyme activity measurements – Activities of NADH:ubiquinone oxidoreductase (CI; EC: 1.6.5.3) and cytochrome *c* oxidase (CIV; EC: 1.9.3.1) were determined in a mitochondrial enriched fraction of cultured fibroblasts as described previously (119). The activity of CI was normalized against that of CIV and expressed as percentage of lowest control (110 mU/U CIV (119,245).

Quantification of superoxide production – Fibroblasts were incubated in HEPES-Tris medium (132 mM NaCl, 4.2 mM KCl, 1 mM $CaCl_2$, 1 mM $MgCl_2$, 5.5 mM D-glucose and 10 mM HEPES, pH 7.4), containing 10 µM hydroethidine (HEt; Molecular Probes, Leiden, The Netherlands) for 10 minutes at 37^o C. HEt is a lipophylic, uncharged compound that readily enters the cell where it reacts with superoxide to form two positively charged products, 2-hydroxyethidium and ethidium, both of which emit red fluorescence (304). The reaction was stopped by thorough washing of the cells with PBS to remove excess HEt. For quantitative analysis of the fluorescent HEt oxidation products, coverslips were mounted in an incubation chamber placed on the stage of an inverted microscope (Axiovert 200 M, Carl Zeiss, Jena, Germany) equipped with a Zeiss 40x/1.3 NA fluor objective. The cells were excited at 490 nm using a monochromator (Polychrome IV, TILL Photonics, Gräfelfing, Germany). Fluorescence emission light was directed by a 525DRLP dichroic mirror (Omega Optical Inc., Brattleboro, VT, USA) through a 565ALP emission filter (Omega) onto a CoolSNAP HQ

monochrome CCD-camera (Roper Scientific, Vianen, The Netherlands). Hardware was controlled with Metafluor 6.0 software (Universal Imaging Corporation, Downingtown, PA, USA). Routinely, 10 fields of view were analyzed per coverslip using an acquisition time of 100 milliseconds.

Blue-native electrophoresis – Cultured skin fibroblasts were harvested by trypsinization, washed, and resuspended (approx. $2 \cdot 10^6$ cells) in 100 µl ice-cold PBS. For isolation of mitochondria, cells were incubated with 2 mg/ml digitonin (Biosciences Inc., La Jolla, CA, USA) in a final volume of 200 µl for 10 min on ice. Next, 1 ml ice-cold PBS was added followed by centrifugation (5 min; 10,000g; 4° C). Mitochondrial pellets were washed twice with 1 ml ice-cold PBS and stored overnight (-20° C). Pellets were solubilized in 100 µl ACBT buffer (Fluka, Steinheim, Germany) containing 1.5 M aminocaproic acid and 75 mM Bis-Tris/HCl (pH 7.0). To extract mitochondrial protein complexes, 20 µl 10% (w/v) β-lauryl maltoside was added and the solution was incubated for 10 min on ice. After centrifugation (30 min; 10,000g; 4° C), 10 µl of blue native sample buffer (Biorad Laboratories, Hercules, CA, USA) was added to the supernatant. Blue native PAGE (BNP) and Western blotting, using monoclonal antibodies with human reactivity against the NDUFA9 (39-kDa) subunit of CI (Molecular Probes) and the 70-kDa subunit of CII (Molecular probes) at a dilution of 1:1000, was performed as described previously (182). For quantitative analysis gels were loaded with exactly 40 µg of mitochondrial protein. After Western blotting, luminescent signals were quantitatively analyzed by exposing illumination films to the blots for different periods of time (5-180 s). Non-saturating films were scanned using a G690 Imaging Densitometer (Biorad). From these scans, the integrated optical density of each band was determined and background corrected. The resulting numerical values were normalized to those obtained with control cells on the same blot.

Data analysis – Processing and analysis of fluorescence images and densitometer scans was performed with Image Pro Plus 5.1 (Media Cybernetics, San Diego, CA, USA) and Metamorph 6.1 (Universal Imaging Corporation, Downingtown, PA, USA). Numerical results were visualized using Origin Pro 7.5 (OriginLab Corp., Northampton, MA, USA) and presented as the mean ± SEM. During linear regression analysis, the degree of bivariate correlation between sets of data was analyzed by calculating Pearson's R. This parameter expresses the proportion of total variation that is explained by the regression. If R is ±1, the total variation in the fit can be explained in terms of the regression curve (58). For R>0 the

correlation is positive, for R<0 the correlation is negative. Statistical differences between average values were determined using an independent two-population Student's *t*-test (Bonferroni corrected). P-values <0.05 were considered significant.

Chemicals – Culture materials were obtained from Invitrogen (Breda, The Netherlands), all other reagents were from Sigma-Aldrich (St. Louis, MO, USA).

RESULTS

Quantitative measurement of superoxide production in human skin fibroblasts - In this study we assessed superoxide production in living cells using hydroethidine (HEt), a membrane-permeable derivative of ethidium bromide that is specifically converted by superoxide into 2-hydroxyethidium and ethidium (304,305). Both products are positively charged and emit red fluorescence when excited at 490 nm. Human skin fibroblasts were grown to ~70% confluence, treated with 10 µM HEt for 10 min and thoroughly washed to remove non-oxidized HEt. Next, video-imaging microscopy was used for subcellular quantification of the fluorescent oxidation products formed during the 10-min incubation period with HEt. We reported before that the fluorescent products formed during the oxidation of HEt accumulated predominantly in the nucleus and a widespread network of tubular structures located within the cytosol (136). **Figure 1A** shows that in both compartments the average fluorescence intensity remained stable for at least 200 s, indicating that non-oxidized HEt was effectively removed during the washing step and that its oxidation products did not translocate during the ensuing recording period. In addition, this result demonstrates that the fluorescent products were resistant to photo-bleaching. **Figure 1A** furthermore shows that dissipation of the mitochondrial membrane potential by FCCP (p-trifluoromethoxy carbonyl cyanide phenyl hydrazone) leads to a rapid decrease in tubular fluorescence. This result identifies the tubular structures as active mitochondria in which positively charged HEt oxidation products are retained in a membrane potential-dependent manner. The FCCP-induced decrease in tubular fluorescence was mirrored by a concomitant increase in nuclear fluorescence, indicating the translocation of HEt oxidation products from the mitochondria to the nucleus. The results obtained with FCCP demonstrate that HEt oxidation products can easily pass mitochondrial membranes. Therefore, it is not possible to make a statement concerning the exact site(s) of primary HEt oxidation.

Chronic rotenone treatment dose-dependently increases superoxide production in human skin fibroblasts – To mimic the pathological condition of chronic CI deficiency, control fibroblasts were cultured in the presence of different concentrations of rotenone for 72 h (136). At concentrations at or below 1 nM, this specific inhibitor of CI had no effect on the amount of fluorescent oxidation products that accumulated in the mitochondrial compartment during the 10-min incubation period with HEt (**Fig. 1B**, closed circles). At higher concentrations, however, the drug dose-dependently increased this amount. For the entire

range of rotenone concentrations, mitochondrial and nuclear fluorescence were linearly correlated (R=0.98, p<0.0001). The increase in mitochondrial fluorescence was virtually mirrored by the decrease in residual CI activity (**Fig. 1B**, open circles), determined in a mitochondrial enriched fraction of cultured fibroblasts (data from 136). Half-maximal concentrations were 110 nM and 20 nM, respectively. These findings show that in human skin fibroblasts drug-induced reduction in CI activity is accompanied by increasing production of cellular superoxide.

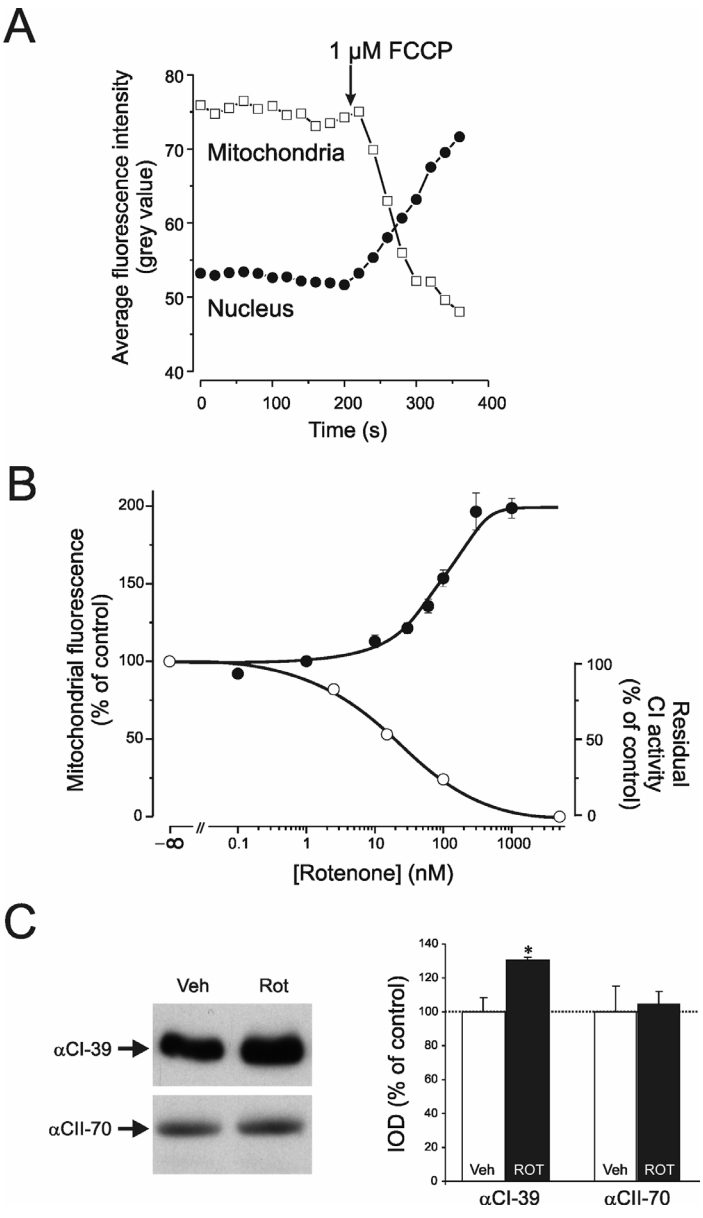

Figure 1: Effect of chronic rotenone treatment on subcellular superoxide production, residual CI activity and cellular CI expression in human skin fibroblasts – (**A**) FCCP-induced redistribution of HEt oxidation products between mitochondria and nucleus. Fibroblasts (CT1, **Table 1**) were incubated with 10 µM hydroethidine (HEt) for 10 min at 37° C, thoroughly washed and visualized using fluorescence microscopy. FCCP was added at the designated time (arrow). Fluorescence signals were obtained from the indicated compartments and background corrected. (**B**) Dose-dependency of the effect of chronic rotenone treatment on the accumulation of HEt oxidation products in the indicated compartment (closed symbols) and the residual CI activity (open symbols). Fibroblasts were pretreated with vehicle or the indicated concentration of rotenone (closed symbols) for 72 h. Residual CI activity (right y-axis) and fluorescence intensity (left y-axis) are expressed as percentage of vehicle-treated control. The data presented are the average ± SEM of 3 independent measurements. (**C**) Effect of chronic rotenone treatment on CI expression. Mitochondrial enriched fractions of vehicle- and rotenone-treated cells were subjected to blue-native electrophoresis and Western blotting. Intensities of the CI and CII bands were determined by densitometry and expressed as percentage of vehicle-treated control. The data presented are the average ± SEM of three independent experiments. *, significantly different from control.

Superoxide production is increased in patient skin fibroblasts – The amount of fluorescent oxidation products that accumulated in the mitochondrial compartment during the 10-min incubation with HEt did not significantly differ between fibroblasts of seven healthy control subjects (**Table 1**, CT1-CT7). Compared to control, however, mitochondrial accumulation of HEt oxidation products was significantly increased in all but two patient cell lines (P2 and P20). As for healthy control fibroblasts treated with various concentrations of rotenone, mitochondrial and nuclear fluorescence were linearly correlated for the whole cohort of patient cell lines ($R=0.98$, $p<0.0001$). Linear regression analysis furthermore revealed an inverse relationship between mitochondrial fluorescence and residual CI activity (**Fig. 2**, $R=-0.83$, $p<0.0001$). In all patient cell lines, acute treatment with rotenone (during the 10-min incubation with HEt) caused a further increase in fluorescence intensity (**Table 1**), demonstrating the presence of a functional rotenone binding site.

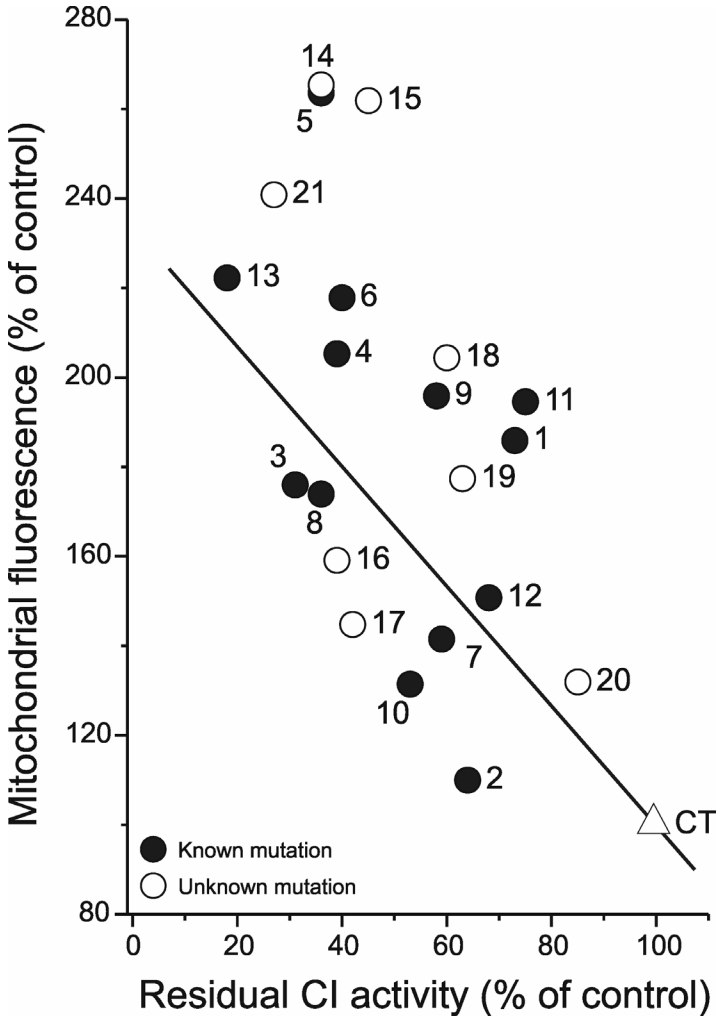

Figure 2: Inverse relationship between superoxide production and residual CI activity in fibroblasts of patients with isolated CI deficiency – Measurement of superoxide production was performed as described in the caption to **figure 1**. Fluorescence intensity in the indicated compartment (left y-axis) is expressed as percentage of vehicle-treated control (CT). Mean values, number of cells analyzed and patient numbers are depicted in **Table 1**. Closed and open symbols represent patient cell lines with a known (13 patients) and hitherto unknown (8 patients) mutation, respectively. Linear regression analysis reveals an inverse correlation between superoxide production and residual CI activity for the whole cohort of patient cell lines.

Fully assembled CI is decreased in patient skin fibroblasts – We reported before that the amount of fully assembled CI is markedly reduced in patient fibroblasts with mutations in nuclear-encoded CI subunits (271). **Figure 3**, depicts assembly data of a subgroup of 13 patients, 7 with a known mutation (**Table 1**, P1-P5 and P12-P13) and 6 with a hitherto unknown mutation (**Table 1**, P14-P16 and P18-P20), and shows that in all but one (P20) of them the amount of fully assembled CI was lower than control. Except cell line P20, the cell lines of the other patients with a hitherto unknown mutation (open symbols) did not differ from those with a known mutation (closed symbols). Linear regression analysis revealed that for the whole cohort of patient cell lines this parameter was negatively related to the cell's superoxide production (R=-0.62, p=0.017) and positively to its residual CI activity (R=0.89, p<0.0001).

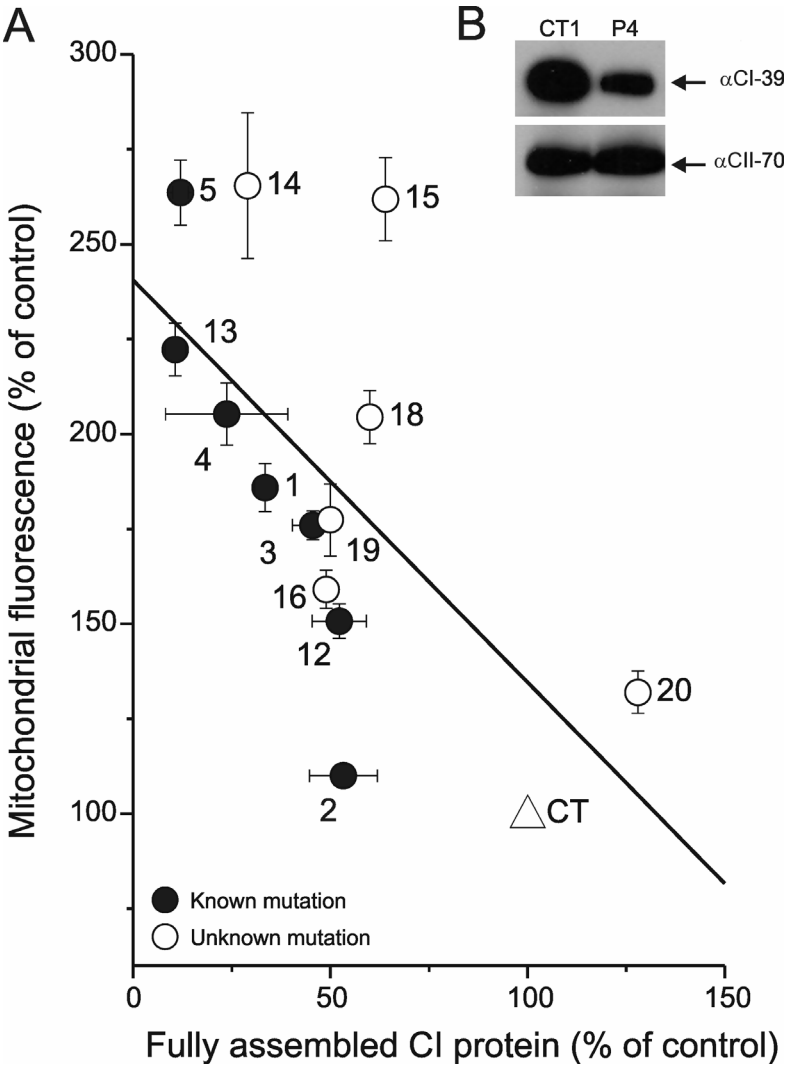

Figure 3: Inverse relationship between superoxide production and fully assembled CI in fibroblasts of patients with isolated CI deficiency – (**A**) Measurement of superoxide production and analysis of fully assembled CI was performed as described in the caption to **figure 1**. Linear regression analysis reveals an inverse correlation between superoxide production and amount of fully assembled CI for 7 patient cell lines with a known (black symbols) and 6 with a hitherto unknown (open symbols) mutation. Assembly data are from 9 (CT), 1 (P5, P14, P15, P16, P18, P19, P20), 2 (P1, P2, P3, P13), 4 (P4) and 5 (P12) independent experiments. Mean fluorescence intensities (± SEM), number of cells analyzed and patient numbers are depicted in **Table 1**. (**B**) The Western blot shows the decrease in fully assembled CI in one of the patient cells lines (P4).

Table 1. Characteristics of the complex I deficient fibroblast cell lines

CELL LINE [$]	AFFECTED SUBUNIT AND MUTATION	CLINICAL PHENOTYPE [%]	PN [ϕ]	CI ACTIVITY [#]	SUPEROXIDE PRODUCTION [&]			
					Nucleus		Mitochondria	
					Untreated	Rotenone	Untreated	Rotenone
CT1 (**#5120**)[†]	None	n.a.	17	113	100±1 (n=526)	237±3 (n=516)	100±1	172±2
CT2 (**#5119**)[†]	None	n.a.	17	105	112±3 (n=89)	237±8 (n=89)	102±2	156±6
CT3 (**#5118**)[†]	None	n.a.	21	103	102±2 (n=126)	229±5 (n=127)	98±3	172±5
CT4 (**#4996**)[†]	None	n.a.	10*	n.d.	112±3 (n=95)	283±9 (n=89)	100±3	182±5
CT5 (**#223V**)[†]	None	n.a.	8*	103	112±3 (n=94)	286±6 (n=90)	99±3	175±4
CT6 (**#5117**)[‡]	None	n.a.	15	223	99±4 (n=92)	n.d.	92±3	n.d.
CT7 (**#5503**)[‡]	None	n.a.	6*	20	91±3 (n=98)	n.d.	93±3	n.d.
P1 (**#5171**)	**NDUFV1**-R59X/T423M	MLM/LL	18	**73**	**214±7** (n=84)	405±10 (n=87)	**186±6**	281±7
P2 (**#5866**)	**NDUFV1**-R59X/T423M	MLM/LL	18	**64**	117±4 (n=61)	244±8 (n=58)	110±3	167±8
P3 (**#6173**)	**NDUFS1**-D618N/R577X	L/LD	13*	**31**	**207±5** (n=83)	271±8 (n=71)	**176±4**	205±6
P4 (**#5170**)	**NDUFS2**-R228Q	HCEM	11*	**39**	**229±7** (n=66)	331±12 (n=69)	**205±8**	243±8
P5 (**#5067**)	**NDUFS2**-P229Q	HCEM	10*	**36**	**331±10** (n=100)	528±15 (n=108)	**264±9**	356±10
P6 (**#4605**)	**NDUFS2**-S413P	HCEM	15*	**40**	**301±21** (n=40)	378±18 (n=47)	**218±13**	272±17
P7 (**#5077**)	**NDUFS4**-W97X	L/LL	23*	**59**	**170±4** (n=100)	339±11 (n=95)	**142±4**	232±7
P8 (**#5260**)	**NDUFS4**-R106X	L/LL	12	**36**	**196±10** (n=64)	293±8 (n=68)	**174±8**	203±6
P9 (**#4827**)	**NDUFS4**-R106X	L/LL	7*	**58**	**238±8** (n=93)	398±13 (n=93)	**196±6**	252±9
P10 (**#5737**)	**NDUFS4**-VPEEHI67/VEKSIstop	L/LL	12	**53**	**150±4** (n=92)	228±6 (n=87)	**131±4**	166±5
P11 (**#4608**)	**NDUFS4**-K158fs	L/LL	18*	**75**	**207±5** (n=106)	377±9 (n=102)	**195±6**	270±7
P12 (**#5175**)	**NDUFS7**-V122M	L/LL	15*	**68**	**161±4** (n=94)	322±9 (n=95)	**151±5**	209±7
P13 (**#6603**)	**NDUFS8**-R94C	L/LL	15	**18**	**263±7** (n=147)	375±9 (n=126)	**222±7**	267±8
P14 (**#4611**)	Unknown	L/LL	14*	**36**	**395±27** (n=36)	581±39 (n=40)	**265±19**	330±28
P15 (**#5409**)	Unknown	FILA	6*	**45**	**265±11** (n=104)	425±22 (n=65)	**262±11**	340±20
P16 (**#4591**)	Unknown	UEM	6*	**39**	**189±5** (n=79)	377±15 (n=60)	**159±5**	234±11
P17 (**#4554**)	Unknown	L/LL	6*	**42**	**175±6** (n=60)	286±11 (n=56)	**145±7**	192±8
P18 (**#4590**)	Unknown	FILA	8*	**60**	**217±7** (n=70)	401±13 (n=59)	**204±7**	315±15
P19 (**#4606**)	Unknown	FILA	6*	**63**	**197±9** (n=42)	302±18 (n=45)	**177±10**	237±14
P20 (**#4617**)	Unknown	L/LL	3*	**85**	127±5 (n=56)	217±6 (n=64)	131±6	174±7
P21 (**#5671**)	Unknown	L/LL	10	**27**	**331±18** (n=38)	402±22 (n=34)	**241±15**	282±16

[$]Numbers indicate the designation of the cell lines within the Nijmegen Centre for Mitochondrial Disorders (NCMD). CT and P indicate control and patient cell lines, respectively. [%]FILA: Fatal infantile lactic acidosis, HCEM: Hypertrophic cardiomyopathy and encephalomyopathy, L/LD: Leigh syndrome and leukodystrophy, L/LL: Leigh syndrome and Leigh-like syndrome, MLM: Macrocephaly, leukodystrophy and myoclonic epilepsy, UEM: Unspecified encephalomyopathy. [ϕ]PN: passage number, an asterisk indicates the passage number after arrival at the Nijmegen Center for Mitochondrial disorders. [#]CI activity is measured in mitochondrial enriched fractions and expressed as % of lowest control. [&]Mean (± SEM) nuclear and mitochondrial fluorescence intensity expressed as percentage of untreated control #5120 (CT1) for the number of cells between brackets. Each cell line was tested on at least two days. Values in bold are below lowest control value (CI activity) or significantly different ($p<0.05$) from highest control (CT2; superoxide production). Rotenone indicates acute treatment with 100 nM rotenone during HEt incubation (10 min, 37° C). [†]Cells obtained from healthy adults. [‡]Cells obtained from healthy age-matched children. **Abbreviations:** n.a., not appropriate, n.d., not determined.

Chapter V

DISCUSSION

Malfunction of the OXPHOS system causes a wide range of neuromuscular, cardiac, and endocrine disorders and, more recently, has also been implicated in age-related diseases and various forms of cancer (242,291,302). In 40% of the cases of inherited OXPHOS disease, the deficiency is associated with an isolated (25%) or combined (15%) defect in CI, the first and largest complex of the OXPHOS system (246). At present, however, there is only very limited information about the cytopathological effects of a disease-causing reduction in CI activity. Here, we quantitatively assessed superoxide production in living skin fibroblasts of a large cohort of 21 patients with inherited isolated CI deficiency, 13 of which with an established mutation in one of the nuclear-encoded CI subunits and 8 in which the disease causing mutation still has to be established, and demonstrate an inverse relationship with the amount and residual activity of this complex. The same inverse relationship between superoxide production and CI activity was observed in healthy fibroblasts treated with increasing concentrations of rotenone. In the latter case, however, the amount of CI increased rather than decreased, indicating that superoxide production can increase in the absence of any mutated subunit. Based on the latter finding we conclude that in isolated human CI deficiency increased cellular superoxide production is primarily a consequence of decreased cellular CI activity and not of further electron leakage due to the presence of a mutated subunit.

In healthy cells, the vast majority (>90%) of reactive oxygen species is produced as a consequence of oxidative phosphorylation (14,68). Work on isolated mitochondrial preparations suggests that CI and CIII are the major contributors to superoxide production (14,68,209). In addition, CII can contribute by donating electrons to CI via reverse electron flow (144,154). As far as CI is concerned, single electron reduction of oxygen can occur at the FMN binding site, the iron-sulfur clusters and/or the Q-binding site (12,47,84,144,154,186). Evidence has been provided that superoxide produced by CI is released into the mitochondrial matrix, whereas that produced by CIII enters both the matrix and the intermembrane space (144). It has been demonstrated that reverse electron flow can be effectively blocked by CI inhibitors, leading to a reduction in superoxide production. Here we show that in all patient cell lines acute addition of rotenone increased rather than decreased the amount of HEt oxidation products, indicating that reverse electron flow is not the underlying cause of increased superoxide production in isolated human CI deficiency.

In addition to CI and CIII, the tricarboxylic acid cycle enzyme α-ketoglutarate dehydrogenase can produce significant amounts of superoxide, especially under conditions that the NADH level in the matrix is increased (267). Moreover, other organelles, such as the endoplasmic reticulum and peroxisomes, may contribute to the production of superoxide (reviewed in (108)). Because HEt oxidation products can easily pass mitochondrial membranes, the method used here to measure cellular superoxide production does not allow to make a statement concerning the exact site(s) of HEt oxidation. Whatever the case may be, the present finding that chronic rotenone decreased the activity of CI and increased the amount of HEt oxidation products with virtually the same potency indicates that a reduction in mitochondrial CI activity is associated with an increase in cellular superoxide production. Importantly, because the inhibitor increased rather than decreased the amount of fully assembled CI, it can be concluded that the observed increase in superoxide production was not due to misassembly of the complex.

The same correlation between cellular superoxide production and residual CI activity was observed within our large cohort of CI deficient patient cell lines. In this case, however, the decrease in residual activity was quantitatively correlated with a decrease in fully assembled CI. In agreement with our results, the NDUFS1-Q522K mutation has recently been published to be associated with a marked reduction in CI amount and activity and a significant increase in mitochondrial superoxide and derived reactive oxygen species (116). Taken together, the present findings may provide first insight into the mechanism of superoxide production in human CI deficiency in that they suggest that decreasing numbers of active complexes produce increasing amounts of superoxide not because of the presence of a mutated subunit but as a consequence of a decrease in cellular CI activity. The alternative explanation that increasing numbers of partially assembled complexes are responsible for the observed increase in superoxide production is not supported by the present finding that chronic rotenone treatment increased rather than decreased the amount of fully assembled CI.

The cohort of patient cell lines used in this study included 13 cell lines with established mutations in nuclear-encoded CI subunits (see, **Table 1**). All 6 affected subunits are predicted to constitute part of the matrix-protruding arm of CI (35). Five of them, NDUFV1 (51-kDa), NDUFS1 (75-kDa), NDUFS2 (49-kDa), NDUFS7 (PSST) and NDUFS8 (TYKY), belong to the group of 14 “central” subunits that are sufficient to perform all bioenergetic functions of the complex, whereas the remaining one, NDUFS4 (AQDQ), belongs to the large group of accessory proteins. Except for NDUFS2, the other 4 “central” subunits carry

iron-sulfur clusters responsible for electron transport from NDUFV1, where NADH is oxidized, to NDUFS7, where ubiquinone is reduced. With the exception of 5 cell lines carrying a mutation in NDUFS4 (see below), 7 (P6 was not analyzed) of the other 8 cell lines displayed a fully assembled complex on a blue-native gel, the amount of which was decreased to a variable degree. Irrespective of the affected subunit, this amount was quantitatively correlated with the cell's residual CI activity, indicating that primarily the expression of the fully assembled complex rather than its intrinsic activity is altered. This conclusion is in agreement with our proposal that the increase in cellular superoxide production is not a direct consequence of further electron leakage from complexes containing a mutated subunit, but of the decrease in cellular CI activity. Importantly, when patient cells were acutely treated with rotenone, superoxide production was even further increased. This indicates that the rotenone-binding site, which is part of the coenzyme Q binding site (14,188), is intact in these CI deficient patients.

Regarding the 5 patient cell lines carrying a mutation in NDUFS4, they all showed a rotenone-sensitive CI activity when assayed in a mitochondrial enriched fraction. On the other hand, all 5 cell lines showed only an inactive subcomplex on a blue-native gel. Previous work revealed the complete absence of any NDUFS4 in patient cell lines P7 and P11 (223). Together with the information that the other 3 patient cell lines of the present study are either homozygous for a premature stop codon (P8 and P9) or carry a premature stop codon and a frameshift (P10) and, therefore, do not express any NDUFS4, these results indicate that in the absence of NDUFS4 catalytically active complexes are formed, which are, however, relatively unstable and fall apart during blue-native electrophoresis. Analysis of the amount of subcomplex as a measure of the amount of catalytically active complex in the mitochondrial enriched fraction then shows that also in these patient cells significantly less catalytically active complex is formed. In contrast to the present study, it was recently shown that fibroblasts of a patient with a nonsense mutation in the first exon of the *NDUFS4* gene (NDUFS4-W15X) produced normal amounts of superoxide (116). Similarly, the present study demonstrates that superoxide production can be increased (P1) or normal (P2) in fibroblasts of two CI deficient brothers. Both cell lines showed the same decrease in fully assembled CI and residual CI activity. These findings indicate that additional factors, such as detoxifying enzymes and nonenzymatic antioxidants, play a role in determining net superoxide production. The involvement of such factors is also evident from the large variation in superoxide production at any given residual CI activity (**Fig. 2**).

Finally, our results partially agree with earlier work showing that superoxide generation was increased in 5 CI deficient patients, whereas it was not different from control or even lower than control in another 8 patients (204). Moreover, in contrast to the latter study, we found no correlation between the rate of superoxide production and clinical phenotype (depicted in **Table 1**). At present, we have no explanation for these discrepancies. Major differences are the use of living fibroblasts rather than frozen-thawed mitochondria and the use of HEt instead of the chemiluminescent probe lucigenin. Both studies had only two clinical phenotypes in common, Leigh's Disease (LD) and Fatal Infantile Lactic Acidosis (FILA). In both studies, the LD patients showed an increase in superoxide, whereas the two FILA patients investigated in the earlier study showed either a decrease or no change in superoxide production. Our study did not include patients displaying Cardiomyopathy with Cataracts and Hepatomegaly with Renal Tubulopathy, shown in the previous study to have a decreased and normal rate of superoxide production, respectively. Obviously, evaluation of these latter clinical phenotypes is required to be confident that under all conditions of isolated CI deficiency a decrease in CI activity is associated with an increase in cellular superoxide production.

In accordance with the above findings, antioxidants were found to improve OXPHOS function in superoxide dismutase 2 null mice (102) and fibroblasts of Parkinson's disease patients (296). Furthermore, chronic antioxidant treatment was shown to increase CV activity and ATP synthesis in cybrids containing the mtDNA of patients with the T8993G mtDNA mutation associated with impaired oxidative phosphorylation in NARP (neuropathy, ataxia and retinitis pigmentosa) and MILS (maternally inherited Leigh's syndrome) (166). Likewise, chronic oral administration of high concentrations of vitamin E was found to prevent the loss of mitochondrial function and reduce protein and lipid oxidation in brain and liver of aging mice (180). These beneficial effects were paralleled by an increased lifespan, better neurological performance and higher exploratory activity. Regarding human CI deficiency, patients have been found to respond differentially to antioxidant treatment (e.g. ref. (193)).

Acknowledgements: This work was supported by equipment grants of ZON (Netherlands Organization for Health Research and Development, No: 903-46-176) and NWO (Netherlands Organization for Scientific Research, No: 911-02-008), and the European Community's sixth Framework Programme for Research, Priority 1 "Life sciences, genomics and biotechnology for health", contract number LSHM-CT-2004-503116.

CHAPTER VI

Mitochondrial and cytosolic redox environment are not detectably altered in isolated human NADH:ubiquinone oxidoreductase deficiency

Sjoerd Verkaart[a,b,d,e]
Werner J.H. Koopman[a,c,d]
Julia Cheek[a,d]
Sjenet E. van Emst-de Vries[a,d]
Lambertus W.P.J. van den Heuvel[b,d,e]
Jan A.M. Smeitink[b,d,e]
Peter H.G.M. Willems[a,c,d]

[a]Department of Membrane Biochemistry, [b]Department of Pediatrics, [c]Microscopical Imaging Centre, [d]Nijmegen Centre for Molecular Life Sciences (NCMLS), [e]Nijmegen Centre for Mitochondrial Disorders (NCMD), Department of Pediatrics, Radboud University Nijmegen Medical Centre

BBA Molecular Mechanisms of Disease, **2007**, ***in press***

ABSTRACT

Isolated complex I (CI) deficiency is the most common enzymatic defect of the oxidative phosphorylation system, causing a wide range of clinical phenotypes including macrocephaly with progressive leukodystrophy, nonspecific encephalopathy, (cardio)myopathy, liver disease, Leigh and Leigh-like syndrome, Leber hereditary optic neuropathy, and some forms of Parkinson disease. We previously reported that cellular superoxide levels are significantly increased in skin fibroblasts of all but one patient (P2 of this study) with nuclear-inherited CI deficiency. Using video-rate confocal microscopy of cells loaded with CM-H_2DCF, we here show a similar increase in superoxide-derived ROS levels. Despite this increase, video microscopy of cells expressing mitochondria-targeted reduction-oxidation sensitive GFP1 (roGFP1) showed no detectable changes in mitochondrial and/or cytosolic thiol redox state. Similarly, neither the glutathione (GSH) nor the glutathione disulfide (GSSG) content differed significantly between patient and healthy control cells. Finally, video-rate confocal microscopy of cells loaded with C11-BODIPY$^{581/591}$ demonstrated that the extent of lipid peroxidation, regarded as a readout of oxidant damage, was not altered in patient fibroblasts. Our results indicate that cultured skin fibroblasts of patients with nuclear-inherited CI deficiency maintain a normal thiol redox state, which is the predominant determinant of the cellular redox environment, even though oxidant levels are markedly increased.

INTRODUCTION

NADH:ubiquinone oxidoreductase or complex I (CI; EC 1.6.5.3.) is the main entry point of metabolic electrons into the mitochondrial electron transport system and its proper function is essential for the adequate production of ATP. In accordance with this function, defects in CI have been found to be associated with a wide range of human disorders including early onset, fatal clinical phenotypes such as Leigh and Leigh-like syndrome, encephalomyopathy and cardiomyopathy (246). In mammals, CI consists of 38 nuclear-encoded and seven mitochondrial-encoded subunits, together having a molecular weight close to 1 MDa (44,45,83). As far as the nuclear genome is concerned, disease-causing mutations have been identified in nine CI subunits (22,40,120,130) and the CI assembly factor B17.2L (185). At the cellular level, these disease-causing mutations were demonstrated to decrease the amount of catalytically active complex (271). Live cell studies revealed that this decrease in CI-specific NADH-oxidizing capacity was associated with disturbed Ca^{2+} and ATP handling (281,283), increased superoxide and derived reactive oxygen species (ROS) levels (116,279) and altered mitochondrial morphology (139). In healthy cells, the large majority of ROS are generated as a consequence of oxidative phosphorylation (OXPHOS; (14,68)). It has been suggested that these OXPHOS-derived ROS play an important signaling role in gearing mitochondrial and cellular physiology for one another (80,153). Of pathological relevance, however, disturbances of the delicate balance between ROS production and ROS scavenging, may lead to cellular injury and, eventually, death (117,209).

The cell's redox environment is crucial in integrating multiple metabolic, signaling and transcriptional processes (153). Because of the high intracellular glutathione concentration (1-11 mM), the glutathione disulfide (GSSG)-glutathione (GSH) redox couple is widely believed to be the major determinant of the cell's redox environment (226,297). Glutathione can either directly react with ROS or function as electron donor for peroxidases (111,297).

In the present study, we used organelle-targeted variants of the reduction-oxidation sensitive green fluorescent protein 1 (roGFP1; (64,95)) to determine the subcellular redox environment in cultured skin fibroblasts of 10 patients with disease-causing mutations in nuclear-encoded CI subunits. It was found that, despite a large increase in superoxide and derived ROS levels, the subcellular redox environment was not detectably altered as compared to healthy control. In agreement with this result, no significant changes in total cellular glutathione content, GSSG to GSH ratio and extent of lipid peroxidation were observed.

MATERIALS AND METHODS

Patient skin fibroblasts – Fibroblasts were derived from skin biopsies of ten patients in the age range of 0-5 years (P1-P10) in whom an isolated NADH:ubiquinone oxidoreductase deficiency was confirmed in both muscle tissue and cultured fibroblasts and ten healthy subjects, five adults (CT1-CT5) and five age-matched children (CT6-CT10), following informed consent and according to relevant institutional review boards (**table 1**). Genetic characterization revealed disease-causing mutations in either the *NDUFV1* (P1-P2), *NDUFS1* (P3), *NDUFS2* (P4-P5), *NDUFS4* (P6-P8), *NDUFS7* (P9) or *NDUFS8* (P10) gene of CI (120). None of the patients harbored mitochondrial DNA mutations previously associated with CI deficiency. Measurement of CI activity was performed in a mitochondrial-enriched fraction obtained from cultured skin fibroblasts as described previously (245). The activity of the complex was normalized against that of complex IV (cytochrome *c* oxidase), which was measured in the same fraction, and expressed as percentage of lowest control (110 mU/U cytochrome *c* oxidase; (245)). Fibroblasts were cultured in medium 199 with Earle's salt supplemented with 10% (v/v) fetal calf serum, 100 IU/ml penicillin and 100 IU/ml streptomycin in a humidified atmosphere of 95% air and 5% CO_2 at 37^o C. Initial passage numbers are given in Verkaart et al., 2007 and measurements were performed within 5 passages. Cell cycle analysis revealed no differences between the various cell lines (139).

Quantification of intracellular superoxide and derived reactive oxygen species levels – Quantitative determination of intracellular superoxide and derived reactive oxygen species levels was performed as described previously (136,137,277). For measurement of intracellular superoxide levels, fibroblasts, grown to ~70% confluence on glass coverslips (Ø 24 mm), were incubated in a HEPES-Tris medium (132 mM NaCl, 4.2 mM KCl, 1 mM $CaCl_2$, 1 mM $MgCl_2$, 5.5 mM D-glucose and 10 mM HEPES, pH 7.4) containing 10 µM hydroethydine (HEt) for exactly 10 min at 37° C. During this period, non-fluorescent HEt enters the cell, where it is converted by superoxide into two fluorescent products, 2-hydroxyethidium and ethidium. After thorough washing to remove non-oxidized HEt, coverslips were mounted in an incubation chamber placed on the stage of an inverted microscope (Axiovert 200 M, Carl Zeiss, Jena, Germany) equipped with a Zeiss 40x/1.3 NA Plan NeoFluar objective. Cells were excited at 490 nm using a monochromator (Polychrome IV, TILL Photonics, Gräfelfing, Germany) and fluorescence emission light was directed by a 525DRLP dichroic mirror (Omega Optical Inc., Brattleboro, VT, USA) through a 565ALP

emission filter (Omega Optical Inc.) onto a CoolSNAP HQ monochrome CCD-camera (Roper Scientific, Vianen, The Netherlands). The imaging setup was controlled by Metafluor 6.0 software (Molecular Devices Corporation, Downingtown, PA, USA). Routinely, 10 fields of view were analyzed per coverslip using an image capturing time of 100 milliseconds. The mean fluorescence intensity was determined in an intracellular region of interest and, for purpose of background correction, an extracellular region of identical size. Quantitative image analysis was performed with Metamorph 6.0 (Molecular Devices Corporation). In each experiment, the average value obtained with healthy fibroblasts was set at 100%, to which all other values were related.

For measurement of superoxide-derived reactive oxygen species levels, fibroblasts were incubated in HEPES-Tris medium containing 1 µM CM-H_2DCFDA for 10 min at 37° C. During this period, the acetate groups are cleaved off by the action of intracellular esterases yielding CM-H_2DCF (dichlorodihydrofluorescein), which is successively oxidized by cytosolic reactive oxygen species to form the highly fluorescent product CM-DCF (dichlorofluorescein). After thorough washing to remove non-hydrolyzed CM-H_2DCFDA, the increase in CM-DCF fluorescence intensity was monitored as a function of time using a video-rate confocal microscope (Oz; Noran Instruments, Middleton, WI, USA) attached to an inverted microscope (Nikon, Diaphot, Tokyo, Japan) equipped with a 40x oil immersion planapochromat objective (NA 1.4; Nikon). Cells were excited with light from an argon ion laser (488 nm; Omnichrome, Chino, CA, USA) and fluorescence emission light was directed by a 500 nm LP barrier filter (Chroma Technology Corp., Rockingham, VT, USA) onto a photomultiplier tube (Hamamatsu Photonics, Bridgewater, NJ, USA). After background correction, the rate of CM-DCF formation was calculated from the slope of the line fitted to the fluorescence intensity versus time. In each experiment, the average value obtained with healthy fibroblasts was set at 100%, to which all other values were related.

Quantification of cytosolic and mitochondrial redox environment – cDNA's encoding roGFP1 and mitochondria-targeted roGFP1 (64,95) were digested from a pEGFP-N1 vector backbone using *Eco*RI/*Xba*I and *Nde*I/*Xba*I, respectively. For expression in mammalian cells, inserts were ligated into a modified pFastbacdual transfer vector (283). RoGFP1 contains surface-exposed cysteine residues that form disulfide bonds upon oxidation. The fluorescence emission ratio after excitation at 400 nm (oxidized state) and 480 nm (reduced state) is a measure of the ambient redox potential (64,95). The ratiometric nature of the probe minimizes errors associated with changes in roGFP1 expression, photobleaching, and

variations in cell thickness (95). Moreover, roGFP1 fluorescence is pH-independent, which allows comparison of roGFP1 signals between the cytosolic and the more alkaline mitochondrial matrix (68). For roGFP1 experiments, human skin fibroblasts, seeded on glass coverslips (Ø 24 mm), were cultured for 24 h, infected with the appropriate baculovirus and cultured for another 48h. Immediately prior to fluorescence measurement, fibroblasts were transferred to HEPES-Tris medium and coverslips were mounted in an incubation chamber placed on the stage of an inverted microscope (Axiovert 200 M) equipped with a Zeiss 40x/1.3 NA Plan NeoFluar objective. RoGFP1 was alternately excited at 400 and 480 nm using a monochromator (Polychrome IV) and fluorescence emission light was directed by a 525DRLP dichroic mirror (Omega Optical Inc.) through a 535DF25 emission filter (Omega Optical Inc.) onto a CoolSNAP HQ monochrome CCD-camera (Roper Scientific). The imaging setup was controlled by Metafluor 6.0 software (Molecular Devices Corporation). Image capturing time was 300 ms and a pair of images was taken every 5 s. For each wavelength, the mean fluorescence intensity was monitored in an intracellular region and, for purpose of background correction, an extracellular region of identical size. After equilibration for 3 min, cells were successively treated with 1 mM hydrogen peroxide (100% oxidation) and 10 mM dithiothreitol (100% reduction). Quantitative image analysis was performed with Metamorph 6.0 (Molecular Devices Corporation). After background correction, the fluorescence emission ratio after excitation at 400 nm (oxidized state) and 480 nm (reduced state) was calculated and the percentage oxidation was determined. In each experiment, the average value with healthy fibroblasts was set at 100%, to which all other values were related.

Determination of GSSG and GSH content in whole-cell homogenates – Preparation of cell extracts and measurement of cellular GSSG and GSH content were performed using HPLC as described previously (57). Values were expressed as nmol/mg protein.

Quantification of the intracellular extent of lipid peroxidation – Measurement of the extent of lipid peroxidation was performed as described before (136). Briefly, fibroblasts, grown to ~70% confluence on glass coverslips, were incubated in HEPES-Tris medium containing 4 µM C11-BODIPY$^{581/591}$ for 30 min at 37° C. Upon oxidation, the red emitting form of the dye (595 nm) is converted into a green emitting form (520 nm). After thorough washing, cells were excited at 488 nm and images were collected using the video-rate confocal microscope. Green and red fluorescence emission signals were separated using a 560 DM

dichroic mirror and appropriate band-pass filters (535D20 and 580LP; Chroma). In each experiment, the average of the green to red fluorescence emission ratios obtained with healthy fibroblasts was set at 100%, to which all other values were related.

Data analysis and statistics – Numerical results were visualized using Origin Pro 7.5 (Originlabs, Northampton, MA, USA) and are expressed as means ± SE. Statistical differences between average values were determined using an independent two-population Student's *t*-test (Bonferroni corrected). P-values <0.05 were considered significant.

Chemicals – Culture materials and fluorescent probes were obtained from Invitrogen (Breda, The Netherlands). All other reagents were from Sigma (Zwijndrecht, the Netherlands).

RESULTS

Reactive oxygen species (ROS) levels are increased in patient fibroblasts – Mitochondria-enriched fractions from cultured skin fibroblasts of patients with isolated CI deficiency exhibit a rotenone-sensitive NADH oxidizing capacity that is lower than the lowest control value (**table 1**). In intact fibroblasts, this condition was found to be associated with a significant increase in superoxide level in all but two cell lines of 21 patients (277). To assess whether this increase is accompanied by a change in cytosolic ROS levels, we here loaded fibroblasts with CM-H_2DCF and monitored its oxidation into fluorescent CM-DCF (137). **Table 1** shows that all but one (P2) of the 10 patient cell lines tested exhibited a significant increase in CM-DCF fluorescence. The table furthermore shows that the fibroblasts of P2 also failed to show an increase in superoxide level.

Total cellular glutathione content and GSSG to GSH ratio are not detectably altered in patient fibroblasts – The results obtained thus far show that the large majority of patient cell lines exhibit a marked increase in oxidant levels. This leaves the question of whether and, if so, how the cellular redox environment is altered under these conditions. An important determinant of this environment is the glutathione disulfide (GSSG)-glutathione (GSH) couple (226). To establish whether CI deficiency affects the redox state of this couple, we determined the GSSG and GSH content in whole-cell homogenates of 10 healthy and 10 patient fibroblast cell lines using high performance liquid chromatography. **Table 2** shows that on average neither the GSSG nor GSH content differed significantly between fibroblasts of healthy subjects and CI deficient patients (p values of 0.55 and 0.36, respectively). Similarly, the ratio of GSSG to GSH did not differ between healthy and patient fibroblasts (p=0.12). Together, these results indicate that the overall cellular redox environment is not detectably altered in human CI deficiency.

Quantification of the subcellular redox environment using organelle-targeted roGFP1 – To investigate the possibility that the subcellular redox environment is altered in human CI deficiency, healthy and patient fibroblasts were transduced with recombinant baculoviruses containing the DNA for roGFP1, a redox-sensitive variant of the green fluorescent protein. RoGFP1 was either expressed in the cytosol (cyt-roGFP1) or targeted exclusively to the mitochondrial matrix (mit-roGFP1). Both proteins were readily expressed and their fluorescence was determined in circular regions marked ‘m’ (**Fig. 1A**) and ‘c’ (**Fig. 1B**),

respectively. For background correction, a cell-free region of similar size (marked 'b') was used. **Figure 1C** depicts the ratio of the fluorescence emission intensities after excitation at 400 and 480 nm as a function of time.

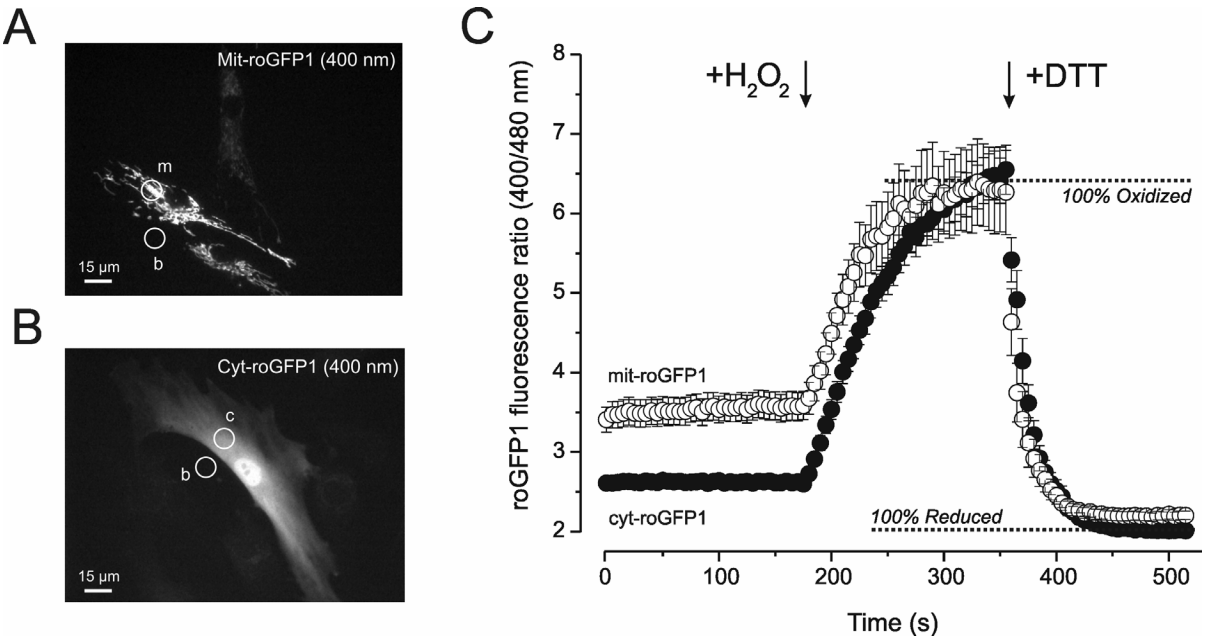

Figure 1: Quantitative measurement subcellular thiol redox state with roGFP1 - (**A**) Fluorescence image (400 nm excitation) of a typical control fibroblast (**table 1**; CT1) transiently expressing the mitochondria-targeted variant of roGFP1 (mit-roGFP1). (**B**) The same following transient expression of the cytosolic variant of roGFP1 (cyt-roGFP1). Circles represent regions of interest used for quantitative measurement of thiol redox state in mitochondrial matrix (m), cytosolic compartment (c) and cell free region used for background correction (b). (**C**) Quantification of the subcellular thiol redox state using 1 mM H_2O_2 (maximal oxidation) and 10 mM DTT (maximal reduction). After background correction, the 400/480 nm fluorescence excitation intensity was calculated. The traces presented depict the average of 42 and 23 cells for mit-roGFP1 and cyt-roGFP1, respectively. Note that roGFP1 is more oxidized in the mitochondrial matrix.

To establish the extent of roGFP1 oxidation, ratio signals were calibrated by successive treatment with 1 mM hydrogen peroxide (H_2O_2) and 10 mM dithiothreitol (DTT) to fully oxidize (100% oxidation) and reduce (0% oxidation) the probe, respectively (95). H_2O_2 gradually increased the fluorescence emission ratio to a maximum reached within 350 s, whereas subsequent addition of DTT rapidly reduced this ratio to below pre-H_2O_2 levels. Higher concentrations of H_2O_2 and DTT caused no further change in fluorescence emission ratio, indicating that the probe was maximally oxidized and reduced, respectively. **Figure 1C** shows that for healthy fibroblasts (**table 1**; CT1), the extent of roGFP1 oxidation was higher in the mitochondrial matrix than in the cytosol.

Chronic rotenone treatment slightly oxidizes the subcellular redox environment in healthy fibroblasts – We previously showed that chronic rotenone treatment dose-dependently reduced the activity of CI in healthy fibroblasts (136). To determine whether CI deficiency could, in principle, alter the subcellular redox environment, healthy fibroblasts (**table 1**; CT1) were treated with 100 nM rotenone for 72 h. This treatment slightly but significantly ($p<0.05$) increased the extent of mit-roGFP1 and cyt-roGFP1 oxidation (**Figs. 2A** and **2B**, respectively). Experiments performed in parallel revealed that chronic rotenone treatment also increased the superoxide level (**Fig. 2C**), whereas, in sharp contrast, it did not affect cytosolic ROS levels (**Fig. 2D**). These results demonstrate that a chronic reduction in CI activity, despite causing a substantial rise in superoxide level, only slightly oxidizes the subcellular redox environment in healthy fibroblasts.

RoGFP1 oxidation is not altered in patient fibroblasts – To establish whether CI deficiency is associated with a change in subcellular redox environment, fibroblasts of 10 healthy subjects and 10 patients were transduced with mit-roGFP1 and cyt-roGFP1 and analyzed as described above. In all cases, mit-roGFP1 was significantly more oxidized than cyt-roGFP1 (**table 2**). Unexpectedly, however, no significant differences in mitochondrial and/or cytosolic roGFP1 oxidation were observed between healthy and CI deficient cell lines. This result shows that CI deficiency is not associated with detectable changes in subcellular redox environment.

RoGFP1 oxidation is markedly increased in BSO-treated healthy fibroblasts – To assess the relevance of the GSSG/GSH couple in preserving the subcellular redox environment, healthy fibroblasts (**table 1**; CT1) were cultured in the presence of 12.5 μM L-buthionine-(S,R)-sulphoximine (BSO) for 72 h. BSO is a potent inhibitor of γ-glutamylcysteine synthetase, the rate limiting enzyme in the synthesis of GSH (89), and it has been demonstrated that chronic treatment with this drug effectively depletes GSH (4,77). BSO dramatically increased the extent of roGFP1 oxidation in both mitochondrial matrix (**Fig. 2A**) and cytosolic compartment (**Fig. 2B**). Moreover, it caused a marked decrease in superoxide level (**Fig. 2C**) and, in sharp contrast, a substantial increase in ROS levels (**Fig. 2D**). These findings demonstrate that the GSSG/GSH couple is essential in preserving the subcellular redox environment in human skin fibroblasts.

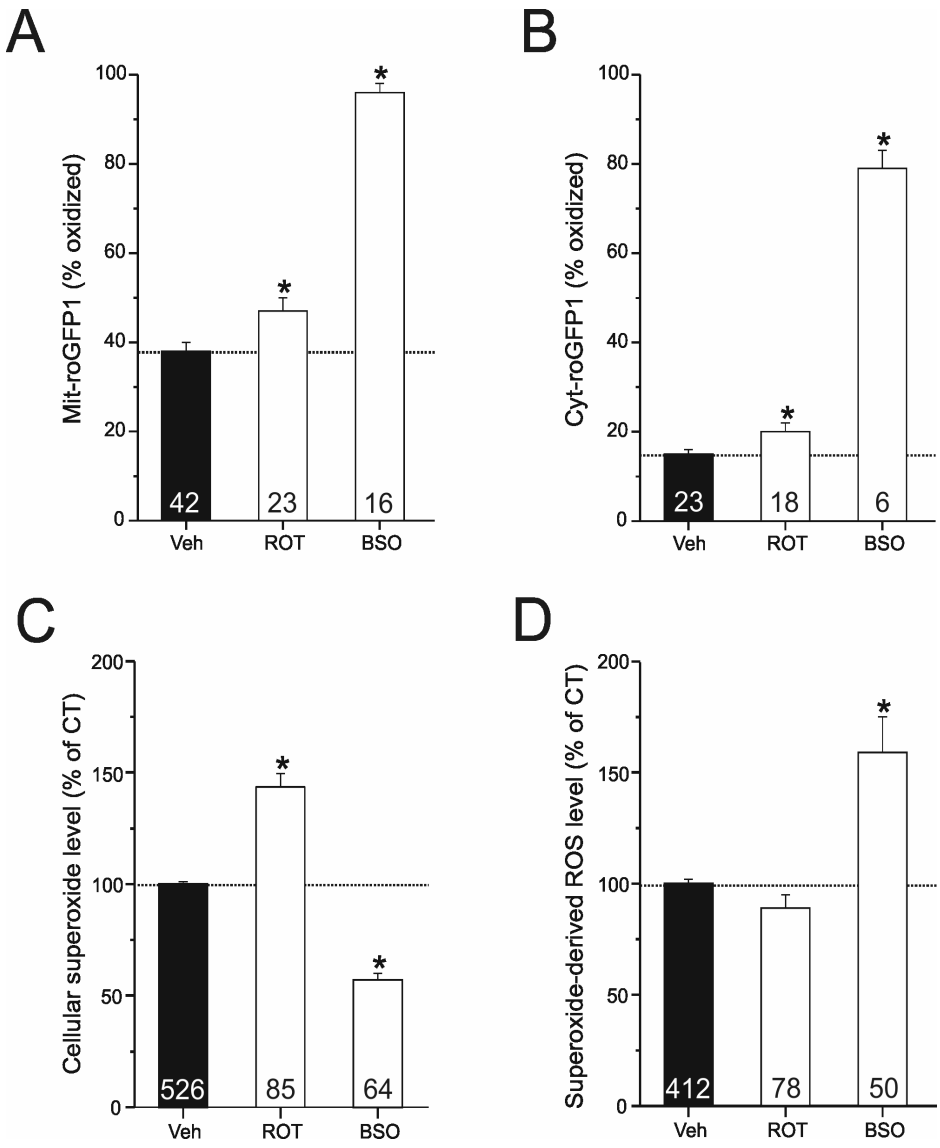

Figure 2: Effect of chronic rotenone and BSO treatment on subcellular thiol redox state and cellular levels of superoxide and derived reactive oxygen species (ROS) - **(A)** CT1 fibroblasts transiently expressing mit-roGFP1 were treated with either rotenone (100 nM) or BSO (12.5 µM) for 72 h. After background correction, the 400/480 nm fluorescence excitation intensity was calculated and expressed as percentage oxidized. **(B)** The same for CT1 fibroblasts transiently expressing cyt-roGFP1. **(C)** CT1 cells chronically treated with either rotenone or BSO were incubated with 10 µM hydroethidine (HEt) for 10 min at 37^{o} C, thoroughly washed to remove non-oxidized dye and subsequently analyzed using digital imaging microscopy for quantification of the fluorescent oxidation products formed during the 10-min incubation period with HEt. The fluorescence emission intensity obtained with vehicle-treated CT1 cells is set at 100%, to which all other values are related. **(D)** CT1 cells chronically treated with either rotenone or BSO were incubated with 1 µM CM-H_2DCFDA for 10 min at 37 °C, thoroughly washed to remove non-hydrolyzed dye and subsequently subjected to video-rate confocal microscopy for quantitative analysis of superoxide-derived ROS levels. The rate of fluorescence increase obtained with vehicle-treated CT1 cells is set at 100%, to which all other values are related. Numerals indicate the number of cells analyzed. *, significantly different from vehicle-treated control (P<0.05).

The extent of lipid peroxidation is not altered in patient fibroblasts – We previously showed that chronic rotenone treatment (100 nM, 72 h) significantly increased the extent of lipid peroxidation in healthy fibroblasts and that this effect of the inhibitor was abolished by the mitochondria-targeted antioxidant mitoquinone (136). Here, we used the same measuring protocol but could not detect any difference in the extent of lipid peroxidation between patient cell lines and cell lines of healthy subjects (**table 1**).

Table 1. Cellular oxidant levels and degree of lipid peroxidation in patient and control fibroblasts

CELL LINE[$]	AFFECTED SUBUNIT AND MUTATION[‡]	CI ACTIVITY[#]	CELLULAR SUPEROXIDE LEVEL[&]	SUPEROXIDE-DERIVED ROS LEVEL[&]	DEGREE OF LIPID PEROXIDATION[‡‡]
Average CT:		**106±2.4**	**100±0.66**	**108±8.33**	**115±10**
CT1 (**#5120**)	None	113	100±1 (n=526)	100±2 (n=412)	100±3 (n=99)
CT2 (**#5119**)	None	105	102±2 (n=89)	100±11 (n=48)	135±5 (n=112)
CT3 (**#5118**)	None	103	98±3 (n=126)	125±13 (n=61)	110±4 (n=108)
CT4 (**#4996**)	None	n.d.	100±3 (n=95)	n.d.	n.d.
CT5 (**#223V**)	None	103	99±3 (n=94)	n.d.	n.d.
Average P:		**49±6.3**	**181±14.0**	**223±20.8**	**112±4**
P1 (**#5171**)	**NDUFV1-**R59X/T423M	**73**	**186±6** (n=84)	**242±19** (n=78)	92±3 (n=73)
P2 (**#5866)**	**NDUFV1-**R59X/T423M	**64**	110±3 (n=61)	135±12 (n=49)	123±3 (n=108)
P3 (**#6173**)	**NDUFS1-**D618N/R577X	**31**	**176±4** (n=83)	**171±13** (n=87)	109±3 (n=74)
P4 (**#5170**)	**NDUFS2-**R228Q	**39**	**205±8** (n=66)	**169±7** (n=124)	115±4 (n=101)
P5 (**#5067**)	**NDUFS2-**P229Q	**36**	**264±9** (n=100)	**351±41** (n=28)	115±5 (n=64)
P6 (**#5260**)	**NDUFS4-**R106X	**36**	**174±8** (n=64)	**187±12** (n=160)	127±4 (n=64)
P7 (**#5737**)	**NDUFS4-**VPEEHI67/VEKSIstop	**53**	**131±4** (n=92)	**202±12** (n=98)	115±4 (n=81)
P8 (**#4608**)	**NDUFS4**-K158fs	**75**	**195±6** (n=106)	**289±46** (n=29)	123±5 (n=76)
P9 (**#5175**)	**NDUFS7**-V122M	**68**	**151±5** (n=94)	**212±15** (n=76)	87±3 (n=99)
P10 (**#6603**)	**NDUFS8**-R94C	**18**	**222±7** (n=147)	**275±20** (n=117)	111±3 (n=90)

[$]Numbers indicate the designation of the cell lines within the Nijmegen Centre for Mitochondrial Disorders (NCMD).
CT and P indicate control and patient cell lines, respectively.
[‡]Mutations are given at the protein level, the affected CI subunit indicated in bold.
[#]Enzymatic activities were measured in mitochondria-enriched fractions and expressed as % of the lowest control value (110 mU/U cytochrome c oxidase).
[&]Cellular superoxide levels were determined previously and are expressed as % of CT1 (**Verkaart, 2007**).
[‡‡]Lipid peroxidation was determined using C11-BODIPY$^{581/591}$ (**Koopman, 2005**) and expressed as % of CT1.
Statistics: Values in bold are below the lowest control value (CI activity) or significantly different ($p<0.05$) from highest control (superoxide level, superoxide-derived ROS level). Values between brackets represent the number of individual cells analyzed on at least two days.

Table 2. Cellular thiol redox status in patient and control fibroblasts

CELL LINE[$]	MIT-ROGFP1[@]	CYT-ROGFP1[@]	GSH+GSSG[&]	GSSG[&] (OXIDIZED)	GSH[&] (REDUCED)	GSSG/GSH
Average CT:	**44.6±2.16**	**17.6±1.25**	**26.9±1.8**	**0.793±0.033**	**26.1±1.8**	**0.031±0.0020**
CT1 (**#5120**)	38±2 (n=42)	15±1 (n=23)	25.1	0.911	24.2	0.038
CT2 (**#5119**)	48±4 (n=24)	20±3 (n=14)	25.4	0.722	24.7	0.029
CT3 (**#5118**)	44±4 (n=22)	14±2 (n=11)	28.0	0.831	27.1	0.031
CT4 (**#4996**)	39±4 (n=21)	20±2 (n=8)	25.7	0.805	24.9	0.032
CT5 (**#223V**)	45±4 (n=18)	18±4 (n=11)	25.6	0.748	24.9	0.030
CT6 (**#MW21**)	49±4 (n=23)	19±3 (n=18)	31.2	0.946	30.3	0.031
CT7 (**#MW25**)	59±4 (n=15)	25±1 (n=12)	26.9	0.749	26.2	0.029
CT8 (**#MW28**)	40±5 (n=11)	19±3 (n=6)	36.3	0.861	35.5	0.024
CT9 (**#MW33**)	48±7 (n=11)	15±4 (n=3)	30.8	0.782	30.0	0.026
CT10 (**#MW35**)	36±6 (n=9)	11±1 (n=10)	14.1	0.577	13.5	0.043
Average P:	**43.3±2.05**	**21.5±1.40**	**24.8±1.4**	**0.830±0.050**	**24±1.4**	**0.035±0.0010**
P1 (**#5171**)	40±3 (n=20)	19±3 (n=23)	29.2	1.014	28.2	0.036
P2 (**#5866)**	44±4 (n=23)	15±1 (n=13)	21.6	0.742	20.9	0.036
P3 (**#6173**)	49±5 (n=14)	20±2 (n=12)	23.0	0.904	22.1	0.041
P4 (**#5170**)	44±5 (n=19)	18±2 (n=14)	27.9	0.783	27.1	0.029
P5 (**#5067**)	36±3 (n=21)	27±2 (n=21)	31.7	0.986	30.7	0.032
P6 (**#5260**)	52±4 (n=22)	26±2 (n=13)	19.4	0.587	18.8	0.031
P7 (**#5737**)	54±3 (n=44)	26±2 (n=31)	19.7	0.732	19.0	0.039
P8 (**#4608**)	40±3 (n=28)	24±3 (n=15)	24.3	0.902	23.4	0.039
P9 (**#5175**)	37±3 (n=20)	16±1 (n=22)	21.9	0.630	21.3	0.030
P10 (**#6603**)	37±3 (n=34)	24±2 (n=29)	29.5	1.017	28.5	0.036

[$]Numbers indicate the designation of the cell lines within the Nijmegen Centre for Mitochondrial Disorders (NCMD).
CT and P indicate control and patient cell lines, respectively.
[@]Data reflects the % of oxidized roGFP1 in the mitochondrion (mit-roGFP1) and cytosol (cyt-roGFP1); values between brackets represent the number of individual cells analyzed on at least four days.
[&]Expressed as nmol/mg protein, determined in two independent experiments

DISCUSSION

In this study, we measured the thiol redox state as an important determinant of the redox environment in both the cytosol and mitochondrial matrix of cultured skin fibroblasts of 10 healthy control subjects and 10 patients with an isolated CI deficiency caused by a mutation in one of the nuclear-encoded subunits of the complex (**table 1**). All but one (P2) of the patient cell lines displayed a marked increase in superoxide and derived ROS levels. Strikingly, however, neither the thiol redox state nor the extent of lipid peroxidation differed significantly between the healthy and patient cell lines.

Cellular ROS levels are increased in inherited CI deficiency – Under normal conditions more than 90% of ROS is generated as a consequence of oxidative phosphorylation (14,68,144,175). In first instance, this involves the production of superoxide and studies with isolated mitochondria indicated that CI and CIII are the major sources of this oxidant (14,68,209). Furthermore, these studies suggested that superoxide produced by CI is released into the mitochondrial matrix, whereas that produced by CIII enters both the matrix and the intermembrane space (144). However, whether CIII contributes to the production of this oxidant in living cells is still debated (184). Although previous work revealed a significant increase in cellular superoxide level in all but one (P2) of the patient cell lines (**table 1**), the method used for its determination precluded any statement about the origin of this oxidant (277). In this context, experimental evidence suggests that under pathological conditions mitochondrial superoxide production may not be confined to CI but may in addition involve α-ketoglutarate dehydrogenase in the mitochondrial matrix (253,267) and monoamine oxidases in the outer mitochondrial membrane (5). Superoxide is rapidly converted into hydrogen peroxide (H_2O_2) by superoxide dismutases present in both the mitochondrial matrix (MnSOD) and cytosolic compartment (CuZnSOD). In agreement with the increase in superoxide level, we observed an increase in cytosolic ROS levels in all but one (P2) of the CI deficient cells lines (**table 1**). Intriguingly, patient 2 is a brother of patient 1 (P1), both harboring exactly the same mutation in the NDUFV1 subunit of CI. We reported before that fibroblast cell lines derived from these two patients show a similar decrease in fully assembled CI and residual CI activity (277). These findings clearly indicate that additional factors play an important role in determining cellular ROS levels. In accordance with this conclusion, fibroblasts of CI deficient patients were demonstrated to express variable amounts of MnSOD (204). The present results are in agreement with recent work showing a

marked elevation in cellular ROS levels in skin fibroblasts of a patient with a mutation in the *NDUFS1* gene (116). In contrast to the latter study, however, we found that cellular ROS levels were increased in fibroblasts of three patients with a mutation in the *NDUFS4* gene. The latter result indicates that the type of mutation in a particular subunit and/or the genetic background of the patient are likely to play a role in the occurrence of a net increase in cellular ROS levels.

Cellular redox environment is not detectably altered in inherited CI deficiency – In the mitochondrial matrix, which is devoid of catalase, H_2O_2 is detoxified by glutathione peroxidase (GPX) (72). The reduction equivalents required for this reaction are provided by the GSSG/GSH redox couple. Importantly, GSH is regenerated from GSSG by glutathione reductase (GR) using NADPH as electron donor (125). It has been suggested that isocitrate dehydrogenase is a major source of NADPH in this compartment (128). In addition, NADH can be converted into NADPH by the action of mitochondrial transhydrogenase (221). In the cytosol, H_2O_2 is removed by the combined action of GPX and catalase. Conditions that increase the production of superoxide and, as a consequence, H_2O_2, will increase the GPX-catalyzed formation of GSSG. Because mitochondria cannot export GSSG to the cytosol (189) and are limited in their ability to synthesize GSH (169), this will lead to a decrease in mitochondrial GSH, if not appropriately balanced by ATP-dependent uptake of GSH from the cytosol (164). In the cytosol, excess GSSG is exported out of the cell, which, if not sufficiently compensated by *de novo* GSH synthesis, will lead to a decrease in total cellular glutathione content. Here, we show that, despite a marked increase in the levels of superoxide and derived ROS, the total cellular glutathione content and the GSSG to GSH ratio are not detectably altered in a large cohort of patient cell lines as compared to a large cohort of healthy control cell lines. In agreement with this result, measurements with roGFP1 revealed no significant differences in thiol redox state between patient and healthy fibroblasts. A similar lack of effect of increased ROS levels on the oxidation state of roGFP1 was observed in EGF-treated NR6 cells (64). Our results disagree with a recent study showing a decrease in total cellular glutathione content in fibroblasts of a patient with a mutation in the *NDUFS1* gene (116). However, the latter study included only one healthy control cell line and we show here that the total cellular glutathione content varied over the same range in both the patient and healthy control group. In agreement with our results, the total cellular glutathione content was found to be unaltered in fibroblasts of a patient with a mutation in the *NDUFS4* gene.

Taken together, our findings show that patient fibroblasts are able to maintain the thiol redox state despite the increased levels of superoxide and derived ROS.

It has been suggested that the redox state of roGFP1 is determined by the reducing capacity of the most important redox buffer within the cell (64). Here, we show that inhibition of GSH synthesis by L-buthionine-(S,R)-sulphoximine (BSO) resulted in virtually complete oxidation of mit- and cyt-roGFP1. This result indicates that the glutathione disulfide (GSSG)-glutathione (GSH) couple is the most important determinant of the cellular redox environment (226). BSO markedly increased cytosolic ROS levels, demonstrating the importance of GSH in oxidant scavenging. At the same time, BSO decreased the superoxide level. Both findings are in agreement with the recent observation that BSO increased the expression of superoxide dismutases (50,79).

Because primary human skin fibroblasts are refractory to most classical transfection methods, we engineered baculoviral vectors for selective expression of roGFP1 in either the cytosol (cyt-roGFP1) or mitochondrial matrix (mit-roGFP1; (140,283). Single cell analysis revealed that in both healthy and patient fibroblasts mit-roGFP1 was significantly more oxidized than cyt-roGFP1 (values of 44% and 20%, respectively). Similar results were obtained with HeLa cells (64,95; values of 33% and 18%, respectively). The finding that the redox environment is more oxidized in the mitochondrial matrix is in accordance with the observation that the vast majority of cellular ROS is produced as a consequence of oxidative phosphorylation (14,68,144,175).

Our results with BSO and rotenone show that the absence of any detectable alteration in cellular redox environment is not due to a lack of sensitivity of roGFP1 because BSO almost completely oxidized this sensor, whereas rotenone, at a concentration shown before to inhibit the activity of CI by approximately 80% (136), only slightly but significantly increased the amount of oxidized roGFP1. Our findings are in agreement with results obtained with an *in vitro* model for Parkinson's disease involving chronic treatment of human neuroblastoma cells with 5 nM rotenone for 4 weeks and showing a significant decrease in cellular GSH content (240). Although at present we have no explanation for the lack of effect of rotenone on cytosolic ROS levels, the results obtained with this potent CI inhibitor substantiate our conclusion that CI deficiency only slightly, if at all, oxidizes the subcellular redox environment in human skin fibroblasts.

Lipid peroxidation is not detectably altered in inherited CI deficiency - When the production of oxidants exceeds the antioxidant capacity of the cell, this may cause damage to lipids, proteins and DNA. Importantly, the extent of damage to a particular target depends, among others, on the type of oxidant involved, the location of the target versus the oxidant, the oxidant to target ratio and the occurrence of repair reactions. It has been demonstrated that inadequate detoxification of H_2O_2 may result in the formation of highly reactive hydroxyl radicals through the classic Fe^{2+}-catalyzed Fenton reaction. As far as human CI deficiency is concerned, experimental evidence suggests that this condition may indeed lead to an increased production of this radical and consequent increase in the extent of lipid peroxidation (160). In accordance with these results, we demonstrated that chronic treatment with rotenone caused a 2-fold increase in the extent of lipid peroxidation (136). Contradictory to these results, however, we now show that the extent of lipid peroxidation is not detectably altered in patient fibroblasts. Together with our conclusion that the GSSG-GSH couple is the most important determinant of the cellular redox environment and our finding that the redox state of this couple is not detectably altered in patient fibroblasts, this finding is compatible with previous conclusions that the presence of sufficient amounts of GSH can prevent the occurrence of oxidant-induced damage (105). In conclusion, the present study demonstrates that cellular superoxide and derived ROS levels are increased complex I deficient human skin fibroblasts but that this condition does not lead to oxidative damage because these cells are able to maintain a normal redox environment.

Acknowledgements: This work was supported by equipment grants of ZON (Netherlands Organization for Health Research and Development, No: 903-46-176), NWO (Netherlands Organization for Scientific Research, No: 911-02-008) and the European Community's sixth Framework Programme for Research, Priority 1 "Life sciences, genomics and biotechnology for health", contract number LSHM-CT-2004-503116. We thank Prof. S.J. Remington (University of Oregon, Eugene, OR, USA) for supplying the cDNA’s encoding redox-sensitive green fluorescent protein 1 and mrs. A. De Graaf-Hess and Dr. H.J. Blom (Dept. of Pediatrics and Neurology, Radboud University Nijmegen Medical Centre) for HPLC measurements.

CHAPTER VII

INHIBITION OF COMPLEX I OF THE ELECTRON TRANSPORT CHAIN CAUSES OXYGEN RADICAL-MEDIATED MITOCHONDRIAL OUTGROWTH

Sjoerd Verkaart[a,b,d,e,%]
Werner J.H. Koopman[a,c,d,%]
Henk-Jan Visch [a,b,d,e]
Francois H. van der Westhuizen[f]
Michael P. Murphy[g]
Lambertus W.P.J. van den Heuvel[b,d,e]
Jan A.M. Smeitink[b,d,e]
Peter H.G.M. Willems[a,c,d]

[a]Department of Membrane Biochemistry, [b]Department of Pediatrics, [c]Microscopical Imaging Centre, [d]Nijmegen Centre for Molecular Life Sciences (NCMLS), [e]Nijmegen Centre for Mitochondrial Disorders (NCMD), Department of Pediatrics, Radboud University Nijmegen Medical Centre, [f]School for Chemistry and Biochemistry, Potchefstroom University for Christian Higher Education, Potchefstroom, South Africa. [g]MRC Dunn Human Nutrition Unit, Cambridge, United Kingdom. [%]These authors contributed equally to this study.

Am.J.Physiol.Cell.Physiol. **2005**, 288(6):C1440-C1450.

ABSTRACT

Recent evidence indicates that oxidative stress is central in the pathogenesis of a wide variety of degenerative diseases, aging, and cancer. Oxidative stress occurs when the delicate balance between production and detoxification of reactive oxygen species is disturbed. Mammalian cells respond to this condition in several ways, among which is a change in mitochondrial morphology. The mechanism underlying this response is still elusive. Here we use rotenone, an inhibitor of complex I of the respiratory chain, which is thought to increase mitochondrial superoxide production, and MitoQ, a mitochondria-targeted antioxidant, to investigate the relationship between mitochondrial superoxide production and morphology change in human skin fibroblasts. Video-rate confocal microscopy of cells pulse-loaded with the mitochondria-specific cation rhodamine 123 (200 μM, 40 seconds) followed by automated analysis of mitochondrial morphology revealed that chronic rotenone treatment (100 nM, 72 hours) caused a significant increase in mitochondrial length and branching without changing the number of mitochondria per cell. Chronic rotenone treatment also caused a 2-fold increase in the extent of lipid peroxidation as was determined by video-rate confocal microscopy of cells loaded with the lipid peroxidation reporter C11-BODIPY$^{581/591}$ (4 μM, 30 minutes). Finally, digital imaging microscopy of cells loaded with hydroethidine (10 μM, 10 minutes), which is oxidized by superoxide to yield fluorescent ethidium, revealed that chronic rotenone treatment caused a 2-fold increase in the rate of superoxide production. MitoQ (10 nM, 72 hours) did not interfere with rotenone-induced ethidium formation but abolished rotenone-induced outgrowth and lipid peroxidation. These findings show that increased mitochondrial superoxide production as a consequence of, for instance, complex I inhibition leads to mitochondrial outgrowth and that MitoQ acts downstream of this oxygen radical to prevent alterations in mitochondrial morphology.

INTRODUCTION

Highly aerobic cells from brain, heart, muscle, liver, kidney and endocrine tissue depend on the ATP-generating capacity of their mitochondria to meet energetic demands. Acute changes in cellular energy consumption are met through feed-back and/or feed-forward regulation of enzymes involved in aerobic ATP production, whereas chronic changes lead to alterations in mitochondrial capacity and/or architecture (11,97,173,174). Marked changes in structure of the cellular mitochondrial network are furthermore observed during differentiation, cellular senescence and apoptosis, whereas subtle rearrangements occur during cellular growth and division (298).

Mitochondria generate ATP through oxidative phosphorylation (OXPHOS) and defects in this system lead to decreased energy production, increased formation of superoxide and derived reactive oxygen species such as hydrogen peroxide and the hydroxyl radical, and the release of death-promoting factors (231,246,290). Defects occur in a wide variety of degenerative diseases, aging, and cancer and primarily affect tissues that have high energy requirements and that are unable to adapt to conditions of reduced mitochondrial energy supply. Cells that can survive under such conditions such as cancer cells show a variety of adaptations including upregulation of glucose transport, glycolysis, and lactate formation (197). At the same time these cells show a marked reduction in mitochondrial content (54) and OXPHOS capacity (244), whereas the mitochondrial reticulum is largely perinuclear (251). Cancer cells that are forced to grow on galactose and glutamine readily switch from anaerobic to aerobic energy production (219). This adaptation is accompanied by an increase in OXPHOS protein, a decrease in mitochondrial matrix pH, a more oxidized matrix redox state, an increase in the amount of cristae but no increase in mitochondrial mass, and a more extended mitochondrial network. Similar observations were initially reached in budding yeast, where a change of substrate induced a 3-fold increase in mitochondrial volume (70). Qualitative and/or quantitative changes in the mitochondrial reticulum are also observed under pathological conditions that are caused by inherited mutations in mitochondrial DNA or in nuclear OXPHOS genes (37,91) and suggest a tight relationship between mitochondrial structure and function (59).

Recent insights suggest that superoxide anions, formed as “by-product” of the oxidative phosphorylation process, may activate specific redox-sensitive signaling pathways (65). Evidence has been provided that these pathways control uncoupling protein-mediated proton conductance (34). In addition, these pathways are implicated in mitochondrial

biogenesis (146,171,172) and regulation of cellular antioxidant capacity (204). Failure to make the appropriate changes is thought to lead to increased oxygen radical production, which, if not properly balanced by the cell's antioxidant mechanisms may cause structural and functional damage to polyunsaturated fatty acids in membrane lipids, proteins, and DNA. There is good evidence that increased oxygen radical formation is the cause of atherosclerosis and possibly also of the major neurodegenerative and chronic inflammatory diseases (92). Moreover, increased radical formation has been implicated in aging (75) and apoptosis (150). However, in the majority of diseases in which tissue damage occurs increased radical formation is regarded as consequence rather than as cause (92). Human mitochondrial complex I (NADH:ubiquinone oxidoreductase; EC: 1.6.5.3) is the largest multisubunit assembly of the OXPHOS system, comprising 39 nuclear encoded and seven mitochondrially encoded subunits (104). Malfunction of this complex is associated with a wide variety of clinical syndromes (246). In order to enhance our understanding of the pathophysiology of these diseases, with the final aim of developing new treatment strategies to stabilize or even cure these conditions, we study genetically characterized human complex I deficient fibroblast cell lines as a model for OXPHOS-system disease, knowing that these cells are glycolytic (216). In doing so, we recently showed that agonist-induced mitochondrial Ca^{2+} accumulation and ensuing ATP production are significantly decreased in skin fibroblasts derived from patients with an isolated complex I deficiency caused by mutations in nuclear-encoded structural subunits of the complex (283).

Robinson and co-workers reported that mitochondrial morphology and dynamics are altered in skin fibroblasts from patients with mitochondrial complex I deficiency (200). Similar observations were reached with control fibroblasts treated with the complex I inhibitor rotenone (40 µM) for 5 minutes. Studies with mitochondrial membranes isolated from patient fibroblasts showed that NADH-stimulated mitochondrial superoxide formation is increased in human complex I deficiency and that 10 µM rotenone readily increases formation of this radical in control membranes (204). Together with observations that exogenous application of hydrogen peroxide increases mitochondrial mass in human lung fibroblasts (146), these findings suggest a causal relationship between increased mitochondrial oxygen radical formation and alterations in mitochondrial reticulum and dynamics in complex I deficiency. However, no definitive proof has yet been offered. Here we show that a sustained increase in mitochondrial superoxide production, brought about by chronic inhibition of complex I of the electron transport chain (100 nM rotenone, 72 hours), causes a marked increase in mitochondrial length and branching.

MATERIALS AND METHODS

Cell culturing, NADH:ubiquinone oxidoreductase measurements and cell cycle analysis
Fibroblasts were obtained from a skin biopsy of a healthy individual and cultured in medium M199 with Earle's salt (Invitrogen, Carlsbad, CA, USA) in a humidified atmosphere of 95% air, 5% CO_2 at 37^o C. The medium contained 5 mg/l Tween 20 and was supplemented with 10% (v/v) fetal calf serum, 100 IU/ml penicillin and 100 µg/ml streptomycin (Invitrogen). The activities of NADH:ubiquinone oxidoreductase (complex I), cytochrome *c* oxidase (complex IV) and citrate synthase (CS) were measured in a mitochondria-enriched fraction as described previously (245). For fluorescence microscopy, fibroblasts were seeded on glass coverslips (Ø 22 mm) and cultured to ~70% confluence. For cell cycle assessment, cells were trypsinized and stored on ice. After staining with propidium iodide, cell suspensions were analyzed using flow cytometry (275).

Quantitative analysis of mitochondrial morphology by video-rate laser-scanning confocal microscopy - Stock solutions of the lipophilic cation rhodamine 123 (R123), Mitotracker Green FM (MG), and Mitotracker Red CMXRos (MR; all from Molecular Probes, Leiden, NL) were freshly prepared in dimethylsulfoxide (DMSO) prior to each measurement. Fibroblasts were incubated in culture medium containing 200 µM (R123) or 5 µM (MR and MG) of the dye for 40 seconds (R123), 3 minutes (MR), or 20 minutes (MG) at 20^o C. After loading cells were thoroughly washed with Hepes-Tris medium (132 mM NaCl, 4.2 mM KCl, 1 mM $CaCl_2$, 1 mM $MgCl_2$, 5.5 mM D-glucose and 10 mM Hepes, pH 7.4). For confocal imaging, coverslips were mounted in an incubation chamber placed on the stage of an inverted microscope (Nikon Diaphot, Tokyo, Japan), attached to an Oz confocal microscope (Noran Instruments, Middleton, WI, USA). Measurements were performed at 20^o C. The light from an Argon ion laser (488 nm; Omnichrome, Chino, CA, USA) was delivered to the cells via a x40 oil immersion planapochromat objective (NA 1.4; Nikon). For all dyes, fluorescence emission light was directed through a 500 nm LP barrier filter (Chroma Technology Corp., Brattleboro, VT, USA) and quantified using a photomultiplier tube (Hamamatsu Photonics, Bridgewater, NJ, USA). Given the flat morphology of the fibroblasts (size <3 µm in the axial direction) slit settings were chosen in such a way that axially, each cell was entirely present within the confocal volume (135). This prevented exclusion of mitochondrial structures from the image and guaranteed an optimal fluorescence signal at minimal laser intensity. Hardware and image acquisition were controlled by Intervision software (Version 1.5, Noran

Instruments) running under IRIX 6.2 on an Indy workstation (Silicon Graphics Inc., Mountain View, CA, USA) equipped with 512 Mb memory. Before image acquisition, brightness and contrast settings were optimized using a custom-made look up table that colored the upper and lower ten greylevels red and blue, respectively. Images (512x480 pixels) were collected at 30 Hz with a pixel dwell time of 100 ns. To reduce random noise, images were averaged in real-time using the running average algorithm of the Intervision Acquisition software with a window size of 32. This acquisition protocol, in combination with the low mitochondrial mobility at 20^{o} C, effectively prevented distortion of the image by mitochondrial movement. Images were recorded from a cross-shaped area transecting the center of the coverslip and converted to TIFF-format using a Silicon Graphics O2 workstation running IRIX 6.5. Quantitative analysis of mitochondrial morphology was performed using Image Pro Plus 4.5 (Media Cybernetics, Silver Spring, MD, USA) as described in the Results section.

Quantitative analysis of mitochondrial superoxide production by digital-imaging microscopy - Fibroblasts were incubated in Hepes-Tris medium containing 10 µM hydroethidine (HEt; Molecular Probes) for 10 minutes at 37^{o} C. HEt is an uncharged compound that readily enters the cell. Within the cell, it reacts with superoxide to form the fluorescent and positively charged product ethidium (Et; 69). The reaction was stopped by thorough washing of the cells with PBS to remove excess HEt. For quantitative analysis of Et, coverslips were mounted in an incubation chamber placed on the stage of an inverted microscope (Axiovert 200 M, Carl Zeiss, Jena, Germany) equipped with a Zeiss 40x/1.3 NA F Fluar objective. Ethidium was excited at 490 nm using a monochromator (Polychrome IV, TILL Photonics, Gräfelfing, Germany). Fluorescence emission light was directed by a 525DRLP dichroic mirror (Omega Optical Inc., Brattleboro, VT, USA) through a 565ALP emission filter (Omega) onto a CoolSNAP HQ monochrome CCD-camera (Roper Scientific, Vianen, The Netherlands). The image capturing time was 100 milliseconds. Routinely, 10 fields of view were analyzed per coverslip. Hardware was controlled with Metafluor 6.0 software (Universal Imaging Corporation, Downingtown, PA, USA). Quantitative image analysis was performed using Metamorph 6.0 (Universal Imaging Corporation) as described in the Results section.

Quantitative analysis of the extent of lipid peroxidation by video-rate laser-scanning confocal microscopy - The extent of lipid peroxidation was quantified using the fluorescent ratio probe C11-BODIPY$^{581/591}$ (Molecular Probes). Upon oxidation, the red emitting form of the dye (595 nm) is converted into a green emitting form (520 nm), which results in an increase in

green/red emission ratio (66). Cells were incubated in Hepes-Tris medium containing 4 µM C11-BODIPY$^{581/591}$ for 30 minutes at 37º C. After thorough washing, images were collected with the Oz confocal system as described above. Green and red fluorescence emission signals were separated by a 560DM dichroic mirror and appropriate bandpass filters (535D20 and 580LP; Chroma). Quantitative image analysis was performed as described in the Results section.

Statistics and data analysis - Numerical values were visualized using Origin Pro 6.1 (OriginLab Corporation, Northampton, MA, USA) and values from multiple experiments were expressed as average ± s.e.m. Statistical significances were assessed by Student's *t*-test.

RESULTS

Visualization of mitochondria in living skin fibroblasts - Successful quantitative analysis of mitochondrial morphology requires a visualization protocol that is compatible with off-line computer-assisted image analysis. The latter requirement implicates that fluorescence originating from mitochondria can be easily separated from background signals. In the ideal case this means that the recorded images contain a discrete range of greylevels solely associated with these organelles. To find a mitochondrial dye most compatible with this requirement, we stained fibroblasts with three widely used mitochondria-specific fluorophores: rhodamine 123 (R123, N=34 cells), Mitotracker Red CMXRos (MR, N=37) and Mitotracker Green FM (MG, N=42). To reduce illumination time of the fluorophores, prevent artifacts associated with mitochondrial movement and increase signal-to-noise ratio, 32 images were captured during 1 second and averaged in real time.

All three dyes revealed extensive mitochondrial reticula as well as individual mitochondrial filaments (**Fig. 1A-C**; left panels). Next, images were segmented using three greylevel intervals (0-50, 51-150 and 151-255; columns below intensity scale in **Fig. 1**). Only for R123 a discrete range of greylevels was exclusively associated with mitochondrial structures (**Fig. 1A**; third image). When R123-stained cells were treated with 1 µM of the protonophore carbonylcyanide-*p*-trifluoromethoxy-phenylhydrazone (FCCP), the mitochondrial staining pattern was acutely lost thus confirming the mitochondrial localization of the dye (not shown).

Fig. 1. Visualization of mitochondria in living human skin fibroblasts - To determine which mitochondria-specific dye suited best for computerized image analysis cells were stained with (**A**) rhodamine 123 (R123), (**B**) mitotracker red CMXRos (MR), or (**C**) mitotracker green FM (MG). Image segmentation into three discrete greylevel ranges (0-50: second column, 51-150: third column and 151 to 255: fourth column) revealed that only in the case of R123 mitochondrial structures are present within a discrete greylevel interval required for computerized image analysis (panel **A**, third image).

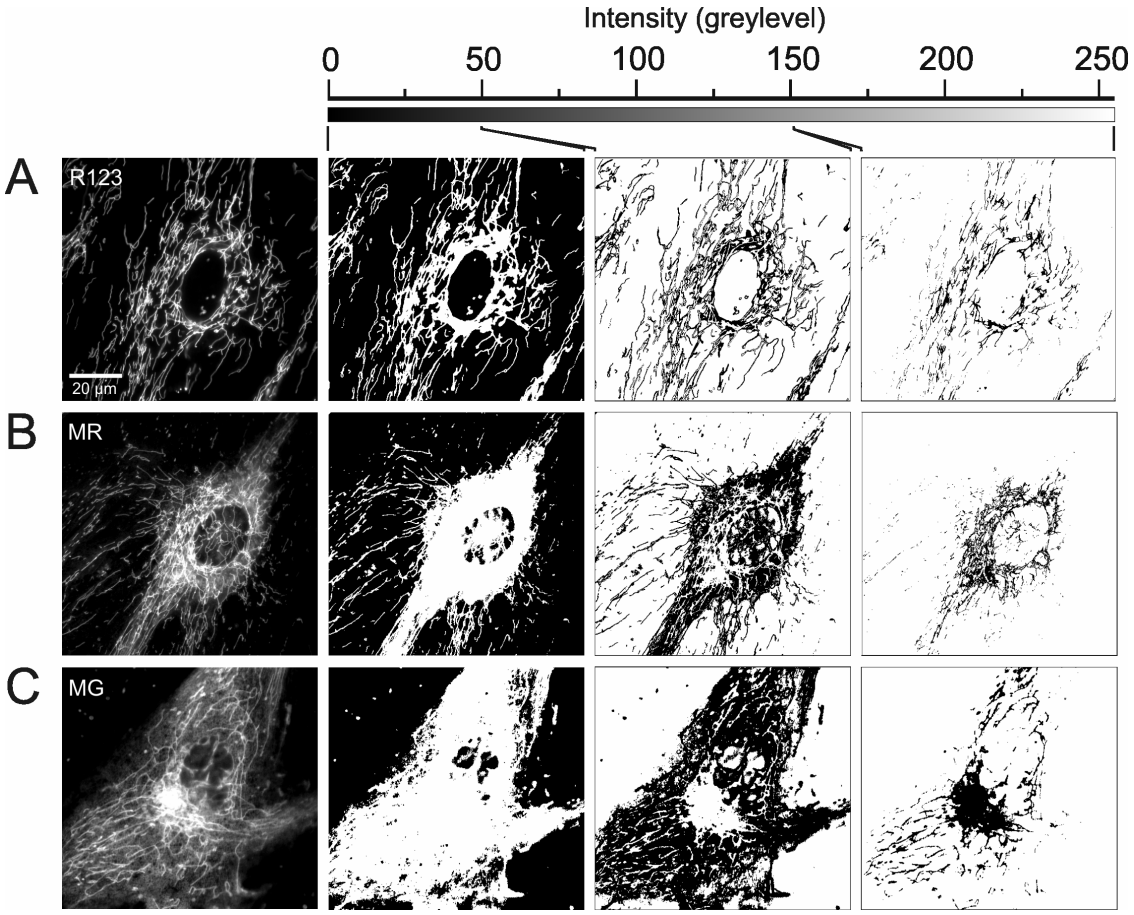

Quantitative analysis of mitochondrial structure - To identify mitochondrial structures in images of R123-stained fibroblasts (**Fig. 2A**; solid line indicates cell boundary), an image-processing algorithm was developed that consisted of three steps. First, the contrast in the image was optimized by reassigning the greyvalues of the pixels to cover the entire available range from 0 to 255 (**Fig. 2B**; intensity histograms before and after optimization are displayed in panel E). Next, a "top-hat" spatial filter was applied (**Fig. 2C**).

This filter is particularly suited to isolate bright features from a dark background and consists of two steps: (**I**) the pixel values in a certain region of the image are multiplied by a matrix *h* (or kernel) of integer filtering coefficients given by:

$$h = \begin{bmatrix} 0 & 0 & -1 & -1 & -1 & 0 & 0 \\ 0 & -1 & -1 & -1 & -1 & -1 & 0 \\ -1 & -1 & +3 & +3 & +3 & -1 & -1 \\ -1 & -1 & +3 & +4 & +3 & -1 & -1 \\ -1 & -1 & +3 & +3 & +3 & -1 & -1 \\ 0 & -1 & -1 & -1 & -1 & -1 & 0 \\ 0 & 0 & -1 & -1 & -1 & 0 & 0 \end{bmatrix}$$

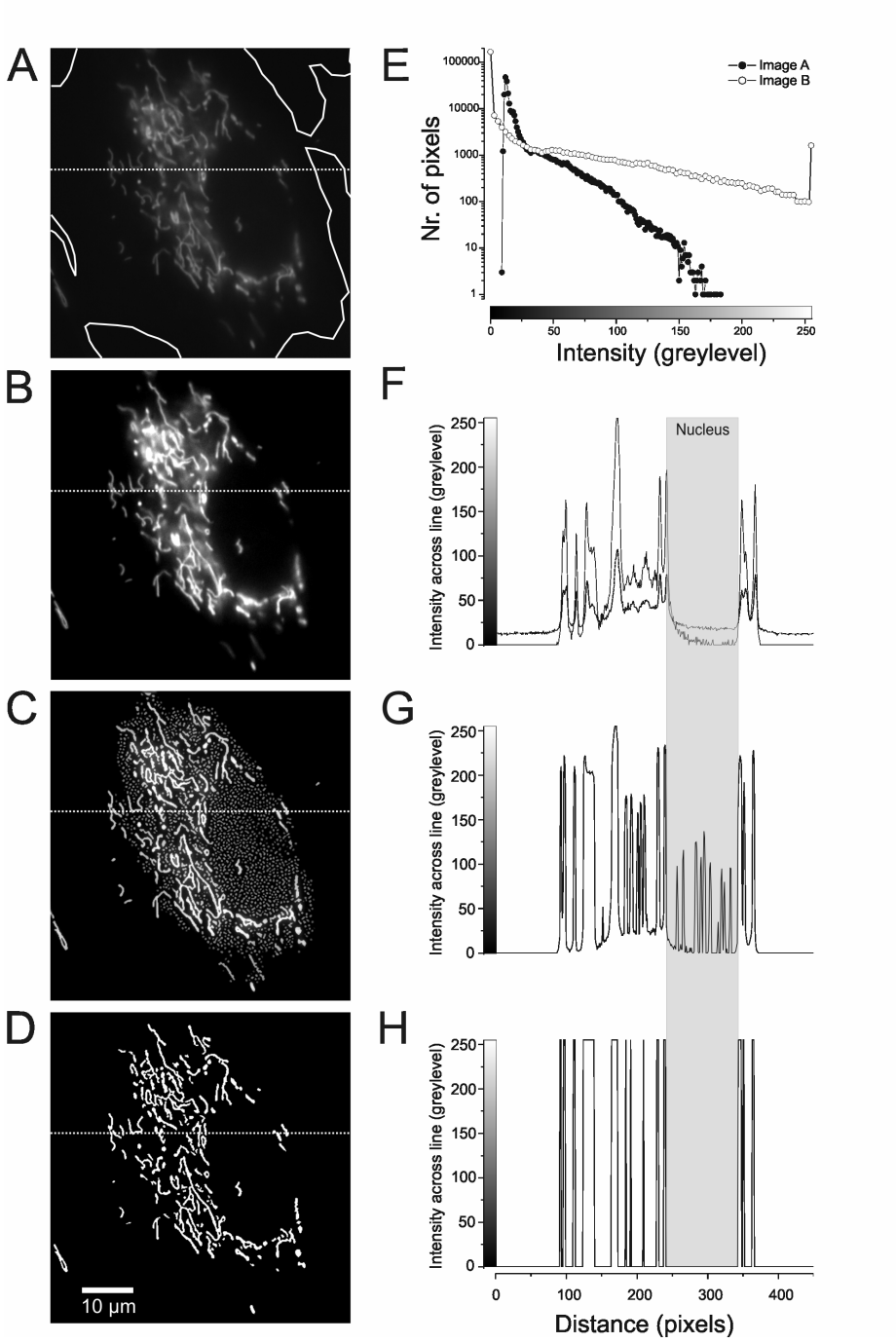

Fig. 2 Quantitative analysis of mitochondrial morphology - For quantitative analysis, (**A**) raw images of R123-stained fibroblasts (solid line indicates the cell boundary) were first (**B**) contrast optimized. Next, (**C**) a spatial filter was applied to highlight mitochondrial structures. (**D**) The small grey particles introduced by this operation were removed by applying a threshold to the image. (**E**) Intensity distribution before (filled symbols) and after (open symbols) contrast optimization, calculated for the images **A** and **B**, respectively. (**F**) Intensity profiles across the lines shown in panels A and B (dotted and continuous line, respectively). (**G** and **H**) intensity profiles for panels C and D. Details are given in the Results section.

(**II**) the newly assigned pixel values are summed and used to replace the original intensity of the central pixel. This process is repeated until each pixel in the image is processed. Of note, the filter always uses the original intensity values of the neighborhood pixels as an input. We chose a dimension of the top-hat filter of 7x7 pixels because this is compatible with the size of the mitochondrial objects. The result in **figure 2C** was obtained by applying the top-hat filter three times using a filter-strength of 30%. The latter value indicates that each time the filter is applied only 30% of the difference between the pixel value after and before filtering is added. Finally, a threshold operation was performed to remove the distinct spherical objects of intermediate intensity introduced by the top-hat filter (**Fig. 2D**). The effects of the various steps of the image processing protocol are visualized in **figures 2F-H**, depicting the intensity profiles across a horizontal line transecting the cell (dotted line in **Figs. 2A-D**). The clear distinction between background (black) and mitochondrial (white) signals in the binary image (**Figs. 2D and H**) allows automated shape-analysis of mitochondrial structures.

For morphological analysis two parameters (descriptors) were calculated for each mitochondrial object: (**I**) the formfactor *F* ($perimeter^2/4\pi \cdot Area$) and (**II**) the aspect ratio *AR* (ratio between the major and minor axis of the ellipse equivalent to the object). Moreover, (**III**) the total number of mitochondria per cell (*Nc*) was determined. Both *F* and *AR* are independent of image magnification, have a minimal value of one (corresponding to a perfect circle) and were used previously to analyze cell shape (133). **Figure 3** illustrates the morphological meaning of *F* and *AR*. Images of R123-stained fibroblasts were contrast optimized (**Fig. 3A**) and mitochondrial structures were isolated by image processing (**Fig. 3B**). Plotting *AR* as a function of *F* for all 392 mitochondria depicted in figure 3C revealed that *AR* is a measure of mitochondrial length, whereas *F* is a measure of both length and degree of branching (representative mitochondrial structures are indicated by black dots). For statistical analysis we routinely calculated the average values of *F* and *AR* for each recorded field of view.

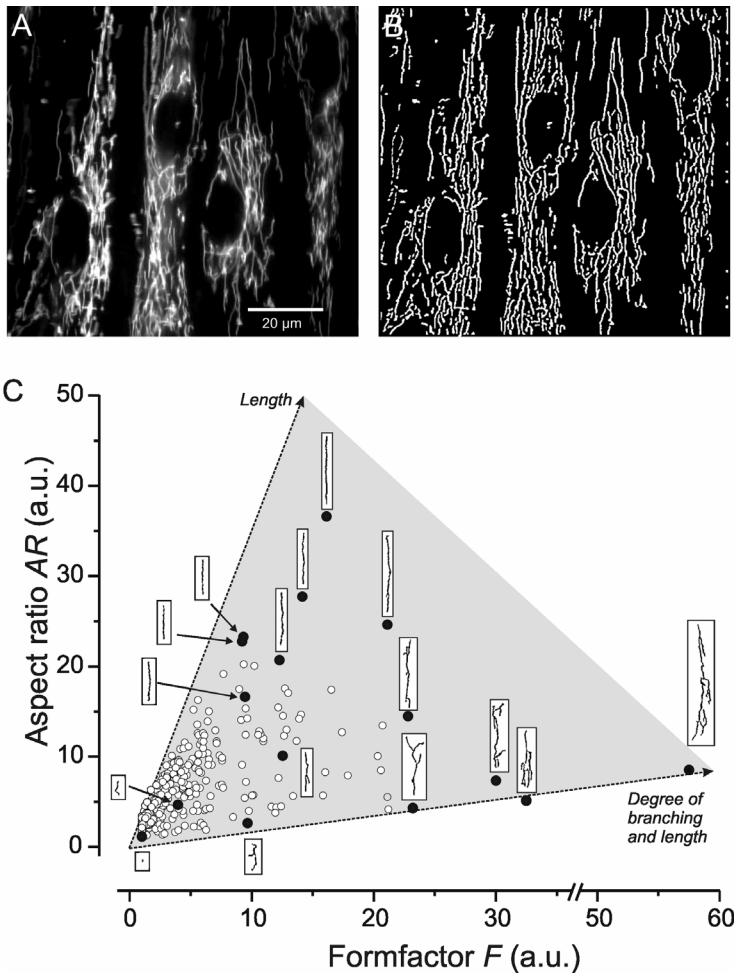

Fig. 3. Morphological descriptors of mitochondrial shape - (**A**) Confocal image of fibroblasts stained with R123. (**B**) The same cells after image processing. (**C**) Aspect ratio (*AR*) plotted as function of formfactor (*F*) for the 392 mitochondrial objects present in the processed image. Morphology is shown for mitochondria with representative combinations of *F* and *AR* (filled symbols). The three corners of the shaded triangle represent morphological extremes.

Chronic rotenone treatment inhibits complex I activity and induces mitochondrial outgrowth in human skin fibroblasts - To assess a possible connection between mitochondrial stress and mitochondrial morphology, cells were cultured in the presence of rotenone, an archetypal inhibitor of complex I of the respiratory chain. Enzyme activity measurements in mitochondria-enriched fractions of cells chronically treated with this drug for 72 hours revealed a dose-dependent decrease in complex I activity (**Fig. 4A**, filled circles). In contrast, the activities of complex IV (open circles) and the Krebs cycle enzyme citrate synthase (squares) were not altered. Visual inspection of R123-stained cells suggested an increase in mitochondrial length and/or branching following rotenone treatment (**Fig. 4B**). Subsequent quantitative analysis revealed that rotenone did not alter *AR* or *Nc*, but caused a dose-dependent increase in *F*, which was significant at a concentration of 100 nM (**Fig. 4C**; $P<0.01$). Importantly, rotenone did not change cell cycle phase. Values of G_0/G_1, G_2/M and S were 86%, 4% and 10% (N=3), 91%, 5% and 5% (N=2) and 92%, 4% and 4% (N=2) for vehicle-treated cells and cells treated with 2.5 and 100 nM rotenone, respectively). The drug

did not detectably alter the mitochondrial membrane potential as indicated by the lack of effect on the R123 fluorescence emission intensity (**Fig. 4C**). Of note, the latter was determined in unprocessed images recorded at identical hardware settings, using the binary image obtained after image processing as a mask.

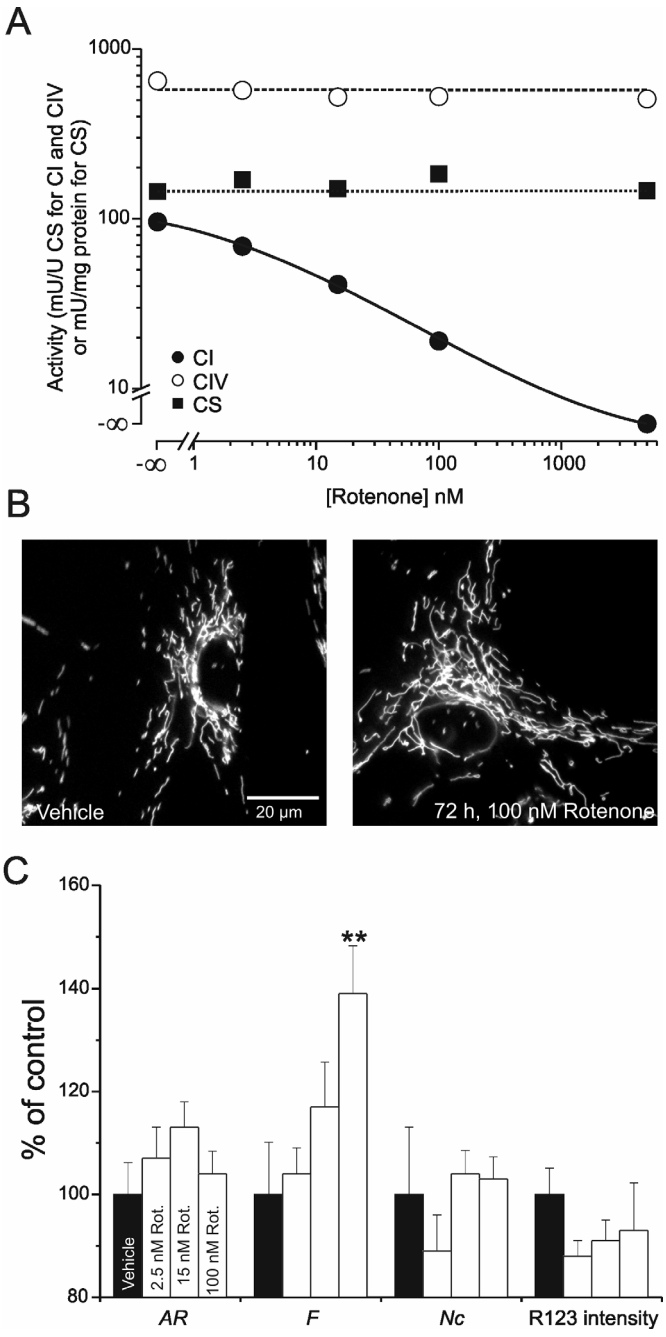

Fig. 4. Chronic rotenone treatment decreases complex I activity and induces mitochondrial outgrowth - (**A**) Chronic treatment of human skin fibroblasts with rotenone (72 h) decreased complex I activity dose-dependently (filled circles) without affecting the activities of complex IV (open circles) and citrate synthase (squares). Activities were measured in a mitochondria-enriched fraction and are expressed as milli-unit per unit citrate synthase (mU/UCS) for complex I and complex IV and milli-unit per mg protein for citrate synthase. (**B**) Control fibroblasts treated with vehicle (containing 0.001% v/v ethanol; left panel) and rotenone (100 nM, 72 hours, right panel) stained with R123. Mitochondria appeared to be more branched in rotenone-treated cells. (**C**) Quantitative analysis of mitochondrial morphology as a function of rotenone concentration. Aspect ratio (*AR*) and R123 emission intensity remained unaffected, whereas the formfactor (*F*) increased dose-dependently (significant at 100 nM rotenone). Experiments were performed on two days. On each day, the average value obtained with vehicle was set at 100% to which the other values were related. Averages are from N=30 cells (vehicle), N=26 cells (2.5 nM rotenone), N=23 cells (15 nM rotenone) and N=52 cells (100 nM rotenone). **Significantly different from vehicle-treated cells ($P<0.01$).

Chronic treatment with rotenone increases superoxide production in human skin fibroblasts - Measurement of the effect of rotenone on oxygen radical formation in living cells has yielded conflicting results. Increases were observed in the human osteosarcoma-derived cell line 143B (16), mesencephalic neurons (179) and HL-60 cells (150), whereas decreases occurred in hepatocytes (289), cultured mice hippocampal neurons (233) and monocytes and macrophages (151). In this study we used hydroethidine (HEt), a redox-sensitive probe that is widely used to measure mitochondrial superoxide production in living cells (30,31,69,305). Hydroethidine is a cell-permeant compound that is oxidized by superoxide to its positively charged product ethidium (Et). Digital imaging microscopy of fibroblasts loaded with 10 μM HEt for 10 minutes and thoroughly washed to remove non-oxidized HEt, revealed the presence of Et in both nucleoli and a widespread network of tubular structures present in the cytosolic compartment (**Fig. 5A**). The intensity of fluorescence emission did not change during 10 minutes of illumination at 0.2 Hz, as demonstrated by a linear fit with a slope of $4.4 \cdot 10^{-5} \pm 2.3 \cdot 10^{-6}$ ($P<0.001$). This indicates that excess HEt was effectively removed, Et did not leak out of the cell and photo-bleaching and/or photo-activation did not occur during at least 10 minutes of image acquisition. The mitochondrial nature of the tubular structures was demonstrated by the immediate loss of Et fluorescence upon addition of the mitochondrial uncoupler FCCP (1 μM; **Fig. 5B**). This confirms that mitochondrial Et accumulation depends on mitochondrial membrane potential (30,31,69).

Fibroblasts treated with 100 nM rotenone for 1 hour prior to the 10-min incubation period with HEt displayed a marked increase in Et fluorescence in both nucleoli and mitochondria (**Fig. 5C and D**). For quantification of the effect of rotenone, we determined the average fluorescence intensity in the nucleoplasm and a cytosolic region of equal size containing a high density of mitochondrial structures (Fig. 5C, circles n and m, respectively). **Figure 5E** shows that the average fluorescence intensities in both regions, determined at different degrees of rotenone inhibition, are linearly correlated (R=0.99; slope = 0.51 ± 0.03, $P<0.05$). This demonstrates that the nucleolar ethidium is of mitochondrial origin. The figure furthermore shows that the average fluorescence intensity in cells treated with 100 nM rotenone for 1 hour (N=35 cells) was 2-fold higher than that in vehicle-treated cells (N=37). A further increase to 3-fold the control value was reached with 1 μM rotenone (N=31). Cells chronically treated with 100 nM rotenone for 72 hours still displayed a 2-fold increase in average fluorescence intensity (N=32). Finally, addition of H_2O_2 (100 μM) did not increase Et fluorescence, demonstrating that HEt is not oxidized by this superoxide derivative. Taken together, these findings show that chronic rotenone treatment causes a rapid and persistent

increase in the rate of mitochondrial superoxide production in cultured human skin fibroblasts.

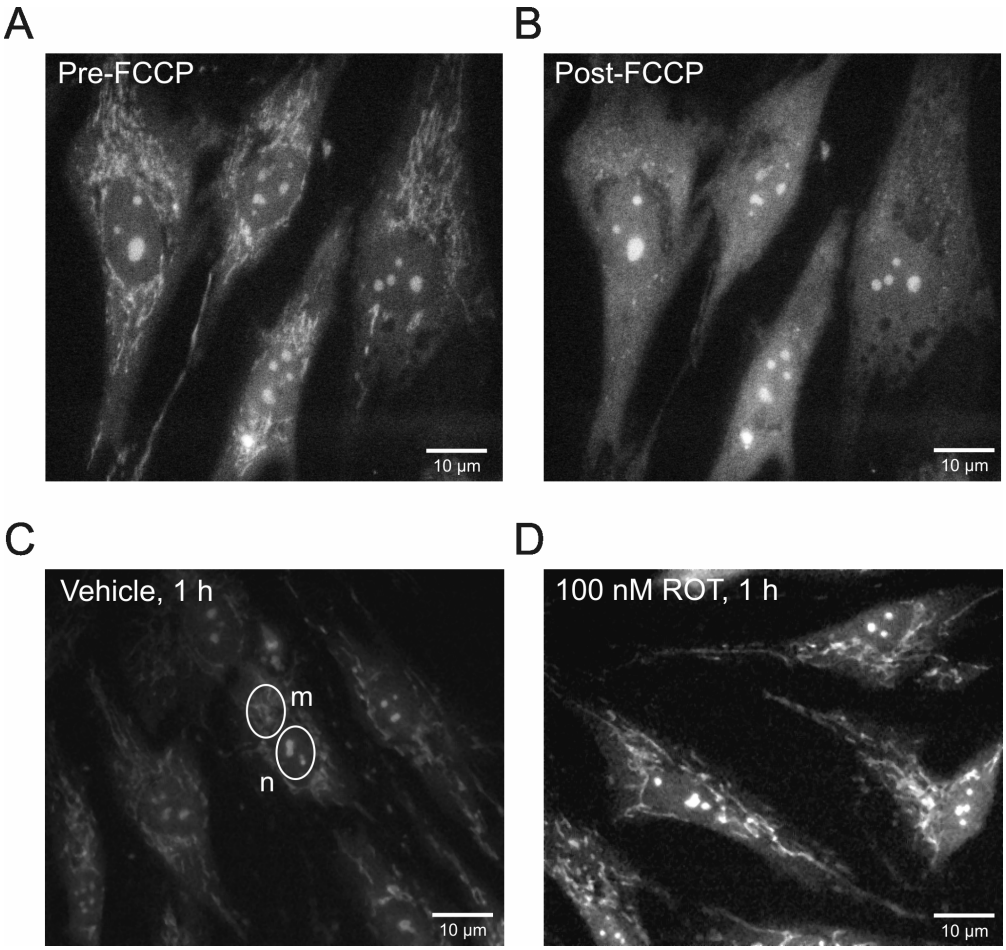

Fig. 5. Rotenone increases mitochondrial superoxide production - (**A**) Human skin fibroblasts incubated in the presence of HEt (10 µM) for 10 min and thoroughly washed to remove non-oxidized HEt, revealed the presence of Et in both nucleoli and a widespread network of tubular structures present in the cytosolic compartment. (**B**) Staining of the cytosolic tubular structures was lost immediately after addition of the mitochondrial uncoupler FCCP (1 µM). (**C,D**) Stimulatory effect of rotenone (100 nM, 1 hour) on Et accumulation in nucleoli (n) and mitochondrial structures (m) during 10 minutes incubation with 10 µM HEt. Vehicle-treated cells were incubated with 0.001% (v/v) ethanol. For quantification of the rotenone effect, the average fluorescence intensity was determined in the nucleoplasm and a cytosolic region of equal size containing a high density of mitochondrial structures (**C**, circles). (**E**) Linear relationship (slope = 0.51 ± 0.03, $P<0.001$) between the average fluorescence intensities in nucleoplasm and cytosolic region for fibroblasts exposed to vehicle (N=35 cells), 100 nM ROT for 1 hour (N=34), 0.1 µM ROT for 1 hour (N=30), or 100 nM ROT for 72 hours (N=28). [a]Significantly different from vehicle-treated cells ($P<0.01$). [b]Significantly different from fibroblasts treated with 100 nM rotenone for 1 hour ($P<0.01$). [c]Significantly different from fibroblasts treated with 100 nM rotenone for 72 hours ($P<0.01$).

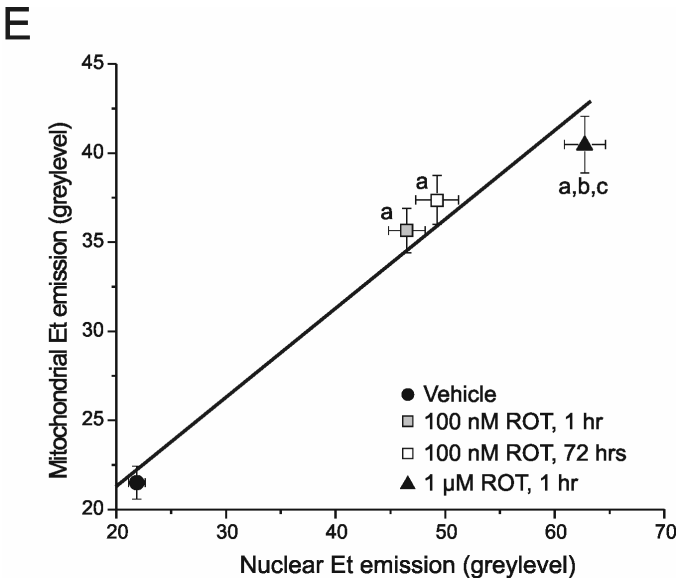

MitoQ prevents rotenone-induced mitochondrial outgrowth without affecting rotenone-induced superoxide formation - To investigate the mechanism underlying rotenone-induced mitochondrial outgrowth we applied the antioxidant mitoquinone (MitoQ; 126). MitoQ is a ubiquinone derivative that is mitochondria-targeted by covalent attachment to a lipophilic triphenylphosphonium cation through an aliphatic carbon chain. Chronic treatment of human fibroblasts with MitoQ for 72 hours did not alter mitochondrial morphology (**Fig. 6A**) or number (not shown). At a concentration of 10 nM, however, MitoQ abolished the effect of chronic rotenone treatment on mitochondrial outgrowth. **Figure 6B** shows that MitoQ alone had no effect on mitochondrial superoxide production. In addition, this figure shows that MitoQ did not inhibit rotenone-induced superoxide formation. These findings demonstrate that MitoQ acts downstream of superoxide to inhibit rotenone-induced mitochondrial outgrowth.

MitoQ prevents the rotenone-induced increase in lipid peroxidation - To address the question of the specificity of MitoQ we used C11-BODIPY$^{581/591}$, a lipid peroxidation reporter molecule that is insensitive to superoxide, nitric oxide and hydroperoxides (66), to assess the effect of rotenone, alone and in combination with MitoQ, on lipid peroxidation. Cells chronically treated with 100 nM rotenone for 72 hours and subsequently incubated in the presence of 4 µM C11-BODIPY$^{581/591}$ for 30 minutes showed a 2-fold increase in the ratio between the oxidized and non-oxidized form of the reporter molecule (**Fig. 6C**). This effect of rotenone was fully absent in cells co-treated with 10 nM MitoQ. MitoQ alone did not alter the relative

amount of oxidized C11-BODIPY$^{581/591}$. These data show that lipid peroxidation is markedly increased in cells chronically treated with 100 nM rotenone and that this effect of rotenone is completely blocked by MitoQ.

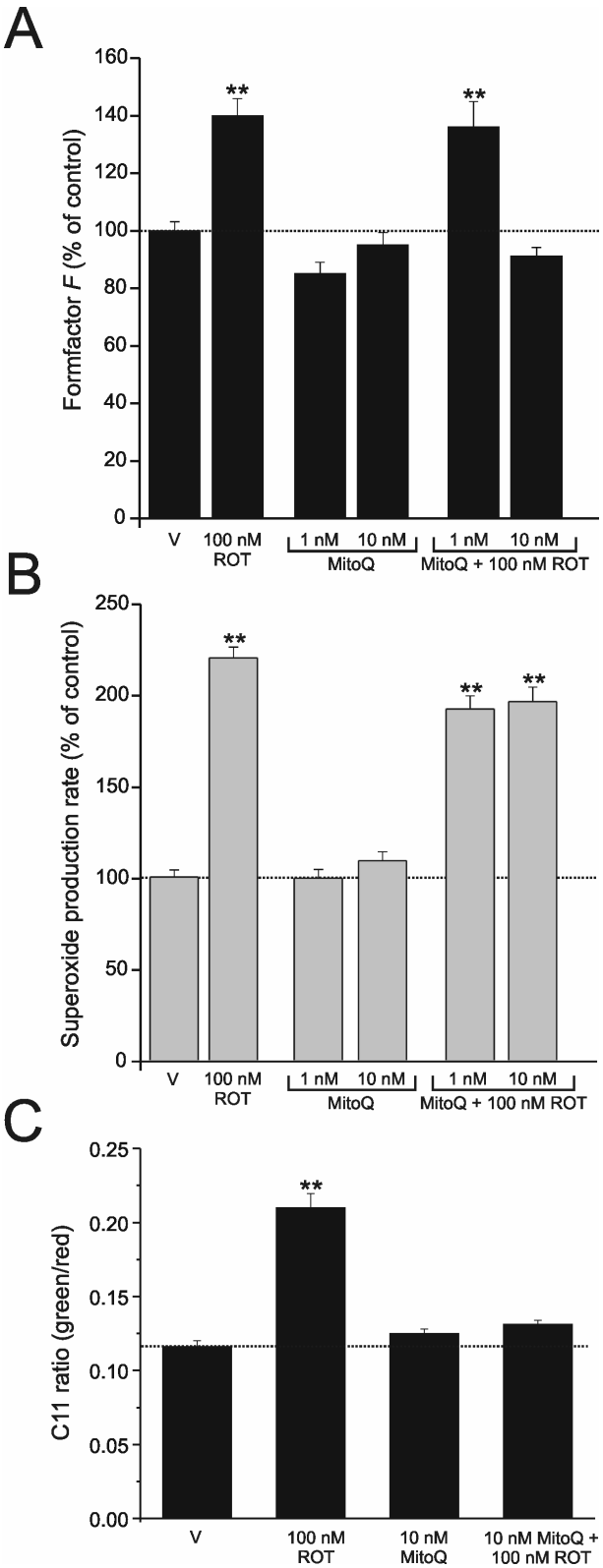

Fig. 6. MitoQ inhibits rotenone-induced mitochondrial outgrowth and lipid peroxidation but not superoxide generation - Human skin fibroblasts were incubated in the presence of ethanol (0.001% (v/v); vehicle), rotenone (100 nM), MitoQ (1 nM, 10 nM), or the combination of both drugs for 72 hours prior to analysis of mitochondrial morphology, rate of mitochondrial superoxide production and extent of lipid peroxidation. (**A**) Effect on formfactor. Experiments were performed on four days. On each day, the average value obtained with vehicle was set at 100% to which the other values were related. The values presented are the average of N=56 cells (vehicle; V), N=71 cells (100 nM ROT), N=84 cells (1 nM MitoQ), N=102 cells (10 nM MitoQ), N=34 cells (100 nM ROT + 1 nM MitoQ) and N=87 cells (100 nM ROT + 10 nM MitoQ). (**B**) Effect on Et accumulation in the nucleoplasm during 10 minutes incubation with 10 µM HEt as a measure of the rate of mitochondrial superoxide production. Experiments were performed on two days. On each day, the average fluorescence intensity in vehicle-treated cells was set at 100% to which the other values were related. The values presented are the average of N=60 cells (V), N=64 cells (100 nM ROT), N=61 cells (1 nM MitoQ), N=63 cells (10 nM MitoQ), N=77 cells (100 nM ROT + 1 nM MitoQ) and N=30 cells (100 nM ROT + 10 nM MitoQ). (**C**) Effect on the emission ratio of C11-BODIPY$^{581/591}$ as a measure of the extent of lipid peroxidation. Data are from two independent measurements. The values presented are the average of N=55 cells (V), N=44 cells (100 nM ROT), N=62 cells (10 nM MitoQ) and N=53 cells (10 nM MitoQ + 100 nM ROT). **Significantly different from vehicle-treated cells ($P<0.01$)

DISCUSSION

Human mitochondrial complex I (NADH:ubiquinone oxidoreductase) is the largest multisubunit assembly of the oxidative phosphorylation (OXPHOS) system. Its malfunction is associated with a wide variety of clinical syndromes ranging from often early lethal disorders, of which Leigh disease, a progressive encephalopathy, is the most frequent, to neurodegenerative disorders in adulthood, including Leber's hereditary optic neuropathy and Parkinson's disease. In recent years, all human nuclear structural complex I genes have been characterized, which allowed us to elucidate the genetic defect in 40% of a cohort of complex I-deficient patients in which the enzyme defect was present in at least skeletal muscle and cultured skin fibroblasts (246). To enhance our understanding of the pathophysiological consequences of complex I deficiency we study fibroblasts from genetically characterized patients (283). Pilot experiments employing the protocol for quantitative analysis of mitochondrial morphology described in this paper, revealed significant differences between control and patient fibroblasts (W.J.H. Koopman, H.-J. Visch, S. Verkaart, J.A.M. Smeitink, L.P. van den Heuvel and P.H.G.M. Willems, unpublished data). This prompted us to investigate the relationship between complex I activity and mitochondrial morphology in control human skin fibroblasts. In order to mimic the pathological condition as closely as possible, control fibroblasts were chronically treated with rotenone concentrations that decreased the activity of complex I to values similar to those measured in patient fibroblasts.

The data presented show that chronic treatment of fibroblasts with 100 nM rotenone for 72 hours decreased complex I activity by 80% and caused significant mitochondrial outgrowth. Importantly, the alterations in mitochondrial shape were not the result of changes in cell cycle phase. This is in agreement with previous studies showing that 100 nM rotenone did not affect cell growth and viability of human B lymphoma cells (9). The morphological parameters analysed were: aspect ratio (*AR*), which is a measure of mitochondrial length, and formfactor (*F*), which is a combined measure of mitochondrial length and degree of branching. Both parameters are independent of objective or zoom factor and therefore most suited for comparison between different microscopes and cell types. To minimize the effects of phototoxicity and mitochondrial movement, images were acquired at video-speed (30 Hz) and averaged in real time. For statistical evaluation, we calculated the average value of *AR*, *F* and *Nc* (the number of mitochondria per cell) for each field of view. These averages were not influenced by the small number of partially imaged mitochondria because typically

between 80-500 mitochondria were present per field of view. Day to day variations in *AR*, *F* and *Nc* were effectively corrected by expressing each value as a percentage of the corresponding control value recorded on the same day. The fact that our R123 staining procedure is very short (40 seconds) and image analysis can be automated allows future application of this protocol in the rapid screening of large numbers of mitochondrial structures.

Chronic treatment with 100 nM rotenone for 72 hours caused a marked increase in formfactor but did not significantly alter the aspect ratio or the number of mitochondrial structures. These findings show that human skin fibroblasts respond to chronic complex I inhibition with the formation of a more complex mitochondrial reticulum. Chronic treatment with 15 nM rotenone tended to increase both *AR* and *F*, suggesting that the effect of rotenone is dose-dependent. When the concentration of rotenone was increased to 100 nM, however, the effect of chronic rotenone treatment on *AR* decreased rather than increased, whereas that on *F* increased further to reach statistical significance. Robinson and co-workers recently reported that human skin fibroblasts displayed increased amounts of mitochondria in the swollen filamentous forms, nodal filaments, and ovoid forms upon acute (5 minutes) treatment with 40 µM rotenone (200). We did not observe such aberrations in mitochondrial morphology in our study, indicating that mitochondria respond completely differently depending on the concentration of the inhibitor and the duration of the treatment. Chronic treatment of fibroblasts with 5 µM rotenone caused massive cell death (data not shown), demonstrating the inability of these cells to cope with relatively high inhibitor concentrations. It should be noted, however, that the relatively low concentration of 100 nM rotenone used in the present study decreased the activity of complex I already by 80%. Moreover, acute addition of 100 nM rotenone caused an immediate increase in the rate of superoxide production (data not shown), indicating that the inhibitor acts instantaneously. These observations suggest that the cytotoxicity of the higher rotenone concentrations is not directly related to its inhibitory effect on complex I activity and that, therefore, results obtained with these concentrations should be treated with caution.

Several studies have shown that high concentrations of rotenone or exogenously added H_2O_2 can induce apoptosis (9,60,131,150,258). In general, this induction is accompanied by permeabilization of the mitochondrial inner membrane, opening of the permeability transition pore, and dissipation of the mitochondrial membrane potential (78). It has been demonstrated that chronic (36 hours) rotenone treatment induces apoptosis through enhancing mitochondrial reactive oxygen production in HL-60 cells (150). However, the

lowest concentration of rotenone that gave a significant increase in percentage of apoptotic cells was 200 nM. In agreement with this finding the present study did not show any adverse effects of chronic treatment with 100 nM rotenone on cell growth and viability. On the contrary, rotenone-treated fibroblasts displayed an increase in complexity of the mitochondrial network that suggests the induction of an adaptive response. A similar increase was observed in cancer cells that were forced to grow on galactose and glutamine (219). Importantly, the latter study showed that the increase in complexity of the mitochondrial reticulum was accompanied by an increase in OXPHOS protein, indicating the adaptive nature of this response. These findings support the existence of a tight relationship between mitochondrial structure and function (59).

The rotenone-induced increase in mitochondrial outgrowth was completely prevented by co-treatment with MitoQ, a mitochondria-targeted derivative of coenzyme Q_{10} (121,126). Given its very large hydrophobicity, MitoQ is preferentially adsorbed to the matrix-facing leaflet of the inner mitochondrial membrane with the triphenylphosphonium moiety at the membrane surface at the level of the fatty acid carbonyls, and the alkyl chain and ubiquinol moiety inserted into the hydrophobic core of the lipid bilayer (10). The inhibitory effect of MitoQ on rotenone-induced mitochondrial outgrowth suggests that an increase in mitochondrial oxidative stress is the primary cause of this cellular response.

MitoQ completely blocked rotenone-induced outgrowth and lipid peroxidation but had no effect on the rotenone-induced increase in mitochondrial superoxide formation. The latter finding shows that MitoQ exerts its effect downstream of this oxygen radical. It has been demonstrated that superoxide radicals produced upon complex I inhibition are released into the mitochondrial matrix (43,255). The rotenone-induced increase in superoxide production found here might very well be at the basis of the rotenone-induced increase in H_2O_2 production observed in previous studies (16,150,258). The observation that exogenous application of H_2O_2 increases mitochondrial mass in human lung fibroblasts (146), indeed suggests the involvement of matrix manganese superoxide dismutase in the mechanism of action of rotenone. Recent work concerning the mechanism by which superoxide activates mitochondrial uncoupling proteins has suggested that superoxide releases ferrous iron from iron-sulfur center-containing enzymes, which reacts with hydrogen peroxide, produced by the action of manganese superoxide dismutase, to form the hydroxyl radical. This radical then extracts a hydrogen atom from an unsaturated fatty acyl chain of a phospholipid to generate carbon-centered radicals that initiate lipid peroxidation, yielding breakdown products that activate the uncoupling proteins (176). Because MitoQ reacts mainly with lipid

peroxidation products (M. Murphy, unpublished observations) the present findings may suggest that rotenone acts through these products to increase mitochondrial outgrowth. However, further research is required to define the exact site of action of MitoQ. The present findings support recent insights that intracellular oxidants may act as specific signaling molecules under both physiological and pathological conditions (75).

The present study shows that 100 nM rotenone causes a 2-fold increase in the rate of mitochondrial superoxide production in intact human skin fibroblasts. In agreement with this finding, NADH-stimulated mitochondrial superoxide formation was found to be increased in mitochondrial membranes isolated from complex I deficient human skin fibroblasts (204,214). These findings support the existence of a site of electron leakage upstream of the rotenone binding site (84). A considerably higher concentration of 10 μM rotenone was used to evoke a significant increase in NADH-stimulated mitochondrial superoxide formation in mitochondrial membranes isolated from control human skin fibroblasts (204). Therefore, the present method of determining the accumulation of Et in intact cells incubated for a short period of time in the presence of HEt is highly sensitive and most suitable for quantification of the rate of mitochondrial superoxide production in patient fibroblasts.

In conclusion, the data presented are compatible with the existence of a superoxide-induced mechanism of mitochondrial outgrowth that is activated at subapoptotic levels of complex I inhibition and leads to a possibly adaptive increase in complexity of the mitochondrial reticulum. Importantly, we show that this mechanism is activated at pathological levels of complex I inhibition. Detailed analysis of mitochondrial morphology in patient fibroblasts will reveal whether this mechanism is activated or whether activation of this mechanism is impaired in human complex I deficiency.

Acknowledgements: This work was supported by equipment grants of ZON (Netherlands Organisation for Health Research and Development, No: 903-46-176) and NWO (Netherlands Organisation for Scientific Research, No: 911-02-008) and the European Community's sixth Framework Programme for Research, Priority 1 "Life sciences, genomics and biotechnology for health", contract number LSHM-CT-2004-503116. We thank A. Janssen and F. van de Brand of the Nijmegen Center for Mitochondrial Disorders (NCMD) and A. Pennings (Department of Hematology, UMC Nijmegen) for technical assistance.

CHAPTER VIII

General discussion and future perspectives

Currently, our understanding of the consequences of mitochondrial complex I (CI) deficiency at the cellular level is still limited, thereby severely hampering the development and testing of possible therapeutics. One of the possible pathological consequences of inherited CI deficiency is enhanced ROS formation by a malfunctioning CI (208). Increased cellular ROS levels could induce a vicious cycle of oxidative injury (2,47,141) or activate redox sensitive signaling pathways in an attempt to counterbalance these detrimental effects (14,80,153). The aim of the research described in this thesis was to gain quantitative insight into the interrelationship between the degree of CI deficiency, CI expression, cellular ROS handling and redox homeostasis in human CI deficiency.

Inherited CI deficiency: a catalytic defect or an expression problem?

To aid clinical diagnosis, CI activity is routinely measured as rotenone-sensitive NADH consumption in crude homogenates of muscle tissue and mitochondria-enriched fractions of cultured skin fibroblasts (119,245). In fibroblasts, CI activity values are routinely normalized to the activity of CIV and subsequently expressed as percentage of lowest control ratio. Although these measurements clearly demonstrate a reduction in CI activity, they are not informative about the mechanism which is causing this decrease. For research purposes, activity of CI can also be determined in an alternative assay by separation of CI protein from other OXPHOS complexes by Blue native electrophoresis (BNP) followed by measurement of its in-gel activity (IGA) (132,182,300). A major advantage of BNP is that it also allows visualization of the amount of fully assembled CI protein (~1 MDa) by Western blot analysis. Quantitative BNP/IGA and subsequent Western Blot analysis revealed a variable reduction in steady-state CI protein and activity (**chapter 3**) and allowed us to estimate the 'intrinsic CI activity' (IGA/BNP) in patient fibroblasts (**chapter 3**).

In addition to the amount of CI protein, it was found that also the intrinsic activity of CI was decreased in patient cells. This finding was further substantiated using the antioxidant Trolox. Trolox-treatment revealed that both CI activity (IGA) and protein content (BNP) increased in control and patient cells. However, calculation of the ratio between the increases in these two parameters (ΔIGA/ΔBNP) revealed that newly formed CI was fully active in control cells (*i.e.* ΔIGA/ΔBNP=1) whereas ΔIGA < ΔBNP in patient cells, indicating that newly formed CI was functionally impaired (**chapter 3**). These findings demonstrate that mutations in nuclear-encoded subunits of CI lead to a decreased amount of intrinsically less active CI protein.

Inherited CI deficiency: do mutations in the NDUFS4 subunit prevent CI assembly?

In addition to the quantitative determination of CI protein content, BNP and subsequent Western Blot analysis is also very informative about the assembly status of CI, regarding the mutated subunit causing disease (**chapter 3,4**). Mutations in the NDUFA1, NDUFS2, NDUFS7, NDUFS8 and the B17.2L protein are all associated with a decline in the steady state amounts of the fully assembled (~1 MDa) CI protein complex (**chapter 3**; 74,185,271). BNP analysis of patient fibroblasts harboring NDUFS4 mutations revealed that they only contain an inactive CI subcomplex of ~830 kDa and no fully assembled CI (**chapter 4**; 223,271). In these patient cells no NDUFS4 protein was detectable by whole cell Western blot analysis (223). Moreover it has been demonstrated that the CI subcomplex does not contain the NADH-binding subunit NDUFV1 (47,185), thereby explaining the lack of IGA. A similar inactive ~830 kDa subcomplex is observed in patients harboring mutations in *NDUFV1*, *NDUFS1* (**chapter 3**; 116,185) and *NDUFS6* (130) in addition to a fully assembled CI. It's therefore suggestive that these subunits are also missing from the ~830 kDa subcomplex.

Surprisingly, a significant rotenone-sensitive NADH consumption (*e.g.* CI activity) was detected in mitochondria-enriched fractions isolated from NDUFS4 patient fibroblasts (40) when a biochemical assay was used. Using the same cells we here demonstrate the presence of rotenone-sensitive NADH consumption using single life cell microscopy (**chapter 4**). These findings indicate that a functional NADH consuming, rotenone-sensitive CI is expressed in NDUFS4 deficient cells in sharp contrast to the inactive CI subassembly found using BNP/IGA analysis.

This conclusion is somewhat controversial and strongly contrasts with previous studies claiming that no functional CI can be assembled in the absence of the NDUFS4 protein (116,199,223). The latter hypothesis is largely based on results obtained in serum starved cells, in which cAMP phosphorylates the NDUFS4 protein and thereby stimulates CI activity. However, serum starvation leads in principle to a decrease in CI activity (202) and specific NDUFS4 phosphorylation is highly debated (48).

Taken together, our findings suggest that fully assembled CI is less stable in patient fibroblasts harboring a mutation in the NDUFS4 protein. As a consequence the CI complex disintegrates during the BNP isolation procedure leaving only an inactive CI subcomplex. This implies a role for NDUFS4 in CI stabilization.

Superoxide levels are specifically increased in fibroblasts of patients with CI deficiency

To investigate if the decline in CI activity and protein content was related to altered ROS production in CI deficient fibroblasts, we first developed two fluorescent reporter assays allowing the selective quantification of the primary source of cellular ROS, superoxide (O_2^-; **chapter 2,3,5,7**) and its downstream products including H_2O_2 (**chapter 4-7**) in a non-invasive way. To obtain a quantitative understanding of its relationship with human CI deficiency we measured O_2^--levels, CI protein content and activity in two model systems for human CI deficiency. To this extent rotenone-treated control cells and skin fibroblasts derived from a cohort of 21 CI deficient patients were used and the obtained results were compared with healthy controls (**chapter 3**). Superoxide levels were elevated in 19 out of 21 CI deficient cell lines and inversely related to CI activity in both rotenone-treated controls and the cohort of patient cell lines. In the cohort of CI deficient cell lines, the decrease in CI activity was paralleled by a decline in CI protein content, whereas protein content increased in the rotenone-treated controls. In the latter case, however, the amount of CI increased rather than decreased, indicating that superoxide production can increase in the absence of mutations in CI subunits. Based on the latter finding we conclude that in isolated human CI deficiency increased cellular superoxide production is primarily a consequence of decreased cellular CI activity and not of further electron leakage due to the presence of a mutated subunit. Superoxide levels were not related to the residual CIII and CIV activities of these CI deficient cell lines (**table 1**, R=0.03, p=0.91 for CIII; R=0.26, p=0.28 for CIV). Importantly, patient-derived cell lines with other single-enzyme OXPHOS deficiencies did not show a detectable increase in O_2^- (**table 2**), suggesting that increased cellular O_2^--levels are a specific consequence of the reduction in CI activity.

As shown in **chapter 3, 5, 6** and **table 1** we observed increased free radical levels in all patients with an identified disease-causing mutation with the exception of patient 2. This patient is one of the two brothers (P1 and P2) with exactly the same mutation in the NDUFV1 subunit of CI (234). Both fibroblast cell lines show a similar decrease CI activity and fully assembled CI (**chapter 3**). Nevertheless, superoxide and cytosolic oxidant levels were only elevated in P1 illustrating that additional factors, such as ROS scavenging activity, play a role in determining cellular ROS production in inherited CI deficiency as found by others (116,204).

The striking difference in ROS levels between these two particular NDUFV1 deficient cell lines might be explained by a difference in the expression of metallothionein (MT). These small (6-7 kDa) metal binding proteins with high cysteine content can scavenge ROS in a similar way to glutathione. Induction of MT-expression occurs after CI inhibition by rotenone treatment (100 nM, 24h) in Hela cells (211) and in CI deficient fibroblasts with a nuclear-inherited mutation during transition from glucose to galactose as carbon source (275). In the latter study, induction of MT-transcripts was similar to controls for P2 (~2-fold) whereas this was 5-fold for P1 and up to 14-fold in other CI deficient cell lines. The lack of MT-induction observed in P2, could mean that the transcripts (and amount of protein) are already elevated in P2, leading to normalization of cellular ROS levels in this particular patient.

Table 1. OXPHOS activities of the complex I deficient fibroblast cell lines used in this thesis

CELL LINE[$]	AFFECTED SUBUNIT AND MUTATION[£]	CLINICAL PHENOTYPE [%]	CI ACTIVITY[#] COX	CIII ACTIVITY[#] COX	CIV ACTIVITY[#] CS	SUPEROXIDE LEVELS[&]	ROS LEVELS[&]	NAD(P)H LEVELS[&]
Control range	n.a.	n.a.	100 – 236%	100 – 206%	100 – 175%	91 – 112%	100-125%	88-108%
P1 (**#5171**)	**NDUFV1-**R59X/T423M	MLM/LL	**73**	126	159	**186±6** (84)	**242±19** (78)	**137±8** (40)
P2 (**#5866**)	**NDUFV1-**R59X/T423M	MLM/LL	**64**	148	147	110±3 (61)	135±12 (49)	**144±4** (112)
P3 (**#6173**)	**NDUFS1-**D618N/R577X	L/LD	**31**	120	126	**176±4** (83)	**171±13** (87)	**138±5** (77)
P4 (**#5170**)	**NDUFS2-**R228Q	HCEM	**39**	141	171	**205±8** (66)	**169±7** (124)	**147±6** (82)
P5 (**#5067**)	**NDUFS2-**P229Q	HCEM	**36**	111	88	**264±9** (100)	**351±41** (28)	**184±6** (119)
P6 (**#4605**)	**NDUFS2-**S413P	HCEM	**40**	239	322	**301±21** (40)	n.d.	n.d.
P7 (**#5077**)	**NDUFS4-**W97X	L/LL	**59**	114	173	**170±4** (100)	n.d.	n.d.
P8 (**#5260**)	**NDUFS4-**R106X	L/LL	**36**	80	132	**174±8** (64)	**187±12** (160)	**128±3** (132)
P9 (**#4827**)	**NDUFS4-**R106X	L/LL	**58**	n.d.	n.d.	**238±8** (93)	n.d.	n.d.
P10 (**#5737**)	**NDUFS4-**VPEEHI67/VEKSIstop	L/LL	**53**	127	114	**131±4** (92)	**202±12** (98)	**128±5** (93)
P11 (**#4608**)	**NDUFS4**-K158fs	L/LL	**75**	97	162	**195±6** (106)	**289±46** (29)	**136±4** (84)
P12 (**#5175**)	**NDUFS7**-V122M	L/LL	**68**	n.d.	141	**151±5** (94)	**212±15** (76)	115±5 (57)
P13 (**#6603**)	**NDUFS8**-R94C	L/LL	**18**	88	229	**222±7** (147)	**275±20** (117)	**178±6** (87)
P14 (**#4611**)	Unknown	L/LL	**36**	107	140	**395±27** (36)	n.d.	n.d.
P15 (**#5409**)	Unknown	FILA	**45**	165	141	**265±11** (104)	n.d.	n.d.
P16 (**#4591**)	Unknown	UEM	**39**	144	112	**189±5** (79)	n.d.	n.d.
P17 (**#4554**)	Unknown	L/LL	**42**	163	135	**175±6** (60)	n.d.	n.d.
P18 (**#4590**)	Unknown	FILA	**60**	160	102	**217±7** (70)	n.d.	n.d.
P19 (**#4606**)	Unknown	FILA	**63**	201	118	**197±9** (42)	n.d.	n.d.
P20 (**#4617**)	Unknown	L/LL	**85**	n.d.	n.d.	127±5 (56)	n.d.	n.d.
P21 (**#5671**)	Unknown	L/LL	**27**	115	133	**331±18** (38)	n.d.	n.d.

[$]Numbers indicate the designation of the cell lines within the Nijmegen Centre for Mitochondrial Disorders (NCMD). P indicate patient cell lines, respectively.
[£]Human subunit designation corresponds to the following nomenclature in *Bos taurus*: NDUFV1 (51-kDa), NDUFS1 (75-kDa), NDUFS2 (49-kDa), NDUFS4 (18-kDa), NDUFS7 (PSST), NDUFS8 (TYKY). Mutations are given at the protein level.
[%]FILA: Fatal infantile lactic acidosis, HCEM: Hypertrophic cardiomyopathy and encephalomyopathy, L/LD: Leigh syndrome and leukodystrophy, L/LL: Leigh syndrome and Leigh-like syndrome, MLM: Macrocephaly, leukodystrophy and myoclonic epilepsy, UEM: Unspecified encephalomyopathy.
[#]Enzymatic activities were measured in mitochondria-enriched fractions and expressed as % of the lowest control value (18.9 mU/mg protein; 100 mU/U CS and 110 mU/U COX for CI activity and 1270 mU/U COX and 680 mU/CS for CIII and CIV activity respectively).
[&]Cellular superoxide, ROS and NAD(P)H levels were expressed as percentage of CT-1 = 100% and tested for significance against the highest control value in the assay. Values in **bold** are significantly different ($p < 0.05$) from the lowest control (CI activity) or highest control value (superoxide, ROS and NAD(P)H. **Abbreviations:** n.a., not appropriate, n.d., not determined.

Table 2. Cellular superoxide levels in OXPHOS deficient fibroblasts and controls

OXPHOS DEFICIENCY[$]	RESIDUAL ACTIVITY[#]	CELLULAR SUPEROXIDE LEVEL[&]	
		Untreated	Rotenone*
Controls (106 ± 2)	145 ± 24	98 ± 1	171 ± 4
CI	**50 ± 4**	**188 ± 10**	249 ± 12
CII	**31 ± 6**	105 ± 7	166 ± 14
CIII	**65 ± 6**	113 ± 11	197 ± 14
CIV	**20 ± 2**	**60 ± 9**	108 ± 15

[$]CI-CIV represent the enzyme complex deficient in the OXPHOS system. [#]Enzymatic activities were measured in mitochondria-enriched fractions and expressed as % of the lowest control value (110 mU/U COX for CI; 536 mU/U COX for CII; 1270 mU/U COX for CIII and 680 mU/CS for CIV activity, respectively).
[&]Cellular superoxide levels were expressed as % of CT1 (277). Values are the mean + SEM of 7 control cell lines; 21 CI; 6 CII; 3 CIII; 4 CIV cell lines for vehicle-treated cells and 5 control cell lines; 21 CI; 6 CII; 2 CIII and 4 CIV cell lines treated with rotenone. **Statistics:** Values in bold are below the lowest control value (OXPHOS activity) or significantly different ($p<0.05$) from CT1 (superoxide level) *Rotenone treatment (10 min, 100 nM, resulted in a significant increase in superoxide levels in all single enzyme deficiencies analyzed.

Strikingly, patient-derived fibroblasts with an isolated CIV deficiency caused by mutations in CIV assembly factor SURF-1 displayed lower superoxide levels than controls. Decreased cellular superoxide levels could mean that superoxide dismutase (SOD) activity is upregulated in these cells. However, decreased superoxide was paralleled by a decline in cytosolic ROS levels in two of the abovementioned patients (data not shown) and SOD activity was unchanged in another study using a similar cell line (85). This suggests a decrease in cellular free radical production rather than enhanced scavenging in CIV deficiency.

Increased superoxide levels are not a consequence of reverse electron-flow

Regarding CI, the use of mitochondrial preparations and purified CI protein have demonstrated that single electron reduction of oxygen can occur at the Q-binding site, the iron-sulfur clusters, or the FMN binding site. (47,84,143,144,154,186). In addition to electrons derived from NADH oxidation, CI can accept electrons from CII via reverse electron flow, resulting superoxide formation (144,154). The latter process can be effectively blocked by CI inhibitors like rotenone (154). To investigate if the observed increase in superoxide in CI deficiency was due to reverse electron flow, cells were acutely treated with rotenone. Rotenone administration elevated cellular O_2^--levels in the whole cohort of CI deficient cell lines (**chapter 3**) and fibroblasts with other single-enzyme deficiencies (**table 2**). These results indicate that reverse electron flow does not underlie the increased O_2^--levels observed in the patient cells. Moreover, we can conclude that CI functions in its forward mode (*i.e.* is oxidizing NADH) in the latter cells.

Increased O_2^--levels are paralleled by elevated cytosolic oxidant and NADH levels

As depicted in **table I**, increased O_2^- levels were paralleled by proportional increases in the levels of O_2^--derived cytosolic oxidant levels (as reported by CM-DCF formation; **chapter 2-4, 6**) in nine out of ten CI deficient patients. However, rotenone-induced O_2^- formation was not associated with increased cytosolic oxidant levels in control cells. As reverse electron flow is not involved in cellular superoxide production, our data suggest that electrons derived from NADH are the most important source of superoxide. Using isolated mitochondrial preparations and purified CI, it has been shown that mitochondrial free radical production is intimately associated with NADH levels as high NADH levels resulted in elevated H_2O_2 (94,141,142,252) and O_2^- formation (143). Life cell analysis of NAD(P)H autofluorescence (**table 1**) revealed that NAD(P)H levels were elevated in all but one patient. Although NADH can also stimulate superoxide production from other cellular sources (2), regression analysis revealed that superoxide and NAD(P)H levels and residual CI activity were linearly correlated (**Figure 1a and b**). These results implicate CI activity as an important determinant for cellular superoxide and mitochondrial NAD(P)H levels.

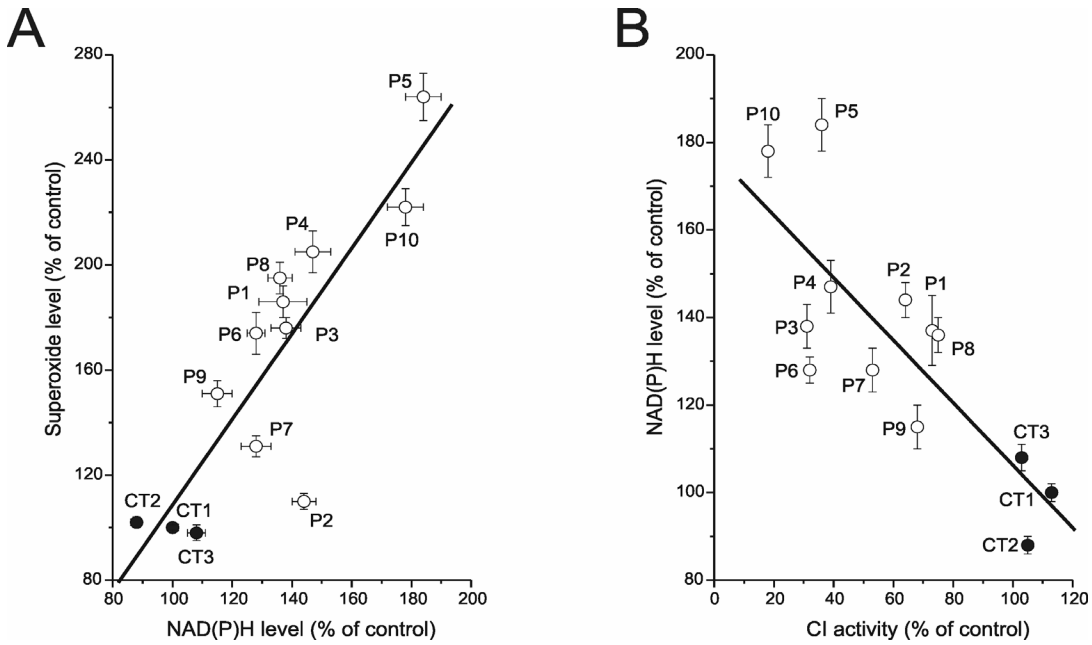

Fig 1. Relationship between cellular NAD(P)H levels and superoxide levels and CI activity - (**A**) Linear correlation between cellular NAD(P)H and superoxide levels in CI deficient fibroblasts (R=0.85, p=0.0002) B) Inverse relationship between CI activity and cellular NAD(P)H levels (R=-0.80, p=0.001). CI activity was determined in a fibroblast-derived mitochondrial enriched fraction and normalized to CIV activity. Next CI/CV activity ratios were expressed as % of lowest control ratio (110mU/U COX). Values for P (patient cell lines) and CT (control cell lines) are depicted in table 1.

Increased O_2^- and cytosolic oxidant levels do not detectably alter cellular redox status or degree of lipid peroxidation in fibroblasts of patients with CI deficiency

Increased ROS production from a malfunctioning CI could lead to oxidative stress and changes in redox environment resulting in cellular damage (117,209). In cells, the GSSG/2GSH redox couple is believed to be the major determinant of cellular redox homeostasis and antioxidant capacity (111,226,297). Despite the increased ROS levels in CI deficient patients, no differences were detected in cellular GSH content (total, oxidized and reduced) between a cohort of ten patient cell lines and ten controls. Furthermore, mitochondrial and cytosolic thiol redox state, determined in living cells with redox sensitive green fluorescent proteins (roGFP1) (64,95), was similar between the cohort of control and patient cell lines (**chapter 6**). In agreement with an unchanged redox environment, cellular damage in the form of lipid peroxidation was not observed.

In contrast to inherited CI deficiency, rotenone treatment caused a small but significant increase in the degree of roGFP1 oxidation (**chapter 6**) and induced a two-fold increase in lipid peroxidation (**chapter 7**). In further contrast with the data obtained in CI deficient patient fibroblasts, rotenone-induced superoxide levels (**chapter 5**) did not result in elevated cytosolic oxidant levels (**chapter 6**). The reason for these discrepancies can be due to the biogenesis of the mitochondrial network (136) as this adaptation has been suggested to lead to increased sharing of mitochondrial oxidants, possibly resulting in normalization of cytosolic oxidant levels (181,277).

Possible ROS- or redox-sensitive factors in human CI deficiency

The abovementioned results suggest that the cohort of CI deficient patient cell lines somehow adapted to the elevated free radical levels possibly via ROS and/or redox-sensitive signaling pathways. Although these pathways remain elusive, they could possibly involve the mitochondrial Fe-S protein glutaredoxin 2 (Grx2) (106) and the hypoxia inducible factor 1a (HIF-1a) (123), a transcription factor which is normally stabilized and activated under hypoxic conditions (238). HIF-1a can be of particular interest in human CI deficiency as it can also be activated under normoxic conditions as a consequence of elevated levels of ROS (243), intermediates of the Krebs cycle (36,114,236) and pyruvate (159), conditions which are also found in CI deficient patients (71) and derived cell lines (this thesis).

Mechanistic aspects of inherited CI deficiency: evidence that the cell's oxidative balance controls CI protein expression

Our results obtained in CI deficient patient fibroblasts demonstrate a link between CI activity, CI protein content, NAD(P)H metabolism and cellular ROS levels. We propose a mechanism (**Fig. 2**) in which nDNA-encoded mutations in CI subunits lower the expression of the fully assembled complex and thereby decrease overall CI activity. As a result, cellular NAD(P)H and free radical levels are increased depending on the severity of the deficiency. If (local) ROS levels are sufficiently high, they can change cellular redox state and might cause additional damage to CI or other cellular constituents (48). However, elevated ROS levels will also induce a signalling cascade counterbalancing increased ROS production by inducing the expression of endogenous antioxidants (204,211,296) or mitochondrial biogenesis (171,183,201,256).

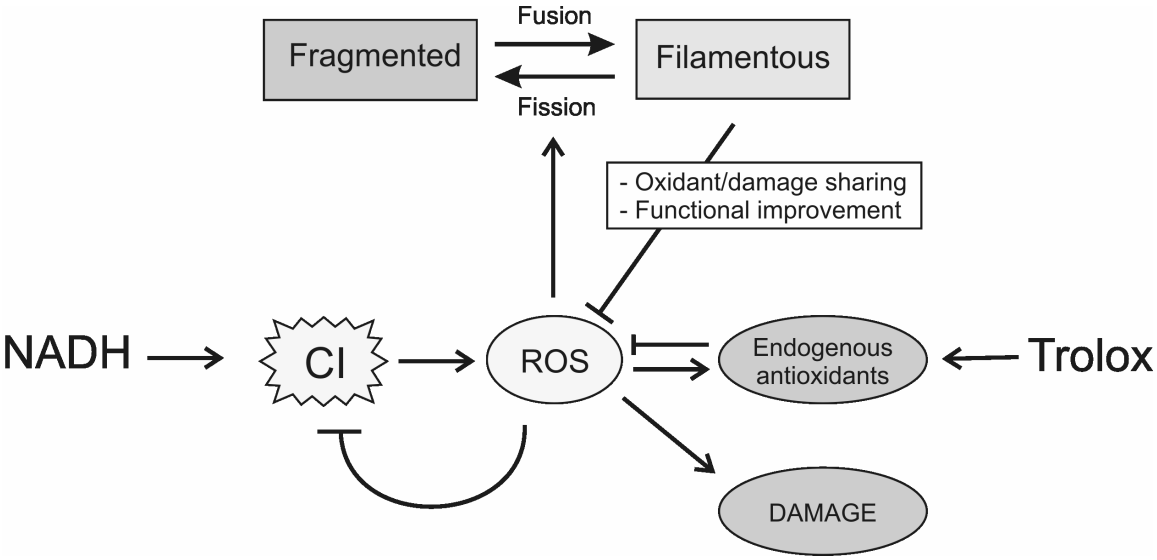

Fig 2. Proposed model for cell biological consequences in human CI deficiency

A similar situation can be envisioned for NADH as physiological concentrations are associated with transcriptional regulation (76,303) whereas excessive cellular [NADH] disturbs the NADH:NAD^+ ratio, leading to altered lactate:pyruvate ratio's and build up of lactic acid (215). Using the antioxidant Trolox we show that the cell's oxidative balance is important for the expression of CI as scavenging of ROS using this compound results in reduced ROS levels and a variable increase in CI protein expression and activity in all CI deficient patients investigated. In addition a functional relation between ROS production and

mitochondrial morphology is proposed. Excessive ROS leads to fragmented mitochondria and is proposed to lead to further functional impairment (46). In contrast mildly elevated ROS levels promote mitochondrial biogenesis (136,147,171) leading to a filamentous mitochondrial structure. It is hypothesized that the latter morphology is directly beneficial for mitochondrial function (203) in that it facilitates the sharing of intramitochondrial antioxidants and ROS-damaged mitochondrial constituents thereby reducing the detrimental effects of ROS (181). This relation is supported by recent findings in Chang cells (an immortalized normal hepatocyte cell line) where chronic (12 h) application of a high concentration of hydrogen peroxide (1 mM) induced mitochondrial fragmentation, whereas lower doses (100 - 200 µM) induced the formation of elongated 'giant' mitochondria (299).

Possible therapeutics and future perspectives

Although there is currently no cure available for inherited CI deficiency, mitigating therapy might be provided using different approaches (61). Most promising are symptomatic therapy in the form of exercise training (260,261) and administration of nutritional cofactors (42,163,220). The assays for quantitative profiling of cellular ROS production and mitochondrial shape and function described in this thesis provide a novel approach for the screening of novel compounds that restore mitochondrial function and/or promote mitochondrial health. The most important conclusion of our integrated quantitative approach is that it provides an experimental basis for antioxidant treatment of inherited human CI deficiency.

As Trolox administration is associated with normalized ROS levels and improved CI protein content and activity, our results suggest that CI expression is under control of the cells oxidative balance. However, similar to vitamin E (232,259,270), Trolox could have other non-ROS related effects on cellular function possibly leading to the observed improvement in CI deficiency. To investigate if Trolox really exerts its beneficial effect on mitochondrial protein expression by scavenging of mitochondria-derived ROS, mitochondrial targeted antioxidants like MitoQ (117,177,241) can be used. Of these compounds, MitoVit E, a mitochondrially targeted Trolox variant, (250) is very promising as it resembles Trolox, can also be delivered to mitochondria *in vivo* (249), and has already proven to have beneficial effects in a cellular model of Friedreich's ataxia (121).

Testing of potential therapeutics requires a platform which allows rapid identification of the effective concentration and incubation time of the compound of interest. As this is rather time-consuming and therefore not feasible using manual single cell imaging, the developed

protocols described in this thesis might be adapted to high-throughput fluorescence microscopy (73,100,145,198). Using the existing array of protocols, a cell biological fingerprint of a particular patient cell line can then be developed and refined using novel sensors to detect mitochondrial superoxide (217), cellular H_2O_2 (19) NO (15) and oxygen consumption (170,191).

Conclusions

The data included in this thesis demonstrate that human isolated CI deficiency caused by mutations in nuclear-encoded CI subunits leads to a reduction in the amount and intrinsic activity of CI protein. The decrease in CI activity increases cellular ROS and NAD(P)H levels but does not induce alterations in cellular thiol redox status or lipid peroxidation. Treatment of these cells with the antioxidant Trolox alleviates cytosolic ROS production and increases CI protein content and activity to a variable extent, stressing the importance of an oxidative component in the pathology of human CI deficiency.

ABBREVIATIONS

$\Delta\Psi$	mitochondrial membrane potential
Ø	diameter
AR	aspect ratio
ADP	adenosine diphosphate
ATP	adenosine triphosphate
BNP	blue native polyacrylamide gel electrophoresis
BSO	D,L-butathione-(S,R)-sulphoximine
CI	complex I or NADH:ubiquinone oxidoreductase
CII	complex II or succinate dehydrogenase:ubiquinone oxidoreductase
CIII	complex III or ubiquinol:cytochrome *c* oxidoreductase
CIV	complex IV or cytochrome *c* oxidase
CV	complex V or F_0/F_1-ATP-synthase
C11-BODIPY$^{581/591}$	4,4-difluoro-5-(4-phenyl-1,3-butadienyl)-4-bora-3a,4a-diaza-s-indacene-3-undecanoic acid
Ca^{2+}	calcium
cDNA	copy DNA
CM-H_2DCFDA	5-(and-6)-chloromethyl-2',7'-dichlorodihydrofluorescein diacetate
CM-H_2DCF	dichlorodihydrofluorescein
CM-DCF	dichlorofluorescein
CoQ	ubiquinone (Coenzyme Q)
$CoQH_2$	ubiquinol
COX	cytochrome *c* oxidase
CO_2	carbon dioxide
CS	citrate synthase
CT	control cell line
CuZnSOD	copper-zinc superoxide dismutase
Cyt *c*	Cytochrome c
DMSO	dimethyl sulfoxide
DNA	deoxyribonucleic acid
DTT	dithiothreitol
Et	ethidium
ETC	electron transport chain

F	formfactor (perimeter^2/4π·area)
FCCP	p-trifluoromethoxy carbonyl cyanide phenyl hydrazone
F/Nc	mitochondrial network complexity
$FADH_2$	flavin adenine dinucleotide (reduced form)
Fe^{2+}	ferrous iron
FILA	fatal infantile lactic acidosis
FMN	flavin mononucleotide
FP	flavoprotein
GSH	glutathione (reduced form)
GSSG	glutathione disulfide (oxidized form)
H^+	proton
HCEM	hypertrophic cardiomyopathy and encephalomyopathy
H_2O_2	hydrogen peroxide
$HO_2^{\cdot}$	hydroperoxyl radical
HE(t)	hydroethidine
HP	hydrophobic protein
HPLC	High-performance liquid chromatography
IGA	in-gel activity
IP	iron-sulfur protein
IMS	inner membrane space
IMM	inner mitochondrial membrane
LD	Leigh disease
L/LD	Leigh syndrome and leukodystrophy
L/LL	Leigh syndrome and Leigh-like syndrome
MDa	megadalton
MG	Mitotracker Green FM
Mfn2	Mitofusin-2
MILS	Maternally inherited Leigh syndrome
MitoQ	Mitoquinone
MLM	macrocephaly, leukodystrophy and myoclonic epilepsy
MnSOD	manganese superoxide dismutase
MR	Mitotracker Red CMXRos
MT	metallothionein
mtDNA	mitochondrial DNA

NAD^+	nicotinamide adenine dinucleotide (oxidized form)
NADH	nicotinamide adenine dinucleotide (reduced form)
NADPH	nicotinamide adenine dinucleotide phosphate (reduced form)
NARP	Neuropathy, Ataxia and Retinitis Pigmentosa
Nc	number of mitochondria per cell
nDNA	nuclear DNA
NDUF	NADH dehydrogenase ubiquinone flavoprotein subunit
ND	NADH dehydrogenase subunit
NBT	nitro blue tetrazolium
NO	nitric oxide
$^1O_2$	singlet oxygen
O_2^-	superoxide
$OH^·$	hydroxyl radical
OMIM	online Mendelian inheritance in man
OMM	outer mitochondrial membrane
$ONOO^-$	peroxynitrite
OXPHOS	oxidative phosphorylation
P	patient cell line
Pi	inorganic phosphate
PBS	phosphate buffered saline
$PUFAOO^·$	polyunsaturated fatty acid peroxyl radicals
roGFP1	reduction-oxidation sensitive green fluorescent protein 1
R123	rhodamine 123
ROI	region of interest
ROS	reactive oxygen species
RNS	reactive nitrogen species
SE(M)	standard error of the mean
SOD	superoxide dismutase
TIM	translocator of the inner mitochondrial membrane
TOM	translocator of the outer mitochondrial membrane
Trolox	6-hydroxy-2,5,7,8-tetramethylchroman-2-carboxylic acid
UEM	Unspecificied encephalomyopathy
$V_{CM\text{-}DCF}$	rate of CM-DCF fluorescence increase
WB	Western Blot

REFERENCE LIST

1. Abou-Sleiman PM, Muqit MM, Wood NW: **Expanding insights of mitochondrial dysfunction in Parkinson's disease.** *Nat.Rev.Neurosci.* 2006, 7(3):207-219.

2. Adam-Vizi V, Chinopoulos C: **Bioenergetics and the formation of mitochondrial reactive oxygen species.** *Trends Pharmacol.Sci.* 2006, 12:639-645.

3. Ahlers PM, Garofano A, Kerscher SJ, Brandt U: **Application of the obligate aerobic yeast *Yarrowia lipolytica* as a eukaryotic model to analyse Leigh syndrome mutations in the complex I core subunits PSST and TYKY.** *Biochim.Biophys.Acta.* 2000, 1459(2-3):258-265.

4. Anderson ME: **Glutathione: an overview of biosynthesis and modulation.** *Chem.Biol.Interact.* 1998, 111-112:1-14.

5. Andreyev AY, Kushnareva YE, Starkov AA: **Mitochondrial metabolism of reactive oxygen species.** *Biochemistry (Mosc)* 2005, 70(2):200-214.

6. Antunes F, Cadenas E: **Estimation of H_2O_2 gradients across biomembranes.** *FEBS Lett.* 2000, 475(2):121-126.

7. Antunes F, Salvador A, Marinho HS, Alves R, Pinto RE: **Lipid peroxidation in mitochondrial inner membranes. I. An integrative kinetic model**. *Free Radic.Biol.Med.* 1996, 21(7):917-943.

8. Armstrong JS: **Mitochondrial membrane permeabilization: the sine qua non for cell death.** *Bioessays* 2006, 28(3):253-260.

9. Armstrong JS, Hornung B, Lecane P, Jones DP, Knox SJ: **Rotenone-induced G2/M cell cycle arrest and apoptosis in a human B lymphoma cell line PW.** *Biochem.Biophys.Res.Commun.* 2001, 289(5):973-978.

10. Asin-Cayuela J, Manas AR, James AM, Smith RA, Murphy MP: **Fine-tuning the hydrophobicity of a mitochondria-targeted antioxidant.** *FEBS Lett.* 2004, 571(1-3):9-16.

11. Bach D, Pich S, Soriano FX, Vega N, Baumgartner B, Oriola J, Daugaard JR, Lloberas J, Camps M, Zierath JR, Rabasa-Lhoret R, Wallberg-Henriksson H, Laville M, Palacin M, Vidal H, Rivera F, Brand M, Zorzano A: **Mitofusin-2 determines mitochondrial network architecture and mitochondrial metabolism. A novel regulatory mechanism altered in obesity.** *J.Biol.Chem.* 2003, 278(19):17190-17197.

12. Bacsi A, Woodberry M, Widger W, Papaconstantinou J, Mitra S, Peterson JW, Boldogh I: **Localization of superoxide anion production to mitochondrial electron transport chain in 3-NPA-treated cells.** *Mitochondrion* 2006, 6(5):235-244.

13. Baglole CJ, Bushinsky SM, Garcia TM, Kode A, Rahman I, Sime PJ, Phipps RP: **Differential induction of apoptosis by cigarette smoke extract in primary human lung fibroblast strains: implications for emphysema.** *Am.J.Physiol.Lung Cell.Mol.Physiol*. 2006, 291(1):L19-L29.

14. Balaban RS, Nemoto S, Finkel T: **Mitochondria, oxidants, and aging.** *Cell* 2005, 120(4):483-495.

15. Balcerczyk A, Soszynski M, Bartosz G: **On the specificity of 4-amino-5-methylamino-2',7'-difluorofluorescein as a probe for nitric oxide.** *Free Radic.Biol.Med.* 2005, 39(3):327-335.

16. Barrientos A, Moraes CT: **Titrating the effects of mitochondrial complex I impairment in the cell physiology.** *J.Biol.Chem.* 1999, 274(23):16188-16197.

17. Basoah A, Matthews PM, Morten KJ: **Rapid rates of newly synthesized mitochondrial protein degradation are significantly affected by the generation of mitochondrial free radicals.** *FEBS Lett.* 2005, 579(28):6511-6517.

18. Bautista J, Corpas R, Ramos R, Cremades O, Gutierrez JF, Alegre S: **Brain mitochondrial complex I inactivation by oxidative modification.** *Biochem.Biophys.Res.Commun.* 2000, 275(3):890-894.

19. Belousov VV, Fradkov AF, Lukyanov KA, Staroverov DB, Shakhbazov KS, Terskikh AV, Lukyanov S: **Genetically encoded fluorescent indicator for intracellular hydrogen peroxide.** *Nat.Methods* 2006, 3(4):281-286.

20. Benit P, Beugnot R, Chretien D, Giurgea I, De Lonlay-Debeney P, Issartel JP, Corral-Debrinski M, Kerscher S, Rustin P, Rotig A, Munnich A: **Mutant NDUFV2 subunit of mitochondrial complex I causes early onset hypertrophic cardiomyopathy and encephalopathy.** *Hum.Mutat.* 2003, 21(6):582-586.

21. Benit P, Chretien D, Kadhom N, de Lonlay-Debeney P, Cormier-Daire V, Cabral A, Peudenier S, Rustin P, Munnich A, Rotig A: **Large-scale deletion and point mutations of the nuclear NDUFV1 and NDUFS1 genes in mitochondrial complex I deficiency.** *Am.J.Hum.Genet.* 2001, 68(6):1344-1352.

22. Benit P, Slama A, Cartault F, Giurgea I, Chretien D, Lebon S, Marsac C, Munnich A, Rotig A, Rustin P: **Mutant NDUFS3 subunit of mitochondrial complex I causes Leigh syndrome.** *J.Med.Genet.* 2004, 41(1):14-17.

23. Ben Mahdi MH, Andrieu V, Pasquier C: **Focal adhesion kinase regulation by oxidative stress in different cell types.** *IUBMB Life* 2000, 50(4-5):291-299.

24. Bernardi P: **Mitochondrial transport of cations: channels, exchangers, and permeability transition.** *Physiol.Rev.* 1999, 79(4):1127-55.

25. Berridge MJ, Bootman MD, Roderick HL: **Calcium signalling: dynamics, homeostasis and remodelling.** *Nat.Rev.Mol.Cell.Biol.* 2003, 4(7):517-529.

26. Bharath S, Andersen JK: **Glutathione depletion in a midbrain-derived immortalized dopaminergic cell line results in limited tyrosine nitration of mitochondrial complex I subunits: implications for Parkinson's disease.** *Antioxid.Redox Signal.* 2005, 7(7-8):900-910.

27. Bianchi C, Genova ML, Parenti Castelli G, Lenaz G: **The mitochondrial respiratory chain is partially organized in a supercomplex assembly: kinetic evidence using flux control analysis.** *J.Biol.Chem.* 2004, 279(35):36562-36569.

28. Bigelow DJ, Squier TC: **Redox modulation of cellular signaling and metabolism through reversible oxidation of methionine sensors in calcium regulatory proteins.** *Biochim.Biophys.Acta.* 2005, 1703(2):121-134.

29. Bilski P, Belanger AG, Chignell CF: **Photosensitized oxidation of 2',7'-dichlorofluorescin: singlet oxygen does not contribute to the formation of fluorescent oxidation product 2',7'-dichlorofluorescein.** *Free Radic.Biol.Med.* 2002, 33(7):938-946.

30. Bindokas VP, Jordan J, Lee CC, Miller RJ: **Superoxide production in rat hippocampal neurons: selective imaging with hydroethidine.** *J.Neurosci.* 1996, 16(4):1324-1336.

31. Bindokas VP, Kuznetsov A, Sreenan S, Polonsky KS, Roe MW, Philipson LH: **Visualizing superoxide production in normal and diabetic rat islets of Langerhans.** *J.Biol.Chem.* 2003, 278(11):9796-9801.

32. Bonini MG, Rota C, Tomasi A, Mason RP: **The oxidation of 2',7'-dichlorofluorescin to reactive oxygen species: a self-fulfilling prophesy?** *Free Radic.Biol.Med.* 2006, 40(6):968-975.

33. Bourgeron T, Rustin P, Chretien D, Birch-Machin M, Bourgeois M, Viegas-Pequignot E, Munnich A, Rotig A: **Mutation of a nuclear succinate dehydrogenase gene results in mitochondrial respiratory chain deficiency.** *Nat.Genet.* 1995, 1(2):144-149.

34. Brand MD, Affourtit C, Esteves TC, Green K, Lambert AJ, Miwa S, Pakay JL, Parker N: **Mitochondrial superoxide: production, biological effects, and activation of uncoupling proteins.** *Free Radic.Biol.Med.* 2004, 37(6):755-767.

35. Brandt U: **Energy converting NADH:quinone oxidoreductase (complex I).** *Annu.Rev.Biochem.* 2006, 75:69-92.

36. Briere JJ, Favier J, Benit P, El Ghouzzi V, Lorenzato A, Rabier D, Di Renzo MF, Gimenez-Roqueplo AP, Rustin P: **Mitochondrial succinate is instrumental for HIF1alpha nuclear translocation in SDHA-mutant fibroblasts under normoxic conditions.** *Hum.Mol.Genet.* 2005, 14(21):3263-3269.

37. Brocard JB, Rintoul GL, Reynolds IJ: **New perspectives on mitochondrial morphology in cell function.** *Biol.Cell.* 2003, 95(5):239-242.

38. Brookes PS: **Mitochondrial nitric oxide synthase.** *Mitochondrion* 2004, 3(4):187-204.

39. Budde SM, van den Heuvel LP, Janssen AJ, Smeets RJ, Buskens CA, DeMeirleir L, Van Coster R, Baethmann M, Voit T, Trijbels JM, Smeitink JA: **Combined enzymatic complex I and III deficiency associated with mutations in the nuclear encoded NDUFS4 gene.** *Biochem.Biophys.Res.Commun.* 2000, 275(1):63-68.

40. Budde SM, van den Heuvel LP, Smeets RJ, Skladal D, Mayr JA, Boelen C, Petruzzella V, Papa S, Smeitink JA: **Clinical heterogeneity in patients with mutations in the NDUFS4 gene of mitochondrial complex I.** *J.Inherit.Metab.Dis.* 2003, 26(8):813-815.

41. Bugiani M, Invernizzi F, Alberio S, Briem E, Lamantea E, Carrara F, Moroni I,Farina L, Spada M, Donati MA, Uziel G, Zeviani M: **Clinical and molecular findings in children with complex I deficiency.** *Biochim.Biophys.Acta.* 2004, 1659(2-3):136-147.

42. Bugiani M, Lamantea E, Invernizzi F, Moroni I, Bizzi A, Zeviani M, Uziel G: **Effects of riboflavin in children with complex II deficiency.** *Brain Dev.* 2006, 28(9):576-581.

43. Cadenas E, Davies KJ. **Mitochondrial free radical generation, oxidative stress, and aging.** *Free Radic.Biol.Med.* 2000, 29(3-4):222-230.

44. Carroll J, Fearnley IM, Shannon RJ, Hirst J, Walker JE: **Analysis of the subunit composition of complex I from bovine heart mitochondria.** *Mol.Cell.Proteomics* 2003, 2(2):117-126.

45. Carroll J, Fearnley IM, Skehel JM, Shannon RJ, Hirst J, Walker JE: **Bovine complex I is a complex of forty-five different subunits.** *J.Biol.Chem.* 2006, 281(43):32724-32727.

46. Chen H, Chan DC: **Emerging functions of mammalian mitochondrial fusion and fission.** *Hum.Mol.Genet.* 2005, 14 Spec No. 2:R283-289.

47. Chen YR, Chen CL, Zhang L, Green-Church KB, Zweier JL: **Superoxide generation from mitochondrial NADH dehydrogenase induces self-inactivation with specific protein radical formation.** *J.Biol.Chem.* 2005, 280(45):37339-37348.

48. Chen R, Fearnley IM, Peak-Chew SY, Walker JE. **The phosphorylation of subunits of complex I from bovine heart mitochondria.** *J.Biol.Chem.* 2004, 279(25):26036-26045.

49. Chen Q, Lesnefsky EJ: **"Hiding out" from chronic ischemia with help from the mitochondria?** *J.Mol.Cell.Cardiol.* 2006, 41(6):956-958.

50. Chen J, Small-Howard A, Yin A, Berry MJ: **The responses of Ht22 cells to oxidative stress induced by buthionine sulfoximine (BSO).** *BMC Neurosci.* 2005c, 6(1):10.

51. Chiarugi P, Pani G, Giannoni E, Taddei L, Colavitti R, Raugei G, Symons M, Borrello S, Galeotti T, Ramponi G: **Reactive oxygen species as essential mediators of cell adhesion: the oxidative inhibition of a FAK tyrosine phosphatase is required for cell adhesion.** *J.Cell.Biol.* 2003, 161(5):933-944.

52. Choksi KB, Boylston WH, Rabek JP, Widger WR, Papaconstantinou J: **Oxidatively damaged proteins of heart mitochondrial electron transport complexes.** *Biochim.Biophys.Acta.* 2004, 1688(2):95-101.

53. Coenen MJ, van den Heuvel LP, Smeitink JA: **Mitochondrial oxidative phosphorylation system assembly in man: recent achievements.** *Curr.Opin.Neurol.* 2001, 14(6):777-781.

54. Cuezva JM, Krajewska M, de Heredia ML, Krajewski S, Santamaria G, Kim H, Zapata JM, Marusawa H, Chamorro M, Reed JC: **The bioenergetic signature of cancer: a marker of tumor progression.** *Cancer Res.* 2002, 62(22):6674-6681.

55. Dahm CC, Moore K, Murphy MP: **Persistent S-nitrosation of complex I and other mitochondrial membrane proteins by S-nitrosothiols but not nitric oxide or peroxynitrite: implications for the interaction of nitric oxide with mitochondria.** *J.Biol.Chem.* 2006, 281(15):10056-10065.

56. Dalle-Donne I, Scaloni A, Giustarini D, Cavarra E, Tell G, Lungarella G, Colombo R, Rossi R, Milzani A: **Proteins as biomarkers of oxidative/nitrosative stress in diseases: the contribution of redox proteomics.** *Mass Spectrom.Rev.* 2005, 24(1):55-99.

57. de Graaf-Hess A, Trijbels F, Blom H: **New method for determining cystine in leukocytes and fibroblasts.** *Clin.Chem.* 1999, 45(12):2224-2248.

58. de Groof AJ, Fransen JA, Errington RJ, Willems PH, Wieringa B, Koopman WJ: **The creatine kinase system is essential for optimal refill of the sarcoplasmic reticulum Ca2+ store in skeletal muscle.** *J.Biol.Chem.* 2002, 277(7):5275-5284.

59. Delettre C, Lenaers G, Griffoin JM, Gigarel N, Lorenzo C, Belenguer P, Pelloquin L, Grosgeorge J, Turc-Carel C, Perret E, Astarie-Dequeker C, Lasquellec L, Arnaud B, Ducommun B, Kaplan J, Hamel CP: **Nuclear gene OPA1, encoding a mitochondrial dynamin-related protein, is mutated in dominant optic atrophy.** *Nat.Genet.* 2000, 26(2):207-210.

60. Diaz-Corrales FJ, Asanuma M, Miyazaki I, Ogawa N: **Rotenone induces disassembly of the Golgi apparatus in the rat dopaminergic neuroblastoma B65 cell line.** *Neurosci.Lett.* 2004, 354(1):59-63.

61. DiMauro S, Hirano M, Schon EA: **Approaches to the treatment of mitochondrial diseases.** *Muscle Nerve*. 2006, 34(3):265-283.

62. DiMauro S, Schon EA: **Mitochondrial respiratory-chain diseases.** *N.Engl.J.Med.* 2003, 348(26):2656-2668.

63. Dispersyn G, Nuydens R, Connors R, Borgers M, Geerts H: **Bcl-2 protects against FCCP-induced apoptosis and mitochondrial membrane potential depolarization in PC12 cells.** *Biochim.Biophys.Acta.* 1999, 1428(2-3):357-371.

64. Dooley CT, Dore TM, Hanson GT, Jackson WC, Remington SJ, Tsien RY: **Imaging dynamic redox changes in mammalian cells with green fluorescent protein indicators.** *J.Biol.Chem.* 2004, 279(21):22284-22293.

65. Droge W: **Free radicals in the physiological control of cell function.** *Physiol.Rev.* 2002, 82(1):47-95.

66. Drummen GP, van Liebergen LC, Op den Kamp JA, Post JA: **C11-BODIPY(581/591), an oxidation-sensitive fluorescent lipid peroxidation probe: (micro)spectroscopic characterization and validation of methodology.** *Free Radic.Biol.Med.* 2002, 33(4):473-490.

67. Duarte M, Schulte U, Ushakova AV, Videira A: **Neurospora strains harboring mitochondrial disease-associated mutations in iron-sulfur subunits of complex I.** *Genetics.* 2005, 171(1):91-99.

68. Duchen MR: **Mitochondria in health and disease: perspectives on a new mitochondrial biology.** *Mol.Aspects Med.* 2004, 25(4):365-451.

69. Dussmann H, Kogel D, Rehm M, Prehn JH: **Mitochondrial membrane permeabilization and superoxide production during apoptosis. A single-cell analysis.** *J.Biol.Chem.* 2003, 278(15):12645-12649.

70. Egner A, Jakobs S, Hell SW: **Fast 100-nm resolution three-dimensional microscope reveals structural plasticity of mitochondria in live yeast.** *Proc.Natl.Acad.Sci. U S A.* 2002, 99(6):3370-3375.

71. Esteitie N, Hinttala R, Wibom R, Nilsson H, Hance N, Naess K, Tear-Fahnehjelm K,von Dobeln U, Majamaa K, Larsson NG: **Secondary metabolic effects in complex I deficiency.** *Ann.Neurol.* 2005, 58(4):544-552.

72. Esworthy RS, Ho YS, Chu FF: **The Gpx1 gene encodes mitochondrial glutathione peroxidase in the mouse liver.** *Arch.Biochem.Biophys.* 1997, 340(1):59-63.

73. Fernandez-Gonzalez R, Munoz-Barrutia A, Barcellos-Hoff MH, Ortiz-de-Solorzano C: **Quantitative in vivo microscopy: the return from the 'omics'.** *Curr.Opin.Biotechnol.* 2006, 17(5):501-510.

74. Fernandez-Moreira D, Ugalde C, Smeets R, Rodenburg RJ, Lopez-Laso E, Ruiz-Falco ML, Briones P, Martin MA, Smeitink JA, Arenas J: **X-linked NDUFA1 gene mutations associated with mitochondrial encephalomyopathy.** *Ann.Neurol.* 2007, 61(1):73-83.

75. Finkel T, Holbrook NJ: **Oxidants, oxidative stress and the biology of ageing.** *Nature* 2000, 408(6809):239-247.

76. Fjeld CC, Birdsong WT, Goodman RH: **Differential binding of NAD+ and NADH allows the transcriptional corepressor carboxyl-terminal binding protein to serve as a metabolic sensor.** *Proc.Natl.Acad.Sci. U S A.* 2003, 100(16):9202-9207.

77. Fojo T, Bates S: **Strategies for reversing drug resistance.** *Oncogene* 2003, 22(47):7512-7523.

78. Fontaine E, Bernardi P: **Progress on the mitochondrial permeability transition pore: regulation by complex I and ubiquinone analogs.** *J.Bioenerg.Biomembr.* 1999, 31(4):335-345.

79. Ford RJ, Graham DA, Denniss SG, Quadrilatero J, Rush JW: **Glutathione depletion in vivo enhances contraction and attenuates endothelium-dependent relaxation of isolated rat aorta.** *Free Radic.Biol.Med.* 2006, 40(4):670-678.

80. Forman HJ, Fukuto JM, Torres M: **Redox signaling: thiol chemistry defines which reactive oxygen and nitrogen species can act as second messengers.** *Am.J.Physiol.Cell.Physiol.* 2004, 287(2):C246-C256.

81. Friedrich T, Bottcher B: **The gross structure of the respiratory complex I: a Lego System.** *Biochim.Biophys.Acta.* 2004, 1608(1):1-9.

82. Friedrich T, Weiss H: **Modular evolution of the respiratory NADH:ubiquinone oxidoreductase and the origin of its modules.** *J.Theor.Biol.* 1997, 187(4):529-540.

83. Gabaldon T, Rainey D, Huynen MA: **Tracing the evolution of a large protein complex in the eukaryotes, NADH:ubiquinone oxidoreductase (Complex I).** *J.Mol.Biol.* 2005, 348(4):857-870.

84. Genova ML, Ventura B, Giuliano G, Bovina C, Formiggini G, Parenti Castelli G, Lenaz G: **The site of production of superoxide radical in mitochondrial Complex I is not a bound ubisemiquinone but presumably iron-sulfur cluster N2.** *FEBS Lett.* 2001, 505(3):364-368.

85. Geromel V, Kadhom N, Cebalos-Picot I, Ouari O, Polidori A, Munnich A, Rotig A,Rustin P: **Superoxide-induced massive apoptosis in cultured skin fibroblasts harboring the neurogenic ataxia retinitis pigmentosa (NARP) mutation in the ATPase-6 gene of the mitochondrial DNA.** *Hum.Mol.Genet.* 2001, 10(11):1221-1228.

86. Ghafourifar P, Cadenas E: **Mitochondrial nitric oxide synthase.** *Trends Pharmacol.Sci.* 2005, 26(4):190-195.

87. Gomes A, Fernandes E, Lima JL: **Fluorescence probes used for detection of reactive oxygen species.** *J.Biochem.Biophys.Methods* 2005, 65(2-3):45-80.

88. Gottlieb E, Tomlinson IP: **Mitochondrial tumour suppressors: a genetic and biochemical update.** *Nat.Rev.Cancer.* 2005, 5(11):857-866.

89. Griffith OW, Meister A: **Potent and specific inhibition of glutathione synthesis by buthionine sulfoximine (S-n-butyl homocysteine sulfoximine).** *J.Biol.Chem.* 1979, 254(16):7558-7560.

90. Grigorieff N: **Structure of the respiratory NADH:ubiquinone oxidoreductase (complex I).** *Curr.Opin.Struct.Biol.* 1999, 9(4):476-483.

91. Griparic L, van der Bliek AM: **The many shapes of mitochondrial membranes.** *Traffic* 2001, 2(4):235-244.

92. Gutteridge JM, Halliwell B: **Free radicals and antioxidants in the year 2000. A historical look to the future.** *Ann.N Y.Acad.Sci.* 2000, 899:136-147.

93. Ha HC, Woster PM, Yager JD, Casero RA Jr: **The role of polyamine catabolism in polyamine analogue-induced programmed cell death.** *Proc.Natl.Acad.Sci.U S A.* 1997, 94(21):11557-11562.

94. Hansford RG, Hogue BA, Mildaziene V: **Dependence of H2O2 formation by rat heart mitochondria on substrate availability and donor age.** *J.Bioenerg.Biomembr.* 1997, 29(1):89-95.

95. Hanson GT, Aggeler R, Oglesbee D, Cannon M, Capaldi RA, Tsien RY, Remington SJ: **Investigating mitochondrial redox potential with redox-sensitive green fluorescent protein indicators.** *J.Biol.Chem.* 2004, 279(13):13044-13053.

96. Harman D: **Aging: a theory based on free radical and radiation chemistry.** *J.Gerontol.* 1956, 11(3):298-300.

97. Harper ME, Himms-Hagen J: **Mitochondrial efficiency: lessons learned from transgenic mice.** *Biochim.Biophys.Acta.* 2001, 1504(1):159-172.

98. Heath-Engel HM, Shore GC: **Mitochondrial membrane dynamics, cristae remodelling and apoptosis.** *Biochim.Biophys.Acta.* 2006, 1763(5-6):549-560.

99. Hempel SL, Buettner GR, O'Malley YQ, Wessels DA, Flaherty DM. **Dihydrofluorescein diacetate is superior for detecting intracellular oxidants: comparison with 2',7'-dichlorodihydrofluorescein diacetate, 5(and 6)-carboxy-2',7'-dichlorodihydrofluorescein diacetate, and dihydrorhodamine 123.** *Free Radic.Biol.Med.* 1999, 27(1-2):146-159.

100. Herrera G, Diaz L, Martinez-Romero A, Gomes A, Villamon E, Callaghan RC, O'connor JE: **Cytomics: A multiparametric, dynamic approach to cell research.** *Toxicol.In Vitro.* 2007, 21(2):176-182.

101. Hervouet E, Godinot C: **Mitochondrial disorders in renal tumors.** *Mitochondrion* 2006, 6(3):105-117.

102. Hinerfeld D, Traini MD, Weinberger RP, Cochran B, Doctrow SR, Harry J, Melov S: **Endogenous mitochondrial oxidative stress: neurodegeneration, proteomic analysis, specific respiratory chain defects, and efficacious antioxidant therapy in superoxide dismutase 2 null mice.** *J.Neurochem.* 2004, 88(3):657-667.

103. Hirst J: **Energy transduction by respiratory complex I an evaluation of current knowledge.** *Biochem.Soc.Trans.* 2005, 33(Pt 3):525-529.

104. Hirst J, Carroll J, Fearnley IM, Shannon RJ, Walker JE: **The nuclear encoded subunits of complex I from bovine heart mitochondria.** *Biochim.Biophys.Acta.* 2003, 1604(3):135-150.

105. Hollins DL, Suliman HB, Piantadosi CA, Carraway MS: **Glutathione regulates susceptibility to oxidant-induced mitochondrial DNA damage in human lymphocytes.** *Free Radic.Biol.Med.* 2006, 40(7):1220-1226.

106. Holmgren A, Johansson C, Berndt C, Lonn ME, Hudemann C, Lillig CH: **Thiol redox control via thioredoxin and glutaredoxin systems.** *Biochem.Soc.Trans.* 2005, 33(Pt 6):1375-1377.

107. Holt IJ, Harding AE, Morgan-Hughes JA: **Deletions of muscle mitochondrial DNA in patients with mitochondrial myopathies.** *Nature* 1988, 331(6158):717-719.

108. Hool LC: **Reactive oxygen species in cardiac signalling: from mitochondria to plasma membrane ion channels.** *Clin.Exp.Pharmacol.Physiol.* 2006, 33(1-2):146-151.

109. Huang HM, Chen HL, Xu H, Gibson GE: **Modification of endoplasmic reticulum Ca2+ stores by select oxidants produces changes reminiscent of those in cells from patients with Alzheimer disease.** *Free Radic.Biol.Med.* 2005, 39(8):979-989.

110. Huang TT, Naeemuddin M, Elchuri S, Yamaguchi M, Kozy HM, Carlson EJ, Epstein CJ: **Genetic modifiers of the phenotype of mice deficient in mitochondrial superoxide dismutase.** *Hum.Mol.Genet.* 2006, 15(7):1187-1194.

111. Hurd TR, Filipovska A, Costa NJ, Dahm CC, Murphy MP: **Disulphide formation on mitochondrial protein thiols.** *Biochem.Soc.Trans.* 2005, 33(Pt 6):1390-1393.

112. Huser J, Blatter LA: **Fluctuations in mitochondrial membrane potential caused by repetitive gating of the permeability transition pore.** *Biochem.J.* 1999, 343 Pt 2:311-317.

113. Imai H, Nakagawa Y: **Biological significance of phospholipid hydroperoxide glutathione peroxidase (PHGPx, GPx4) in mammalian cells.** *Free Radic.Biol.Med.* 2003, 34(2):145-169.

114. Isaacs JS, Jung YJ, Mole DR, Lee S, Torres-Cabala C, Chung YL, Merino M, Trepel J, Zbar B, Toro J, Ratcliffe PJ, Linehan WM, Neckers L: **HIF overexpression correlates with biallelic loss of fumarate hydratase in renal cancer: novel role of fumarate in regulation of HIF stability.** *Cancer Cell.* 2005, 8(2):143-153.

115. Ishihara N, Jofuku A, Eura Y, Mihara K: **Regulation of mitochondrial morphology by membrane potential, and DRP1-dependent division and FZO1-dependent fusion reaction in mammalian cells.** *Biochem.Biophys.Res.Commun.* 2003, 301(4):891-898.

116. Iuso A, Scacco S, Piccoli C, Bellomo F, Petruzzella V, Trentadue R, Minuto M, Ripoli M, Capitanio N, Zeviani M, Papa S: **Dysfunctions of cellular oxidative metabolism in patients with mutations in the NDUFS1 and NDUFS4 genes of complex I.** *J.Biol.Chem.* 2006, 281(15):10374-10380.

117. James AM, Cocheme HM, Murphy MP: **Mitochondria-targeted redox probes as tools in the study of oxidative damage and ageing.** *Mech.Ageing Dev.* 2005, 126(9):982-986.

118. Janssen RJ, Nijtmans LG, Heuvel LP, Smeitink JA: **Mitochondrial complex I: Structure, function and pathology.** *J.Inherit.Metab.Dis.* 2006, 29(4):499-515.

119. Janssen AJ, Smeitink JA, van den Heuvel LP: **Some practical aspects of providing a diagnostic service for respiratory chain defects.** *Ann.Clin.Biochem.* 2003, 40(Pt 1):3-8.

120. Janssen RJ, van den Heuvel LP, Smeitink JA: **Genetic defects in the oxidative phosphorylation (OXPHOS) system.** *Expert Rev.Mol.Diagn.* 2004, 4(2):143-156.

121. Jauslin ML, Meier T, Smith RA, Murphy MP: **Mitochondria-targeted antioxidants protect Friedreich Ataxia fibroblasts from endogenous oxidative stress more effectively than untargeted antioxidants.** *FASEB J.* 2003, 17(13):1972-1974.

122. Kang SW, Rhee SG, Chang TS, Jeong W, Choi MH: **2-Cys peroxiredoxin function in intracellular signal transduction: therapeutic implications.** *Trends Mol.Med.* 2005, 11(12):571-578.

123. Ke Q, Costa M: **Hypoxia-inducible factor-1 (HIF-1).** *Mol.Pharmacol.* 2006, 70(5):1469-1480.

124. Keller A, Mohamed A, Drose S, Brandt U, Fleming I, Brandes RP: **Analysis of dichlorodihydrofluorescein and dihydrocalcein as probes for the detection of intracellular reactive oxygen species.** *Free Radic.Res.* 2004, 38(12):1257-1267.

125. Kelner MJ, Montoya MA. **Structural organization of the human glutathione reductase gene: determination of correct cDNA sequence and identification of a mitochondrial leader sequence.** *Biochem.Biophys.Res.Commun.* 2000, 269(2):366-368.

126. Kelso GF, Porteous CM, Coulter CV, Hughes G, Porteous WK, Ledgerwood EC, Smith RA, Murphy MP: **Selective targeting of a redox-active ubiquinone to mitochondria within cells: antioxidant and antiapoptotic properties.** *J.Biol.Chem.* 2001, 276(7):4588-4596.

127. Kerscher S, Grgic L, Garofano A, Brandt U: **Application of the yeast Yarrowia lipolytica as a model to analyse human pathogenic mutations in mitochondrial complex I (NADH:ubiquinone oxidoreductase).** *Biochim.Biophys.Acta.* 2004, 1659(2-3):197-205.

128. Kil IS, Park JW: **Regulation of mitochondrial NADP+-dependent isocitrate dehydrogenase activity by glutathionylation.** *J.Biol.Chem.* 2005, 280(11):10846-10854.

129. Kim YM, Lim JM, Kim BC, Han S: **Cu,Zn-superoxide dismutase is an intracellular catalyst for the H(2)O(2)-dependent oxidation of dichlorodihydrofluorescein**. *Mol.Cells* 2006, 21(1):161-165.

130. Kirby DM, Salemi R, Sugiana C, Ohtake A, Parry L, Bell KM, Kirk EP, Boneh A, Taylor RW, Dahl HH, Ryan MT, Thorburn DR: **NDUFS6 mutations are a novel cause of lethal neonatal mitochondrial complex I deficiency.** *J.Clin.Invest.* 2004, 114(6):837-845.

131. Kitamura Y, Inden M, Miyamura A, Kakimura J, Taniguchi T, Shimohama S: **Possible involvement of both mitochondria- and endoplasmic reticulum-dependent caspase pathways in rotenone-induced apoptosis in human neuroblastoma SH-SY5Y cells.** *Neurosci.Lett.* 2002, 333(1):25-28.

132. Klement P, Nijtmans LG, Van den Bogert C, Houstek J. **Analysis of oxidative phosphorylation complexes in cultured human fibroblasts and amniocytes by blue-native-electrophoresis using mitoplasts isolated with the help of digitonin.** *Anal.Biochem.* 1995, 231(1):218-224.

133. Koopman WJ, Bosch RR, van Emst-de Vries SE, Spaargaren M, De Pont JJ, Willems PH: **R-Ras alters Ca2+ homeostasis by increasing the Ca2+ leak across the endoplasmic reticular membrane.** *J.Biol.Chem.* 2003, 278(16):13672-13679.

134. Koopman WJ, Hink MA, Visser AJ, Roubos EW, Jenks BG: **Evidence that Ca2+-waves in Xenopus melanotropes depend on calcium-induced calcium release: a fluorescence correlation microscopy and linescanning study.** *Cell Calcium* 1999, 26(1-2):59-67.

135. Koopman WJ, Scheenen WJ, Errington RJ, Willems PH, Bindels RJ, Roubos EW, Jenks BG: **Membrane-initiated Ca(2+) signals are reshaped during propagation to subcellular regions.** *Biophys.J.* 2001, 81(1):57-65.

136. Koopman WJ, Verkaart S, Visch HJ, van der Westhuizen FH, Murphy MP, van den Heuvel LW, Smeitink JA, Willems PH: **Inhibition of complex I of the electron transport chain causes $O2^{\cdot-}$–mediated mitochondrial outgrowth.** *Am.J.Physiol.Cell.Physiol.* 2005, 288(6):C1440-C1450.

137. Koopman WJ, Verkaart S, van Emst-de Vries SE, Grefte S, Smeitink JA, Willems PH: **Simultaneous quantification of oxidative stress and cell spreading using 5-(and-6)-chloromethyl-2',7'-dichlorofluorescein.** *Cytometry A.* 2006, 69(12):1184-1192.

138. Koopman WJ, Visch HJ, Smeitink JA, Willems PH: **Simultaneous quantitative measurement and automated analysis of mitochondrial morphology, mass, potential, and motility in living human skin fibroblasts.** *Cytometry A.* 2006, 69(1):1-12.

139. Koopman WJ, Visch HJ, Verkaart S, van den Heuvel LW, Smeitink JA, Willems PH: **Mitochondrial network complexity and pathological decrease in complex I activity are tightly correlated in isolated human complex I deficiency.** *Am.J.Physiol.Cell.Physiol.* 2005, 289(4):C881-C890.

140. Kost TA, Condreay JP, Jarvis DL: **Baculovirus as versatile vectors for protein expression in insect and mammalian cells.** *Nat.Biotechnol.* 2005, 23(5):567-575.

141. Kudin AP, Bimpong-Buta NY, Vielhaber S, Elger CE, Kunz WS: **Characterization of superoxide-producing sites in isolated brain mitochondria.** *J.Biol.Chem.* 2004, 279(6):4127-4135.

142. Kushnareva Y, Murphy AN, Andreyev A: **Complex I-mediated reactive oxygen species generation: modulation by cytochrome c and NAD(P)+ oxidation-reduction state.** *Biochem.J.* 2002, 368(Pt 2):545-553.

143. Kussmaul L, Hirst J: **The mechanism of superoxide production by NADH:ubiquinone oxidoreductase (complex I) from bovine heart mitochondria.** *Proc.Natl.Acad.Sci. U S A.* 2006, 103(20):7607-7612.

144. Lambert AJ, Brand MD: **Inhibitors of the quinone-binding site allow rapid superoxide production from mitochondrial NADH:ubiquinone oxidoreductase (complex I).** *J.Biol.Chem.* 2004, 279(38):39414-39420.

145. Lang P, Yeow K, Nichols A, Scheer A: **Cellular imaging in drug discovery.** *Nat.Rev.Drug.Discov.* 2006, 5(4):343-356.

146. Lee HC, Yin PH, Chi CW, Wei YH: **Increase in mitochondrial mass in human fibroblasts under oxidative stress and during replicative cell senescence.** *J.Biomed.Sci.* 2002, 9(6 Pt 1):517-526.

147. Lee HC, Wei YH: **Mitochondrial biogenesis and mitochondrial DNA maintenance of mammalian cells under oxidative stress.** *Int.J.Biochem.Cell.Biol.* 2005, 37(4):822-834.

148. Leigh D: **Subacute necrotizing encephalomyelopathy in an infant.** *J.Neurol.Neurosurg. Psychiatry* 1951, 14(3):216-221.

149. Li Y, Huang TT, Carlson EJ, Melov S, Ursell PC, Olson JL, Noble LJ, Yoshimura MP, Berger C, Chan PH, Wallace DC, Epstein CJ: **Dilated cardiomyopathy and neonatal lethality in mutant mice lacking manganese superoxide dismutase.** *Nat.Genet.* 1995, 11(4):376-381.

150. Li N, Ragheb K, Lawler G, Sturgis J, Rajwa B, Melendez JA, Robinson JP: **Mitochondrial complex I inhibitor rotenone induces apoptosis through enhancing mitochondrial reactive oxygen species production.** *J.Biol.Chem.* 2003, 278(10):8516-8525.

151. Li Y, Trush MA: **Diphenyleneiodonium, an NAD(P)H oxidase inhibitor, also potently inhibits mitochondrial reactive oxygen species production.** *Biochem.Biophys.Res.Commun.* 1998, 253(2):295-299.

152. Lill R, Muhlenhoff U: **Iron-sulfur-protein biogenesis in eukaryotes.** *Trends Biochem.Sci.* 2005, 30(3):133-141.

153. Liu H, Colavitti R, Rovira II, Finkel T: **Redox-dependent transcriptional regulation.** *Circ.Res.* 2005, 97(10):967-974.

154. Liu Y, Fiskum G, Schubert D: **Generation of reactive oxygen species by the mitochondrial electron transport chain.** *J.Neurochem.* 2002, 80(5):780-787.

155. Loeffen J, Elpeleg O, Smeitink J, Smeets R, Stockler-Ipsiroglu S, Mandel H, Sengers R, Trijbels F, van den Heuvel L: **Mutations in the complex I NDUFS2 gene of patients with cardiomyopathy and encephalomyopathy.** *Ann.Neurol.* 2001, 49(2):195-201.

156. Loeffen J, Smeitink J, Triepels R, Smeets R, Schuelke M, Sengers R, Trijbels F, Hamel B, Mullaart R, van den Heuvel L: **The first nuclear-encoded complex I mutation in a patient with Leigh syndrome.** *Am.J.Hum.Genet.* 1998, 63(6):1598-1608.

157. Loeffen JL, Smeitink J, Trijbels J, Janssen A, Triepels R, Sengers R, van den Heuvel L: **Isolated complex I deficiency in children: clinical, biochemical and genetic aspects.** *Hum.Mutat.* 2000, 15(2):123-134.

158. Lopez LC, Schuelke M, Quinzii CM, Kanki T, Rodenburg RJ, Naini A, Dimauro S, Hirano M. **Leigh syndrome with nephropathy and CoQ10 deficiency due to decaprenyl diphosphate synthase subunit 2 (PDSS2) mutations.** *Am.J.Hum.Genet.* 2006, 79(6):1125-1129.

159. Lu H, Dalgard CL, Mohyeldin A, McFate T, Tait AS, Verma A: **Reversible inactivation of HIF-1 prolyl hydroxylases allows cell metabolism to control basal HIF-1.** *J.Biol.Chem.* 2005, 280(51):41928-41939.

160. Luo X, Pitkanen S, Kassovska-Bratinova S, Robinson BH, Lehotay DC: **Excessive formation of hydroxyl radicals and aldehydic lipid peroxidation products in cultured skin fibroblasts from patients with complex I deficiency.** *J.Clin.Invest.* 1997, 99(12):2877-2882.

161. Maechler P, Carobbio S, Rubi B: **In beta-cells, mitochondria integrate and generate metabolic signals controlling insulin secretion.** *Int.J.Biochem.Cell.Biol.* 2006, 38(5-6):696-709.

162. Marchesi E, Rota C, Fann YC, Chignell CF, Mason RP: **Photoreduction of the fluorescent dye 2'-7'-dichlorofluorescein: a spin trapping and direct electron spin resonance study with implications for oxidative stress measurements.** *Free Radic.Biol.Med.* 1999, 26(1-2):148-161.

163. Marriage B, Clandinin MT, Glerum DM: **Nutritional cofactor treatment in mitochondrial disorders.** *J.Am. Diet.Assoc.* 2003, 103(8):1029-1038.

164. Martensson J, Lai JC, Meister A: **High-affinity transport of glutathione is part of a multicomponent system essential for mitochondrial function.** *Proc.Natl.Acad.Sci. U S A.* 1990, 87(18):7185-7189.

165. Martin MA, Blazquez A, Gutierrez-Solana LG, Fernandez-Moreira D, Briones P, Andreu AL, Garesse R, Campos Y, Arenas J: **Leigh syndrome associated with mitochondrial complex I deficiency due to a novel mutation in the NDUFS1 gene.** *Arch.Neurol.* 2005, 62(4):659-661.

166. Mattiazzi M, Vijayvergiya C, Gajewski CD, DeVivo DC, Lenaz G, Wiedmann M, Manfredi G: **The mtDNA T8993G (NARP) mutation results in an impairment of oxidative phosphorylation that can be improved by antioxidants.** *Hum.Mol.Genet.* 2004, 13(8):869-879.

167. Meeusen S, McCaffery JM, Nunnari J: **Mitochondrial fusion intermediates revealed in vitro.** *Science* 2004, 305(5691):1747-1752.

168. Meeusen SL, Nunnari J: **How mitochondria fuse.** *Curr.Opin.Cell.Biol.* 2005, 17(4):389-394.

169. Meister A: **Mitochondrial changes associated with glutathione deficiency.** *Biochim.Biophys.Acta.* 1995, 1271(1):35-42.

170. Mik EG, Stap J, Sinaasappel M, Beek JF, Aten JA, van Leeuwen TG, Ince C: **Mitochondrial PO2 measured by delayed fluorescence of endogenous protoporphyrin IX.** *Nat.Methods* 2006, 3(11):939-945.

171. Miranda S, Foncea R, Guerrero J, Leighton F: **Oxidative stress and upregulation of mitochondrial biogenesis genes in mitochondrial DNA-depleted HeLa cells.** *Biochem.Biophys.Res.Commun.* 1999, 258(1):44-49.

172. Mitsumoto A, Takeuchi A, Okawa K, Nakagawa Y: **A subset of newly synthesized polypeptides in mitochondria from human endothelial cells exposed to hydroperoxide stress.** *Free Radic.Biol.Med.* 2002, 32(1):22-37.

173. Moyes CD: **Controlling muscle mitochondrial content.** *J.Exp.Biol.* 2003, 206(Pt 24):4385-4391.

174. Moyes CD, Hood DA: **Origins and consequences of mitochondrial variation in vertebrate muscle.** *Annu.Rev.Physiol.* 2003, 65:177-201.

175. Muller FL, Liu Y, Van Remmen H: **Complex III releases superoxide to both sides of the inner mitochondrial membrane.** *J.Biol.Chem.* 2004, 279(47):49064-49073.

176. Murphy MP, Echtay KS, Blaikie FH, Asin-Cayuela J, Cocheme HM, Green K, Buckingham JA, Taylor ER, Hurrell F, Hughes G, Miwa S, Cooper CE, Svistunenko DA, Smith RA, Brand MD: **Superoxide activates uncoupling proteins by generating carbon-centered radicals and initiating lipid peroxidation: studies using a mitochondria-targeted spin trap derived from alpha-phenyl-N-tert-butylnitrone.** *J.Biol.Chem.* 2003, 278(49):48534-48545.

177. Murphy MP, Smith RA: **Targeting antioxidants to mitochondria by conjugation to lipophilic cations.** *Annu.Rev.Pharmacol.Toxicol.* 2007, 47:629-656.

178. Murrant CL, Reid MB: **Detection of reactive oxygen and reactive nitrogen species in skeletal muscle.** *Microsc.Res.Tech.* 2001, 55(4):236-248.

179. Nakamura K, Bindokas VP, Kowlessur D, Elas M, Milstien S, Marks JD, Halpern HJ, Kang UJ: **Tetrahydrobiopterin scavenges superoxide in dopaminergic neurons.** *J.Biol.Chem.* 2001, 276(37):34402-34407.

180. Navarro A, Gomez C, Sanchez-Pino MJ, Gonzalez H, Bandez MJ, Boveris AD, Boveris A. **Vitamin E at high doses improves survival, neurological performance, and brain mitochondrial function in aging male mice.** *Am.J.Physiol.Regul.Integr.Comp.Physiol.* 2005, 289(5):R1392-R1399.

181. Neuspiel M, Zunino R, Gangaraju S, Rippstein P, McBride H: **Activated mitofusin 2 signals mitochondrial fusion, interferes with Bax activation, and reduces susceptibility to radical induced depolarization.** *J.Biol.Chem.* 2005, 280(26):25060-25070.

182. Nijtmans LG, Henderson NS, Holt IJ: **Blue Native electrophoresis to study mitochondrial and other protein complexes.** *Methods* 2002, 26(4):327-334.

183. Noack H, Bednarek T, Heidler J, Ladig R, Holtz J, Szibor M: **TFAM-dependent and independent dynamics of mtDNA levels in C2C12 myoblasts caused by redox stress.** *Biochim.Biophys.Acta.* 2006, 1760(2):141-150.

184. Nohl H, Gille L, Staniek K: **Intracellular generation of reactive oxygen species by mitochondria.** *Biochem.Pharmacol.* 2005, 69(5):719-723.

185. Ogilvie I, Kennaway NG, Shoubridge EA: **A molecular chaperone for mitochondrial complex I assembly is mutated in a progressive encephalopathy.** *J.Clin.Invest.* 2005, 115(10):2784-2792.

186. Ohnishi ST, Ohnishi T, Muranaka S, Fujita H, Kimura H, Uemura K, Yoshida K,Utsumi K: **A possible site of superoxide generation in the complex I segment of rat heart mitochondria.** *J.Bioenerg.Biomembr.* 2005, 37(1):1-15.

187. Ohnishi T, Salerno JC: **Conformation-driven and semiquinone-gated proton-pump mechanism in the NADH-ubiquinone oxidoreductase (complex I).** *FEBS Lett.* 2005, 579(21):4555-4561.

188. Okun JG, Lummen P, Brandt U: **Three classes of inhibitors share a common binding domain in mitochondrial complex I (NADH:ubiquinone oxidoreductase).** *J.Biol.Chem.* 1999, 274(5):2625-2630.

189. Olafsdottir K, Reed DJ: **Retention of oxidized glutathione by isolated rat liver mitochondria during hydroperoxide treatment.** *Biochim.Biophys.Acta.* 1988, 964(3):377-382.

190. O'Malley YQ, Reszka KJ, Britigan BE: **Direct oxidation of 2',7'-dichlorodihydrofluorescein by pyocyanin and other redox-active compounds independent of reactive oxygen species production.** *Free Radic.Biol.Med.* 2004, 36(1):90-100.

191. O'riordan TC, Fitzgerald K, Ponomarev GV, Mackrill J, Hynes J, Taylor C, Papkovsky DB: **Sensing intracellular oxygen using near infrared phosphorescent probes and live-cell fluorescence imaging.** *Am.J.Physiol.Regul.Integr.Comp.Physiol.* 2007, 292(4):R1613-1620.

192. Pagliarini DJ, Dixon, JE: **Mitochondrial modulation: reversible phosphorylation takes center stage?** *Trends Biochem.Sci.* 2005, 31(1):26-34.

193. Panetta J, Smith LJ, Boneh A: **Effect of high-dose vitamins, coenzyme Q and high-fat diet in paediatric patients with mitochondrial diseases.** *J.Inherit.Metab.Dis.* 2004, 27(4):487-498.

194. Papa S, Scacco S, Sardanelli AM, Vergari R, Papa F, Budde S, van den Heuvel L, Smeitink J: **Mutation in the NDUFS4 gene of complex I abolishes cAMP-dependent activation of the complex in a child with fatal neurological syndrome.** *FEBS Lett.* 2001, 489(2-3):259-262.

195. Paradies G, Petrosillo G, Pistolese M, Ruggiero FM: **Reactive oxygen species affect mitochondrial electron transport complex I activity through oxidative cardiolipin damage.** *Gene* 2002, 286(1):135-141.

196. Pearce LL, Kanai AJ, Epperly MW, Peterson J: **Nitrosative stress results in irreversible inhibition of purified mitochondrial complexes I and III without modification of cofactors.** *Nitric Oxide* 2005, 13(4):254-263.

197. Pedersen PL: **Tumor mitochondria and the bioenergetics of cancer cells.** *Prog.Exp.Tumor Res.* 1978, 22:190-274.

198. Pepperkok R, Ellenberg J: **High-throughput fluorescence microscopy for systems biology.** *Nat.Rev.Mol.Cell.Biol.* 2006, 7(9):690-696.

199. Petruzzella V, Vergari R, Puzziferri I, Boffoli D, Lamantea E, Zeviani M, Papa S: **A nonsense mutation in the NDUFS4 gene encoding the 18 kDa (AQDQ) subunit of complex I abolishes assembly and activity of the complex in a patient with Leigh-like syndrome.** *Hum.Mol.Genet.* 2001, 10(5):529-535.

200. Pham NA, Richardson T, Cameron J, Chue B, Robinson BH: **Altered mitochondrial structure and motion dynamics in living cells with energy metabolism defects revealed by real time microscope imaging.** *Microsc.Microanal.* 2004, 10(2):247-260.

201. Piantadosi CA, Suliman HB: **Mitochondrial transcription factor A induction by redox activation of nuclear respiratory factor 1.** *J.Biol.Chem.* 2006, 281(1):324-333.

202. Piccoli C, Scacco S, Bellomo F, Signorile A, Iuso A, Boffoli D, Scrima R, Capitanio N, Papa S. **cAMP controls oxygen metabolism in mammalian cells.** *FEBS Lett.* 2006, 580(18):4539-4543.

203. Pich S, Bach D, Briones P, Liesa M, Camps M, Testar X, Palacin M, Zorzano A: **The Charcot-Marie-Tooth type 2A gene product, Mfn2, up-regulates fuel oxidation through expression of OXPHOS system.** *Hum.Mol.Genet.* 2005, 14(11):1405-1415.

204. Pitkanen S, Robinson BH: **Mitochondrial complex I deficiency leads to increased production of superoxide radicals and induction of superoxide dismutase.** *J.Clin.Invest.* 1996, 98(2):345-351.

205. Procaccio V, Wallace DC: **Late-onset Leigh syndrome in a patient with mitochondrial complex I NDUFS8 mutations.** *Neurology* 2004, 62(10):1899-1901.

206. Quinzii C, Naini A, Salviati L, Trevisson E, Navas P, Dimauro S, Hirano M: **A Mutation in Para-Hydroxybenzoate-Polyprenyl Transferase (COQ2) Causes Primary Coenzyme Q10 Deficiency.** *Am.J.Hum.Genet.* 2006, 78(2):345-349.

207. Radi R, Cassina A, Hodara R, Quijano C, Castro L: **Peroxynitrite reactions and formation in mitochondria.** *Free Radic.Biol.Med.* 2002, 33(11):1451-1464.

208. Raha S, Robinson BH: **Mitochondria, oxygen free radicals, disease and ageing.** *Trends Biochem.Sci.* 2000, 25(10):502-508.

209. Raha S, Robinson BH: **Mitochondria, oxygen free radicals, and apoptosis.** *Am.J.Med.Genet.* 2001, 106(1):62-70.

210. Rahman S, Blok RB, Dahl HH, Danks DM, Kirby DM, Chow CW, Christodoulou J, Thorburn DR: **Leigh syndrome: clinical features and biochemical and DNA abnormalities.** *Ann.Neurol.* 1996, 39(3):343-351.

211. Reinecke F, Levanets O, Olivier Y, Louw R, Semete B, Grobler A, Hidalgo J, Smeitink J, Olckers A, Van der Westhuizen FH: **Metallothionein isoform 2A expression is inducible and protects against ROS-mediated cell death in rotenone-treated HeLa cells.** *Biochem.J.* 2006, 395(2):405-415.

212. Rimbach G, Minihane AM, Majewicz J, Fischer A, Pallauf J, Virgli F, Weinberg PD: **Regulation of cell signalling by vitamin E.** *Proc.Nutr.Soc.* 2002, 61(4):415-425.

213. Rizzuto R, Pozzan T: **Microdomains of intracellular Ca^{2+}: molecular determinants and functional consequences.** *Physiol.Rev.* 2006, 86(1):369-408.

214. Robinson BH: **Human complex I deficiency: clinical spectrum and involvement of oxygen free radicals in the pathogenicity of the defect.** *Biochim.Biophys.Acta.* 1998, 1364(2):271-286.

215. Robinson BH. **Lactic acidemia and mitochondrial disease.** *Mol.Genet.Metab.* 2006, 89(1-2):3-13.

216. Robinson BH, Glerum DM, Chow W, Petrova-Benedict R, Lightowlers R, Capaldi R: **The use of skin fibroblast cultures in the detection of respiratory chain defects in patients with lactic acidemia.** *Pediatr.Res.* 1990, 28(5):549-555.

217. Robinson KM, Janes MS, Pehar M, Monette JS, Ross MF, Hagen TM, Murphy MP, Beckman JS: **Selective fluorescent imaging of superoxide in vivo using ethidium-based probes.** *Proc.Natl.Acad.Sci. U S A* 2006, 103(41):15038-15043.

218. Rossignol R, Faustin B, Rocher C, Malgat M, Mazat JP, Letellier T: **Mitochondrial threshold effects.** *Biochem.J.* 2003, 370(Pt 3):751-762.

219. Rossignol R, Gilkerson R, Aggeler R, Yamagata K, Remington SJ, Capaldi RA: **Energy substrate modulates mitochondrial structure and oxidative capacity in cancer cells.** *Cancer Res.* 2004, 64(3):985-993.

220. Rotig A, Appelkvist EL, Geromel V, Chretien D, Kadhom N, Edery P, Lebideau M, Dallner G, Munnich A, Ernster L, Rustin P: **Quinone-responsive multiple respiratory-chain dysfunction due to widespread coenzyme Q10 deficiency.** *Lancet* 2000, 356(9227):391-395.

221. Rydstrom J: **Mitochondrial transhydrogenase--a key enzyme in insulin secretion and, potentially, diabetes.** *Trends Biochem.Sci.* 2006, 31(7):355-358.

222. Sainz RM, Mayo JC, Tan DX, Lopez-Burillo S, Natarajan M, Reiter RJ: **Antioxidant activity of melatonin in Chinese hamster ovarian cells: changes in cellular proliferation and differentiation.** *Biochem.Biophys.Res.Commun.* 2003, 302(3):625-634.

223. Scacco S, Petruzzella V, Budde S, Vergari R, Tamborra R, Panelli D, van den Heuvel LP, Smeitink JA, Papa S: **Pathological mutations of the human NDUFS4 gene of the 18-kDa (AQDQ) subunit of complex I affect the expression of the protein and the assembly and function of the complex.** *J.Biol.Chem.* 2003, 278(45):44161-44617.

224. Scaglia F, Towbin JA, Craigen WJ, Belmont JW, Smith EO, Neish SR, Ware SM, Hunter JV, Fernbach SD, Vladutiu GD, Wong LJ, Vogel H: **Clinical spectrum, morbidity, and mortality in 113 pediatric patients with mitochondrial disease.** *Pediatrics* 2004, 114(4):925-931.

225. Scarpulla RC: **Nuclear control of respiratory gene expression in mammalian cells.** *J.Cell.Biochem.* 2006, 97(4):673-683.

226. Schafer FQ, Buettner GR: **Redox environment of the cell as viewed through the redox state of the glutathione disulfide/glutathione couple.** *Free Radic.Biol.Med.* 2001, 30(11):1191-1212.

227. Schafer E, Seelert H, Reifschneider NH, Krause F, Dencher NA, Vonck J: **Architecture of active mammalian respiratory chain supercomplexes.** *J.Biol.Chem.* 2006, 281(22):15370-15375.

228. Schagger H, de Coo R, Bauer MF, Hofmann S, Godinot C, Brandt U: **Significance of respirasomes for the assembly/stability of human respiratory chain complex I.** *J.Biol.Chem.* 2004, 279(35):36349-36353.

229. Schagger H, Pfeiffer K: **Supercomplexes in the respiratory chains of yeast and mammalian mitochondria.** *EMBO J.* 2000, 19(8):1777-1783.

230. Schapira AH: **Mitochondrial disease.** *Lancet* 2006, 368(9529):70-82.

231. Scheffler IE: **A century of mitochondrial research: achievements and perspectives.** *Mitochondrion* 2001, 1(1):3-31.

232. Schneider C: **Chemistry and biology of vitamin E.** *Mol.Nutr.Food Res.* 2005, 49(1):7-30.

233. Schuchmann S, Heinemann U: **Increased mitochondrial superoxide generation in neurons from trisomy 16 mice: a model of Down's syndrome.** *Free Radic.Biol.Med.* 2000, 28(2):235-250.

234. Schuelke M, Smeitink J, Mariman E, Loeffen J, Plecko B, Trijbels F, Stockler-Ipsiroglu S, van den Heuvel L: **Mutant NDUFV1 subunit of mitochondrial complex I causes leukodystrophy and myoclonic epilepsy.** *Nat.Genet.* 1999, 21(3):260-261.

235. Segel, I.H: **Enzyme kinetics: Behavior and analysis of rapid equilibrium and steady state enzyme systems.** *New York: John Wiley & Sons Inc.* 1975, 43-44.

236. Selak MA, Armour SM, MacKenzie ED, Boulahbel H, Watson DG, Mansfield KD, Pan Y, Simon MC, Thompson CB, Gottlieb E: **Succinate links TCA cycle dysfunction to oncogenesis by inhibiting HIF-alpha prolyl hydroxylase.** *Cancer Cell.* 2005, 7(1):77-85.

237. Sell H, Deshaies Y, Richard D: **The brown adipocyte: update on its metabolic role.** *Int.J.Biochem.Cell.Biol.* 2004, 36(11):2098-2104.

238. Semenza GL: **Hypoxia-inducible factor 1: master regulator of O2 homeostasis.** *Curr.Opin.Genet.Dev.* 1998, 8(5):588-594.

239. Serrano MC, Pagani R, Pena J, Portoles MT: **Transitory oxidative stress in L929 fibroblasts cultured on poly(epsilon-caprolactone) films.** *Biomaterials* 2005, 26(29):5827-5834.

240. Sherer TB, Betarbet R, Stout AK, Lund S, Baptista M. Panov AV, Cookson MR, Greenamyre JT: **An in vitro model of Parkinson's disease: linking mitochondrial impairment to altered alpha-synuclein metabolism and oxidative damage.** *J.Neurosci.* 2002, 22(16):7006-7015.

241. Sheu SS, Nauduri D, Anders MW: **Targeting antioxidants to mitochondria: a new therapeutic direction.** *Biochim.Biophys.Acta.* 2006, 1762(2):256-265.

242. Shoubridge EA: **Nuclear genetic defects of oxidative phosphorylation.** *Hum.Mol.Genet.* 2001, 10(20):2277-2284.

243. Simon MC: **Mitochondrial reactive oxygen species are required for hypoxic HIF alpha stabilization.** *Adv.Exp.Med.Biol.* 2006, 588:165-170.

244. Simonnet H, Alazard N, Pfeiffer K, Gallou C, Beroud C, Demont J, Bouvier R, Schagger H, Godinot C: **Low mitochondrial respiratory chain content correlates with tumor aggressiveness in renal cell carcinoma.** *Carcinogenesis* 2002, 23(5):759-768.

245. Smeitink J, Sengers R, Trijbels F, van den Heuvel L: **Human NADH:ubiquinone oxidoreductase.** *J.Bioenerg.Biomembr.* 2001, 33(3):259-266.

246. Smeitink J, van den Heuvel L, DiMauro S: **The genetics and pathology of oxidative phosphorylation.** *Nat.Rev.Genet.* 2001, 2(5):342-352.

247. Smeitink JA, van den Heuvel LW, Koopman WJ, Nijtmans LG, Ugalde C, Willems PH: **Cell biological consequences of mitochondrial NADH:ubiquinone oxidoreductase deficiency.** *Curr.Neurovasc.Res.* 2004, 1(1):29-40.

248. Smeitink JA, Zeviani M, Turnbull DM, Jacobs HT: **Mitochondrial medicine: a metabolic perspective on the pathology of oxidative phosphorylation disorders.** *Cell Metab.* 2006, 3(1):9-13.

249. Smith RA, Porteous CM, Gane AM, Murphy MP: **Delivery of bioactive molecules to mitochondria in vivo.** *Proc.Natl.Acad.Sci. U S A.* 2003, 100(9):5407-5412.

250. Smith RA, Porteous CM, Coulter CV, Murphy MP: **Selective targeting of an antioxidant to mitochondria.** *Eur.J.Biochem.* 1999, 263(3):709-716.

251. Springer EL: **Comparative study of the cytoplasmic organelles of epithelial cell lines derived from human carcinomas and nonmalignant tissues.** *Cancer Res.* 1980, 40(3):803-817.

252. Starkov AA, Fiskum G: **Regulation of brain mitochondrial H2O2 production by membrane potential and NAD(P)H redox state.** *J.Neurochem.* 2003, 86(5):1101-1107.

253. Starkov AA, Fiskum G, Chinopoulos C, Lorenzo BJ, Browne SE, Patel MS, Beal MF: **Mitochondrial alpha-ketoglutarate dehydrogenase complex generates reactive oxygen species.** *J.Neurosci.* 2004, 24(36):7779-7788.

254. Stone JR, Yang S: **Hydrogen peroxide: a signaling messenger.** *Antioxid.Redox Signal.* 2006, 8(3-4):243-270.

255. St-Pierre J, Buckingham JA, Roebuck SJ, Brand MD: **Topology of superoxide production from different sites in the mitochondrial electron transport chain.** *J.Biol.Chem.* 2002, 277(47):44784-44790.

256. Suliman HB, Welty-Wolf KE, Carraway M, Tatro L, Piantadosi CA: **Lipopolysaccharide induces oxidative cardiac mitochondrial damage and biogenesis.** *Cardiovasc.Res.* 2004, 64(2):279-288.

257. Swift LM, Sarvazyan N: **Localization of dichlorofluorescin in cardiac myocytes: implications for assessment of oxidative stress.** *Am.J.Physiol.Heart.Circ.Physiol.* 2000, 278(3):H982-H990.

258. Tada-Oikawa S, Hiraku Y, Kawanishi M, Kawanishi S: **Mechanism for generation of hydrogen peroxide and change of mitochondrial membrane potential during rotenone-induced apoptosis.** *Life Sci.* 2003, 73(25):3277-3288.

259. Tafazoli S, Wright JS, O'Brien PJ: **Prooxidant and antioxidant activity of vitamin E analogues and troglitazone.** *Chem.Res.Toxicol.* 2005, 18(10):1567-1574.

260. Taivassalo T, Haller RG: **Implications of exercise training in mtDNA defects--use it or lose it?** *Biochim.Biophys.Acta.* 2004, 1659(2-3):221-231.

261. Taivassalo T, Haller RG: **Exercise and training in mitochondrial myopathies.** *Med.Sci.Sports Exerc.* 2005, 37(12):2094-2101.

262. Tarpey MM, Wink DA, Grisham MB: **Methods for detection of reactive metabolites of oxygen and nitrogen: in vitro and in vivo considerations.** *Am.J.Physiol.Regul.Integr.Comp.Physiol.* 2004, 286(3):R431-R444.

263. Taylor ER, Hurrell F, Shannon RJ, Lin TK, Hirst J, Murphy MP: **Reversible glutathionylation of complex I increases mitochondrial superoxide formation.** *J.Biol.Chem.* 2003, 278(22):19603-19610.

264. Taylor RW, Turnbull DM: **Mitochondrial DNA mutations in human disease.** *Nat.Rev.Genet.* 2005, 6(5):389-402.

265. Thannickal VJ, Fanburg BL: **Reactive oxygen species in cell signaling.** *Am.J.Physiol.Lung Cell. Mol.Physiol.* 2000, 279(6):L1005-1028.

266. Tompkins AJ, Burwell LS, Digerness SB, Zaragoza C, Holman WL, Brookes PS: **Mitochondrial dysfunction in cardiac ischemia-reperfusion injury: ROS from complex I, without inhibition.** *Biochim.Biophys.Acta.* 2006, 1762(2):223-231.

267. Tretter L, Adam-Vizi V: **Generation of reactive oxygen species in the reaction catalyzed by alpha-ketoglutarate dehydrogenase.** *J.Neurosci.* 2004, 24(36):7771-7778.

268. Triepels RH, van den Heuvel LP, Loeffen JL, Buskens CA, Smeets RJ, Rubio Gozalbo ME, Budde SM, Mariman EC, Wijburg FA, Barth PG, Trijbels JM, Smeitink JA: **Leigh syndrome associated with a mutation in the NDUFS7 (PSST) nuclear encoded subunit of complex I.** *Ann.Neurol.* 1999, 45(6):787-790.

269. Trifunovic A: **Mitochondrial DNA and ageing.** *Biochim.Biophys.Acta.* 2006, 1757(5-6):611-617.

270. Tucker JM, Townsend DM: **Alpha-tocopherol: roles in prevention and therapy of human disease.** *Biomed.Pharmacother.* 2005, 59(7):380-387.

271. Ugalde C, Janssen RJ, van den Heuvel LP, Smeitink JA, Nijtmans LG: **Differences in assembly or stability of complex I and other mitochondrial OXPHOS complexes in inherited complex I deficiency.** *Hum.Mol.Genet.* 2004, 13(6):659-667.

272. Ugalde C, Vogel R, Huijbens R, Van Den Heuvel B, Smeitink J, Nijtmans L: **Human mitochondrial complex I assembles through the combination of evolutionary conserved modules: a framework to interpret complex I deficiencies.** *Hum.Mol.Genet.* 2004, 13(20):2461-2472.

273. van den Heuvel L, Ruitenbeek W, Smeets R, Gelman-Kohan Z, Elpeleg O, Loeffen J, Trijbels F, Mariman E, de Bruijn D, Smeitink J: **Demonstration of a new pathogenic mutation in human complex I deficiency: a 5-bp duplication in the nuclear gene encoding the 18-kD (AQDQ) subunit.** *Am.J.Hum.Genet.* 1998, 62(2):262-268.

274. van den Heuvel L, Smeitink J: **The oxidative phosphorylation (OXPHOS) system: nuclear genes and human genetic diseases.** *Bioessays* 2001, 23(6):518-525.

275. van der Westhuizen FH, van den Heuvel LP, Smeets R, Veltman JA, Pfundt R, van Kessel AG, Ursing BM, Smeitink JA: **Human mitochondrial complex I deficiency: investigating transcriptional responses by microarray.** *Neuropediatrics.* 2003, 34(1):14-22.

276. Vasquez-Vivar J, Kalyanaraman B, Kennedy MC: **Mitochondrial aconitase is a source of hydroxyl radical. An electron spin resonance investigation.** *J.Biol.Chem.* 2000, 275(19):14064-14069.

277. Verkaart S, Koopman WJH, Nijtmans LGJ, van den Heuvel LWPJ, Smeitink JAM, Willems, PHGM: **Superoxide production is inversely related to complex I activity in inherited complex I deficiency.** *Biochim.Biophys.Acta* 2007, 1772(3) 373-381.

278. Verkaart S, Willems PHGM, Visch HJ, Grefte S, Rodenburg RJ, Grovenstein M, van Emst-de Vries SE, van den Heuvel LWPJ, Smeitink JAM, Nijtmans LGJ, Koopman WJH: **Cellular and molecular basis of nuclear-inherited isolated NADH:ubiquinone oxidoreductase deficiency: Improvement by chronic treatment with a vitamin E analogue.** 2007, ***submitted***.

279. Verkaart S, Koopman WJH, Cheek J, van Emst-de Vries SE, van den Heuvel LWPJ, Smeitink JAM, Willems PHGM: **Mitochondrial and cytosolic redox environment are not detectably altered in isolated human NADH:ubiquinone oxidoreductase deficiency.** 2007, ***submitted***.

280. Vinogradov AD: **Respiratory complex I: structure, redox components, and possible mechanisms of energy transduction.** *Biochemistry (Mosc)* 2001, 66(10):1086-1097.

281. Visch HJ, Koopman WJ, Leusink A, van Emst-de Vries SE, van den Heuvel LP, Willems PH, Smeitink JA: **Decreased agonist-stimulated mitochondrial ATP production caused by a pathological reduction in endoplasmic reticulum calcium content in human complex I deficiency.** *Biochim.Biophys.Acta.* 2006, 1762(1):115-123.

282. Visch HJ, Koopman WJ, Zeegers D, van Emst-de Vries SE, van Kuppeveld FJ, van den Heuvel LP, Smeitink JA, Willems PH. **Ca^{2+} mobilizing agonists increase mitochondrial ATP production to accelerate cytosolic Ca^{2+} removal: aberrations in human complex I deficiency.** *Am.J.Physiol.Cell.Physiol.* 2006, 291(2):C308-316.

283. Visch HJ, Rutter GA, Koopman WJ, Koenderink JB, Verkaart S, de Groot T, Varadi A, Mitchell KJ, van den Heuvel LP, Smeitink JA, Willems PH: **Inhibition of mitochondrial Na^{+}-Ca^{2+} exchange restores agonist-induced ATP production and Ca^{2+} handling in human complex I deficiency.** *J.Biol.Chem.* 2004, 279(39):40328-40336.

284. Vogel RO, Dieteren CE, van den Heuvel LP, Willems PH, Smeitink JA, Koopman WJ, Nijtmans LG: **Identification of mitochondrial complex I assembly intermediates by tracing tagged NDUFS3 demonstrates the entry point of mitochondrial subunits.** *J.Biol.Chem.* 2007, 282(10):7582-7590.

285. Vogel RO, Janssen RJ, van den Brand MA, Dieteren CE, Verkaart S, Koopman WJ, Willems PH, Pluk W, van den Heuvel LW, Smeitink JA, Nijtmans LG: **Cytosolic signalling protein Ecsit also localises to mitochondria where it interacts with chaperone NDUFAF1 and functions in complex I assembly.** *Genes Dev.* 2007, 21(5):615-624.

286. Vogel RO, Janssen RJ, Ugalde C, Grovenstein M, Huijbens RJ, Visch HJ, van den Heuvel LP, Willems PH, Zeviani M, Smeitink JA, Nijtmans LG: **Human mitochondrial complex I assembly is mediated by NDUFAF1.** *FEBS J.* 2005, 272(20):5317-5326.

287. Vogel R, Nijtmans L, Ugalde C, van den Heuvel L, Smeitink J: **Complex I assembly: a puzzling problem.** *Curr.Opin.Neurol.* 2004, 17(2):179-186.

288. von Kleist-Retzow JC, Cormier-Daire V, de Lonlay P, Parfait B, Chretien D, Rustin P, Feingold J, Rotig A, Munnich A: **A high rate (20%-30%) of parental consanguinity in cytochrome-oxidase deficiency.** *Am.J.Hum.Genet.* 1998, 63(2):428-435.

289. Vrablic AS, Albright CD, Craciunescu CN, Salganik RI, Zeisel SH: **Altered mitochondrial function and overgeneration of reactive oxygen species precede the induction of apoptosis by 1-O-octadecyl-2-methyl-rac-glycero-3-phosphocholine in p53-defective hepatocytes.** *FASEB J.* 2001, 15(10):1739-1744.

290. Wallace DC: **Mitochondrial diseases in man and mouse.** *Science.* 1999, 283(5407):1482-1488.

291. Wallace DC: **A mitochondrial paradigm of metabolic and degenerative diseases, aging, and cancer: a dawn for evolutionary medicine.** *Annu.Rev.Genet.* 2005, 39:359-407.

292. Wallace DC, Singh G, Lott MT, Hodge JA, Schurr TG, Lezza AM, Elsas LJ 2nd, Nikoskelainen EK: **Mitochondrial DNA mutation associated with Leber's hereditary optic neuropathy.** *Science* 1988, 242(4884):1427-1430.

293. Walter L, Hajnoczky G: **Mitochondria and endoplasmic reticulum: the lethal interorganelle cross-talk.** *J.Bioenerg.Biomembr.* 2005, 37(3):191-206.

294. Wang Y, Meng A, Zhou D: **Inhibition of phosphatidylinostol 3-kinase uncouples H2O2-induced senescent phenotype and cell cycle arrest in normal human diploid fibroblasts.** *Exp.Cell Res.* 2004, 298(1):188-196.

295. Wiedemann N, Pfanner N, Chacinska A: **Chaperoning through the mitochondrial intermembrane space.** *Mol.Cell* 2006, 21(2):145-148.

296. Winyard PG, Moody CJ, Jacob C: **Oxidative activation of antioxidant defence.** *Trends Biochem.Sci.* 2005, 30(8):453-461.

297. Wu G, Fang YZ, Yang S, Lupton JR, Turner ND: **Glutathione metabolism and its implications for health.** *J.Nutr.* 2004, 134(3):489-492.

298. Yaffe MP: **The cutting edge of mitochondrial fusion.** *Nat.Cell.Biol.* 2003, 5(6):497-499.

299. Yoon YS, Yoon DS, Lim IK, Yoon SH, Chung HY, Rojo M, Malka F, Jou MJ, Martinou JC, Yoon G: **Formation of elongated giant mitochondria in DFO-induced cellular senescence: involvement of enhanced fusion process through modulation of Fis1.** *J.Cell.Physiol.* 2006, 209(2):468-480.

300. Zerbetto E, Vergani L, Dabbeni-Sala F: **Quantification of muscle mitochondrial oxidative phosphorylation enzymes via histochemical staining of blue native polyacrylamide gels.** *Electrophoresis* 1997; 18(11):2059-2064.

301. Zeviani M, Di Donato S: **Mitochondrial disorders.** *Brain* 2004, 127(Pt 10):2153-2172.

302. Zeviani M, Spinazzola A, Carelli V: **Nuclear genes in mitochondrial disorders.** *Curr.Opin.Genet.Dev.* 2003, 13(3):262-270.

303. Zhang Q, Piston DW, Goodman RH: **Regulation of corepressor function by nuclear NADH.** *Science.* 2002, 295(5561):1895-1897.

304. Zhao H, Joseph J, Fales HM, Sokoloski EA, Levine RL, Vasquez-Vivar J, Kalyanaraman B: **Detection and characterization of the product of hydroethidine and intracellular superoxide by HPLC and limitations of fluorescence.** *Proc.Natl.Acad.Sci. U S A.* 2005, 102(16):5727-5732.

305. Zhao H, Kalivendi S, Zhang H, Joseph J, Nithipatikom K, Vasquez-Vivar J, Kalyanaraman B: **Superoxide reacts with hydroethidine but forms a fluorescent product that is distinctly different from ethidium: potential implications in intracellular fluorescence detection of superoxide.** *Free Radic.Biol.Med.* 2003, 34(11):1359-1368.

SUMMARY

Mitochondria fulfill a central role in cellular physiology. They are composed of a double membrane encompassing two aqueous compartments (the mitochondrial matrix and intermembrane space, IMS) and posses their own genetic material (mtDNA). Virtually all mitochondrial functions require the presence of a negative potential ($\Delta\Psi$) across the inner mitochondrial membrane (IMM). The generation of $\Delta\Psi$ is coupled to the production of cellular energy (adenosine triphosphate or ATP) by the oxidative phosphorylation (OXPHOS) system. The OXPHOS system consists of five multi-protein assemblies (complex I-V, CI-CV) and is embedded in the IMM. The first four complexes comprise the electron transport chain, which oxidizes NADH at CI and succinate at CII to release electrons. These are transported to CIV via two mobile electron carriers (ubiquinone and cytochrome *c*) and CIII, ultimately resulting in oxygen consumption and water formation. Energy released during electron transport is used by CI, CIII and CIV to transfer protons (H^+) from the mitochondrial matrix into the IMS resulting in the electrochemical proton gradient $\Delta\Psi$ that powers the fifth complex (CV) to produce ATP. With the exception of CII, which is entirely nuclear-encoded, all OXPHOS complexes are under dual genetic control of both the mtDNA and nuclear DNA (nDNA).

One in approximately 5000 children is born with a severe deficiency in the ATP generating system due to a genetic alteration affecting one or more of the OXPHOS complexes. OXPHOS deficiency mainly affects tissues with a high energy demand including brain, heart, and skeletal muscle. Frequently, the disease course is progressive, leading to multi-system deterioration and early death. In most cases, defective OXPHOS function is associated with a deficiency of NADH:ubiquinone oxidoreductase (complex I, CI), the first and largest complex of the OXPHOS system.

Complex I forms a ~1 MDa, L-shaped structure and is composed of 45 different proteins. Seven of these subunits are encoded by the mtDNA whereas genetic information for the remainder is on the nDNA. Mutations in nuclear-inherited CI genes are the most frequent cause of human CI deficiency. At present, our understanding of the molecular and cellular consequences of these mutations is still limited, which severely hampers the rational design and testing of effective therapeutics.

Although CI deficiency is generally associated with a decreased capacity to produce cellular energy, this may not be the only cause of disease. For example, abnormalities in cellular calcium homeostasis and mitochondrial morphology have been demonstrated in patient-

derived cell lines. In addition, CI deficiency is associated with alterations in reduction-oxidation (redox) homeostasis, which is of critical importance to a wide variety of cellular processes. A disturbed redox homeostasis can lead to oxidative stress and is associated with elevated levels of reactive oxygen species (ROS). Under physiological conditions, ROS are formed as 'by products' of oxidative phosphorylation. They comprise a group of chemically diverse molecules (e.g. superoxide (O_2^-), hydrogen peroxide (H_2O_2) and hydroxyl radical ($OH^\cdot$)) and differ in their mechanism of production, diffusion range, biological targets and detoxification pathways. Although excessive formation of these molecules is hazardous to a cell, inflicting damage to all cellular constituents, low level ROS production is implicated to play a role in diverse cellular signaling pathways.

The aim of the research described in this thesis was to gain more insight into the cell biological consequences of human CI deficiency in relation to ROS (patho)physiology. For this purpose we used control fibroblasts treated with rotenone (a CI inhibitor) and patient-derived skin fibroblast cell lines harboring a mutation in a nuclear-encoded structural CI subunit. With the aid of fluorescent reporters and life-cell imaging combined with biochemical, immunohistochemical and enzymatic techniques, we investigated the effect of these mutations on CI activity and expression, cellular ROS levels and redox homeostasis.

In **chapter 1** a detailed introduction is given about the concept of OXPHOS and CI deficiency in relation to ROS production and cellular redox state and describes the objectives of this thesis. **Chapter 2** describes and validates a novel method for simultaneous quantification of oxidative stress. **Chapter 3** describes the use of the antioxidant Trolox to study the effect of cellular ROS levels on CI expression and activity in cultured fibroblasts of six children with inherited CI deficiency. It was demonstrated that CI deficient cell lines displayed increased cellular ROS levels which could be alleviated by Trolox-treatment. In addition to ROS scavenging, Trolox-treatment also increased CI protein content and activity in all patient cell lines studied and in controls. The use of this antioxidant revealed a variable intrinsic catalytic problem in most CI deficient patient cell lines as Trolox increased CI protein content to a larger extent than it's activity. In controls both CI activity and CI protein content increased proportionally after Trolox-treatment. **Chapter 4** deals with the use of Trolox as a tool to investigate the pathological mechanism of CI deficiency in a subset of patient-derived cell lines harboring a mutation in the NDUFS4 subunit of CI. Although NDUFS4 deficient cell lines display an inactive CI subassembly in a gel-based assay, our results indicate that they retain functionally active CI protein in living cells albeit in lower amount as controls. In **chapter 5**, a cohort of 21 CI deficient cell lines was studied to investigate a possible

relationship between superoxide levels, CI activity and CI protein content. Our results demonstrate that inherited CI deficiency results in reduced CI activity and CI protein content, the extent of which is inversely related to elevated superoxide levels. In **chapter 6** we investigated whether the observed decrease in CI protein and elevation in cellular ROS levels in human deficiency were associated with an altered cellular redox state and caused cellular damage. However, no differences in cellular thiol redox status were observed between control and patient cell lines in living cells using the redox-sensitive green fluorescent protein 1 or after biochemical determination of cellular glutathione content (oxidized and reduced). Similarly, lipid peroxidation was not different from controls. **Chapter 7** reports on a cellular model for CI deficiency using healthy human skin fibroblasts, treated with the classic inhibitor of CI activity, rotenone. It is demonstrated that chronic (72h) rotenone treatment leads to increased levels of superoxide and lipid damage, and induces changes in mitochondrial morphology. Treatment of these CI inhibited cells with the antioxidant Mitoquinone (MitoQ) normalized cellular lipid damage and mitochondrial morphology but had no effect on superoxide levels or the abovementioned parameters in healthy cells. Therefore it is suggested that CI deficiency results in altered mitochondrial morphology through superoxide formation and lipid damage. In **chapter 8**, the result described in this thesis are discussed

In summary, we have demonstrated that CI deficiency caused by mutations in nuclear-inherited structural CI subunits results in a decline in the amount of active CI protein which is associated with elevated superoxide, NAD(P)H levels and cytosolic ROS levels. Although free radical production is increased in these CI deficient cell lines, no changes are observed in cellular thiol redox status. Finally, treatment of these cells with the antioxidant Trolox alleviates cytosolic ROS production and increases CI protein content and activity to a variable extent, stressing the importance of an oxidative component in the pathology of human CI deficiency in a cellular model. So far no treatment strategy is available for human CI deficiency. Hopefully, these cell biological findings might aid in the development of future therapeutics to slow down the disease progress and improve the quality of life of these patients.

SAMENVATTING

Mitochondriën zijn essentiële subcellulaire structuren die een centrale rol vervullen binnen de cel. Ze bestaan uit twee membranen die een barrière vormen voor twee waterig milieus (de mitochondriële tussenmembraan ruimte en de matrix). Ook bezitten deze organellen hun eigen genetisch materiaal, het mitochondriële DNA (mtDNA). Vrijwel alle mitochondriële functies zijn afhankelijk van de mitochondriële membraanpotentiaal ($\Delta\Psi$). Dit is een negative lading over de mitochondriële binnenmembraan. De generatie van $\Delta\Psi$ is gekoppeld aan de productie van adenosine trifosfaat (ATP), de universele brandstof van de cel. Dit wordt bewerkstelligd door het oxidatieve fosforylerings (OXPHOS) systeem.

Het OXPHOS systeem bestaat uit vijf multi-eiwit complexen (complex I-V of CI-CV) die zijn gelegen in de mitochondriële binnenmembraan. De eerste vier complexen vormen samen met de electronen dragers coenzym Q (CoQ) en cytochroom *c* (Cyt *c*) de electronen transportketen. Oxidatie van energie dragende substraten door CI en CII maakt electronen vrij. Deze worden vervolgens via CoQ, CIII en Cyt *c* naar CIV geleid, wat uiteindelijk resulteerd in zuurstof consumptie en de vorming van water. Tijdens dit transport komt energie vrij, die door CI, CIII en CIV wordt gebruikt om protonen (H^+) vanuit de mitochondriële matrix naar de tussenmembraanruimte te transporteren. Dit resulteert in de electrochemische gradient $\Delta\Psi$, die gebruikt wordt door CV om ATP te produceren. Het merendeel van de OXPHOS complexen is opgebouwd uit eiwitten van nucleaire en mitochondriële origine. De uitzondering hierop is CII, waarvan alle bouwstenen door het kern DNA (nucleair DNA/nDNA) worden gecodeerd.

Eén op de 5000 kinderen wordt geboren met een ernstige functionele tekortkoming (deficiëntie) van het OXPHOS systeem. Deze wordt veroorzaakt door een mutatie in het mtDNA of nDNA en zorgt ervoor dat één of meerdere OXPHOS complexen minder goed werken. OXPHOS deficiëntie resulteert in een verlaagde capaciteit om energie (ATP) te produceren en manifesteert zichzelf vooral in weefsels met een hoge energievraag zoals hart- en skeletspier en de hersenen. Het verloop van de ziekte is progressief en resulteert meestal in vroegtijdig overlijden. In de meeste gevallen wordt OXPHOS deficiëntie veroorzaakt door een slecht functionerend NADH:ubiquinone oxidoreductase (complex I of CI). Complex I heeft een molaire massa van ~1 MegaDalton, heeft een L-vormige structuur en bestaat uit 45 verschillende subunits. Zeven eiwitten worden door het mtDNA gecodeerd terwijl de genen voor de overige subunits op het nDNA gelegen zijn. De meeste gevallen

van CI deficiëntie worden veroorzaakt door mutaties in kern-gecodeerde subunits van CI. Tot op heden is er weinig inzicht in de consequenties van deze mutaties op moleculair en cellulair niveau. Dit vormt een duidelijke belemmering in de ontwikkeling en het testen van therapeutica.

Hoewel CI deficiëntie in het algemeen geassocieerd wordt met een verlaagde energie productie, is dit waarschijnlijk niet de enige oorzaak die leidt tot ziekte. Cellijnen van CI deficiënte patiënten, vertonen een veranderde cellulaire calcium huishouding en veranderingen in de uiterlijke kenmerken van de mitochondriën, de mitochondriële morfologie. Tevens leidt CI deficiëntie tot veranderingen in cellulaire reductie-oxidatie (redox) status. Een gezonde redox status is zeer belangrijk voor een grote verscheidenheid aan cellulaire processen. Pathologische condities zoals CI deficiëntie kunnen leiden tot een veranderde redox status en resulteren in oxidatieve stress. Dit gaat gepaard met verhoogde niveaus van reactieve zuurstof radicalen, of 'reactive oxygen species' (ROS). Normaliter worden ROS gevormd als bijproducten van oxidatieve fosforylering. ROS bestaan uit een groep chemisch diverse moleculen, zoals superoxide (O_2^-), waterstof peroxide (H_2O_2) en het hydroxyl radicaal ($OH^\cdot$). Ze verschillen in hun productie mechanisme, diffusie mogelijkheden, biologische targets en afbraak routes. Hoewel ROS alle primaire cellulaire bouwstenen (eiwitten, suikers, vetten en DNA) kunnen beschadigen en dus een potentieel gevaar vormen voor cellulaire functie, vervullen deze moleculen ook een belangrijke positieve rol in tal van cellulaire signaaltransductie routes.

Het doel van het in dit proefschrift beschreven onderzoek was het verkrijgen van meer inzicht in de celbiologische consequenties van humane CI deficiëntie in relatie tot ROS biologie. Hierbij is gebruik gemaakt van gezonde huid fibroblasten, wel of niet behandeld met de CI remmer rotenone en patiënten cellijnen met een geïdentificeerde mutatie in één van de kern-gecodeerde eiwitten van CI. Met behulp van fluorescente reporter moleculen en kwantitatieve video-microscopie in combinatie met biochemische, immunochemische en enzymatische technieken is het effect van CI deficiëntie op CI activiteit, expressie, ROS niveaus en redox status op cellulair niveau onderzocht.

Hoofdstuk 1 geeft een introductie over het OXPHOS systeem en CI deficiëntie in relatie tot ROS productie en cellulaire redox status en beschrijft de doelstellingen van het onderzoek beschreven in dit proefschrift. **Hoofdstuk 2** beschrijft de validatie van een nieuwe methode waarmee gelijktijdig cellulaire oxidanten en spreiding van cellen gemeten kan worden. In experimenten beschreven in **hoofdstuk 3** en **4** is het antioxidant Trolox gebruikt. Antioxidanten zijn stoffen die ROS of oxidanten kunnen wegvangen. In **hoofdstuk 3** is

Trolox gebruikt om het effect van cellulaire ROS op de expressie en activiteit van CI te onderzoeken in fibroblasten van zes kinderen met een geïsoleerde CI deficiëntie. Deze cellijnen vertoonden verhoogde ROS niveaus die normaliseerden na Trolox-behandeling. De verlaging in ROS was geassocieerd met een verhoging van de hoeveelheid CI eiwit en activiteit in alle patiënten cellijnen en in controle cellen. Door het gebruik van dit antioxidant werd een intrinsiek catalytisch probleem in CI binnen dit patiëntencohort blootgelegd. In deze cellijnen was de Trolox geïnduceerde toename in de hoeveelheid CI eiwit namelijk altijd groter dan de toename in CI activiteit terwijl in Trolox behandelde controle cellen CI activiteit en eiwit proportioneel toenamen. In **hoofdstuk 4** is met behulp van Trolox het pathogene mechanisme van CI deficiëntie onderzocht dat veroorzaakt wordt door mutaties in de NDUFS4 subunit van CI. Mitochondriële fracties van NDUFS4 deficiënte cellijnen vertonen een CI eiwit complex dat niet volledig geassembleerd is en ook geen activiteit vertoont in een in-gel CI activiteitsassay. Deze resultaten suggereren dat onvolledige CI assemblage de oorzaak van ziekte is in patiënten met een mutatie in NDUFS4. In tegenstelling tot de resultaten in mitochondriële fracties, tonen onze bevindingen in levende cellen aan dat NDUFS4 deficiënte cellen wel degelijk een functioneel CI kunnen maken. Behandeling met Trolox zorgde verder voor een afname in de hoeveelheid ROS en een verhoging van de hoeveelheid CI eiwit en activiteit. In **hoofdstuk 5** is materiaal van 21 CI deficiënte patiëntencellijnen gebruikt om een mogelijke relatie tussen superoxide niveaus, de hoeveelheid CI eiwit en CI activiteit te onderzoeken. Hieruit is naar voren gekomen dat humane CI deficiëntie veroorzaakt wordt door een verminderde hoeveelheid actief CI eiwit en geassocieerd is met verhoogde superoxide niveaus. In **hoofdstuk 6** is onderzocht of de verlaging in actief CI eiwit en de verhoging in cellulaire ROS in CI deficiënte cellen resulteerde in een veranderde cellulaire redox status en celschade. Hiervoor is gebruik gemaakt van de redox gevoelige probe ‘redox-sensitive green fluorescent protein 1’ en zijn de cellulaire concentraties glutathione en glutathione disulfide (geoxideerd glutathione) gemeten. Ondanks verhoogde ROS productie zijn er geen verschillen gevonden in cellulaire thiol redox status tussen patiënten en controle cellen. Ook lipide schade was niet veranderd tussen controle en CI deficiënte patiënten cellijnen. **Hoofdstuk 7** beschrijft de bevindingen met een cellulair model voor CI deficiëntie, gebruikmakend van gezonde huid fibroblasten die behandeld zijn met een klassieke remmer van CI activiteit, rotenone. Chronische remming van CI (72 uur) leidt tot verhoogde superoxide niveaus, schade aan vetzuren en veroorzaakt een verandering in de mitochondriële morfologie. Behandeling van deze CI geremde cellen met het mitochondriële antioxidant Mitoquinone (MitoQ) leidde tot een

normalisatie van vetzuur schade en mitochondriële morfologie maar had geen effect op superoxide productie. Deze resultaten suggereren dat CI deficiëntie gepaard gaat met een veranderde mitochondriële morfologie via verhoogde superoxide productie en lipide schade. In **hoofdstuk 8** worden de bevindingen beschreven in dit proefschrift bediscussieerd.

Samenvattend is er aangetoond dat humane CI deficiëntie veroorzaakt door mutaties in kern-gecodeerde structure CI eiwitten resulteert in een verlaagde hoeveelheid actief CI eiwit. De verlaagde CI activiteit is geassocieerd met verhoogde superoxide, NAD(P)H en cytosolische ROS niveaus. Hoewel de cellulaire vrije radicaal niveaus verhoogd zijn, zijn er geen veranderingen gemeten in cellulaire thiol redox status. Behandeling van deze cellen met het antioxidant Trolox leidt tot een verlaging in ROS niveaus en een verhoging in de hoeveelheid CI eiwit en activiteit. Dit illustreert het belang van een oxidative component in de pathologie van humane CI deficiëntie in een celmodel. Tot op heden is er geen effectieve behandeling aanwezig voor patiënten met een geïsoleerde CI deficiëntie. Hopelijk dragen deze celbiologische bevindingen bij aan de ontwikkeling van therapeutica om de progressie in het ziekteproces te verminderen en de kwaliteit van het leven voor deze patiënten te verbeteren.

DANKWOORD

Zo, nu het meest gelezen onderdeel van mijn proefschrift. Onderzoek doe je niet alleen en de resultaten beschreven in dit proefschrift zouden niet tot stand gekomen zijn zonder de steun en medewerking van een heleboel mensen. Zonder iemand te kort te willen doen zou ik graag een aantal mensen persoonlijk willen bedanken.

Zonder gekarakteriseerde cellen zou dit onderzoek onmogelijk zijn. Daarom wil ik de ouders van de patiëntjes en de verschillende diagnostische onderdelen (celkweek, enzym- en DNA diagnostiek) van de afdeling Kindergeneeskunde en Neurologie hartelijk bedanken voor hun medewerking.

Ten tweede zou ik Jan en Peter willen bedanken voor de uitdagende werkomgeving die de basis heeft gevormd voor dit proefschrift. Ondanks jullie overvolle dagprogramma kon ik altijd binnenlopen met vragen en ideeën en was er tijd voor een wekelijkse werkbespreking waarin deze werden uitgewerkt. Verder wil ik Bert en Richard bedanken voor de karrevracht aan OXPHOS getallen die zij in de loop der jaren op mijn verzoek hebben aangeleverd.

Dit proefschrift had nooit tot stand kunnen komen zonder de hulp van Werner. Beste Dr. Koopman, Dr. Corel Draw, Dr. Mic en zo kan ik wel doorgaan, ik vond het ontzettend leuk om met je samen te werken en op congres / werkbezoek te gaan. Je ongeremde enthousiasme, motivatie en werklust beginnen zich nu uit te betalen in een groot aantal publicaties en projecten. Heel veel succes toegewenst en misschien kunnen we onze samenwerking, al dan minder direct, in de toekomst voortzetten.

Een dag niet gelachen is een dag niet geleefd. Gelukkig bestond onze werkgroep uit een gezonde mix van junior onderzoekers, senior analisten, postdocs en studenten waardoor het werken op het lab erg gezellig was. Ook was ik vaak op het ziekenhuis te vinden voor celkweek, mutatie informatie en de laatste nieuwtjes. Bij deze wil ik dan ook graag Cindy, Edinio, Henk-Jan, Jan Koenderink, Leo, Li Yan en mijn collegas van de afdeling Kindergeneeskunde en Neurologie bedanken voor hun samenwerking en succes wensen in de toekomst.

De categorie senior analisten bestaat uit Herman en Sjenet. Zij hebben samen ongeveer 40 jaar labervaring en zijn niet te beroerd om ons advies te geven en hun eigen kennis uit te breiden. Herman, bedankt voor je hulp bij het modificeren en opzetten van het baculovirus systeem dat van grote waarde is gebleken voor mij en je huidige collega's.

Sjenet, zonder al jouw Blue-Native analyses was dit proefschrift nooit tot stand gekomen. Binnen een half jaar is het je gelukt om met deze techniek kwantitatieve data te genereren. Je laat je niet gek maken en ondanks alles blijf je met beide benen op de grond en sterk in je schoenen staan. Ontzettend bedankt voor jouw bijdrage aan dit proefschrift en ik hoop dat je het leuk vindt één van mijn paranimfen te zijn.

Tijdens mijn onderzoek heb ik ook een aantal studenten mogen begeleiden. Bij deze wil ik Maarten, Eva en Julia dan ook hartelijk bedanken voor hun medewerking aan de diverse hoofdstukken van dit proefschrift. Miss Julia Cheek, I had the pleasure of working with you for almost a year in which you struck me as a motivated, punctual and well-ordered student with excellent pipetting skills. I wish you all the best and hopefully we will meet again in the future.

Omdat ik graag business with pleasure afwissel in de vorm van koffiepauzes ging ik ook veel om met de afdeling Farmacologie/Toxicologie. Met name wil ik noemen Juffrouw Janny, Jeroen, Joke, Miriam en Suzanne. Het drinken van koffie/thee werd al snel uitgebreid met diners en barbecues en werkbezoeken in Leuven en Tessin. Dit heeft geleid tot een hechte vriendschap die we hopelijk nog lang in stand kunnen houden. Hartelijk bedankt voor de luisterende oren en al jullie steun.

Hetzelfde geldt voor mijn tweede paranifm Martijn. Celkweken in Nijmegen en bierdrinken in Aarhus gaat je goed af (en mij ook). Ook jij bent het promotietraject ingegaan. Bij deze wil ik je bedanken voor je steun de afgelopen jaren en succes wensen met jouw promotie.

Tot slot wil ik mijn ouders, Joost (voor de laatste loodjes) vrienden en familie bedanken voor hun onvoorwaardelijke steun als ik het even niet zag zitten.

En last but not least: Viv. Jij hebt de minst leuke kanten van mijn promotie van dichtbij meegemaakt maar hebt me altijd gesteund en opgebeurt. Samen hebben we er ons doorheen geslagen. We zijn de trotse ouders geworden van onze zoon Bram waaraan we heel veel plezier beleven.

Dit is afgerond, op naar een nieuwe uitdaging.

Sjoerd

CURRICULUM VITAE

Sjoerd Verkaart word op 10 december 1977 geboren in Bergen op Zoom en groeit het grootste deel van zijn jeugd op in het Brabantse Son en Breugel. Nadat hij zijn HAVO-diploma heeft behaald aan het Eckart College in Eindhoven begint hij in 1995 met de opleiding tot HLO-analist in Etten-Leur. Na een praktische stage aan de Erasmus Universiteit Rotterdam (afdeling Hematologie onder leiding van Dr. E. Wiemer) wordt deze opleiding in 1999 afgerond met biotechnologie als specialisatie. Vervolgens gaat hij verder studeren aan de Radboud Universiteit Nijmegen, opleiding Medische Biologie. Deze opleiding wordt na een wetenschappelijk stage aan dezelfde universiteit (afdeling Autoimuunbiochemie onder leiding van Dr. M. Fouraux en Dr. G. Pruijn) begin 2002 afgerond. In juni 2002 start hij verbonden aan de afdelingen Kindergeneeskunde en Neurologie en Membraanbiochemie zijn promotieonderzoek aan de Radboud Universiteit Nijmegen onder leiding van Prof. Dr. J. Smeitink en Dr. P. Willems. Vanaf februari 2007 is hij werkzaam als postdoc op de afdeling Celfysiologie aan de Radboud Universiteit Nijmegen onder leiding van Dr. J. Hoenderop en Prof. Dr. R. Bindels.

LIST OF PUBLICATIONS

Fouraux MA, Bouvet P, **Verkaart S**, van Venrooij WJ, Pruijn GJ: Nucleolin associates with a subset of the human Ro ribonucleoprotein complexes. *J.Mol.Biol.* 2002, 320(3):475-488.

Visch HJ, Rutter GA, Koopman WJ, Koenderink JB, **Verkaart S**, de Groot T, Varadi A, Mitchell KJ, van den Heuvel LP, Smeitink JA, Willems PH. Inhibition of mitochondrial Na+-Ca2+ exchange restores agonist-induced ATP production and Ca^{2+} handling in human complex I deficiency. *J.Biol.Chem.* 2004, 279(39):40328-40336.

Koopman WJ, Visch HJ, **Verkaart S**, van den Heuvel LW, Smeitink JA, Willems PH: Mitochondrial network complexity and pathological decrease in complex I activity are tightly correlated in isolated human complex I deficiency. *Am.J.Physiol.Cell.Physiol.* 2005, 289(4):C881-C890.

Koopman WJ, **Verkaart S**, Visch HJ, van der Westhuizen FH, Murphy MP, van den Heuvel LW, Smeitink JA, Willems PH: Inhibition of complex I of the electron transport chain causes $O2^{-\cdot}$–mediated mitochondrial outgrowth. *Am.J.Physiol.Cell.Physiol.* 2005, 288(6):C1440-C1450.

Koopman WJ, **Verkaart S**, van Emst-de Vries SE, Grefte S, Smeitink JA, Willems PH: Simultaneous quantification of oxidative stress and cell spreading using 5-(and-6)-chloromethyl-2',7'-dichlorofluorescein. *Cytometry A.* 2006, 69(12):1184-1192.

Verkaart S, Koopman WJ, Nijtmans LG, van den Heuvel LW, Smeitink JA, Willems PH: Superoxide production and CI expression are inversely related in CI deficiency. *Biochim.Biophys.Acta.* 2007, 1772(3):373-381.

Vogel RO, Janssen RJ, van den Brand MA, Dieteren CE, **Verkaart S**, Koopman WJ, Willems PH, Pluk W, van den Heuvel LW, Smeitink JA, Nijtmans LG: Cytosolic signalling protein Ecsit also localises to mitochondria where it interacts with chaperone NDUFAF1 and functions in complex I assembly. *Genes Dev.* 2007, 21(5):615-624.

Koopman WJ, **Verkaart S**, Visch HJ, van Emst-de Vries SE, Nijtmans LG, Smeitink JA, Willems PH: Human NADH:ubiquinone oxidoreductase deficiency: radical changes in mitochondrial morphology? *Am.J.Physiol.Cell.Physiol.* 2007, ***in press***

Koopman WJ, Hink MA, **Verkaart S**, Visch-HJ, Smeitink JA, Willems PH: Partial complex I inhibition decreases mitochondrial motility and increases matrix protein diffusion as revealed by fluorescence correlation spectroscopy *Biochim.Biophys.Acta.* 2007, ***in press***.

Verkaart S, Koopman, WJ, Cheek J, van Emst-de Vries SE, van den Heuvel LW, Smeitink JA, Willems PH. Mitochondrial and cytosolic redox environment are not detectably altered in isolated human NADH:ubiquinone oxidoreductase deficiency *Biochim.Biophys.Acta.* 2007, ***in press.***

Verkaart S, Willems PH, Visch HJ, Grefte S, Rodenburg RJ, van den Heuvel LW, Smeitink JA, Nijtmans LG, Koopman WJ. Cellular and molecular basis of nuclear-inherited isolated NADH:ubiquinone oxidoreductase deficiency: improvement by chronic treatment with a vitamin E analogue (***submitted***).

Verkaart S, Koopman WJ, van Emst-de Vries SE, Rodenburg RJ, van den Heuvel LW, Nijtmans LG, Smeitink JA, Willems PH. Patients with a mutation in the NDUFS4 subunit of NADH:ubiquinone oxidoreductase display an active but unstable form of the enzyme (***in preparation***).